QUANTITATIVE MICROSPECTROSCOPIC STUDIES OF DNA-DRUG COMPLEXES

by

GEOFFREY DOUGHERTY

B.Sc. (Manc.)

A Thesis Submitted for the Degree of

Doctor of Philosophy

in the

University of Keele

Department of Physics,

University of Keele,

England.

August 1979

ABSTRACT

The interactions in solution and in the fibre state of the trypanocidal phenanthridine drugs, ethidium bromide, dimidium bromide and prothidium (di)bromide with DNA have been investigated using a variety of physical techniques. A number of analytical techniques applicable to polymer-ligand interactions have been developed and used in the analysis of these results.

For each of the drugs, complexes were prepared with three natural DNA's of different nucleotide compositions using a novel mixing scheme. The solution spectra were analysed in terms of binding affinity, number and size of binding sites and base-pair specificity. The binding of ethidium and dimidium is limited by neighbour exclusion effects, whilst prothidium is able to bind to higher levels.

Fibre X-ray diffraction showed that dimidium and ethidium caused a substantial increase in the DNA pitch at high humidities, probably through intercalative binding. In contrast, the binding of prothidium appears to cause no change in the DNA secondary structure at any humidity. The birefringence and linear dichroism of the fibres used in the diffraction study were measured over a range of humidities, using a microspectrophotometer. The results are interpreted in terms of the tilt angle of the base-pairs and/or drug chromophores, the disorientation of the DNA helices (estimated from the diffraction patterns) and the fractions of bound drug. At high humidities, a substantial fraction of ethidium or dimidium is oriented perpendicular to the helix axis, consistent with intercalation. The X-ray diffraction and dichroism measurements considered together give an unwinding angle at the intercalation site of about 34°. This is unexpectedly large but there are difficulties in combining the results from these two techniques. Prothidium shows little preferred orientation in its binding.

A combined external binding scheme is presented with some molecules inclined parallel to the sugar-phosphate chain, and others binding across adjacent chains. Computer drawings and molecular models illustrate these suggested binding schemes.

ACKNOWLEDGEMENTS

I am grateful to Professor W. Fuller for provision of the research facilities and equipment used in this work. I would like to thank Dr. W.J. Pigram for his supervision, advice and encouragement freely given throughout the duration of this project.

I should like to thank Dr. T. Markvart for his assistance with the linear dichroism simulations, Dr. P.K. Grannell for help with the electronics, Mr. R.J. Greenall for advice on the model-building program and Mr. N.J. Rhodes for technical aid with the X-ray generators. I would like to thank Dr. G. Jones for an interesting discussion on the stereochemistry of phenanthridines. I am grateful to the technical staff of the Physics Department for the support they provided, to Mr. M. Daniels and Mr. M.T. Cheney for the photographic work, and to the consultants of the Computer Centre at the University of Keele for their assistance with some of the computer programs. My thanks are due to Mrs. J. Gill for her careful typing of the manuscript.

I would like to thank my parents for their encouragement throughout this period. Special thanks are due to Nab, who stencilled most of the drawings and re-wrote the manuscript legibly for typing. She has given me valuable support throughout the period of this work.

CONTENTS

CHAPTER 1

INTRODUCTION

1.1 DNA Structure and Function

The fundamental role of deoxyribonucleic acid (DNA) in the replication of living cells is well established. It encodes the genetic information and transmits it from one generation to the next. The information can then be deciphered by the messenger RNA - ribosome-transfer RNA system to synthesise the enzymatic and structural proteins for the new organism. DNA, conjugated with protein, is a major constituent of the genes, which are the regions of a chromosome that determine particular genetic traits.

DNA is a long polymer, made up of monomers called nucleotides. Each nucleotide consists of three components - a heterocyclic base, a deoxyribose sugar and a phosphate group - and has a molecular weight of about 330. There are four different bases that occur commonly in DNA; two purines, adenine (A) and guanine (G), and two pyrimidines, thymine (T) and cytosine (C). The nucleotides are polymerised to form a sugar-phosphate chain (Fig. 1.1) whose direction can be specified by reference to the sugar 3' and 5' carbon atoms. The molecular weight of DNA is extremely high, ranging from several million to several hundred million depending on the species, and this corresponds to many thousands of nucleotides.

The two polynucleotide chains are joined by a specific interaction between certain bases. This interaction is in the form of a hydrogen bonding scheme in which adenine is always paired with thymine, and guanine always with cytosine. The resulting double helix is stabilised with the hydrophobic bases in the centre and the negatively charged phosphate groups, usually neutralised by alkali metal ions such as Na^+, arranged externally. The two chains run antiparallel (Fig. 1.2), being related by a dyad axis perpendicular to the helix axis and passing through each base-

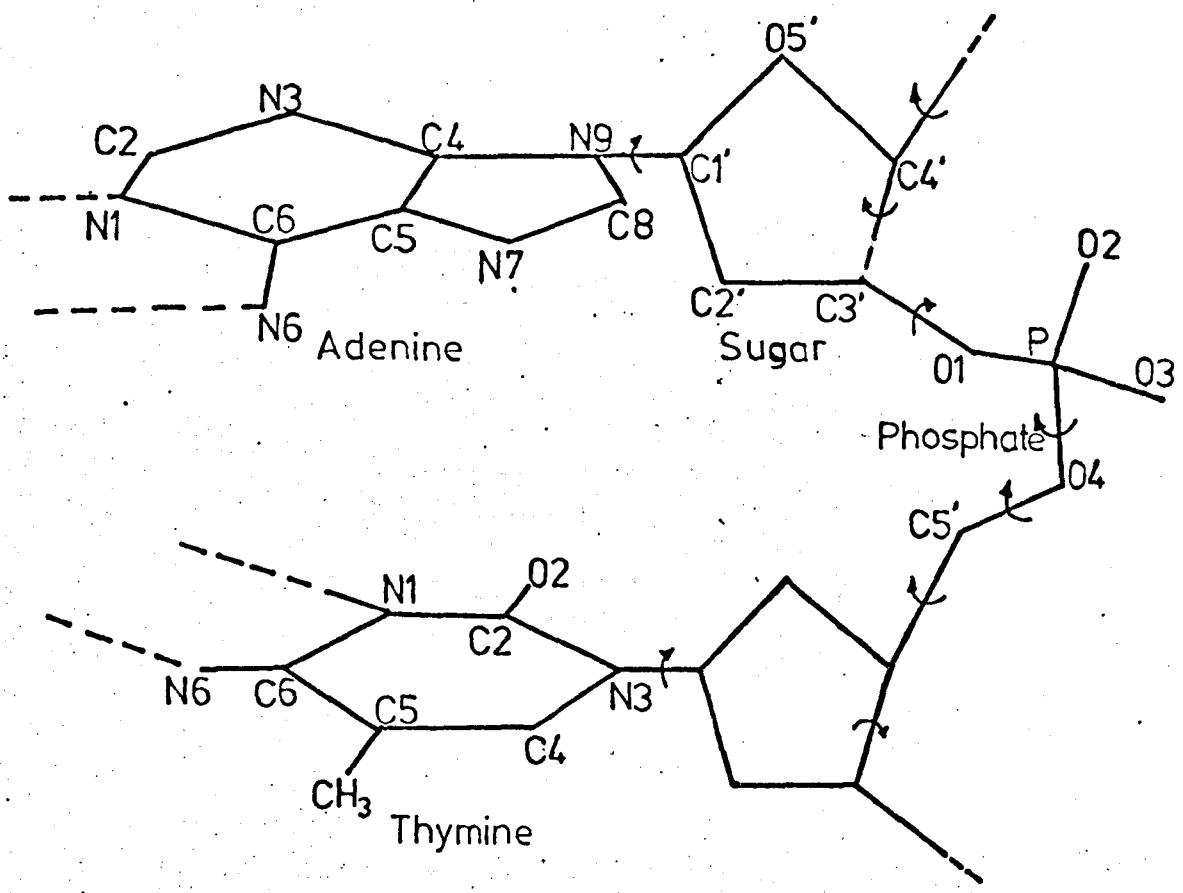

Fig. 1.1 Schematic representation of DNA structure showing the nomenclature for pyrimidine and purine bases and the conformational angles that define the structure.

Fig. 1.2 Schematic representation of the Watson-Crick DNA model with strands of opposite polarity

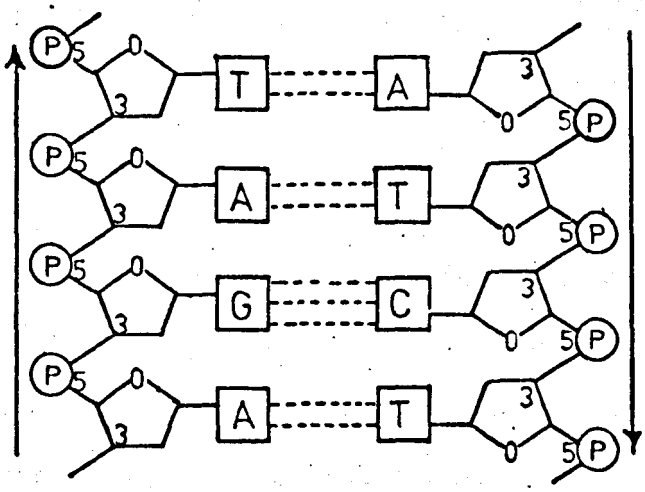

With this model, TpA = TpA

ApG = CpT

GpA = TpC

pair (Fig. 1.3). The sugar-phosphate backbones are regular, even though the base sequence is random, because the dimensions of the A - T and G - C base-pairs are virtually identical.

The importance of the base-pairing scheme with regard to DNA replication is that it allows the DNA to act as its own template, since the base sequence on one strand specifies the sequence on the other. The genetic information itself is coded in terms of the sequence of bases along a polynucleotide chain. Groups of three bases, termed codons, code for the insertion of a particular amino-acid into a protein.

1.1.1 DNA Conformation

Early fibre X-ray diffraction studies (Wilkins et al., 1953; Franklin and Gosling, 1953; Marvin et al., 1958) established that there were three distinct conformations, the A, B and C forms, for natural DNA, which are all modifications of the same basic structure. The structure of the A form was described in detail by Fuller et al. (1965); that of the B form by Langridge et al. (1960); and that of the C form by Marvin et al. (1961). Recently, more refined structures of the A and B forms have been presented (Arnott and Hukins, 1972). The model proposed by Watson and Crick (1953) corresponds most closely to the B conformation.

The three conformations of DNA differ in the number of nucleotides per helix turn, the helix pitch and the nucleotide conformation (Table 1.1). The A and B forms are quite different and can be characterised by the type of sugar puckering present (Fig. 1.4) and the disposition of the base-pairs relative to the helix axis (Fig. 1.3). The sugar pucker is determined by the position of C2' or C3' relative to the plane defined by C1' - O5' - C4'. The conformation is endo if the most out of plane atom is on the same side of the plane as C5', and exo if it is on the opposite side to C5'. In B DNA the distance D, of the base-pairs from the helix axis is small and negative, the base tilt is almost zero, and the sugar

Fig. 1.3 The parameters defining the disposition of a base-pair relative to the helix axis

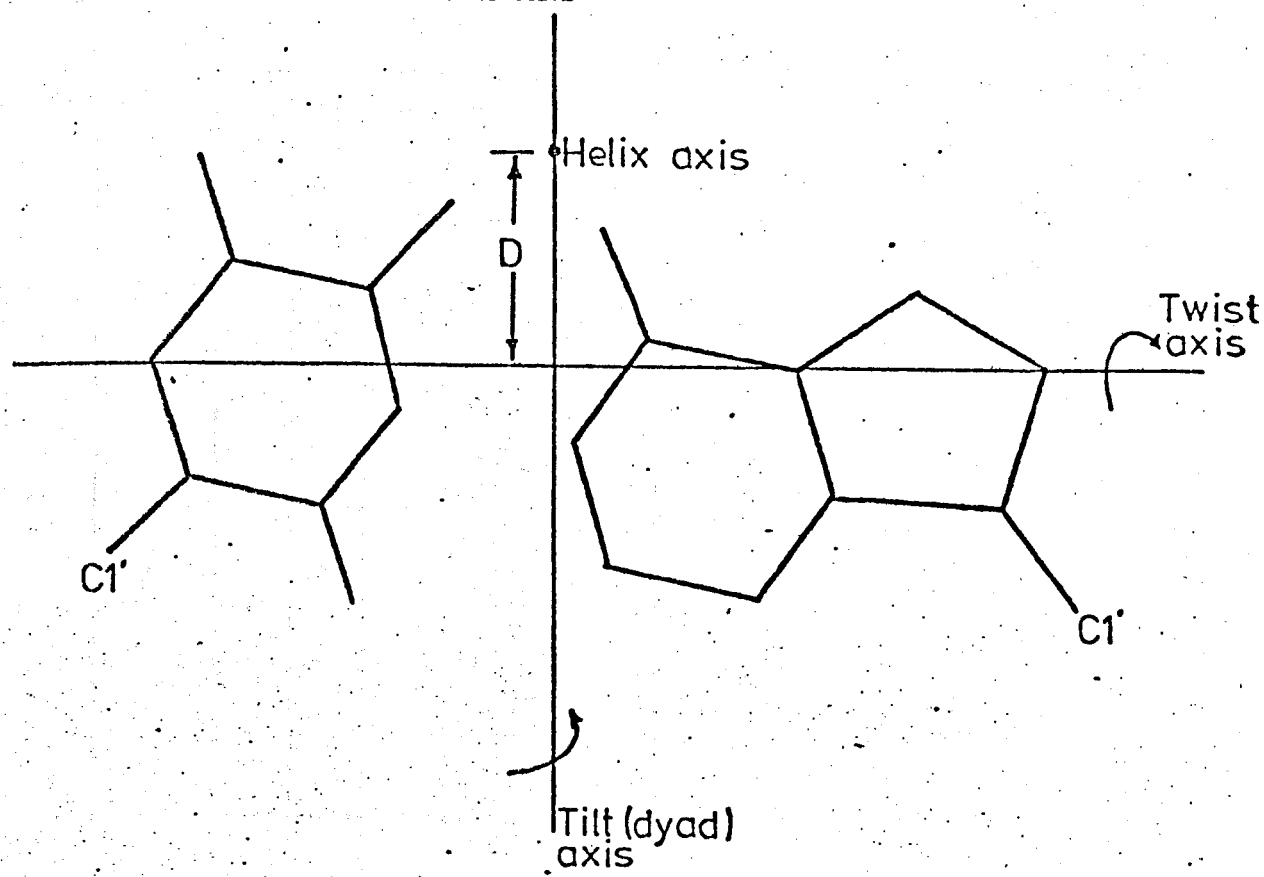

Fig. 1.4 Projections parallel to C1' - O5' - C4' to show the four possible sugar puckers: (i) C2'-endo (ii) C3'-endo (iii) C2'-exo (iv) C3'-exo

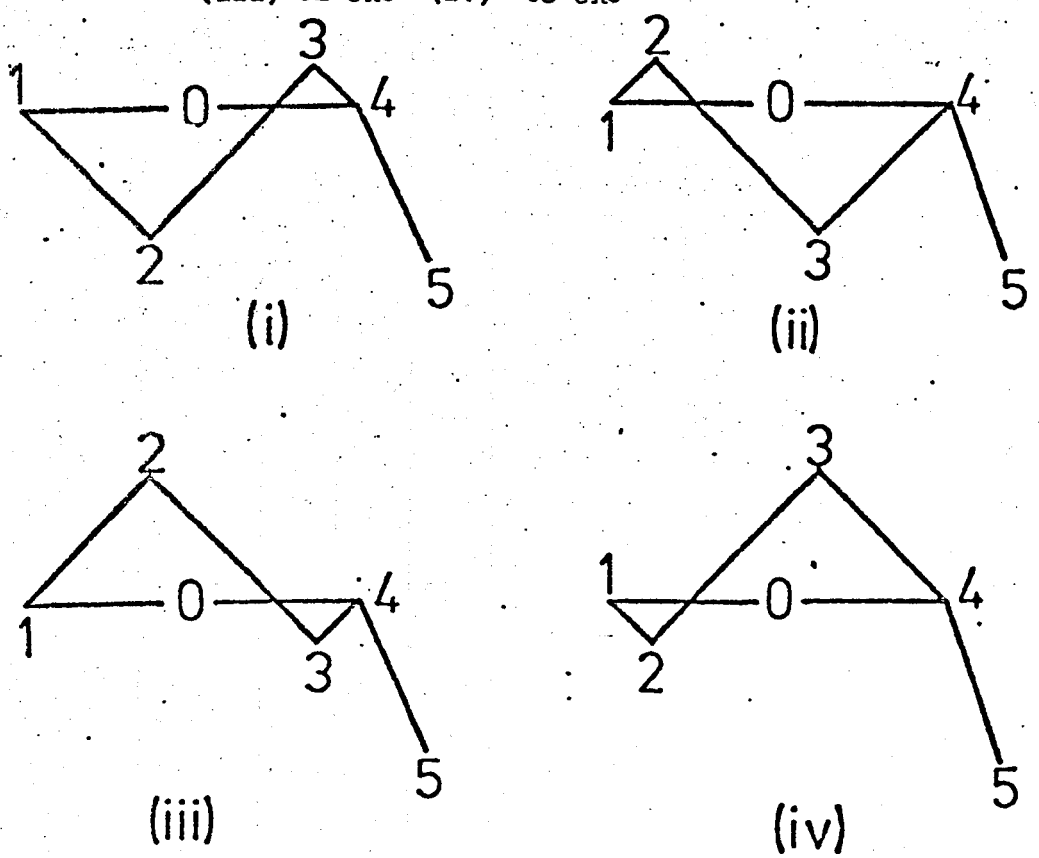

Form	Sugar Pucker	Pitch (A)	Residues per turn	Rise per Nucleotide (A)	Distance D (A)	Tilt (°)	Twist (°)	References
A	C3 endo	28.15	11	2.56	4.72	20	-1.2	Arnott and Hukins, 1972
B	C3 exo	33.8	10	3.4	-0.16	-5.9	-2.1	Arnott and Hukins, 1972
C	C3 exo	30.9	9.3	3.22 .	-2.13	-6.0	5	Marvin et al., 1961

TABLE 1.1 Helical Parameters of the Three Main Conformations of DNA

pucker is C3' exo. The two polynucleotide chains are wound around each other such that two helical grooves, a large one and a smaller one, run along the polymer between the two strands. The characteristic 3.4Å base-pair repeat distance along the helix axis gives rise to strong reflections on the meridian of X-ray diffraction photographs. In the A form the base-pairs are moved nearly 5Å forward (D positive) from the helix axis and the tilt angle is large and positive, whilst the sugar ring pucker is C3' endo. Although the C form has a number of features which make it distinct from the B form, it is similar in having C3' exo sugar puckering and negative values both for the distance, D, and the tilt angle.

The conformation depends on the type and concentration of the counterion present, and on the relative humidity. At low ionic strengths (< 5% excess NaCl) the A form has always been observed at humidities up to and including 92%, and occasionally at 98% (Cooper and Hamilton, 1966); whilst fibres containing more counterions (> 9% excess NaCl) gave B-patterns at 75% relative humidity. Fibres containing salt contents intermediate between these two values, gave the A form at 75% R.H. and the B form at 92% R.H. and above. X-ray diffraction studies have shown that the A form is crystalline, giving Bragg reflections over much of the diffraction pattern, whereas the B form is semi-crystalline and gives less well defined reflections in the centre of the pattern and diffuse diffraction streaks over the remainder of the pattern.

With fibres made from the lithium salt of DNA, the A form is not observed. Instead the semi-crystalline C form is observed at low salt concentrations (< 3% excess LiCl) and low humidities ($\leqslant$ 60% R.H.), and a crystalline B pattern is obtained at higher ionic concentrations.

Hamilton et al. (1959) showed that the above conformations could be obtained from natural DNA's from a wide variety of sources. Bram (1973) has reported some differences of the B conformation with G - C content, and in particular the possibility of a D conformation, but the effect is not

great. Premilat and Albiser (1975) and Goodwin (1977) have found that the base-pair composition of DNA has only a negligible effect on the diffracted X-ray intensities, which can be explained by slight changes in the base-pair tilt. So far, no variations of the A form of DNA have been reported, although in dried specimens the intermolecular separation of the double helices is dependent on the relative humidity.

DNA structure is so closely related to its function that it is possible that the different conformations are involved in the cell mechanisms. It is generally accepted that the B form of DNA, which is most stable at high humidities, is the most probable conformation in solution in the living cell. If different segments of DNA adopt slightly different conformations under the same environmental conditions, perhaps as a result of the base-pair composition within that segment, it would provide a possible molecular basis for control mechanisms in DNA replication and transcription.

A number of recent papers (Rodley et al., 1976; Sasisekharan and Pattabiraman, 1976, 1978; Sasisekharan et al., 1977, 1978; Cyriax and Gäth, 1978; Pohl and Roberts, 1978) have suggested that the two strands of DNA do not coil around one another but lie side-by-side (the so-called SBS model). Crick et al. (1979) refute this suggestion using evidence from recent gel electrophoresis experiments (Keller and Wendel, 1974; Keller, 1975; Shure and Vinograd, 1976; Wang, 1978, 1979). They do however concede that the experimental evidence for the righthandedness of the original model (Watson and Crick, 1953) is still only suggestive and not yet completely compelling. Fourier transform studies on the SBS model (R.J. Greenall et al., to be published) have shown serious discrepancies between the X-ray diffraction intensities observed and those calculated using the model.

1.2 The Interaction of Drugs with DNA

Albert et al.(1961) showed that the antimicrobial activity of phenanthridines and acridines, both of which possess a triple aromatic ring (Fig. 1.5), is dependent on the compounds existing as cations. They suggested that the drugs act by competing with hydrogen ions for certain anionic groups in the organism. These anionic groups probably have a pK_a of 9 or higher (for example, the hydroxyl groups in the purine or pyrimidine bases in DNA). Albert pointed out that there is a correlation between the activity of these drugs and the area of flatness in the drug molecule. The triple aromatic rings often present in drugs are referred to as chromophores, since they are the basis of the characteristic colours of these drugs. The chromophores of the phenanthridines and acridines are fully conjugated and hence are flat (the atoms in the chromophores deviating by less than 0.1Å from the mean plane through the chromophore (Giacomoni, 1973)) and have an area of approximately 38Å^2. Hydrogenation of one ring of 5-aminoacridine to yield 5-aminotetrahydroacridine reduces the flat area of the molecular to 28Å^2 and also reduces its bacteriostatic activity by a factor of thirty to a level comparable to that of the drug 4-aminoquinoline, which also has a flat area of 28Å^2.

The requirement for planarity was investigated by Lerman (1961) in studies on the interaction of acridines with DNA. X-ray diffraction patterns of DNA-acridine fibres revealed closer side by side packing of DNA molecules, suggesting that external binding to DNA was not the dominant binding process. Layer lines corresponding to the helical repeat of the DNA were not observed but the meridional reflections indicating a monomer repeat distance of 3.4Å along the structure were still strong. DNA-acridine complexes in solution exhibit a marked increase in viscosity and decrease in sedimentation coefficient compared with DNA (see also Kersten et al., 1966; O'Brien et al., 1966; Müller and Crothers, 1968). Other

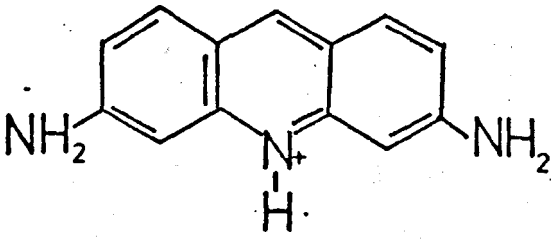

Proflavine

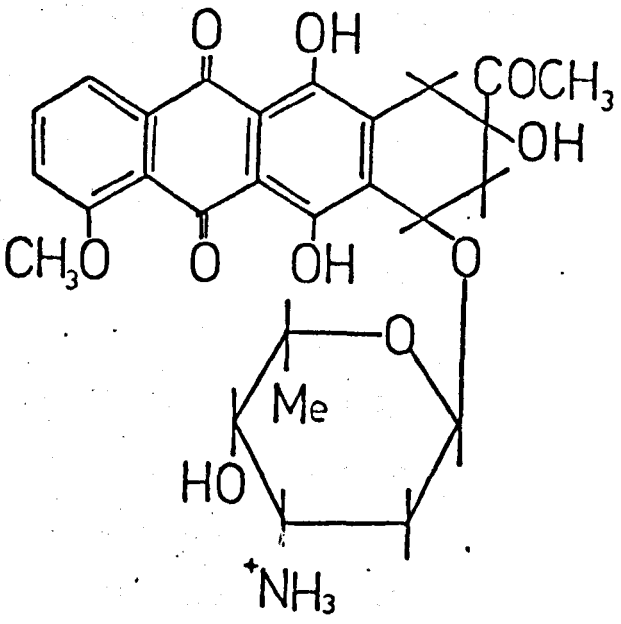

Daunomycin

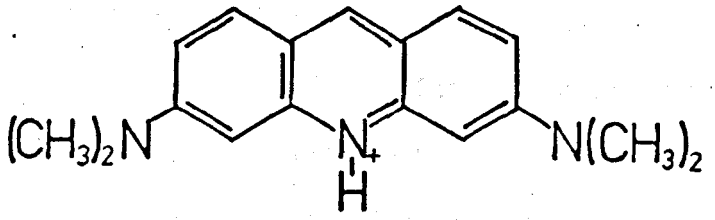

Acridine orange

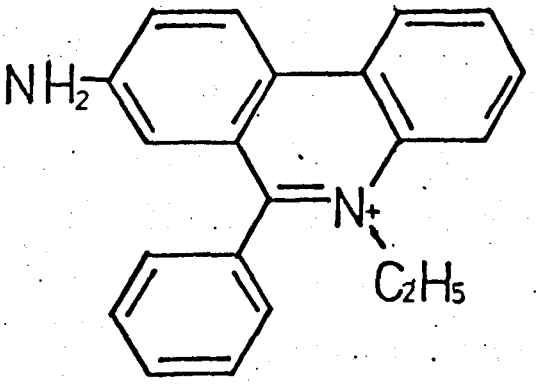

Ethidium bromide

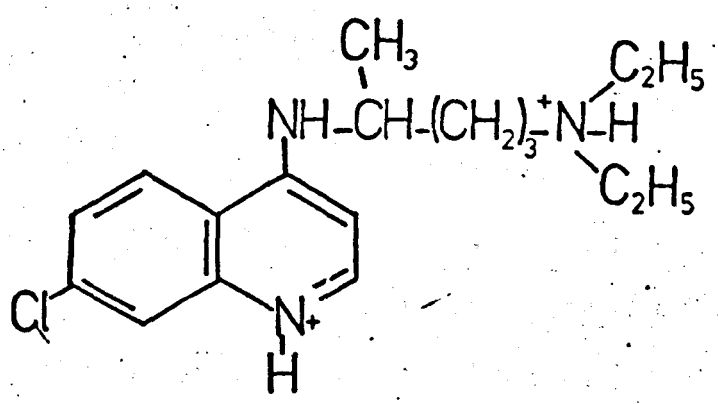

Chloroquine

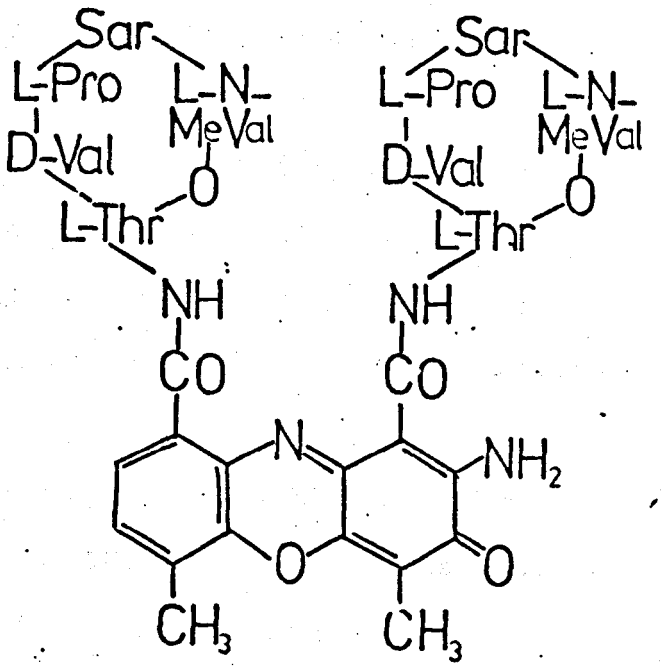

Actinomycin D

Fig. 1.5 Structural formulae of some compounds which bind to DNA

cations, lacking the planarity of the acridines, were found to reduce the viscosity of DNA. These observations are compatible with a thinner, stiffer DNA helix and Lerman proposed that the drug interacted with DNA largely by a process which he called intercalation. This involved the sandwiching of a drug molecule between two adjacent DNA base-pairs (Fig. 1.6). The base-pairs remain perpendicular to the helix axis, but they are moved apart to accommodate the drug molecule (of approximately 3.4Å thickness) which lies in Van der Waal's contact with the base-pairs above and below. The intimate contact between the π-orbitals of the drug molecule and the base-pairs would help to stabilise the complex via hydrophobic and charge-transfer forces.

Since the DNA sugar-phosphate chain is virtually fully extended in native DNA (no doubt partly due to electrostatic repulsion between successive negatively charged phosphate groups), Lerman proposed that the helix had to unwind (Fig. 1.7) in order to admit the drug. This leads to a local distortion of the helix. An initial estimate of 45° unwinding was suggested, but this was later modified to 36° (Lerman, 1964). This distortion of the helix at intercalated sites would destroy the long-range regularity of the helix (as long as the sites were not located at regular intervals along the DNA molecule), which accounts for the loss of sharp layer-line reflections in the X-ray diffraction patterns when a substantial amount of drug is bound.

An X-ray diffraction and model building study of ethidium bromide binding to DNA by Fuller and Waring (1964) likewise concluded that ethidium intercalated into DNA. They proposed that the minimum and possibly the preferred unwinding angle for intercalation of ethidium was 12°, since this would maintain maximal separation of the charged phosphate groups in the perturbed helix. In general, the binding of drugs to DNA has a stabilising effect on the double stranded structure, as deduced from the increased melting temperature (Lerman, 1964). More recent studies (Wang, 1974;

Fig. 1.6 Sketches representing the secondary structure of (i) DNA and (ii) DNA containing intercalated acridine molecules (after Lerman (1961))

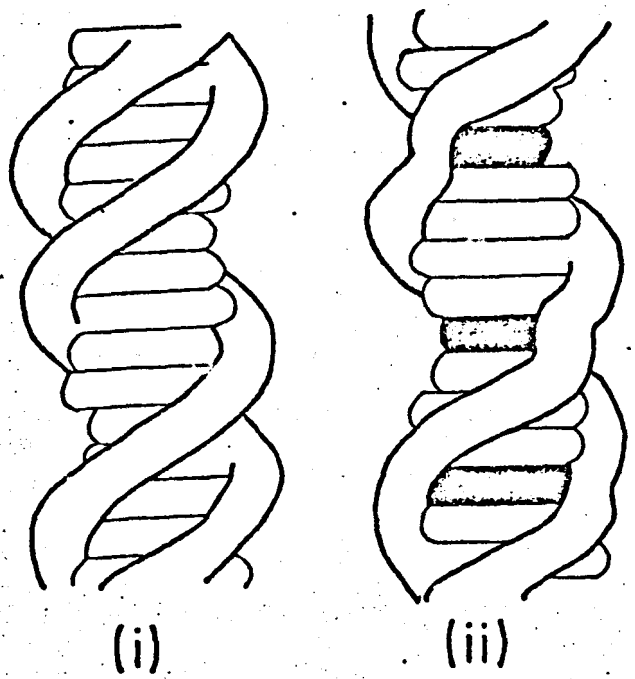

Fig. 1.7 Schematic representation of a DNA-drug complex, to show unwinding of the helix.

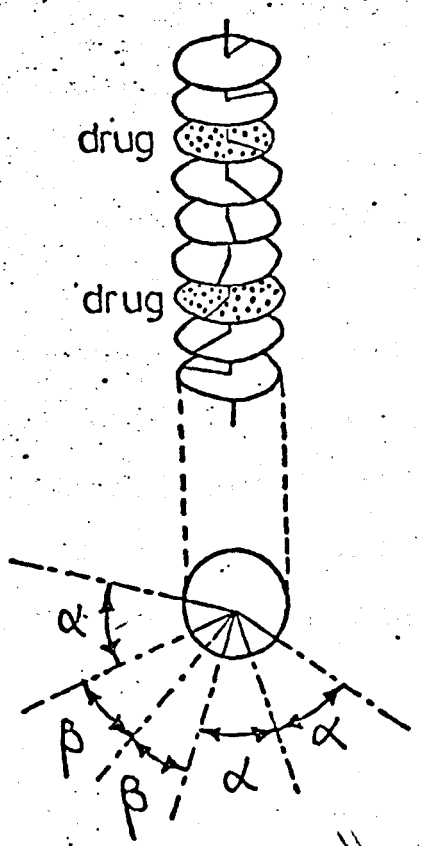

The distance between base-pairs is 3.4Å, and they are related by a rotation of α between each. The intercalated drug conserves this 3.4Å separation, but the rotation on either side of it is β ($\neq\alpha$).

The unwinding angle, $\phi = 2\beta - \alpha$

Keller, 1975; Sobell and Jain, 1972; Tsai et al.,1975) have questioned this figure for the unwinding angle and have suggested a value of around 26°. Fuller and Waring pointed out the similarity in structure between the phenanthridine and acridine rings (Fig. 1.5) and suggested that bound ethidium lies across and between successive base pairs, with the phenyl and ethyl groups lying in the large groove of the DNA. Such a position allows the formation of hydrogen bonds between the 3- and 8-amino groups of the ethidium cation (Fig. 1.8) and phosphate groups on both strands of the DNA. This was similar to the position for proflavine intercalation postulated by Lerman; the nitrogen heteroatom of proflavine did not lie in the same position as that of ethidium but the same hydrogen bonds could be made although there would be less overlap with the base-pairs.

Craig and Isenberg (1970) tested a number of polycyclic aromatic hydrocarbons and validified the criterion that drugs that were small enough to fit between the base-pairs of DNA and be well protected from the acqueous medium were more likely to bind.

Later DNA-drug diffraction patterns (Neville and Davies, 1966 - acridines; Pigram, 1968 - daunamycin) showed more clearly defined layer lines than in the earlier studies, and the lines were more closely spaced than in the control DNA pattern indicating that the helix pitch had increased. The generally poor definition of the layer lines compared to those in DNA patterns was evidence of a disordering of the helix pitch, and the increase in magnitude of the pitch was a natural consequence of the insertion of the drug and the unwinding of the helix. The increase in pitch of the DNA-drug fibres with increasing humidity is in accord with the expected hydrophobic nature of intercalation.

Since Lerman's original proposal other evidence supporting an intercalation model has accumulated. An autoradiographic study (Cairns, 1962) showed that DNA molecules increased in length after proflavine was bound to them, and this has been confirmed recently (Butour et al., 1978) by

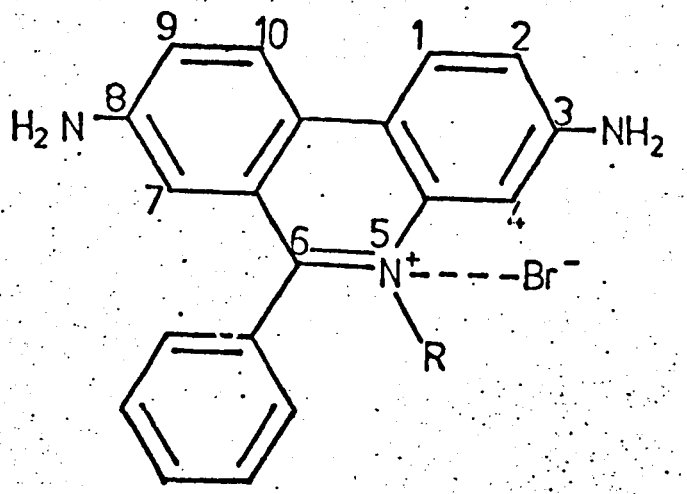

(i) Dimidium R = CH_3

(ii) Ethidium R = C_2H_5

(i) Dimidium bromide, $C_{20}H_{18}N_3^+Br^-$

(3,8-diamino-5-methyl-6-phenylphenanthridium bromide)

(ii) Ethidium bromide, $C_{21}H_{20}N_3^+Br^-$

(3,8-diamino-5-ethyl-6-phenylphenanthridium bromide)

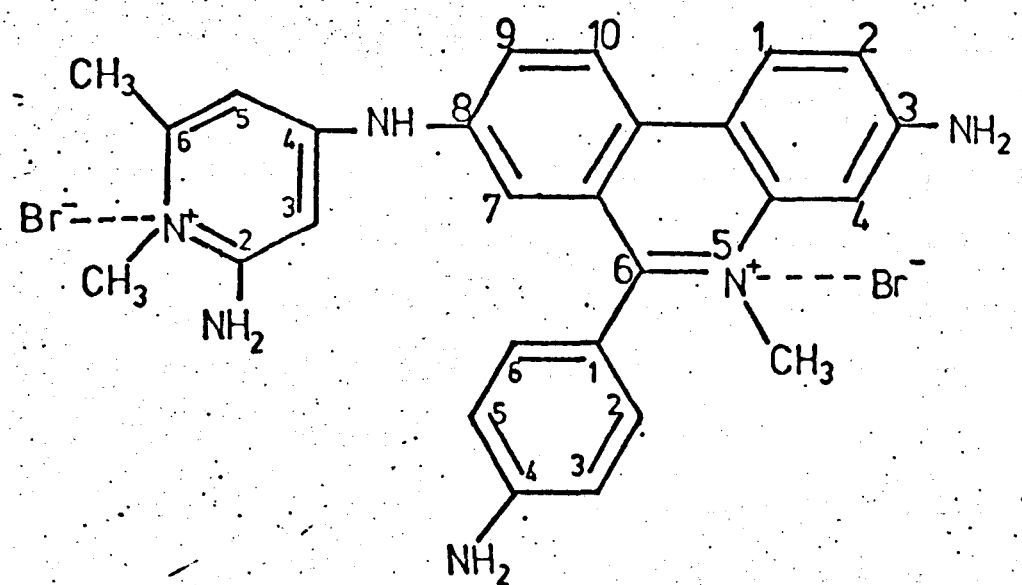

(iii) Prothidium (di)bromide, $C_{26}H_{27}N_7^{2+}Br_2^{2-}$

(3-amino-8-[3-amino-1,6-dimethylpyrinidinium-4-yl) amino]-6-(4-aminophenyl)-5-methyl-phenanthridium-dibromide

Fig. 1.8 Structural formulae of the three phenanthridine drugs used in this study

electron microscopy of PM_2 DNA molecules treated with either ethidium bromide or a covalently dimerised form of acridine. Light scattering and low angle X-ray scattering studies (Mauss et al., 1967; Luzzati et al.,1961) confirmed a reduced mass per unit length for the DNA-drug complex, and flow dichroism, circular dichroism and fluorescence polarisation studies (Lerman, 1963; Le Pecq and Paoletti, 1967; Dalgleish and Peacocke, 1971; Genest and Wahl, 1972; Leng et al., 1973; Houssier et al., 1974) indicated that the drug chromophores were bound approximately perpendicular to the DNA axis. Unwinding of the supercoils of closed circular DNA (Waring, 1970), revealed by changes in the sedimentation coefficient, is consistent with the idea of an intercalated drug unwinding the DNA molecule. Electron-spin resonance studies (Hong and Piette, 1976) strongly favour an intercalative binding mode for spin-labelled ethidium, and NMR work (Krugh and Reinhardt, 1975) has suggested a base-pair specificity for the intercalation of ethidium bromide.

There is now evidence on an increasing number of other drugs that are able to bind to DNA in this fashion. These include the antitumour antibiotics daunomycin, adriamycin and nogalamycin (Calendi et al., 1965; Ward et al., 1965; Kersten et al., 1966; Neogy et al., 1973), the schistomicidal drug, miracil D (Carchman et al., 1969), the antimalarial drug chloroquine (O'Brien et al., 1966) as well as many carcinogenic hydrocarbons (Lesko et al., 1971). Intercalation is also a likely mode of binding for actinomycin D (Müller and Crothers, 1968) and propidium iodide (Hudson et al., 1969).

Structural formulae of some of these drugs are shown in Fig. 1.5, and it will be noted that all possess a planar triple aromatic ring system except for chloroquine which has only a two-ring chromophore. The flat ring systems are important, since it is an obvious requirement of the intercalation theory that the drug molecule must possess a reasonably large flat portion (but not too large or bulky) if it is to slip in between

the flat base-pairs of the DNA helix. In fact it has been shown (Müller et al., 1973) that a proflavine derivative, 2, 7-di-t-butyl-proflavine, does not intercalate, and this had been predicted by molecular model building studies which showed that the steric hindrance involving the bulky side groups would prevent intercalation of the ring system.

There is evidence from equilibrium studies of the binding of drugs to DNA (Waring, 1965; Blake and Peacocke, 1968; Zunino et al., 1972) for the co-existence of more than one binding mode, although the original interpretation of some of these results may be open to question (see Chapter 3). Intercalation is thought to predominate at low drug/DNA ratios, but an external binding (i.e. non intercalative) mode may be important at large drug/DNA content. Relaxation kinetics experiments (Li and Crothers, 1969; Schmechel and Crothers, 1971) have suggested that some external binding is present even at low drug content. In fact, intercalation may occur via a multi-step reaction, with the external binding mode as an intermediate stage (Sobell et al., 1977). The external binding mode probably involves an electrostatic attachment of the cationic drug molecules to the negatively charged phosphate groups along the outside of the DNA helix, since this mode appears to be more sensitive to the ionic strength of the complex. External binding may also exhibit a specificity towards particular DNA types by forming specific hydrogen bonds to certain base-pairs, and externally bound planar drug molecules (such as the acridines) may stack together along the sugar-phosphate backbones.

Intercalation has been used as a model to explain how frameshift mutations are caused by aminoacridines and how some drugs may act as translation/replication inhibitors (Brenner et al., 1961; Streisinger et al., 1966). The insertion of a drug molecule into DNA could alter the reading sequence of a hypothetical genetic code such that a radically altered non-functional gene product would result, if indeed any product were made at all. It is likely that the normal copying and transcribing of DNA will

only occur if both the sequence and geometry of the bases are correct. Intercalation of a small molecule into the helix can be expected to seriously affect these processes and it may prove less easy for the strands to separate. In addition, the side chains of the drug may partially block one of the grooves in the helix and prevent enzymes from recognising appropriate regions. Drugs may cause mis-translation of the DNA (e.g. proflavine) and act as mutagens or carcinogens. Other drugs (e.g. daunomycin, adriamycin) are extensively used in the chemotherapeutic treatment of acute leukaemia and solid tumours in humans (Tan et al., 1967; Bolron et al., 1969).

The three drugs considered in this work are phenanthridines and, in common with many other suspected intercalators, they each possess a triple aromatic ring (Fig. 1.8). They are trypanocidal, and have been used extensively in the treatment both of sleeping sickness in man and nagana in cattle. Dimidium bromide was used until 1952 when, in an attempt to overcome drug resistance, increased doses were used and found to result in high fatility, delayed toxicity and photosensitisation (Burdin and Plowright, 1952). The ethyl homologue, ethidium bromide, was found to be ten times more active and much less toxic than dimidium and is still used in both East and West Africa. At the pH of the blood, ethidium forms twice as much pseudobase as dimidium, and it has been suggested (Watkins, 1952) that this may enhance its ability to penetrate cell membranes. A further successful modification was achieved in 1956 by attaching the pyrimidyl moiety of quinapyramine on to the 8-amino group of the triple ring to form prothidium (di)bromide, which was found to possess prophylactic as well as curative activity giving protection to cattle for periods up to four months (Robson, 1961). These drugs also have antiviral properties and interfere with the synthesis of nucleic acids in a variety of organisms (Kerridge, 1958; Kandaswamy and Henderson, 1962; Tomchik and Mandel, 1964).

1.3 Outline of the Present Project

This study is aimed at elucidating the mode of attachment of drugs to DNA at a molecular level. Information about the binding at this level, and in particular the comparison of closely related drugs, is essential for the development of new, more specific chemotherapeutic agents with reduced toxic side effects. Moreover, understanding of the way in which small molecules modify the structure of DNA may shed light on the interaction between DNA and more complex systems, such as enzymes and regulatory proteins.

The full chemical nomenclature and structure of the three phenanthridine drugs used in this work - dimidium bromide, ethidium bromide and prothidium (di)bromide - are shown in Fig. 1.8. Previous research on DNA-drug interactions has been carried out on complexes either in solution or in the solid state. This study has used various physical techniques to characterise the interactions in both phases, in an effort to bridge the gap between them.

Spectroscopic analysis of the binding (Chapter 4) was used to provide information on the common features and differences between the binding of the three drugs. Binding parameters, such as the association constants and the number of binding sites associated with each base-pair, were obtained for the binding to DNA's of differing base-pair content. These were used to determine any base-pair or base sequence specificity operating in the interactions.

Fibre X-ray diffraction (Chapter 5) was used to monitor the changes in helix pitch and intermolecular separation with increased drug content and changing humidity. This information was used to determine which binding modes were taking place. Measurement of the arcing of the diffraction streaks was used to indicate the probable disorientation within the DNA-drug fibres.

Absorption spectra from fibres were used (Chapter 7) to compare the binding modes in the solid state with those in solution. Linear dichroism and birefringence measurements, used in conjunction with the X-ray diffraction results, can provide information on the orientation of the drug chromophores. These measurements were recorded at different humidities so that the fraction of free drug and bound drug (whether intercalated or externally bound) could be followed for different environmental conditions.

Preliminary studies with space-filling models (Chapter 8) were undertaken to investigate the stereochemical feasibility of certain DNA-drug models in the light of the accumulated data. A model building study, using a computerised linked atom least squares refinement routine, was used to compare more precisely the different models.

CHAPTER 2

MATERIALS AND EXPERIMENTAL TECHNIQUES

2.1 The Materials

2.1.1 The Nucleic Acids

Some of the more commonly available DNA types are listed below in order of descending G-C content:-

	G-C (%)
Micrococcus lysodeikticus	72
Sarcina lutea	72
Serratia marcescens	58
Escherichia coli	50-52
Salmon testes	44
Calf thymus	42
Cytophaga johnsonii	33
Clostridium perfringens	30

In order to investigate possible base-pair specificity or sequence specificity in the binding of drugs to DNA, a number of varieties were required which would adequately cover this range of G-C content and which would be available in a fairly purified form at reasonable cost. On the basis of these criteria the varieties shown in Table 2.1 were chosen.

A theoretical paper (Felsenfeld and Hirschmann, 1965) has shown, using a model in which hypochromism arises from the interaction of base-pairs along the helix, that the absorptivity should increase quadratically with A-T content so long as the base-pair sequence is random. But because their figures and the results from several experimental papers (Schildkraut et al., 1962 - buoyant density in CsCl; Gray et al., 1978 - circular dichroism; Blake and Lefoley, 1978 - spectrophotometry of direct-derivative melting curves) do not correspond, and because the experimental values vary

TABLE 2.1

DNA Varities Chosen by the Author for Study

Species	G-C content (%)	Maximum absorptivity (M^{-1} cm^{-1})
M. lysodeikticus	72 (1,2)	6300 (3) 6400 (2) 6923 (4)
Calf Thymus	42 (5)	6600 (6,7) 6412 (4)
Cl. perfringens	30 (5)	6225 (4) 6700 (8)

References

1. Ramstein and Leng, 1975.
2. Kleinwächter et al., 1969.
3. Wakelin and Waring, 1976.
4. Müller and Crothers, 1975.
5. Chan and van Winkle, 1969.
6. Pigram, 1968.
7. Plumbridge et al., 1978.
8. Ramstein et al., 1972

so widely amongst themselves, it was decided to adopt the value 6600 M^{-1} cm^{-1} as the maximum absorptivity (at 255 - 258nm) for all three samples.

The three DNA's were purchased from the Sigma Chemical Company -

(i) M. lysodeikticus Type XI (containing approximately 1% protein, 0.2% RNA)

(ii) Calf Thymus Type I (containing less than 1% protein, and less than 3% RNA)

(iii) Cl. perfringens Type XII (containing less than 2% protein, 0.02% RNA)

The shape of their absorption spectra were similar, though there were slight differences in the wavelength at which maximum absorptivity was observed (viz. M. lysodeikticus - 255nm, Calf Thymus - 258nm, Cl. perfringens - 256nm).

Several spectrophotometric tests on the purity of a nucleic acid solution have been cited in the literature. Dalgleish et al. (1973) considered a sample adequately deproteinized if A_{260}/A_{230} was greater than 1.85. Goodwin (1977) adopted the criterion that A_{260}/A_{280} should be greater than or about 1.90. Groves et al. (1968) have shown that the absorbance of proteins around 280nm is due primarily to tryptophan and tyrosine, and that the peptide bond linkage and the other amino-acids are responsible for the absorbance around 230nm. Marmur (1961) quoted that $A_{260} : A_{230} : A_{280} = 1.0 : 0.45 : 0.515$, equivalent to $A_{260}/A_{230} = 2.12$ and $A_{260}/A_{230} = 1.94$, corresponds to an amino-acid content of 0.3 - 0.5%.

For solution spectroscopy, values of A_{260}/A_{230} greater than 2.2 and A_{260}/A_{280} greater than 1.9 were considered acceptable and samples received that satisfied both these conditions were not deproteinized further. On the other hand, all the DNA used for fibre-making was routinely purified in an effort to improve the quality of the subsequent X-ray diffraction patterns. Comparisons of the patterns taken using purified DNA have all shown a significant improvement in picture quality over earlier patterns

which were taken using unpurified DNA.

A phenol extraction stage was included in the purification stage since phenol has been reported to be effective in removing proteins from DNA samples (Massie and Zimm, 1956). Freshly-distilled analar grade phenol was used to avoid oxidation products, and the distillate was allowed to drip into a 0.1M NaCl solution.

The DNA was shredded gently and dissolved in 0.003M NaCl to give a concentration of approximately 1mg/ml. This salt concentration is sufficient to prevent denaturing of the DNA, but is low enough to allow it to dissolve easily. All samples were left for at least six days to dissolve completely. Before adding to the phenol, the salt concentration of the DNA solution was raised to 0.1M NaCl by addition of the appropriate volume of 2.0M NaCl.

The DNA solution is added to the same volume of the phenolic (lower) layer of the phenol/salt mixture and shaken gently for 20 minutes. The resulting mixture is then centrifuged at 3000 r.p.m. for 20 minutes and the upper (acqueous) layer is then carefully removed using a hooked Pasteur pipette to minimise gathering material from the lower layer. This solution is poured on to an equal volume of propanol, and allowed to stand for 15 minutes. The precipitated DNA is then wound on to a glass rod and washed in 80% ethanol (to remove excess salt), 95% ethanol (to remove water) and finally acetone (to remove the ethanol). It can then be cut from the rod and stored at $4^{\circ}C$ until ready for use.

Purification was found to increase the A_{260}/A_{230} ratio by between 0.05 and 0.15 relative to the value for unpurified DNA, but had little effect on the A_{260}/A_{280} ratio. No evidence of denaturation of the DNA due to the phenol extraction stage has been observed, contrary to the fears of Leng et al. (1973).

The DNA samples were dissolved in either 0.01M tris-HCl/0.01M NaCl pH 7.6 (low ionic strength buffer) or 0.01M tris-HCl/0.1M NaCl pH 7.6 (high ionic strength buffer). Tris is tris-hydroxymethyl

methylamine. The tris concentration was kept low so that the main ionic component of each buffer would be the sodium chloride, but it was sufficient to maintain the pH to within $\pm$ 0.1.

The pH was measured using a Pye model 79 pH meter using a combined glass and reference electrode, and calibrated using standard buffers. Checks on the pH of the DNA, the drug and the DNA-drug solutions throughout the investigation always resulted in values of 7.6 $\pm$ 0.1, close to the physiological level.

2.1.2 The Drugs

Ethidium bromide was obtained from BDH Chemicals Ltd., and dimidium bromide and prothidium di(bromide) were gifts from Dr. T.I. Watkins, The Boots Co. Ltd. In the dry state they were stored in a desiccator in the dark at 0 - 4°C.

Each was used without further purification, being dissolved in either the low or the high ionic strength buffer. Only with prothidium was difficulty in dissolving the crystals experienced. For the low ionic strength solution warming to about 35°C was sufficient to permit dissolving, whilst the high ionic strength solution had to be prepared first at low ionic concentration and then brought up to the higher value when completely dissolved. All solutions were stored at 0 - 4°C, and wrapped in metal foil to minimise photolytic degradation.

The structural formulae of the drugs are given in Chapter 1. The molecular weight of ethidium bromide was taken as 415.5, and all concentrations calculated taking its absorptivity at 480nm to be 5850 $M^{-1}cm^{-1}$ (Bresloff and Crothers, 1975). This is higher than the 5600 $M^{-1}cm^{-1}$ figure extensively quoted in earlier literature (e.g. Waring, 1965; Pigram, 1968), but it takes into account the ethanol impurity (approximately 0.46 mole/mole ethidium bromide, according to Bresloff and Crothers (1975)) associated with commercial ethidium and is in good agreement with the figure of

5900 $M^{-1}cm^{-1}$ used by Wakelin and Waring (1974).

A molecular weight of 380 and absorptivity of 6200 $M^{-1}cm^{-1}$ at 480nm were used for dimidium bromide (Wakelin and Waring, 1974). The absorptivities for ethidium and dimidium are reliable to $\pm$ 100 $M^{-1}cm^{-1}$ (M.J. Waring, private communication).

For prothidium (di)bromide a molecular weight of 597.4 was adopted, with concentrations calculated assuming a peak absorptivity (at ~465nm) of 7100 $M^{-1}cm^{-1}$. This figure was obtained by the author experimentally, and because of variations with ionic strength (Chapter 4) is considered precise to $\pm$ 200 $M^{-1}cm^{-1}$.

2.2 Preparation of Complexes and Fibre-making

The required volumes of the stock solutions were separately diluted by approximately equal volumes of the appropriate buffer, and the drug solution was then slowly added to the DNA, stirring continuously, to give a final volume of 14 - 15ml containing approximately 1.5mg DNA. Control samples of DNA without drug were also prepared. From each complex, 4ml was extracted and used for spectroscopic analysis. The remaining solution was sedimented in an MSE ultracentrifuge at 40,000 r.p.m. for 12 hours. The supernatants were carefully removed and their absorption spectra recorded; the amounts of free and bound drug in a gel can be calculated from subtracting the amounts left in the supernatant from those found prior to centrifugation.

A drop of the gel was placed between the rounded tips of two thin glass rods about 1mm apart. As the gel dried down the DNA helices tended to align along the direction joining the two tips, resulting in an oriented fibre about 100 - 150μm in diameter. Orientation is improved if the tips are gently separated at stages during the drying, but overstretching must be avoided as this will result in "necking" and possible rupture of the fibre. Well-oriented fibres of DNA and DNA-drug mixtures containing only moderate amounts of drug could be prepared at room temperature. However, the more viscous gels associated with high drug content only produced suitable fibres when prepared at low temperature (4°C) and high humidity (92% R.H.); at higher temperatures the outer surface dries down too quickly and the interior is poorly oriented.

2.3 Methods of Investigating the Binding Process

Detection of a complex between a small molecule and DNA, and quantifying the parameters of the binding process, often relies on finding some physical property of the complex that differs from the sum of the properties of the separate species. One of the most convenient tools for detecting complex formation is by monitoring the visible absorbance of the complex at a range of wavelengths for different drug / DNA ratios, but many other methods have been used as well (Chapter 1). In this investigation information on the binding process has been collected from solution spectroscopy, equilibrium dialysis, fibre X-ray diffraction and birefringence and linear dichroism measurements in the fibre state and subsequently analysed.

2.3.1 Solution Spectroscopy

2.3.1(a) Definitions

In this report the binding ratio r will be taken as the number of drugs bound per base-pair, which is the system adopted by Müller and Crothers (1975). Earlier papers (e.g. Blake and Peacocke, 1968; Waring, 1965) have taken r to be the number of drugs bound per phosphate, but the definition adopted here is considered preferable since the base-pair is the natural unit involved in intercalative binding.

In discussing the results of the X-ray diffraction and model-building work, it will prove more convenient to refer to the number of base-pairs present for each bound drug; this is just the inverse of r.

2.3.1(b) The Method

The phenanthridines, in common with other drugs that incorporate a heterocyclic structure, have characteristic visible absorption spectra, whereas DNA itself does not absorb light in the visible region. When mixed with DNA a change in the colour of the drug occurs. More precisely,

as increasing amounts of DNA are added the absorbance maximum shifts towards longer wavelengths and reduces in magnitude.

The free drug spectrum ($r = \infty$) and a DNA-drug spectrum taken at a low value of r (such that further addition of DNA produces no further change in the spectrum i.e. all the drug is bound) are considered as the two library (or reference) spectra. Spectra of complexes with intermediate values of r can be regarded as linear combinations of the two library spectra, and the concentrations of the two components may be computed using a least-squares minimisation procedure applied to the digitised absorbances (Section 4.3). From the results of this analysis, binding equilibrium data can be determined.

Different mixing schemes have been used in the past to obtain DNA-drug complexes in solution with differing binding ratios. These have included (i) adding small quantities of a concentrated drug solution sequentially to a stock solution of DNA (Waring, 1970; Angerer and Moudrianakis, 1972; Douthart et al., 1973) (ii) adding aliquots of concentrated DNA to a standard drug solution (Krugh et al., 1975; Patel and Shen, 1978; Blakeley, 1976) (iii) making separate mixtures each with a constant concentration of drug but differing concentrations of DNA (Peacocke and Skerrett, 1956; Porumb, 1976; Plumbridge and Brown, 1977) and (iv) mixing drug and DNA stock solutions to form a complex of low binding ratio r, and subsequently increasing r by adding appropriate volumes of the original drug stock solution (Waring, 1965; Dalgleish et al., 1971).

The first method suffers greatly in that the total drug concentration within the various mixtures varies by a factor similar to the range in r values required, resulting in vastly different absorbance readings. The photodetector of the Cary 118C spectrophotometer has its minimum relative error around A = 0.86, with a relative error of about 1% for absorbance values between 0.5 and 1.5 ("Optimum Spectrophotometer Parameters", Application Report AR14-2, Varian Instruments, 1970). This method would

not only result in having to record values outside the optimum range, but would involve taking spectra on different absorbance range settings with the consequent danger of considerable baseline errors.

The second method involves corrections to the absorbances to allow for the increases in volumes of the mixtures, and since it begins at large r there it some danger of precipitation. Method (iii) uses rather large quantities of both drug and DNA. The fourth method overcomes these drawbacks but, like method (i), it involves using a wide range of total drug concentration.

By using a constant concentration of drug (method (iii)), not only can readings be limited to the optimal range (A = 0.5 to 1.5) but the isosbestic behaviour (Section 4.2) can be viewed directly during the course of the experiment, if it occurs for that particular complex. A method which uses only small quantities of drug and DNA (like method (iv)) is also expedient, and a scheme whereby the complex could remain in the spectrophotometer and have its binding ratio, r, changed in situ without altering the position of the cuvette would have the advantage that exactly the same optical path was being sampled for each mixture.

A novel method incorporating all of these advantages has been devised by the author. A DNA-drug complex was mixed thoroughly and used to fill a cylindrical cuvette of 5cm pathlength and 15ml capacity. The amount of drug in the mixture was chosen such that the absorbance maximum would be at about A = 1.0, and the binding ratio r was sufficiently low to ensure that the ensuing spectrum corresponded to the case in which all the drug was bound. Experience indicated that this binding ratio was between 0.07 and 0.10 for the drugs used, although Waring (1965) has used a binding ratio of 0.21 (i.e. a phosphate/drug ratio of 9.6) for his bound spectrum for ethidium bromide.

To alter the binding ratio an autopipette (Oxford Laboratories macro-pipette, maximum capacity 5ml) was used to withdraw a quantity, x ml, of

the DNA-drug mixture from the cuvette and replace it with the same volume of a solution of the drug alone. The drug in this solution had the same concentration as that in the mixture so that the net effect was to leave the total amount of drug unaltered but to remove some of the DNA. These operations were performed with the cuvette still in position in the spectrophotometer, and to ensure adequate mixing a portion of the new mixture was repeatedly withdrawn from and returned to the cuvette by autopipette. To establish a protocol, this was done ten times and the new mixture was allowed to remain in the spectrophotometer for a further five minutes before an absorbance trace was taken. This procedure was repeated several times, with a spectral trace being obtained for each mixture, and the series was completed by removing the cuvette, cleaning and drying it, and filling it with the drug stock solution to obtain the spectrum of the completely free drug. The spectrophotometer was operated in its "auto slit" mode since this provides automatic compensation of the changing reference signal and a fixed noise level when scanning over an extended wavelength region ("Auto Slit versus Auto Gain", Application note UV-73-1, Varian Instruments, 1973).

A similar procedure was carried out in parallel with the reference cuvette. Initially it is filled with a DNA solution of the same concentration as the DNA in the original mixture, and it is progressively diluted by extracting x ml from it and replacing it with x ml of the buffer. This compensates for the effect of light scattering by the DNA in the mixture.

With this scheme the binding ratio increases in a geometric progression, giving a convenient spacing of the data in the subsequent analysis (Chapters 3, 4) to find the binding site size. The changed binding ratio is related to the previous binding ratio by -

$$\frac{\text{changed } r}{\text{previous } r} = \frac{V}{V - x} \qquad (2.1)$$

where V is the total volume of the mixture, equal to 15ml in this study.

The autopipette was set to extract/deliver a nominal 4ml and was calibrated by weighing, on an electronic balance, the amounts of water it delivered. At this setting it was found to deliver 3.89ml with a precision better than 1% (i.e. $x = 3.89 \pm 0.04$ml).

Before each spectral series the cuvettes were cleaned with distilled water and rinsed internally with acetone and rubbed carefully on the outside with a lens tissue dipped in ethanol to facilitate drying. (With this scheme the cuvettes only required cleaning twice - prior to beginning the series, and before taking the final free drug spectrum.) The multipots on the spectrophotometer were then adjusted to compensate for any cuvette mismatching.

To run a spectral series on a particular drug with a specific type of DNA and at a given ionic strength requires only a small amount of DNA (about 12mM, equivalent to about 6-7mg in its hydrated sodium salt form) and even less drug (about 3μM for a drug of maximum absorptivity around 6000 $M^{-1}cm^{-1}$).

At the end of each series, before running the free drug spectrum, the cuvette and its contents were weighed and compared with the weight that would be expected for a 15ml mixture of that binding ratio. In every case, the figures for the mixtures agreed to within 2-3%. Since each series involves about twelve extractions and deliveries of solution, each limited to a precision of 1%, there appears to have been no cumulative errors within the series.

2.3.1(c) The limitations

The spectrophotometric method can only cover a limited range of binding ratios, since at low values of r it is difficult to distinguish the mixture spectrum from the completely bound spectrum and at large r

values the free drug and/or the bound drug may be present at such high concentrations that their absorbance contribution is no longer directly proportional to their concentration (due to self-aggregation and/or instrumental stray light). The mixing scheme adopted by the author minimises the dangers at large r values by keeping the total drug concentration several times lower than the concentration at which the free drug self-aggregates (Chapter 4).

2.3.2 Equilibrium Dialysis

2.3.2(a) The Method

The equilibrium dialysis method allows investigation of the binding over a wider range of binding ratios, and the values obtained require no special theoretical assumptions regarding the binding process.

The free drug is allowed to equilibrate across a membrane of sufficiently small pore size that it is impermeable to the macromolecule. In the scheme considered here, the macromolecule (viz. DNA) is contained within dialysis tubing which had previously been boiled in a buffer solution for two hours to remove soluble plasticizers. A length of about 25cm of Visking cellophane tubing, 8mm in diameter, was used to contain 5ml of solution and was tied at both ends.

With reference to Fig. 2.1, the tubing containing the DNA and a similar sac containing 5ml of the appropriate buffer (to act as a control) were immersed in a graduated cylinder, of 50ml capacity, containing the drug solution at a concentration C. After three days in the dark, continuously agitated using a magnetic stirrer, the system was judged to have reached equilibrium i.e. the concentration of free drug inside and outside the dialysis sacs were the same.

If the total amount of drug is conserved, using the notation of Fig. 2.1, it follows that

$$CV = C_1'V + (C_2 + C_1)v + C_1 v + 2A \qquad (2.2)$$

Fig. 2.1 Schematic Representation of the equilibrium dialysis study

(i) Before dialysis

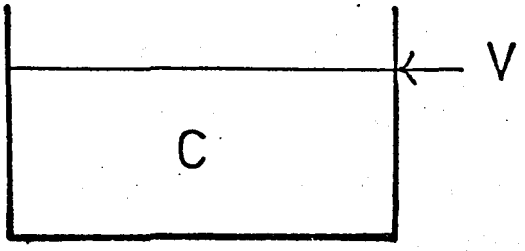

(ii) After dialysis

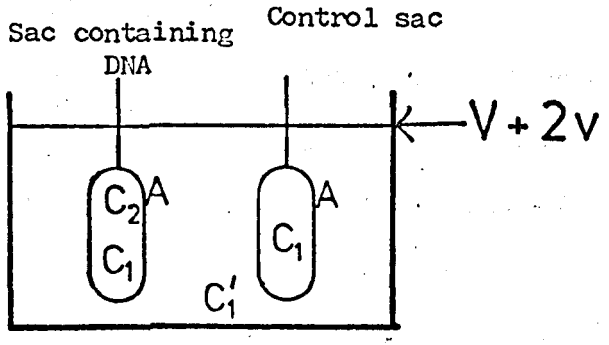

(iii) Ancillary experiment to determine A

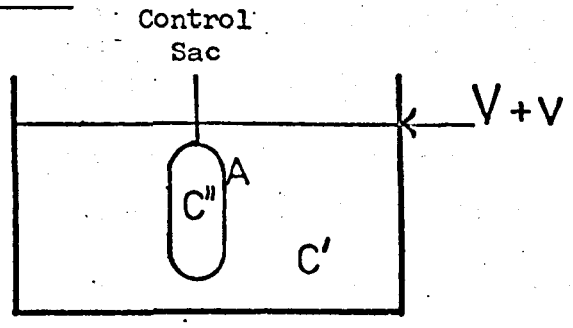

Where: C = Free drug concentration before dialysis

V = Volume of drug solution

C_1, C_1' = Free drug concentrations inside and outside the sacs after dialysis

C_2 = Concentration of drug bound to DNA

A = The amount of drug adsorbed by the membrane

v = Volume of solution within each sac

C'', C' = Free drug concentrations inside and outside the control sac of (iii)

The volumes V and v are known (50ml and 5ml respectively), and the concentration C will have been determined spectrophotometrically. After equilibrating, samples from the control sac and the graduated cylinder are removed and their visible spectra recorded to determine C_1 and C_1'. Their values were always within 5% of each other, in agreement with work performed by Armstrong et al. (1970) using acridine dyes.

The amount of drug adsorbed to the membrane, A, is found from an ancillary experiment (Fig. 2.1 (iii)) using the relation

$$CV = C'V + C''v + A \qquad (2.3)$$

A value for C_2, the bound drug concentration, can then be found from equation (2.2). Knowing the DNA concentration, and now the quantities C_1 and C_2, a data point on the binding curve can be obtained (Chapter 3).

2.3.2(b) The Limitations

The disadvantages of the method include the long time required to achieve equilibrium; the complicating nature of the Donnan effect at low ionic strengths (Standke, 1975); the difficulty in determining A precisely; the fact that v increases during the course of the experiment due to osmotic uptake of water; and the large quantities of materials required.

The maximum accuracy is obtained when V is as small, and both v and the DNA concentration are as large as possible. Errors in C_2 are proportionately greater when C_2 is small (Peacocke and Skerrett, 1956).

Values of r/C_1 and C_1 determined by this method have a precision of about $\pm$ 10% compared with about $\pm$ 3% for the spectrophotometrically determined data. However, the method is useful for providing values in a range inaccessible to a spectroscopic study ($r \lesssim 0.1$), and in providing a check on the spectral data in the region where both can be used.

2.3.3 Fibre X-ray Diffraction

2.3.3.1 The Generators and Cameras

X-ray diffraction photographs from DNA-drug fibres were taken using

nickel filtered copper K_α radiation (λ = 1.5418 Å) from either a Hilger and Watts microfocus generator or a Marconi-Elliott GX6 rotating anode generator. Sets were operated at 35kV, with tube currents of 3mA and 60mA respectively. Exposure times varied with the thickness of the fibre (and, to a lesser extent, with its drug content) but were typically 5-7 days using the Hilger and Watts generator and 6-8 hours using the rotating anode generator.

Pinhole cameras with a specimen-to-film distance of about 3cm were used with the microfocus generators. A focussing camera with toroidal optics and a specimen-to-film distance of 3.5cm was used with the rotating anode generator. The pinhole cameras sample only a small region of a fibre, whereas the toroidal arrangement with a beam of annular cross-section averages over a larger volume of a fibre.

In order to minimise scattering of the X-rays by air, the cameras were continuously flushed at a moderate rate with helium gas. This produces relatively little scattering because of the small number of electrons in the helium atom compared with the numbers in nitrogen and oxygen molecules. In order to control the environment of the fibre, the helium was humidified prior to flushing by passing it through water and then through a saturated salt solution (Section 2.3.4.2). A pot of the appropriate saturated salt solution was also placed inside the camera. At least one hour was allowed for the fibre to equilibrate to the desired humidity before each exposure, and for photographs taken at 98% R.H. a minimum of two hours was allowed. Some difficulty was experienced at high humidities ($\geq$ 92% R.H.) with films exposed in the pinhole cameras. Due to the long exposure times the backing paper tended to adhere to the X-ray film. Soaking of the film in water prior to developing alleviated this problem but did not overcome it completely.

2.3.3.2 Measurement of Diffraction Patterns

The diffraction photographs were printed on to Kodak KPP positive paper, and the positions of reflections on this were digitised using a D-Mac pencil follower. Using a computer program based on one developed by Dr. W.J. Pigram, the co-ordinates were then converted into reciprocal space co-ordinates, from which the pitch, residue repeat distance and the intermolecular separation of the helices were obtained.

In order to obtain an accurate value of the specimen-to-film distance the fibres were sprayed with aragonite powder which produces diffraction rings corresponding to spacings of 3.396Å and 3.273Å. Calcite impurity in the powder also produces a ring corresponding to 3.029Å. Digitised co-ordinates from one of these rings are used to scale the patterns and locate their centres.

Co-ordinates of reflections can be measured much more quickly with this method than with the 2-dimensional travelling microscope previously employed by this research group. The agreement between the reciprocal co-ordinates originating from the four quadrants of a pattern is at least as good with this method, indicating that there is no significant loss of accuracy incurred through photographic distortion for example.

A Joyce-Loebl recording microdensitometer was used to scan some reflections tangentially in order to find the degree of arcing and hence an estimate of the disorientation within a fibre.

2.3.4 Birefringence and Linear Dichroism

2.3.4.1 The Techniques

Birefringence measurements on DNA and DNA-drug fibres provide information on the orientation of the base-pairs and/or the drug chromophores relative to the helix axes, and on the disorientation of the helices within the fibre. Dichroic ratio measurements of DNA-drug fibres can indicate

the fraction of drug chromophores oriented parallel to the base pairs if their orientation and the general disorientation within the fibre is known (from X-ray diffraction and birefringence data).

As with solution spectroscopy, neither of these techniques can show that intercalation occurs though the results may be interpreted along these lines especially in conjunction with results from the X-ray diffraction studies.

2.3.4.2 Birefringence Measurements

Measurements were taken in white light (viz. the internal illumination of the Zeiss microscope described in Chapter 7), using a calibrated Ehringhaus rotary compensator. The fibres were placed at an angle of 45° to the crossed polariser and analyser, and the compensator positioned so that its slow axis was aligned with the fast axis of the fibre (Chapter 6).

Interference colours were difficult to distinguish through the colour of a DNA-drug fibre, and in order to ease this problem these readings were taken with the microscope illuminator at maximum intensity and the condenser aperture (which controls the contrast) fully open. An infra-red filter was placed below the condenser to protect the specimen from heating.

The fibre and its glass rod support were enclosed in a 3mm thick humidity cell which fitted on the specimen stage of the polarising microscope (Section 7.2). The cell was flushed at a moderate rate with air which had been humidified by passing through water and then through a saturated salt solution. The relative humidity was monitored by paper hygrometers placed before and after the humidity cell. The experimental readings (at 20 - 22°C) agreed well with each other, but were noticeably different to the standard values quoted by O'Brien (1948).

These findings are similar to those reported by Porumb (1976), and are consistent in giving increasing R.H. in the same order as O'Brien (1948).

	Nominal R.H. % (O'Brien)	Average R.H. % obtained
Dry air	-	52
Sodium bromide	57	75
Sodium chlorate	75	84
Potassium chloride	86	90
Sodium tartrate	92	92
Potassium chlorate	98	95

Each fibre was measured at a series of increasing humidites, with an equilibration time of at least one hour at each humidity. The fibre length and diameter were also recorded at the time of each measurement.

2.3.4.3 Visible Absorption Spectra of Fibres and Linear Dichroism Measurements

Visible absorption spectra of DNA-drug fibres were recorded for polarised light in the wavelength range 400 to 650nm using a micro-spectrophotometer system based on a Zeiss Universal microscope and described in Chapter 7. The fibre was placed on the rotating stage of the microscope between crossed analyser and polariser and oriented for complete extinction. The analyser was then removed, and absorption spectra taken for polariser orientations perpendicular and parallel to the fibre axis under various relative humidity conditions.

The spectra are similar to those obtained from the same complexes in solution, and at the low r values used the positions of the absorbance maxima indicate that most of the drug is in the bound state.

The dichroic ratio, D, is defined as the ratio of the absorbance recorded with light polarised perpendicular to the fibre axis, $A_{\perp}$, to the absorbance recorded with light polarised parallel to the fibre axis, $A_{\parallel}$.

$$D = A_{\perp} / A_{\parallel} \qquad (2.4)$$

Due to the large absorbance of the drug component, only the spectra for

fibres of small binding ratios ($r \lesssim 0.1$ for ethidium-DNA and dimidium-DNA) could be measured directly. So long as there is only one mode of binding and the fraction of drug bound is known, this condition need not be too restricting. The magnitude of the dichroic ratio does not depend necessarily on the amount of drug in the fibre, only on the orientation of the drug chromophores (both free and bound) relative to the fibre axis.

By using the values of the dichroic ratio at different humidities in conjunction with the X-ray diffraction data, information on the binding mode(s) and the fraction of drug binding intercalatively in the fibre state was determined (Chapter 7).

2.3.5 Model Building and Computer Graphics

The quantity and quality of data from X-ray diffraction patterns of fibres are often limited due to the lack of crystallinity within the fibre. This often results in patterns which consist largely of diffuse diffraction streaks rather than distinct Bragg reflections. With increasing drug content the fibres may become so non-crystalline (i.e. the conformation of the helices and their packing becomes so irregular) that even the layer lines overlap and the resolution deteriorates even further.

Fibre data is so sparse that the structure cannot be solved conventionally by the inversion of the observed Fourier transform. Instead, standard stereochemical parameters (such as covalent bond lengths and angles) are adopted on the basis of the known chemical structure. These are used to construct a model that conforms to the gross features indicated by the diffraction data - overall diameter, helix pitch, rise per residue, etc.. The Fourier transform of this model can be computed and compared with the observed diffraction data, and the model can be adjusted until agreement is reached. Initial models are usually constructed manually but in later stages computer model building often takes place, in which case the

conformational energy can be more readily minimised at the same time.

In this work the structure of the undistorted DNA was known and the drug binding was presumed to cause perturbations to this structure. Since there is no adequate Fourier transform theory for the random DNA-drug binding situation (Goodwin, 1977) all that could be attempted was to build stereochemically satisfactory models that satisfied the gross (geometric) features of the diffraction data from the DNA-drug fibres.

Preliminary studies with CPK space-filling models (Koltun, 1965) were made to investigate the stereochemical feasibility of certain models of drug binding. A model of the B-DNA double helix had been constructed with the central rod supporting the bases divided between two base-pairs (Pigram, 1968; N.J. Rhodes and W.J. Pigram, to be published). The two sections of the DNA model could be separated and rotated to study intercalation models with various degrees of unwinding, as well as external binding schemes. More accurate skeletal models can then be built from which sets of torsion (dihedral) angles can be measured. (In practice some intercalation models had been constructed previously (Goodwin, 1977) and it was only necessary to adapt these results for the particular drugs used in this study.)

These torsion angles were then refined to give a more favourable conformation using a program written by Pigram (1968), which had been rewritten by Goodwin (1977) and has recently been modified by Mr. R.J. Greenall of this Department. The program was run on the CDC 7600 Computer at the University of Manchester Regional Computer Centre via a link from the Keele Computer Centre. Once refined co-ordinates for a model were obtained they were input to a data file at Keele, and then used in a graphics program written by the author to display the structure on an Imlac refresh display interfaced to the Keele GEC 4082 computer. Facilities to scale and rotate the drawing, to apply 3-dimensional

"windowing" to the data (i.e. isolating and displaying only specially desired regions of the model), and to produce perspective views from user-nominated positions (using a light-sensitive pen) were included. As written the program can be used to produce a drawing of the models on the graph-plotter. However, the GINO-F graphics routines referred to in the program had not yet been implemented on the graph-plotter at Keele at the time of writing and it was necessary to photograph the drawings off the Imlac screen for this thesis.

CHAPTER 3

SPECTROSCOPIC ANALYSIS OF DNA-DRUG BINDING DATA: THEORY

The visible absorption spectra of drugs alter when they are bound to DNA. In particular, the bound drug spectrum is shifted to longer wavelengths and its maximum absorptivity is reduced in magnitude. There may even be more than one type of binding, and the bound species may or may not be spectroscopically distinct. The spectra taken at a series of binding ratios, r, can be analysed in most instances as a linear combination of two library spectra corresponding to the cases of a completely free drug and a drug completely bound to the DNA. The analysis gives the concentrations of free and bound drug in each of the mixtures comprising the series, and is described fully in Section 4.3. This data can then be interpreted using a particular binding model to yield the binding parameters of the DNA-drug interaction, such as the association constant and the number of binding sites associated with each base-pair.

3.1 Simple Single-Species Binding

If there is only one bound species the reaction may be described by

$$\underset{\text{(free sites)}}{\text{DNA}} + \underset{\text{(free drug)}}{\text{DRUG}} \rightleftharpoons \underset{\text{(bound drug)}}{\text{COMPLEX}}$$

Assuming that the binding sites are independent, the Law of Mass Action gives

$$k_a = \frac{[\text{bound drug}]}{[\text{free sites}][\text{free drug}]}$$

where k_a is the association constant (an equilibrium constant, not a rate constant) and the square brackets denote "concentration of".

Defining the following quantities:

c_1 = free drug concentration

c_2 = bound drug concentration

$c = c_1 + c_2$ = total drug concentration

n = number of binding sites per base-pair

$[BP]$ = total concentration of DNA base-pairs,

then

$$k_a = \frac{c_2}{(n[BP] - c_2)c_1}$$

The bound drug concentration, c_2, can be replaced by $r[BP]$, where r is the binding ratio defined in Section 2.3.1(a), giving

$$k_a = \frac{r}{(n - r)c_1}$$

Rearranging,

$$\frac{r}{c_1} = k_a(n - r) \qquad (3.1)$$

For the evaluation of the parameters n and k_a, several linear transformations of this equation have been used (Klotz and Hunston, 1971; Scatchard, 1949) and three of these are shown in Fig. 3.1. With transformation (i), $\frac{1}{r}$ vs. $\frac{1}{c_1}$, the value of $\frac{1}{n}$ corresponds to the value of $\frac{1}{r}$ when $\frac{1}{c_1} = 0$. The extrapolation required is from the largest experimental value of c_1 to $c_1 = \infty$, which is a much larger extrapolation than is apparent from the graphical plot. Transformation (ii), $\frac{c_1}{r}$ vs c_1, has been used rarely and transformation (iii), $\frac{r}{c_1}$ vs. r, leads to the so-called Scatchard plot which has enjoyed widespread usage.

The association constant, k_a, is related to the standard free energy of the binding by the expression

$$k_a = e^{\frac{-\Delta G}{RT}}$$

where ΔG is the change in the standard free energy, and is a negative quantity for binding

R is the gas constant

and T is the temperature (in K).

An energetically strong reaction will therefore result in k_a being large, leading to a steep negative gradient on the Scatchard plot, and a

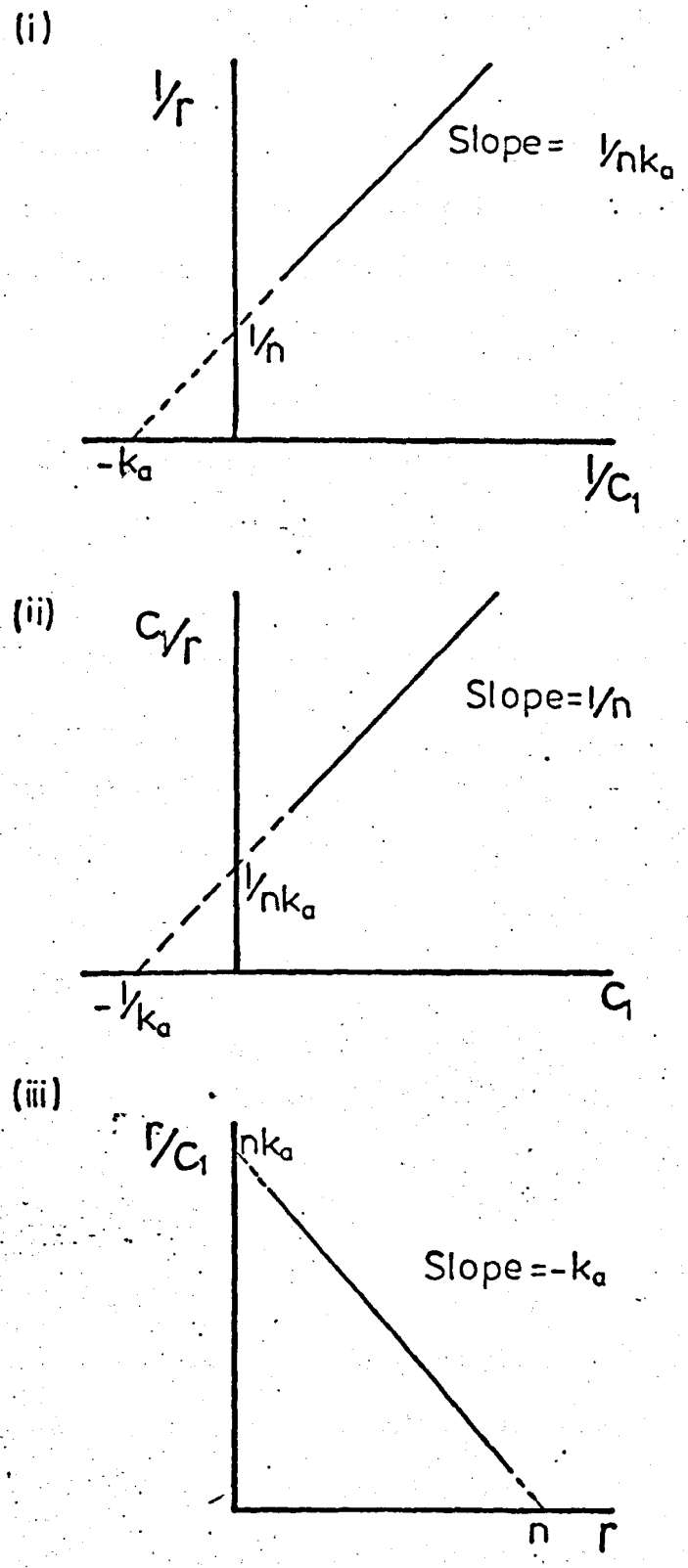

Fig. 3.1 Graphical representation of three possible linear transformations of the binding equation for a single binding model (see Equation 3.1)

weaker reaction will result in a shallow gradient. A typical case of strong binding, such as the binding of acridines at low binding ratios to DNA, results in a value for ΔG between -6 and -9 kcal/mole (Blake and Peacocke, 1968).

A binding curve (i.e. a plot of r against c_1) is another useful plot, especially since it presumes no special relationship between r and c_1. For the case of simple single-species binding its form is shown in Fig. 3.2. The initial slope is large for a strong binding reaction and the value of r asymptotically approaches n, the maximum number of binding sites available per base-pair, at large values of c_1. A similar shape is obtained by plotting r against c/[BP], and this has been used as an alternative by Porumb (1976).

In an experimental situation the Scatchard plot is often curved when r is moderately large. The value of n obtained by extrapolation of the linear region is frequently less than unity even for homopolymers. This cannot be explained in terms of base-pair or base sequence specifity of the binding. With DNA containing a single type of base-pair only, at each base-pair either binding (of an integral number of drugs) or no binding should occur. For the homopolymers which bind the drug the value obtained from the Scatchard plot should be integral. Non-integral values of n imply that this simple theory is inadequate in describing the prevailing physical situation.

Various, more complex theories have been advanced to account for the curvature of experimental Scatchard plots. There may be more than one type of binding operating, resulting in more than one bound species. Interactions between drugs could be envisaged which could either favour the binding of additional drugs or discourage further binding. Binding at a particular base-pair might preclude binding at a neighbouring site, perhaps due to the steric hindrance of a side group of the initially bound drug molecule. Binding specificity could operate with a particular drug,

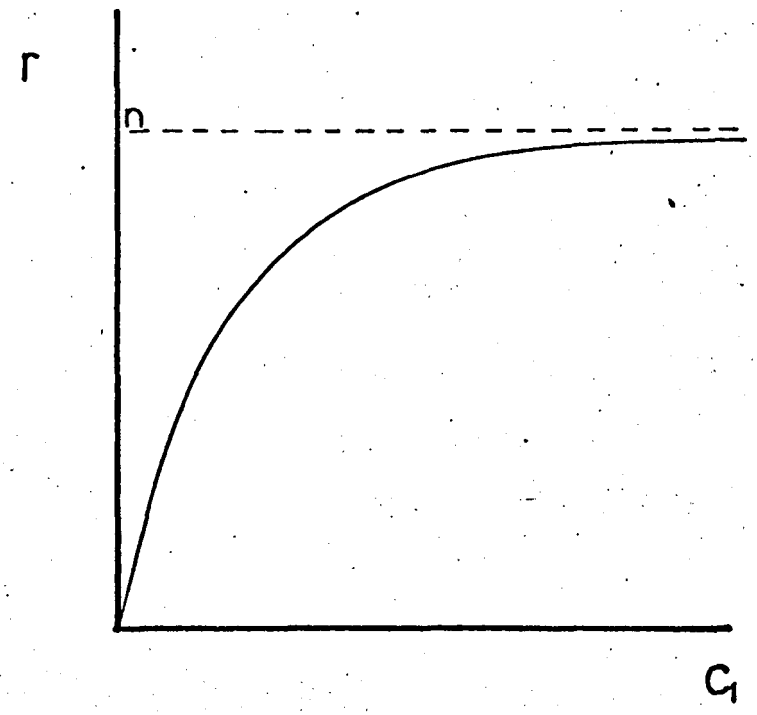

Fig. 3.2 A schematic binding curve for single-site binding. r (the no. of drugs bound per base-pair) vs. c_1 (the free drug concentration); n is the maximum number of binding sites per base-pair

whereby the drug preferentially binds to a particular base-pair or to a particular sequence of base-pairs. These possibilities are discussed in the following sections.

3.2 More Than One Independent Bound Species

Equation (3.1) applies for only one species of bound drug and can be re-arranged as

$$r = \frac{nk_a c_1}{1+k_a c_1}$$

If the drug can bind by m different binding modes at each base-pair and the number of binding sites per base-pair for mode i is given by n_i with a corresponding association constant k_i, then the binding ratio is given by

$$r = \sum_{i=1}^{m} \frac{n_i k_i c_1}{1 + k_i c_1} \qquad (3.2)$$

The total number of sites per base-pair is then given by

$$n = \sum_{i=1}^{m} n_i$$

As m increases, the number of binding parameters increases as well. Given that the experimental data is not perfect it becomes increasingly difficult to obtain precise solutions for these parameters. Considering the case where m = 2, a Scatchard plot would result in a shape similar to that shown in Fig. 3.3. This can be treated as being comprised of two approximately linear regions separated by a curved portion. The data in these two linear regions can be analysed to yield two gradients and four intercepts, all of which are generally complex functions of n_i and k_i. The only parameter directly obtainable is $n(= n_1 + n_2)$, the total number of binding sites per base-pair, although experimentally this is often difficult to determine accurately. Data at large r is difficult to obtain because of aggregation or precipitation of the drug, and in this region the plot tends to approach the axis asymptotically.

It should be noted that the apparent intercepts and gradients associated with the two linear regions are not what one might expect from an intuitive generalisation of the single binding site case. In fact,

Fig. 3.3 Schematic curve of $\frac{r}{c_1}$ vs. r with intercepts and limiting slopes, where 2 independent binding modes are present

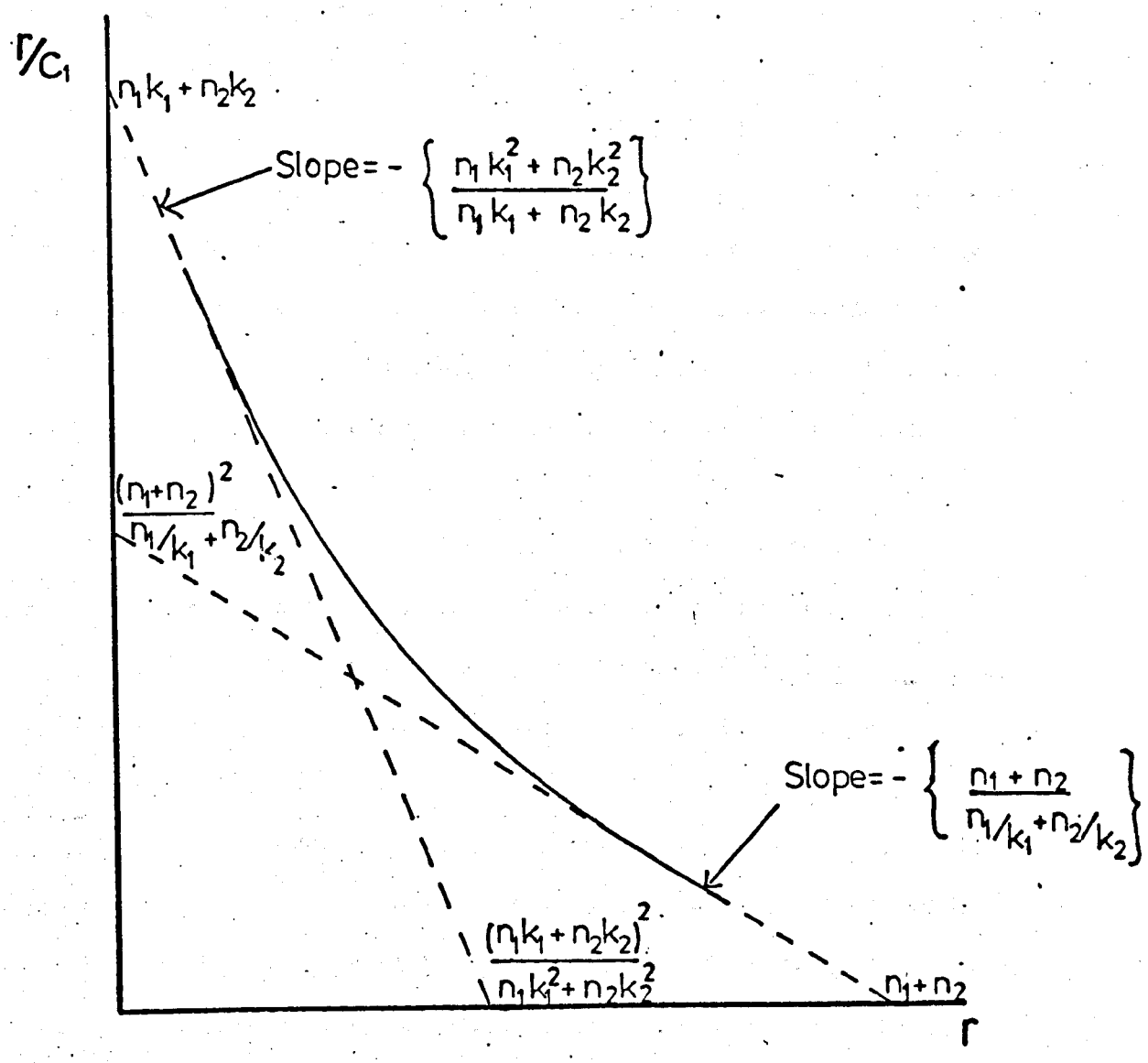

Where: n_1, k_1 are the maximum number of binding sites and the association constant for binding by Method I

n_2, k_2 are the parameters similarly defined, for binding by Method II

r, c are the total number of bound drugs per base-pair and the total free drug concentration

the two regions are only separable as such when the binding parameters involved, k_1 and k_2, are appreciably different. Consider the case where $n_1 = n_2 = 1$. If $\frac{k_1}{k_2} = 10$ then an 8% error would result if the slope of the stronger binding region were taken as $-k_1$, and there would be an error of 9% in taking the slope of the weaker binding region as $-k_2$. If $\frac{k_1}{k_2} = 100$, the slope of the strong binding region could be taken as $-k_1$ and result in only 1% error, but if the slope of the weak binding region were taken as $-k_2$ a 98% error would result. This latter case would hardly arise in practice since if k_2 were so small, the analysis would have been carried out presuming only single-species binding. The situation is more complicated if n_1 and n_2 are not known explicitly, which is usually the case.

Spectroscopic data obtained from proflavine binding to DNA has been analysed according to a model assuming two independent bound species (Peacocke and Skerrett, 1956). These authors took the gradients of the two linear portions as being equal to $-k_1$ and $-k_2$, and obtained values corresponding to a ΔG of between -6 and -9 kcal/mole for the strong binding mode, and between -2 and -3 kcal/mole for the weak binding mode. The stronger binding was later associated (Blake and Peacocke, 1968) with intercalation in conjunction with results obtained from X-ray diffraction studies. The weaker binding was considered to be an external binding scheme with a strong electrostatic character, since it was found to be more dependent on the ionic concentration of the complex.

In a particular analysis if the intercept, Σn_i, is less than m, and the individual values n_i do not seem to correlate with any structural features of possible DNA-drug models, then an alternative binding model may have to be considered. The binding curve, r vs. c, is often helpful in deciding whether or not a model with more than one bound species is appropriate. For the case of two bound species, in which k_1 and k_2 are well separated, the binding curve will exhibit the characteristic shape illustrated in Fig. 3.4.

Fig. 3.4 Binding curve, where 2 independent binding modes are present

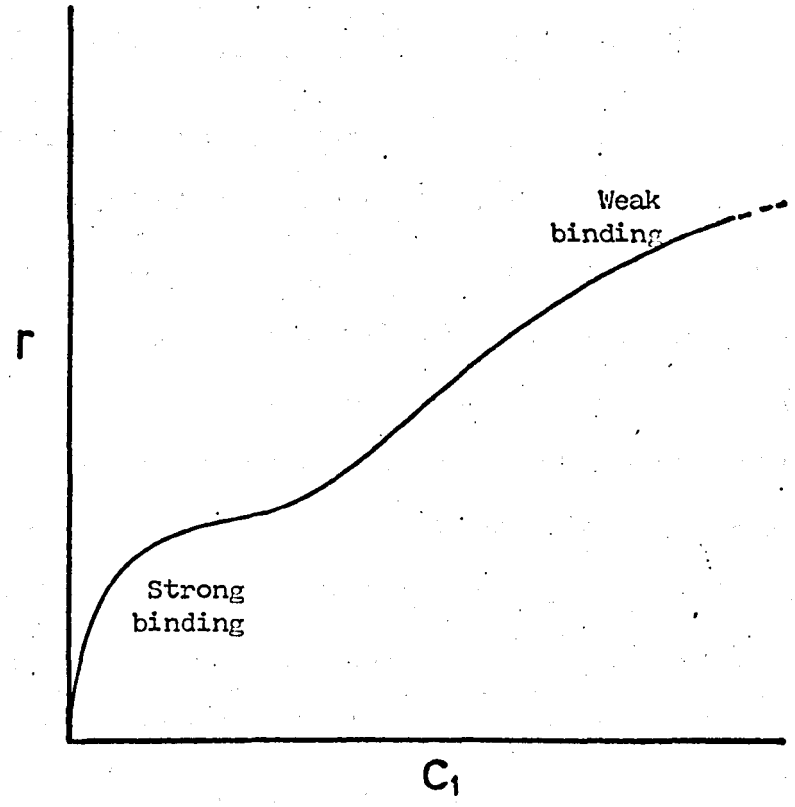

Fig. 3.5 Theoretical plots of $\frac{\theta}{k_a c_1}$ vs. θ for several values of $e^{\frac{w}{kT}}$ (after Steiner and Beer, 1961)

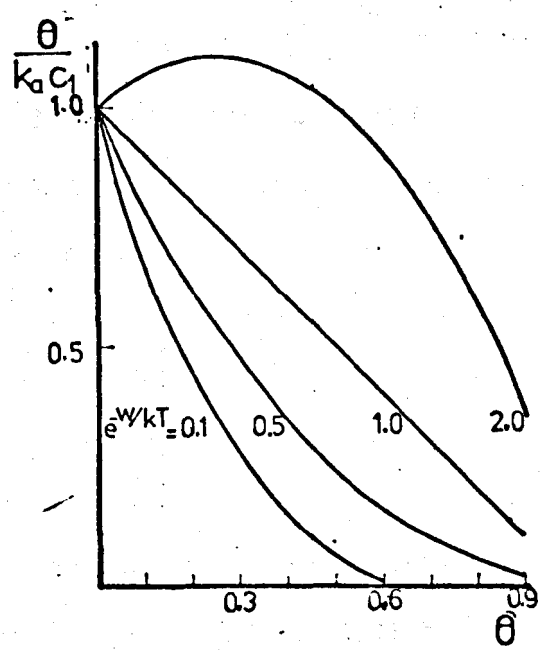

3.3 Co-operativity and Anti-Co-operativity

Electrostatic interactions between bound cationic drug molecules may have the effect of discouraging further binding at nearby sites (anti-co-operativity). However, in some cases it seems that attractive Van der Vaal's forces may overshadow electrostatic effects and favour the attachment of further drug molecules at adjacent sites (co-operativity).

For the very simple case in which interactions of bound drugs involving only nearest neighbours are considered, and neither the co-operativity nor the binding constant is affected by any change in the DNA secondary structure caused by the binding of the drugs, the following relationship has been proposed (after Fowler and Guggenheim, 1952),

$$\lambda x = \left(\frac{\beta - 1 + 2\theta}{\beta + 1 - 2\theta}\right) e^{\frac{W}{kT}} \qquad (3.3)$$

where λ = the absolute activity of the drug

x = the partition function for a molecule of bound drug

θ = the fraction of occupied sites (i.e. $\frac{r}{n}$)

W = the free energy of interaction of a nearest neighbour pair of bound drug molecules

k = Boltzmann's constant

and $\beta = \{1 - 4\theta(1 - \theta)(1 - e^{-\frac{W}{kT}})\}^{\frac{1}{2}}$

For dilute solutions the left hand side of Equation (3.3) can be replaced by $k_a c_1$ to give

$$k_a c_1 = \left(\frac{\beta - 1 + 2\theta}{\beta + 1 - 2\theta}\right) e^{\frac{W}{kT}} \qquad (3.4)$$

If nearest neighbour interactions are negligible ($W \approx 0$) this reduces simply to Equation (3.1).

If the forces of interaction are purely electrostatic in origin, further simplifications to Equation (3.4) lead to a binding equation of the form

$$\frac{r}{c_1} = k'k_a(n - r) \qquad (3.5)$$

k' is an interaction coefficient which is related to the ionic charges and the dielectric constant of the medium, but it can be more conveniently treated as an adjustable empirical parameter. For instance, if

$$k' = e^{-\frac{\Delta G^o(r)}{RT}}$$

then $\Delta G^o(r)$ can be taken as an electrostatic free energy term which depends on the binding ratio, r (Ramstein and Leng, 1975).

In cases where non-electrostatic interactions may be important, the more exact approach of Equation (3.3) is preferable. A theoretical plot of $\frac{\theta}{k_a c_1}$ against θ (equivalent to a Scatchard plot with both k_a and n normalised to unity) for several values of $e^{\frac{-W}{kT}}$, as computed from Equation (3.3), is shown in Fig. 3.5.

When W is non-zero, pronounced curvature is obtained. For positive values of W (i.e. anti-co-operativity, due to a repulsive interaction) the plots are curved downwards below the simple linear case, and for negative values of W (i.e. co-operativity, resulting from attractive forces) the curvature is opposite and the plot lies above the classical Scatchard line. It will be noticed that the anti-co-operative case could be difficult to distinguish from the curvature arising from the two independent binding species model. Co-operative binding is easier to recognise because of the characteristic direction of the curvature of the Scatchard plot, and the sigmoidal nature of the binding curves as shown in Fig. 3.6.

The acridines, being simple planar molecules, exhibit a strong tendency to aggregate by stacking in concentrated solutions and the aggregate spectrum is blue-shifted relative to that of the free monomer. A similar co-operative effect has been found amongst acridine molecules, thought to be externally bound to DNA, at r values close to unity (Peacocke and Skerrett, 1956; Bradley and Felsenfeld, 1959). This stacking behaviour

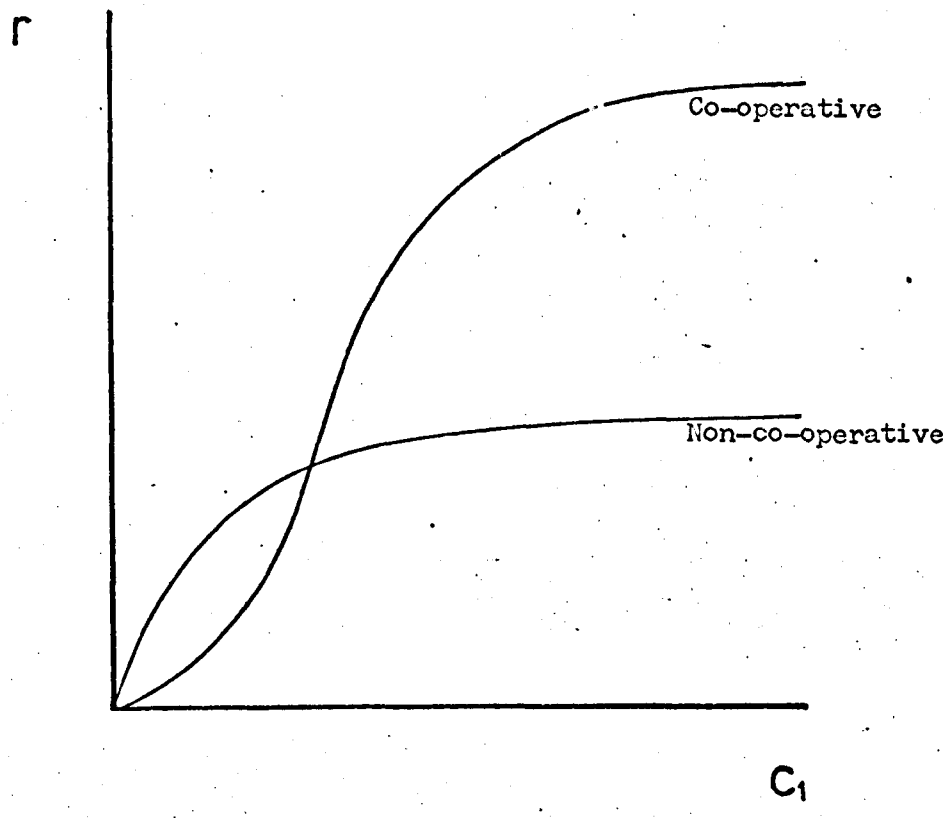

Fig. 3.6 Schematic binding curves to illustrate the difference in shape between data for non-co-operative and co-operative binding

along the DNA is not observed with ethidium bromide because the phenyl side group prevents close contact, but anti-co-operativity could operate either because of this steric restriction or because of changes in the DNA secondary structure due to local distortion at the strong binding sites (now believed to be intercalative).

3.4 The Excluded Site Model

3.4.1 The Rationale

It is possible to conceive of a situation where a bound drug occupies more than one binding site. The drug does not need to physically cover more than one site: all that is required is that binding at a particular site precludes binding at neighbouring sites. This could arise from

(i) Steric hindrance. For example, the phenyl substituent on ethidium and dimidium, and the phenyl group and the pyrimidine moiety on prothidium, could prevent the approach of another potential binding drug.

(ii) An anti-co-operative effect, e.g. due to the local electrostatic shielding of the lattice phosphate by a bound drug. It will be seen later in this section that this anti-co-operative character which we already have considered separately in Section 3.3 can be conveniently included in the excluded site model. Indeed it is difficult to separate it out as a term independent from the steric hindrance and secondary distortion effects.

(iii) Distortion of the DNA secondary structure. Binding of a drug could cause stereo-modification of the DNA at or near a binding site. If its effect spreads to adjacent sites then it may not prove feasible to implement the same modification at the neighbouring sites. According to the intercalative binding model of Sobell et al. (1977), DNA kinks or bends prior to accepting an intercalative drug. This is made possible by altering the normal C2' endo sugar ring puckering in B DNA to a mixed puckering pattern of the type C2' endo (5'-3') C3' endo and partially unstacking the bases. This mixed pucker system necessarily limits intercalation to every other base-pair (i.e. nearest neighbour exclusion).

3.4.2 The Binding Analysis

In the treatment of the excluded site model by McGhee and von Hippel (1974) the drug covers n base-pairs* on a DNA molecule N base-pairs in length (Fig. 3.7).

At any degree of binding the number of free binding sites depends not only on the number of drug molecules already bound, but also on their distribution along the DNA lattice. This is a major departure from the classical Scatchard analysis of Section 3.1. Fig. 3.8 shows some of the immediate differences. At complete saturation, $\frac{N}{n}$ drug molecules are bound. The classical analysis presumes that at any degree of saturation, the numbers of bound and free sites should add up to this number. Fig. 3.8(i) shows that this is not the case. For this particular example, although the lattice is not completely saturated, there are no acceptable vacant binding sites because the bound drugs had not been constrained to bind n base-pairs apart. Fig. 3.8(ii) shows that the number of binding sites on a naked lattice is $(N - n + 1)$. A consequence at low binding ratios (Fig. 3.8(iii)) is that the classical analysis would underestimate the number of free sites (in this instance, as four instead of seven) and thus overestimate k_a (see Table 3.1).

By incorporating these features and using simple conditional probabilities, McGhee and von Hipple were able to begin with the Law of Mass Action and develop it to obtain an equation analagous to Equation (3.1),

$$\frac{r}{c_1} = k(1 - nr)\left(\frac{1 - nr}{1 - (n-1)r}\right)^{n-1} \qquad (3.6)$$

where n, c_1 and r have been previously defined, and k is the association constant of an isolated site.

When n = 1 the last factor in this expression becomes equal to unity,

---

* Note that this differs from the n defined in Section 4.1 and used up until now. The current n is the number of base-pairs occluded per bound drug molecule, whereas the previous n was the number of binding sites per base-pair. They are related by their inverses.

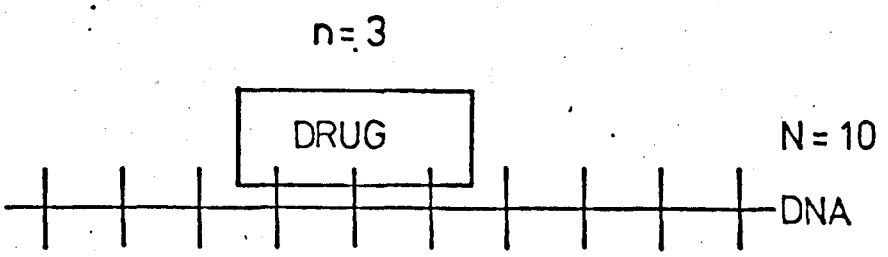

Fig. 3.7 An example to illustrate the terms n (the number of base-pairs covered by a drug molecule) and N (the number of base-pairs in the DNA molecule) for the excluded site model

Fig. 3.8 Diagrams to illustrate some of the special features, described in the text, of the excluded site model of McGhee and von Hippel (1974).

For these examples, n = 2 and N = 10

(i)

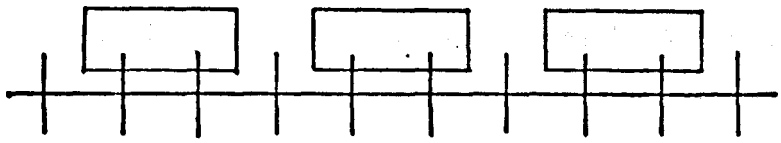

No. of bound sites = 3

No. of free sites = 0

(ii)

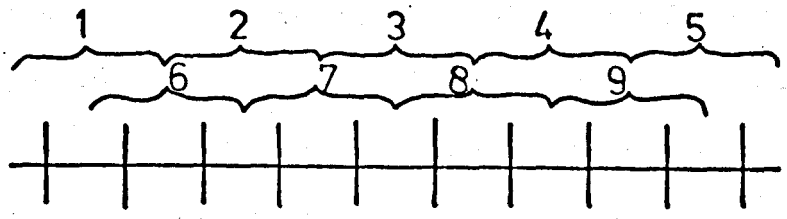

No. of binding sites on a naked lattice = N-n+1

= 9, in this instance

(iii)

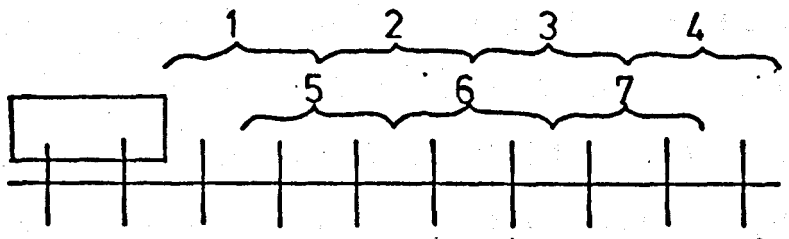

In this example of low binding density, the number of free sites is 7 .

and the equation reduces to

$$\frac{r}{c} = k(1 - r)$$

This is identical to the classical equation (3.1), except for the "one" inside the brackets. Its appearance, rather than Scatchard's n, results from the assumption in this treatment that every base-pair is a potential binding site for a single drug. If the bound drug molecule occupies more than one base-pair on the DNA, the last factor in Equation (3.6) is less than unity and is a function of n and r. The resulting Scatchard plot is curved and falls below the classical straight line plot (Fig. 3.9).

The intercept on the abscissa is $\frac{1}{n}$ as required for complete saturation, though the plots become very shallow at large r for even moderately sized drug molecules. Crothers (1968) noted that this implied a reluctance of the drugs to bind, and resulted from the accumulation of gaps smaller than n base-pairs in length.

The slope of Equation (3.6) at low r is $-k(2n - 1)$ so that extrapolation of data from this portion of the curve leads to an intercept of about $\frac{1}{(2n-1)}$. This results in an overestimation of the binding site size (see Table 3.1). Many earlier DNA-drug binding studies have produced extrapolated intercepts of around 0.3 drugs per base-pair, which was difficult to explain in terms of the classical analysis. It can now be seen that these values are consistent with an exclusion site model in which n = 2 (viz. nearest neighbour exclusion).

Equation (3.6) is the most convenient but not the sole formulation of the solution for the excluded site model. The results of Zasedatelev *et al.* (1971), obtained by a combinatorial method, can be arranged to give this expression; and both Crothers (1968), using a Monte Carlo method, and Schellman (1974), using sequence generating functions, have proposed similar equations. In addition, there have been a number of more restricted analyses which have produced less general solutions (Hill, 1957;

Fig. 3.9 Theoretical plots calculated from Equation (3.6) for the binding of drugs ranging in size from n=1 to n=20, for k=1 M^{-1} (after McGhee and von Hippel , 1974).

The absicca is scaled in units of $\frac{1}{n}$, and the dashed line represents the limiting slope of the n=20 curve (see text)

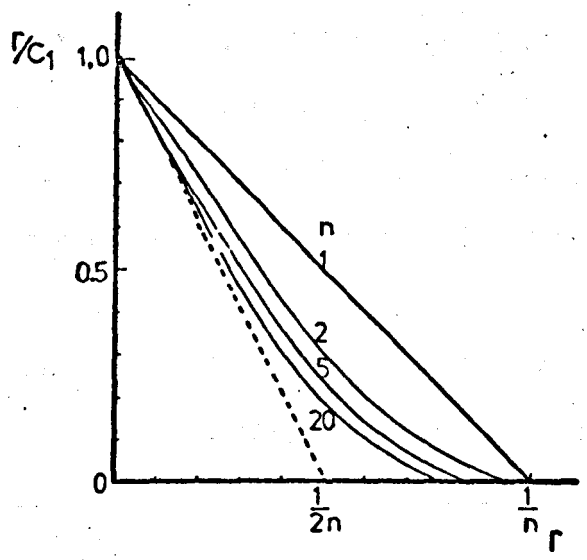

Fig. 3.10 Theoretical plots for the co-operative binding of a ligand of n=1 (for k= 1 M^{-1}) with w ranging from 0 to 5 (after McGhee and von Hippel, 1974)

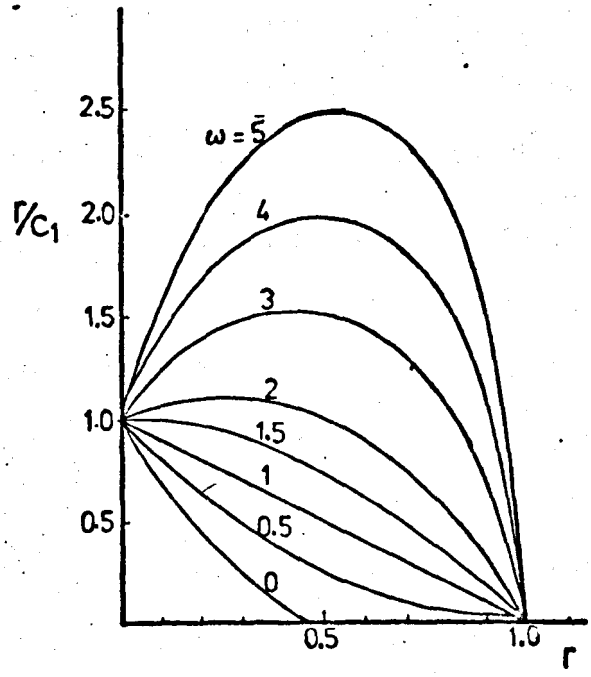

Schwarz, 1970; Bauer and Vinograd, 1970; Armstrong et al., 1970).

Recently, good quality X-ray diffraction patterns (Bond et al., 1975) from a platinum-substituted ethidium-DNA complex have strongly supported the nearest neighbour exclusion theory by demonstrating a 10.2Å periodicity along the helix axis. Unfortunately, however, no estimate of the pitch was made from the diffraction data and because the 10.2Å meridional is considerably less intense than that corresponding to the 3.4Å base-pair repeat, there are doubts (Goodwin, 1977) as to whether saturation of the binding had been reached.

Ethiduim bromide binding to DNA is a particularly difficult case to analyse spectroscopically. If an external binding mode is present, it is likely that it causes a similar shift to the free drug spectrum as is caused by intercalative binding (Porumb, 1976). Previously the curved Scatchard plot had been analysed according to a two binding mode scheme (Waring, 1965), but more recently the data has been shown to fit accurately a single binding species model in which nearest neighbour exclusion effects are operating (Bresloff and Crothers, 1975).

Theoretical calculations have been quoted (Gale et al., 1972; Cairns, 1962) to support a saturation of binding at less than r = 0.5 for the nearest neighbour exclusion model. It has been suggested that the maximum occupancy under this scheme would be $\frac{(1 - e^{-2})}{2} = 0.436$. The original paper (Page, 1959) considered the random selection of adjacent pairs of points from a line of N points, but the theory is inapplicable to drug binding. Once pairs of points had been selected they were not considered again, whereas in drug binding a dynamic situation prevails in which a rearrangement of drugs along the DNA is continuously occurring.

The excluded site model can be generalised further to include more than one binding species and/or to include drug interactions, but in most such extensions the number of unknown parameters proliferates at a greater

rate than do the experimental means of distinguishing the different effects. The introduction of a drug interaction parameter w (McGhee and von Hippel, 1974), for instance, modifies the theory to produce the plots of Fig. 3.10. Values of w greater than unity correspond to co-operativity, and values less than unity to anti-co-operativity. Anti-co-operativity and binding site overlap are seen to result in the same effect on the plot (viz. a curving below the classical straight line), and for most applications it will suffice to abscrb the interaction term within the largely steric overlap factor to produce an "apparent site size" which includes both effects.

3.4.3 The Computer Programs

A computer program, "SCATCH", written by Dr. James McGhee (to be discussed fully in a publication in preparation) uses the Regula falsi iterative method to minimise (with respect to n and k) the sum of the squares of the differences between the two sides of Equation (3.6), in order to fit experimental binding data to that expression. A listing kindly supplied by Dr. McGhee has been modified so that the program would run on the link to the CDC 7600 computer at Manchester.

Convergence to the best fitting values can be accelerated using a quadratic convergence scheme and the author has developed independently a program, "SCATFIT", which uses the Simplex method (Nelder and Mead, 1965). This program also outputs graphically the curve generated by Equation (3.6) using the best-fit values of n and k, and superimposes it on the data points.

Both programs were tested using previously published data for ethidium bromide (Bresloff and Crothers, 1975) and actinomycin C3 (Müller and Crothers, 1968). The values obtained for n and k are compared with those quoted in the original papers in Table 3.1. As previously noted, use of

TABLE 3.1

Comparison of Binding Parameters Using Different Analyses

	Original Values		Values using 'SCATCH'		Values using 'SCATFIT'	
	n	k	n	k	n	k
Ethidium bromide	2.76 (2.00	5.03×10^4 (1) 1.83×10^4) (2)	2.02	1.836×10^4	2.923	1.838×10^4
Actinomycin C3 (low salt)	11.11	2.4×10^6 (3)	6.388	- (4)	6.230	2.003×10^5
Actinomycin C3 (high salt)	12.50	1.2×10^7 (3)	7.662	- (4)	7.349	8.055×10^5

1. Values obtained from the classical Scatchard analysis (Equation (3.1), applied to the linear portion of the data of Müller and Crothers (1975)).
2. Values obtained by Bresloff and Crothers (1975) using the analysis of Crothers (1968), which is equivalent to Equation (3.6), with n constrained to equal two.
3. Values obtained by Müller and Crothers (1968) applying Equation (3.1) to their data.
4. Program failed to converge with the starting parameters chosen (n = 7 and $k = 2.0 \times 10^5$).
5. Program failed to converge with the starting parameters chosen (n = 7 and $k = 8.0 \times 10^5$).

Equation (3.1) (applicable to the simple single binding species model) rather than Equation (3.6) (resulting from the excluded site theory) leads to an overestimation of both n and k.

Figs. 3.11 and 3.12 show the results from "SCATFIT" for these sets of data. Each figure shows the generated best fit curve, and two other curves generated by taking values of n 5% lower and k 5% higher than the best-fit values (the upper dotted curve), and then n 5% higher and k 5% lower than the best values (the lower dotted curve). This is used to give an idea of how well the best-fit curve fits the experimental data. The ethidium data is seen to be well described by Equation (3.6), but the actinomycin data deviates markedly from the theoretical fitted curve at large r (as previously noted by McGhee and von Hippel (1974)). This implies that an additional complication is operating in the actinomycin binding, and this is probably that actinomycin C3 prefers to bind to a G(5' - 3')C sequence (Sobell, 1973). Equation (3.6) is sufficiently inflexible that variations from it due to binding site heterogeneity (discussed fully in the following section) can be detected by a poor fitting of the generated curve to the data.

"SCATFIT" was used in preference to "SCATCH" for analysing the data presented in Chapter 4, because of its more rapid convergence and its improved robustness (i.e. its ability to cope with somewhat poorer starting values of n and k). A further advantage of "SCATFIT" is the ability to specify, prior to minimisation, the error tolerable in the final result.

A surface plotting program, "SURFPLOT" was developed with the assistance of Dr. P. Collis of the Keele University Computer Centre. The log of the sum of the residuals from Equation (3.6) is plotted against a range of values of n and k enabling the region where the minimum occurs to be located, and hence starting values of n and k to be obtained for use in "SCATFIT". Figs. 3.13 and 3.14 show these plots for the ethidium and actinomycin data. The steps at the right hand side of the plots show regions in which a minimum will not be found. The absence of readily

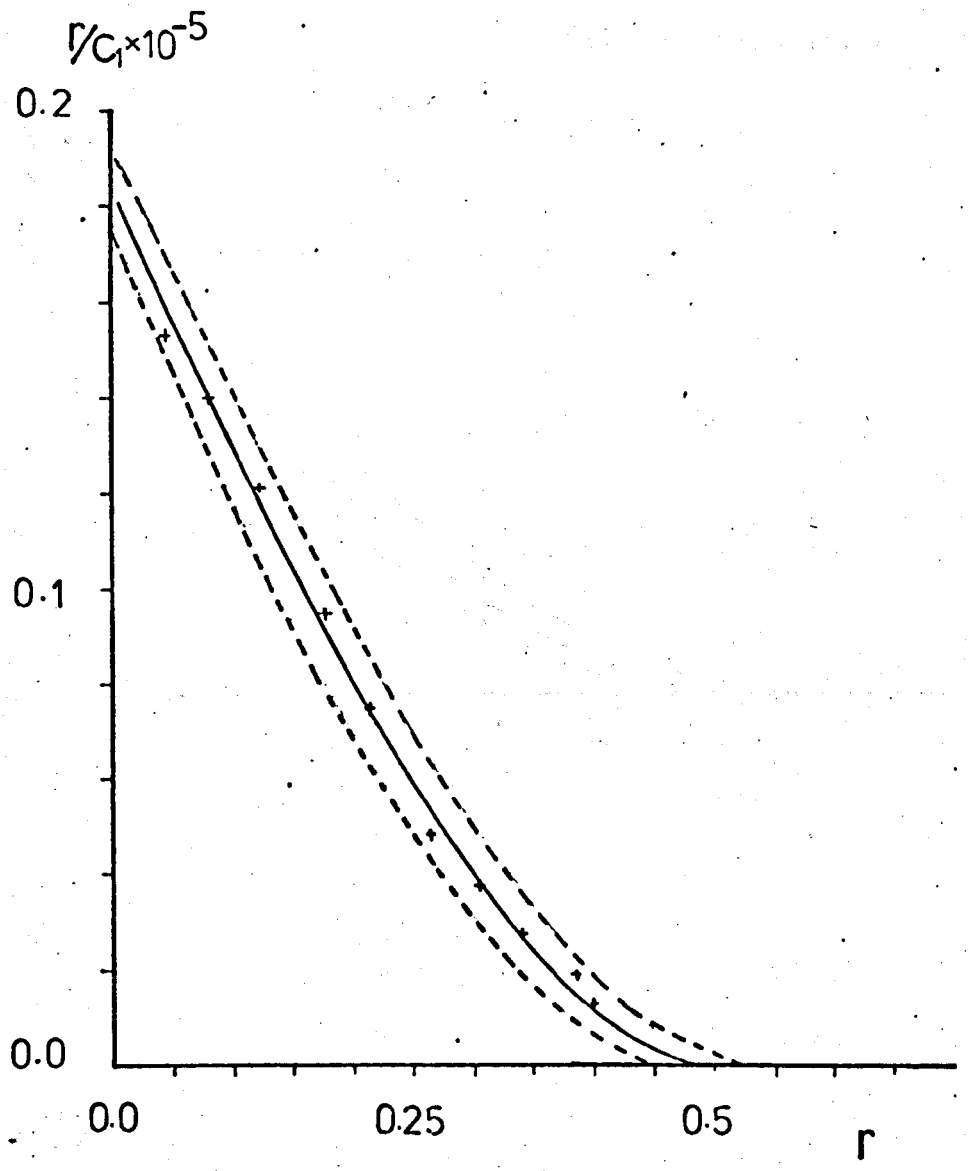

Fig. 3.11 Ethidium bromide - DNA binding data (from Bresloff and Crothers, 1975) fitted to Equation (3.6) using the program 'SCATFIT'. The dotted lines indicate the goodness of fit (see text)

Fig. 3.12 Actinomycin C3 - DNA binding data (from Müller and Crothers, 1968) fitted to Equation (3.6) using 'SCATFIT'.

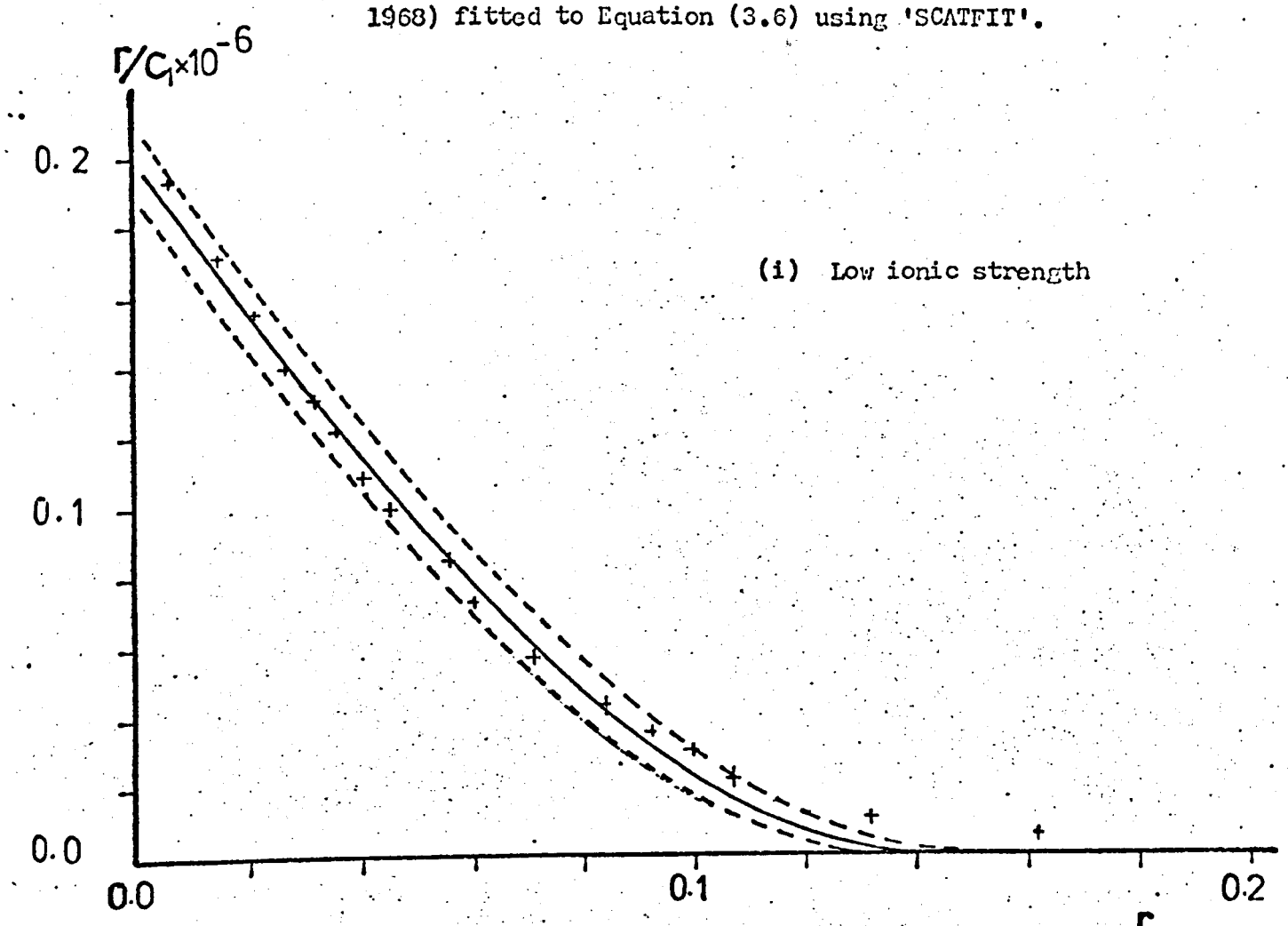

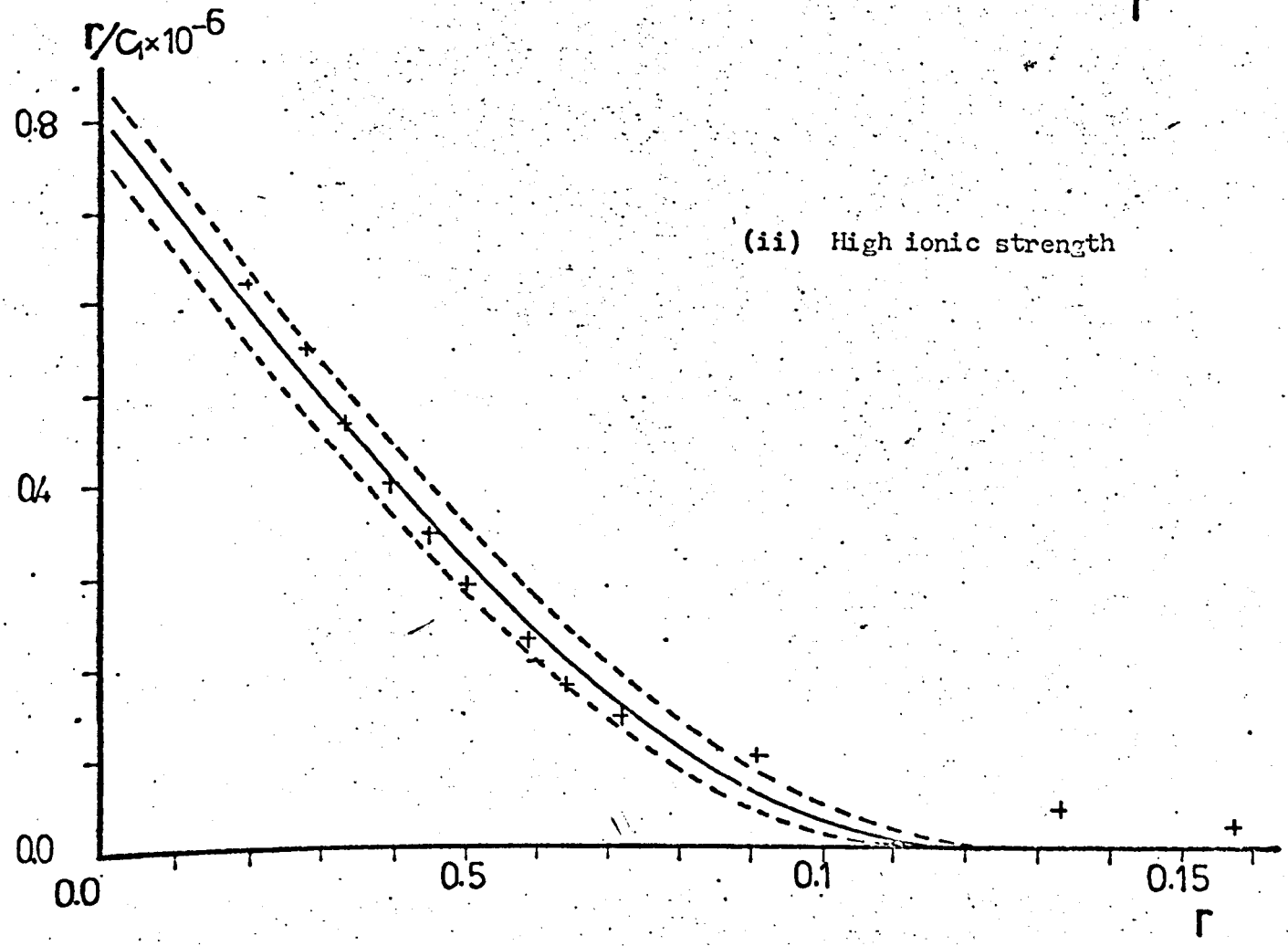

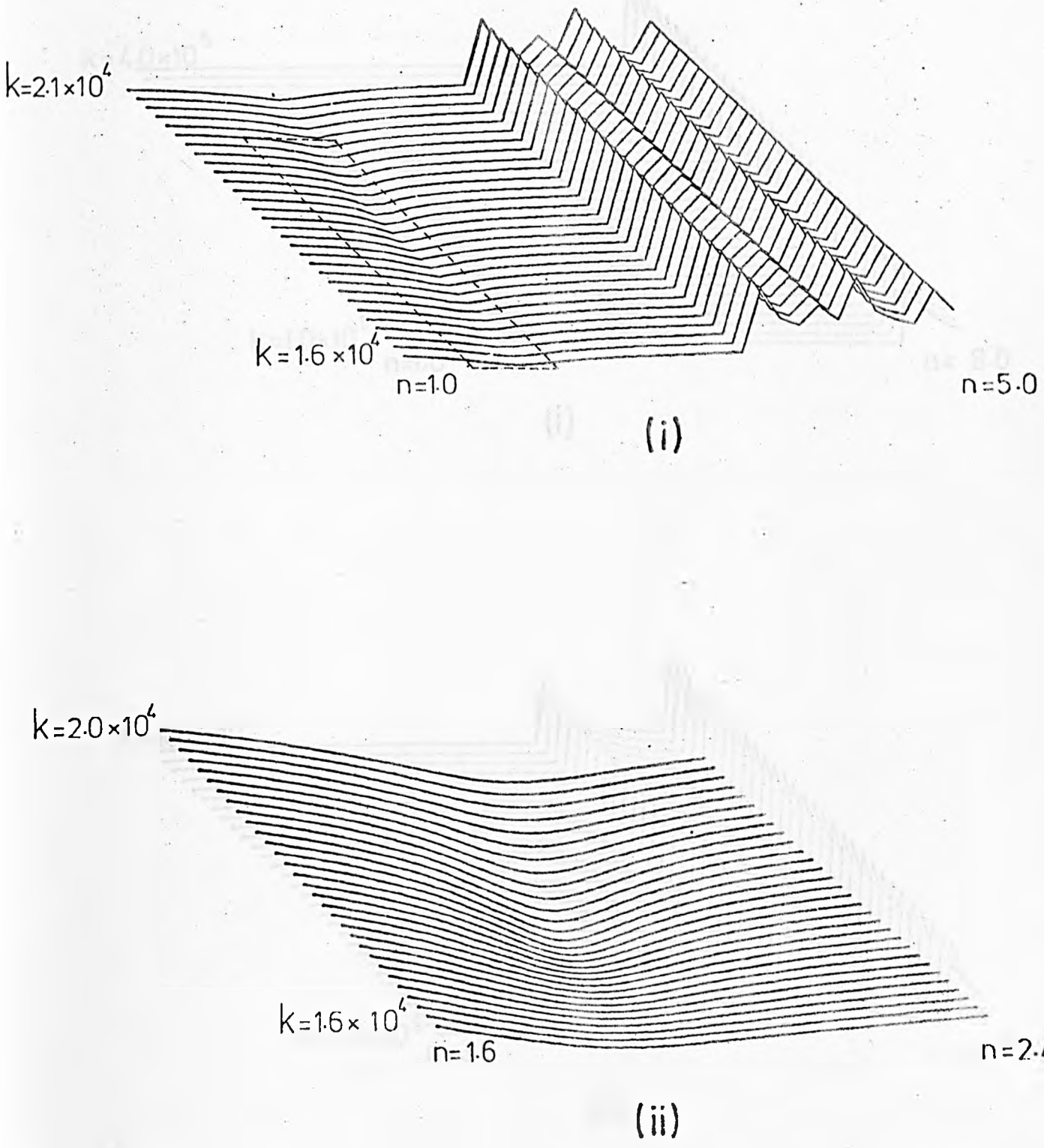

Figure 3.13 Surface plots produced by "SURFPLOT" from DNA–ethidium bromide data (from Bresloff and Crothers, 1975). The dotted portion of diagram (i) is shown, increased in scale, as diagram (ii).

Fig. 3.14 Surface plots produced by "SURFPLOT" from DNA-actinomycin C3 binding data at (i) low ionic concentration and (ii) high ionic concentration

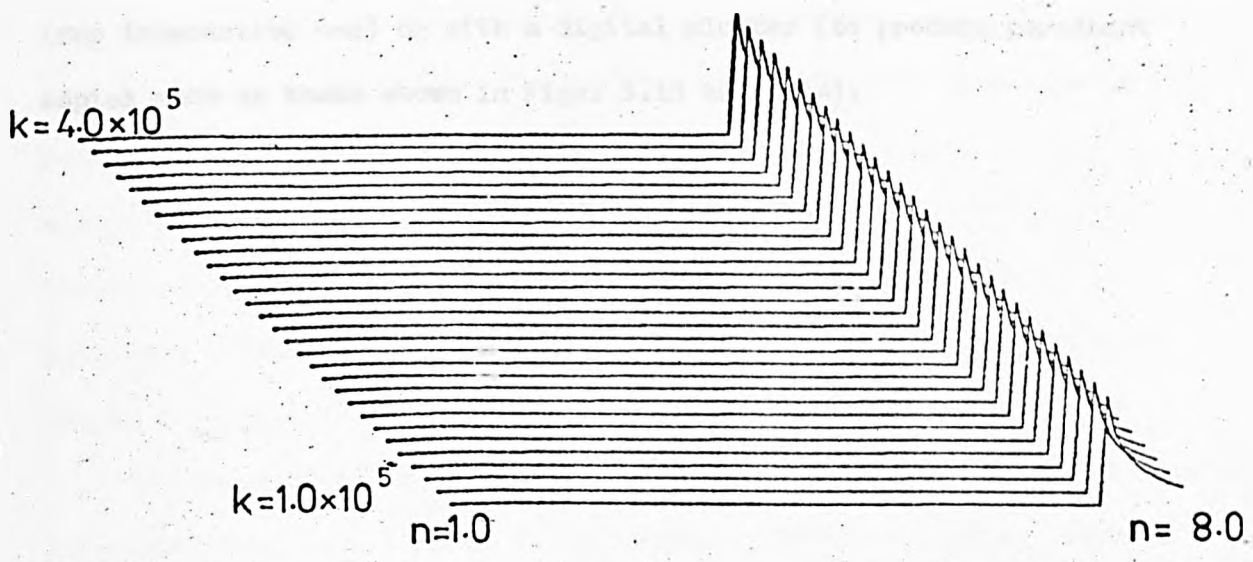

(i)

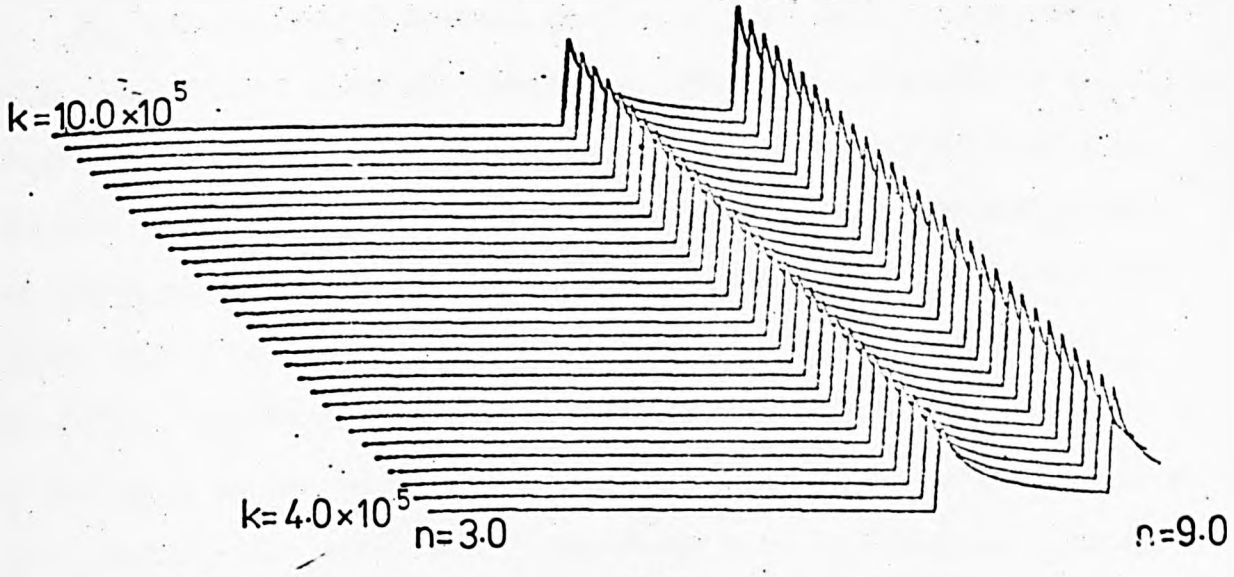

(ii)

identifiable minima in Fig. 3.15 for actinomycin indicates that Equation (3.6) may be a poor description of the experimental situation. "SURFPLOT" has been designed to be used either with a Tektronix graphical display unit (for interactive use) or with a digital plotter (to produce permanent copies such as those shown in Figs. 3.13 and 3.14).

3.5 Heterogeneous Binding Sites

3.5.1 Base-pair Specificity

A curved Scatchard plot could result from either base-pair or base sequence specificity in the binding reaction. Present knowledge of the existence of base-pair specificities is restricted largely to the actinomycin-DNA system (Müller and Crothers, 1968; Sobell et al., 1971), to the interaction of several acridine dyes (Ramstein et al., 1972) and analogues (Müller and Crothers, 1975), and to the antibiotic netropsin (Wartell et al., 1974).

Crothers (1968) produced a non-linear Scatchard plot for a heterogeneous polynucleotide using a Monte Carlo method. For a drug which can bind between two base-pairs (Fig. 3.15) in which at least one member is G-C, and for which n = 4, he obtained the plots shown in Fig. 3.16. Crothers considered the binding to be intercalative, but this is not necessary for the theory. All that is required is that the drug show this preference for a G-C base-pair.

For this simulation Crothers considered a DNA molecule comprising 5000 base-pairs, a value which permitted advance specification of the base-pair composition of the random sequence to within roughly 2%. If f is the fractional G-C content, then the probability of one base-pair chosen at random being G-C is f. The probability of choosing two adjacent base-pairs with at least one of them being G-C is $(1 - (1 - f)^2)$, that is, $(2f - f^2)$. This probability holds no matter what the binding site size, n, of the drug, so long as the identifying site (Fig. 3.17) on the drug (i.e. the chemical group which actually binds) is fixed in a certain position. This would be the case for most binding schemes, although an exception would be the bifunctional intercalators (e.g. echinomycin - Wakelin and Waring, 1976).

In the simpler case of a homogeneous lattice the intercept on the $\frac{r}{c_1}$

Fig. 3.15 A schematic representation of the conditions applicable to the plots of Fig. 3.20

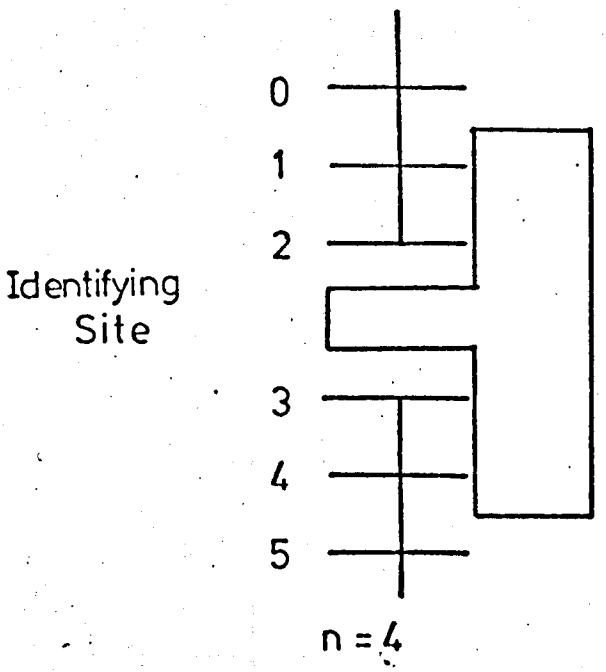

Either 2 or 3 is G-C, or both of them are G-C's

Fig. 3.16 Theoretical Scatchard plot for a model in which a drug (n=4) binds between two base-pairs when at least one of them is G-C ($P=2f-f^2$). (After Crothers, 1968) k has been set to $1M^{-1}$.

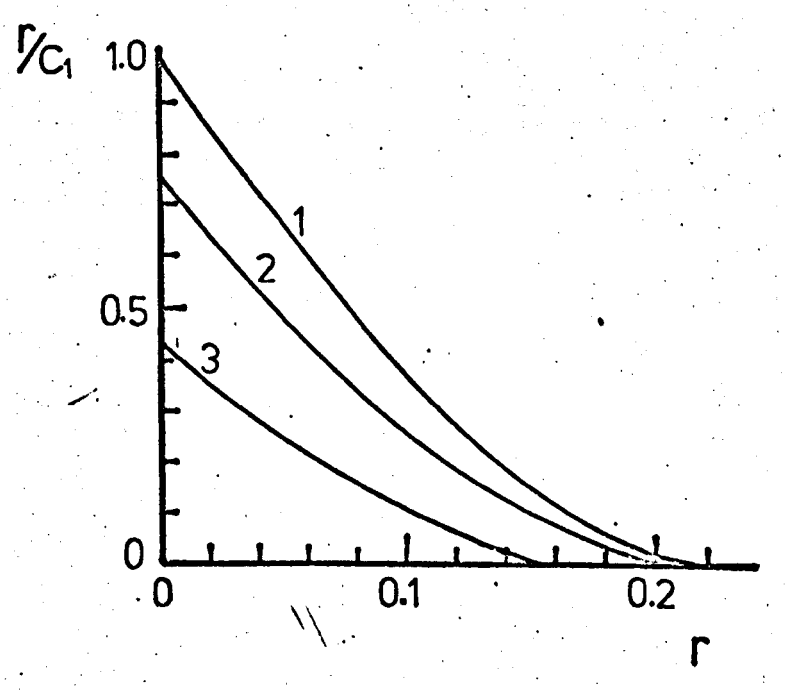

1. f = 1.00 2. f = 0.505 3. f = 0.257

Fig. 3.17 Two different identifying sites for the case where n = 4

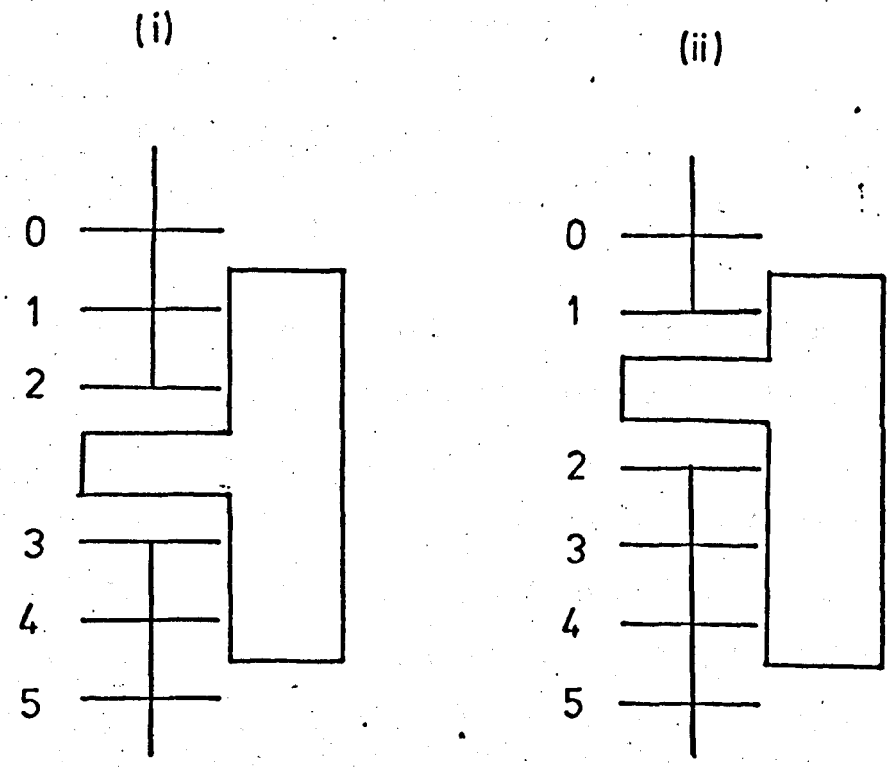

Identifying site is 2 (or 3)

Identifying site is 1 (or 4)

axis of the Scatchard plot is k, the intrinsic association constant of each binding site. Because of the need to satisfy the base-pair preference in a heterogeneous lattice system, the level of binding will always be less for a given total drug concentration. The $\frac{r}{c_1}$ intercept will be reduced by the probability factor, P, to Pk. P depends on the fractional G-C content, f, according to the details of the binding preference. For the scheme considered by Crothers, the dependence of P on f is shown below -

f	$P(= 2f - f^2)$
1.0	1.0
0.5	0.755
0.257	0.448

If binding were to occur exclusively on only one particular side of a G-C pair then the probability factor would equal the fractional G-C content (i.e. P = f), and if it required two adjacent G-C pairs then the probability, P, would be equal to f^2. Thus a plot of the $\frac{r}{c_1}$ intercept (called the affinity, α, by Müller and Crothers (1975)), determined for a variety of DNA's, against a specific expression for P in terms of f, the G-C content, could be useful in testing different models for the binding site specificity requirements. Fig. 3.18 shows the theoretically expected variation of the affinity, α, with the fractional G-C content, f, for the cases where $P = 2f - f^2$, $P = f$ and $P = f^2$.

These relationships hold only for a heteropolymer with random base-pair sequence, whereas in DNA the sequence is generally non-random. Josse et al. (1961) showed that the base-pair sequence in DNA from odd numbered type T phages is close to random if sufficiently long segments of DNA are examined, whilst in thymal and bacterial DNA there is a correlation in the arrangement of immediate neighbours. Shugalin et al. (1971) have concluded that these latter types can be considered as blocks of quasirandom sequence, although

Fig. 3.18 The theoretical variation of the affinity, α, (normalised to unity) with the fractional G-C content, f.

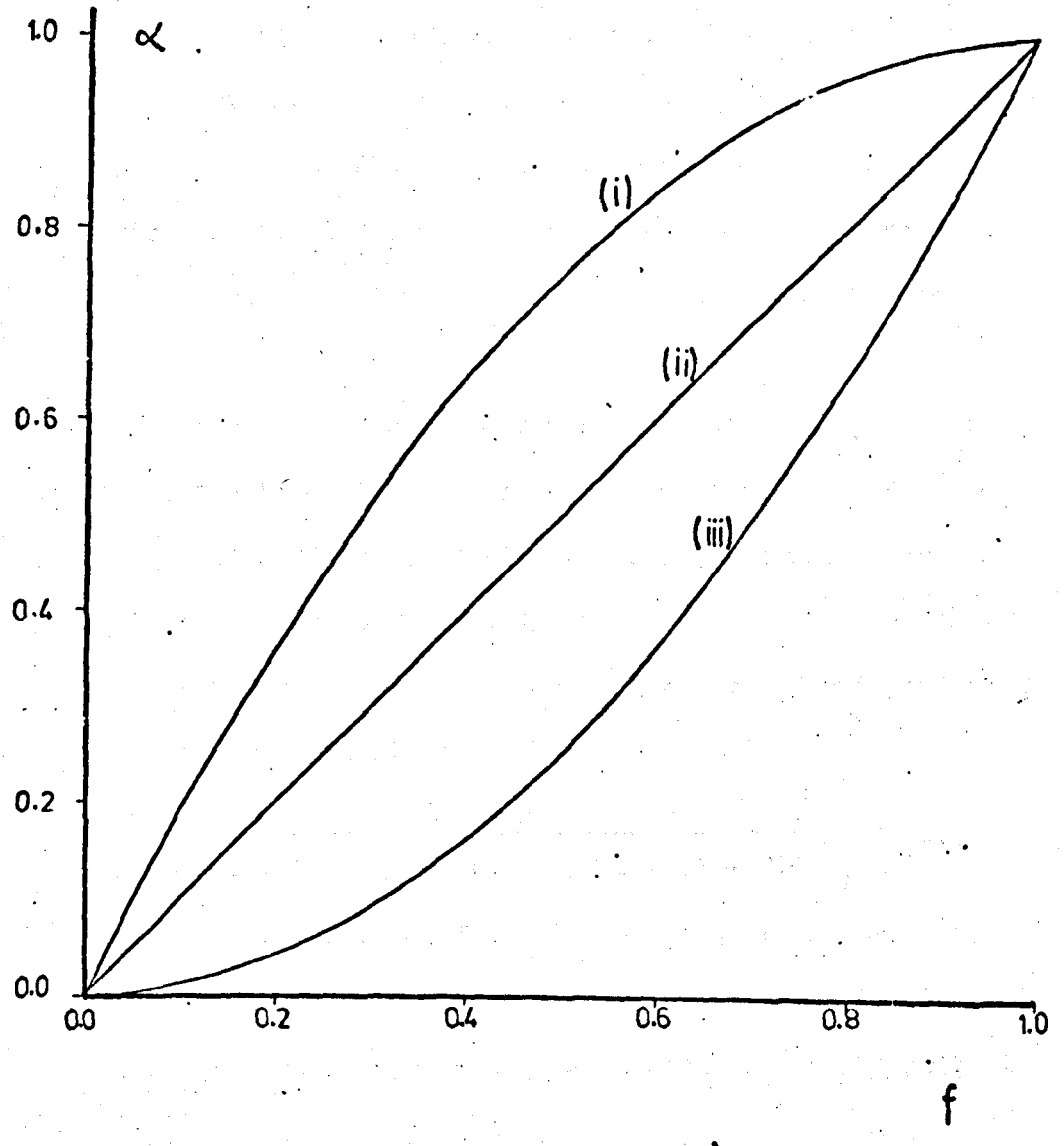

Case (i) $P = 2f - f^2$

(ii) $P = f$

(iii) $P = f^2$, where P is the probability factor (see text for details)

each block contains a differing G-C content. For calf thymus DNA the mean molecular weight of the block is 10 - 15 million with a mean square deviation of the content of the blocks from the average of an entire genome as 9.5%, and for E. coli the respective figures are 5 - 10 million and 4%. However, Gurskii et al. (1972) using these values for thymal DNA, have shown that the resulting value of the binding site size, n, for actimomycin binding to DNA is only about 5% away from the estimate made on the assumption of a completely random heteropolymer. This deviation is lower than the normal experimental error in these investigations. In any case, the molecular weights of the DNA fragments used in the experiments described in this work are likely to be less than the mean value of a block so that the sequence within each fragment can be taken as being completely random.

For the situation where $n > 2$ the concept of an identifying site (Gurskii et al., 1972) becomes important. The affinity is independent of the position of the identifying site with the drug, but the saturation value of r, r_{max}, for a random heteropolymer does depend on the position of this site. For the case where binding requires a G-C pair adjacent to the identifying site, r_{max} is given by

$$r_{max} = \frac{f}{1 + f(n-1) + (1-f)\left\{1 - (1-f)^{t-1}\right\}} \quad (3.7)$$

where t denotes the position of the identifying site. In Fig. 3.17(i) t could be taken as either 2 or 3, and in Fig. 3.17(ii) it could be taken as either 1 or 4. For use with Equation (3.7) t should be taken such that $1 \leq t \leq \frac{n}{2}$.

The equation can be generalised by replacing f by the probability factor P, so that it will describe other base-pair specificity schemes -

$$r_{max} = \frac{P}{1 + P(n-1) + (1-P)\left\{1 - (1-P)^{t-1}\right\}} \quad (3.8)$$

For n=2, when the position of the identifying site is unimportant, this reduces to

$$r_{max} = \frac{P}{1 + P} \qquad (3.9)$$

Table 3.2 illustrates the dependence of r_{max} on f for random-sequence DNA samples of differing G-C content. The relationship between r_{max} and f is shown fully in Fig. 3.19, for the three different probability factors considered previously.

For n=4, the case considered by Crothers, Equation (3.8) reduces to

$$r_{max} = \frac{P}{1 + 3P} \quad \text{for } t = 1. \qquad (3.10)$$

and $$r_{max} = \frac{P}{1 + 4P - P^2} \quad \text{for } t = 2 \qquad (3.11)$$

The intercepts, r_{max}, for these two distinct cases are tabulated in Table 3.3 for the G-C contents considered by Crothers, and the relationships between r_{max} and f are plotted in Fig. 3.20.

Crothers considered the case where the identifying site requires at least one G-C pair (i.e. $P = 2f - f^2$). However, it is difficult to tell from his results whether his example corresponded to having the identifying site at t = 1 or t = 2.

Because of reduced binding due to base-pair specificities, the intercept r_{max} is less than the value expected for that particular binding site size, n. It is the inverse of the intercept which gives a measure of the binding site size. If the values of r_{max} are smaller due to base-pair specificities, inverting them will result in values for the apparent binding site size, n_{app} $(= \frac{1}{r_{max}})$, which are larger than the actual site size, n. This is illustrated, for the different types of specificity considered, in Fig. 3.21 for an actual site size of two (n = 2) and in Fig. 3.22 for an actual site size of four (n = 4).

To recap on the significance of the intercepts measured from the Scatchard plots -

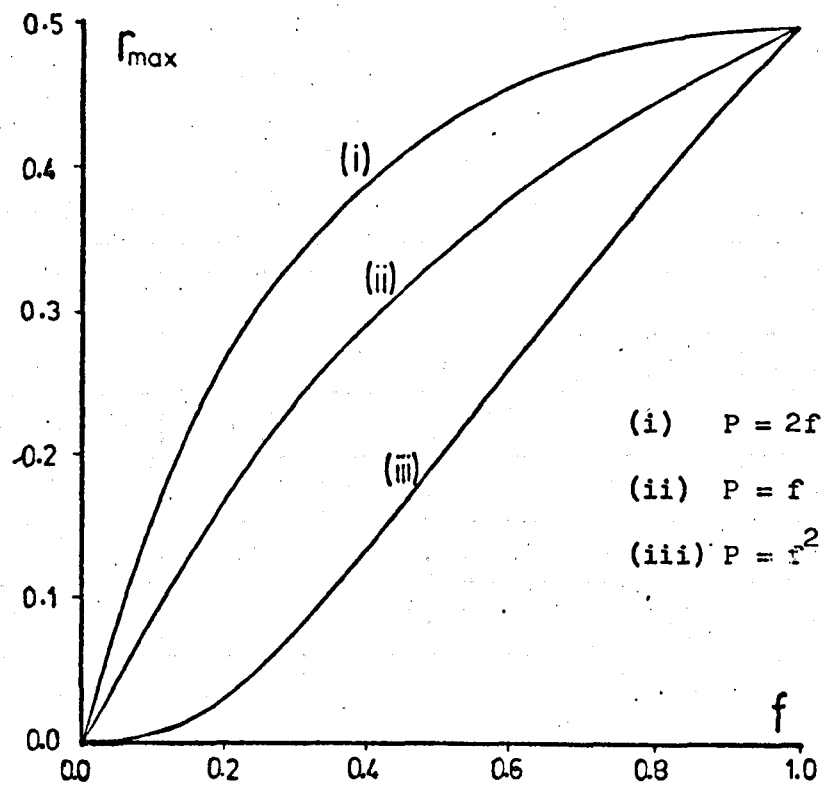

Fig. 3.19 The r intercept, r_{max}, from a Scatchard plot shown as a function of the G-C content f, for n=2

Fig. 3.20 The r intercept, r_{max}, as a function of G-C content f, for n=4

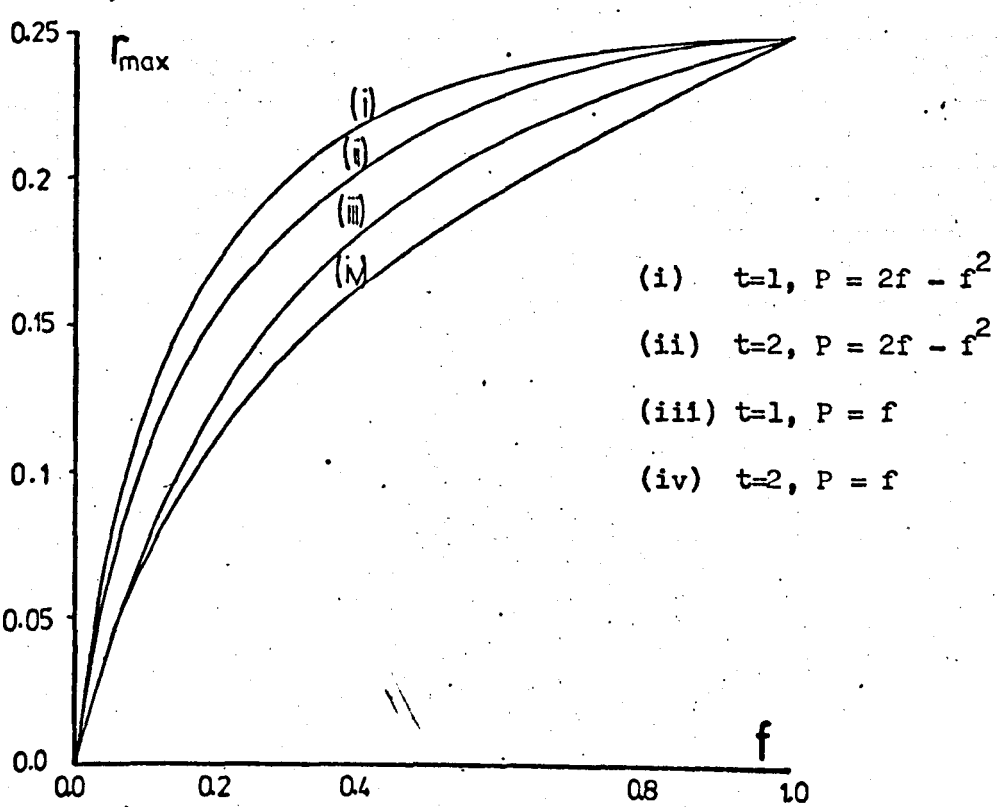

TABLE 3.2

The Intercept, r_{max}, for various f Values when n=2

DNA type	f	r_{max}		
		$P = 2f - f^2$	$P = f$	$P = f^2$
Poly dG - poly dC	1.00	0.50	0.50	0.50
M. lyso	0.72	0.48	0.42	0.34
Calf thymus	0.42	0.40	0.30	0.15
Cl. perfringens	0.30	0.34	0.23	0.08

TABLE 3.3

The Intercept, r_{max}, for various f Values when n=4

f	r_{max} for t=1		r_{max} for t=2	
	$P = 2f - f^2$	$P = f$	$P = 2f - f^2$	$P = f$
1.00	0.250	0.250	0.250	0.250
0.50	0.231	0.201	0.219	0.183
0.257	0.191	0.145	0.173	0.131

Fig. 3.21 Apparent binding site size, n_{app}, as a function of the fractional G-C content f for n=2

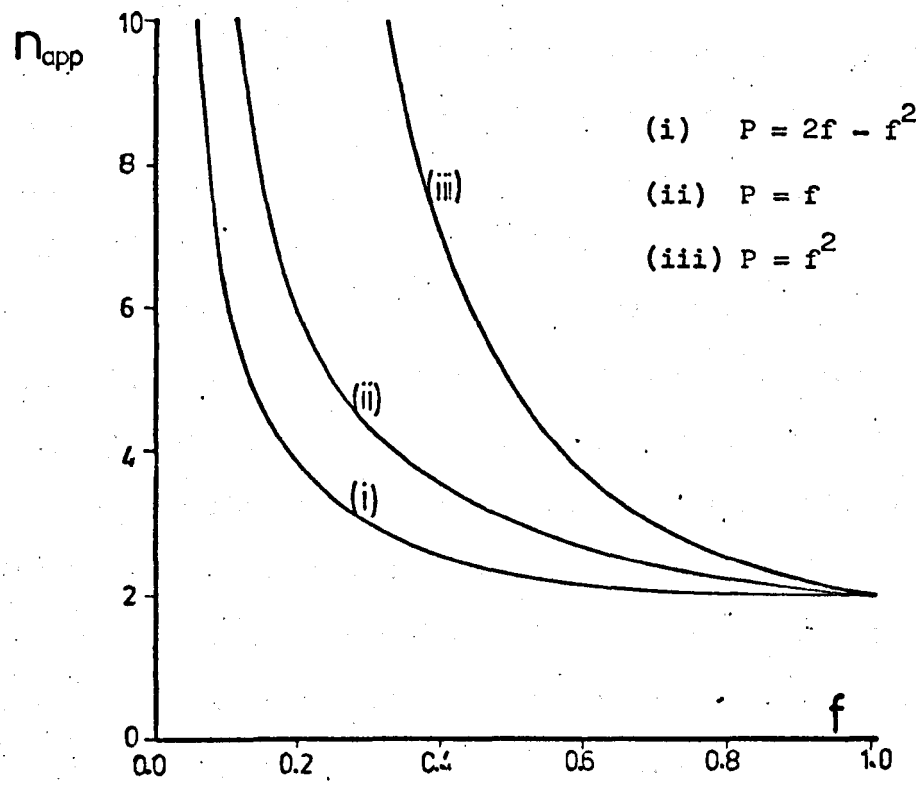

Fig. 3.22 Apparent binding site size, n_{app}, as a function of the fractional G-C content f for n=4

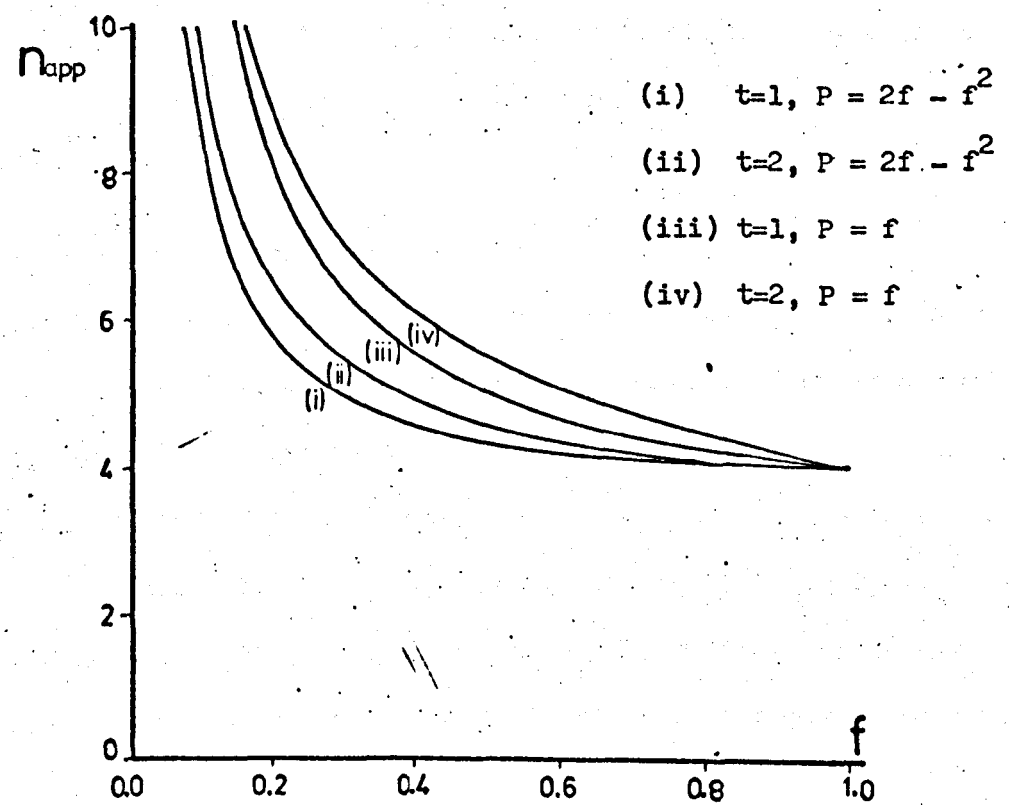

(i) the $\frac{r}{c}$ intercept (the affinity, α) is independent of the size of the binding site and of the position of the identifying site within a drug molecule. Its variation with the fractional G-C content depends on the particular type of base-pair specificity operating, and its value is always less than in the case where there is no specificity in the binding (Fig. 3.18).

(ii) the r intercept (r_{max}) depends both on the binding site size and, when $n > 2$, on the position of the identifying site (Figs. 3.19 and 3.20). Its value is always smaller than the expected value when no base-pair specificity is present. Although it depends on more variables than does the affinity, it may prove useful to consider its variation with G-C content if r_{max} is known more reliably than α.

A further complication would be that binding occurs to both A-T and G-C pairs but with differing affinities (k_{AT} and k_{GC}), a circumstance that could hardly be detected by these methods.

Müller and Crothers (1975) studied the base-pair specificities of a series of proflavine and acridine orange analogues by differential dialysis of the drugs against DNA samples of differing G-C content. For the bis (dimethyl-amino) phenazoxonium ion, the results fitted closely a linear relationship between the affinity, α, and the fractional G-C content indicating that binding requires one G-C pair.

3.5.2 Base Sequence Specificity

Analysing the dependence of α and r_{max} on the G-C content, as described in the previous section, may provide information on the preference of a drug for a particular sequence of bases. The situation where a drug is found to prefer binding to a site containing two adjacent G-C's (i.e. $p = f^2$) is equivalent to a sequence specificity for GpG (or CpC).

It can be shown that, as a consequence of the right-handed nature of the Watson-Crick DNA double helix with its strands of opposite polarity

(Fig. 1.2), there are ten distinctly different binding sites (Fig. 3.23). Although the experimental evidence is conflicting (Chan and van Winkle, 1969; Gersch and Jordan, 1965; Kleinwächter et al., 1969; Bidet et al., 1971), each of these sites could theoretically possess a different association constant (k_1, k_2, k_3.....k_{10}) and the differences amongst them would be more apparent at low binding ratios. These ten sites could be built into a double-helical model of eleven base-pairs, or into a circular double helix of ten base-pairs, for inspection purposes (Fig. 3.24). It is clear, for example, that sites 1, 2 and 3 in Fig. 3.24 are not equivalent and that they present different environments to a binding drug molecule.

In a random arrangement of base-pairs in a DNA molecule, the frequency of any nearest neighbour pair (viz. a sequence of two) should be predictable as the product of the frequencies of its constituent monomers (e.g. F(ApT) = F(TpA) = F(Ap) x F(Tp), where F indicates "frequency of"). Josse et al. (1961) observed that whilst most sequence frequencies fell within these predictions, for several DNA's they differed sharply. In particular, the sequence C(5' - 3')G seems to occur with a frequency which is invariably less than the random value in animal and plant cells (0.016 in calf thymus, instead of an expected 0.21 x 0.21 = 0.044); and, by contrast, its isomeric sequence G(5' x 3')C differs little from the random expectation (in calf thymus, 0.044 experimentally). In bacteria, the reverse of this tendency appears to be the case. Some of the results of Josse et al. are reproduced in Table 3.4, together with the corresponding expected (random) frequencies.

Base-pair specificity can be determined through binding experiments using DNA samples of varying base-pair composition (Wartell et al., 1974 - netropsin; Wakelin and Waring, 1976 - echinomycin). Direct determination of sequence specificity (Müller et al., 1973) is facilitated by using synthetic double helical polynucleotides, but these are limited in their

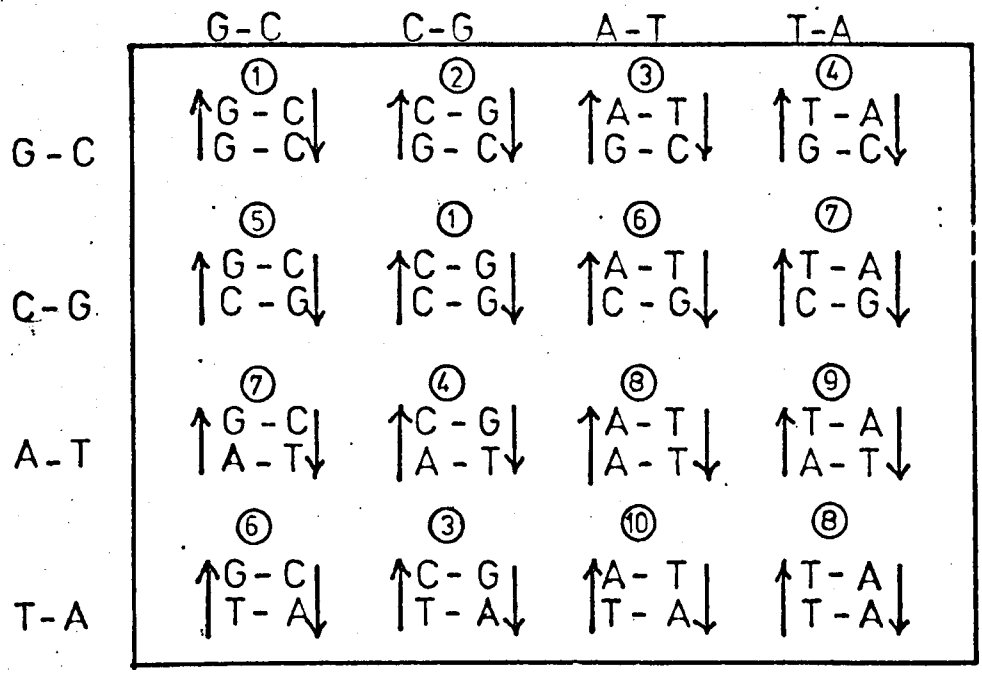

Fig. 3.23 Schematic drawing of the possible intercalating sites in DNA. A degeneracy exists so that of the 16 possibilities, only 10 are distinctly different

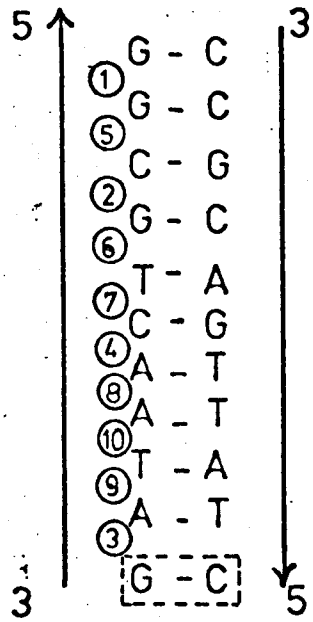

Fig. 3.24 The 10 distinguishable sites may be built into a DNA model 11 base-pairs long, or into a circular DNA model 10 base-pairs long with 5 G-C's and 5 A-T's

TABLE 3.4

Nearest Neighbour Frequencies for some Common DNA Types

(Experimental data from Josse et al., 1961)

Nearest Neighbour Sequence (5' - 3')	Cl. perfringens	Calf thymus		M. lysodeikticus	
	Theoretical	Theoretical	Experimental	Theoretical	Experimental
ApA, TpT	0.123	0.084	0.089, 0.087	0.020	0.019, 0.017
CpA, TpG	0.053	0.061	0.080, 0.076	0.050	0.052, 0.054
GpA, TpC	0.053	0.061	0.064, 0.067	0.050	0.065, 0.063
CpT, ApG	0.053	0.061	0.067, 0.072	0.050	0.050, 0.049
GpT, ApC	0.053	0.061	0.056, 0.052	0.050	0.056, 0.057
GpG, CpC	0.023	0.044	0.050, 0.054	0.130	0.112, 0.113
TpA	0.123	0.084	0.053	0.020	0.011
ApT	0.123	0.084	0.073	0.020	0.022
CpG	0.023	0.044	0.016	0.130	0.139
GpC	0.023	0.044	0.044	0.130	0.121

Theoretical values using: $f_{C,\,G} = 0.15$ and $f_{A,\,T} = 0.35$ (Cl. perfs.)

$f_{C,\,G} = 0.21$ and $f_{A,\,T} = 0.29$ (Calf thymus)

$f_{C,\,G} = 0.36$ and $f_{A,\,T} = 0.14$ (M. lyso.)

availabi L.ty.

Krugh et al. (1975) have investigated the strong (intercalative) binding of ethidium bromide to dinucleotides using visible spectrophotometry, circular dichroism and NMR techniques and have reported a base sequence specificity. A definite preference for binding to a purine (5' - 3') pyrimidine sequence (GpC) compared with the isomeric pyrimidine (5' - 3') purine sequence (CpG) has been detected. They predict the existence of different equilibrium constants for the ten different intercalation sites based on the importance of stabilising stacking interactions between the base-pair and the intercalated phenanthridium ring. Patel and Canuel (1976) have extended sequence studies to the tetranucleotide level, and have observed stronger binding of ethidium to the self-complementary GpCpGpC (i.e. two GpC intercalation sites) and GpGpCpC (i.e. one GpC site) duplexes compared to the CpCpGpG (i.e. no GpC sites) by monitoring the UV absorbance at 480nm of various mixtures.

A recent theoretical analysis (Pack and Loew, 1978) of the origins of the base sequence specificity in the intercalative binding of ethidium to DNA has considered the binding in two stages. In the first stage, the double helix changes conformation (unwinds) to accept the intercalating molecule; and in the second stage, the drug is bound and its interaction energy (primarily with the bases) compensates for the energy required for unwinding. They conclude that the sequence specificity of ethidium is more readily explained in terms of the conformational energy changes than by preferential stacking interactions. NMR studies (Patel and Canuel, 1977) of the binding of proflavine and propidium diiodide have shown that both exhibit a specificity for G(5' - 3')C sites, similar to that shown by ethidium, and it is probable (Pack and Loew, 1978) that all drugs which unwind DNA in the same manner as ethidium would exhibit this particular

sequence specificity.*

* 9-amino acridine (Seeman et al., 1975) shows a sequence preference for a pyrimidine (5' - 3') purine sequence, ApU, but it is a non-intercalator. Actinomycin D shows a strong specificity for G(5' - 3')C sequences, but this has been explained in terms of specific hydrogen bonding by the lactone rings (Müller and Crothers, 1968; Jain and Sobell, 1972).

3.6 Concluding Remarks

The change in the free energy when drugs bind to DNA results from a complex mixture of electrostatic effects, π-electron interactions, hydrophobic bonding and dipole/polarisability factors, all constrained by steric considerations. Estimation of the relative importance of each of these effects would not be easy even with detailed thermodynamic and kinetic studies. Free energy calculations (e.g. Gersch and Jordan, 1965, on the aminoacridines) remain at a formative stage and, because of the complexity of the situation, must continue to function only in a supporting capacity to empirical observations.

Useful information can be obtained from a careful interpretation of a Scatchard plot of the binding parameters. It is important to realise that much (if not all) of the non-linearity in such a plot can be attributed to a binding overlap effect (i.e. an exclusion site model). Experimental data should be first analysed according to this model, and only if this proves inadequate should one consider a multi-binding species or a co-operativity treatment. Analysis using DNA samples of different G-C content will reveal any base-pair specificity of a drug, and may indicate a base sequence specificity in its binding.

The presence of different binding sites may prove to be of great importance in the recognition process involved in protein-nucleic acid interactions and in DNA replication and transcription. Simple electrostatic and hydrogen bonding interactions cannot by themselves be very selective since there are many such sites on the helix, but selectivity due to stacking/steric/electronic/unwinding factors would allow a sequence within the DNA to be recognised. Highly specific antibiotic and anti-tumour drugs could then be designed to bind at or adjacent to these sequences. If a correspondence were established between the unwinding angle of DNA and the helical conformation of the intercalative complex,

specifities could be predicted directly from measured unwinding angles and this would greatly facilitate the design of sequence-specific intercalators.

CHAPTER 4

Spectroscopic Analysis of DNA-Drug Binding Data : Experimental

4.1 The Absorption Spectra of the Drugs

The three phenanthridine drugs under investigation possess the characteristic planar phenanthridinium ring, the electronic structure of which is little affected by the methyl or ethyl substituents of dimidium and ethidium bromide (Giacomoni and Le Bret, 1973). Fig. 4.1 shows the geometry of the main ring and the π-electron distribution. Theoretical calculations (Giacomoni and Le Bret, 1973) on this structure have predicted an absorbance spectrum with a strong visible component around 445nm. The red shifting of the peak to 480nm for dimidium and ethidium, observed experimentally, is due to the bathochromic effect of alkyl groups (Jones, 1945).

The absorbance of ethidium bromide obeys Beer's Law (i.e. the absorbance increases linearly with the concentration of the solution) up to concentrations of about 1.0mM (Waring, 1965) above which departures occur due to aggregation of the drug molecules (Thomas and Roques, 1972). The author has found that dimidium obeys Beer's Law up to a similar concentration, and that prothidium obeys it up to at least 0.10mM (which is lower than the free drug concentration ($\sim$ 0.02mM) used in the spectroscopic series). Above these concentrations the drugs can form antisymmetric dimers causing the spectra to become red-shifted and hypochromic (Fig. 4.2). The proposed structure of the ethidium dimer is shown in Fig. 4.3. In this configuration both the steric hindrance, due to the phenyl groups, and the electrostatic repulsion of the charged nitrogens are minimised, and the large surface areas in contact maximise the hydrophobic effect. A similar stacking geometry applies to the acridines (Zanker et al., 1959).

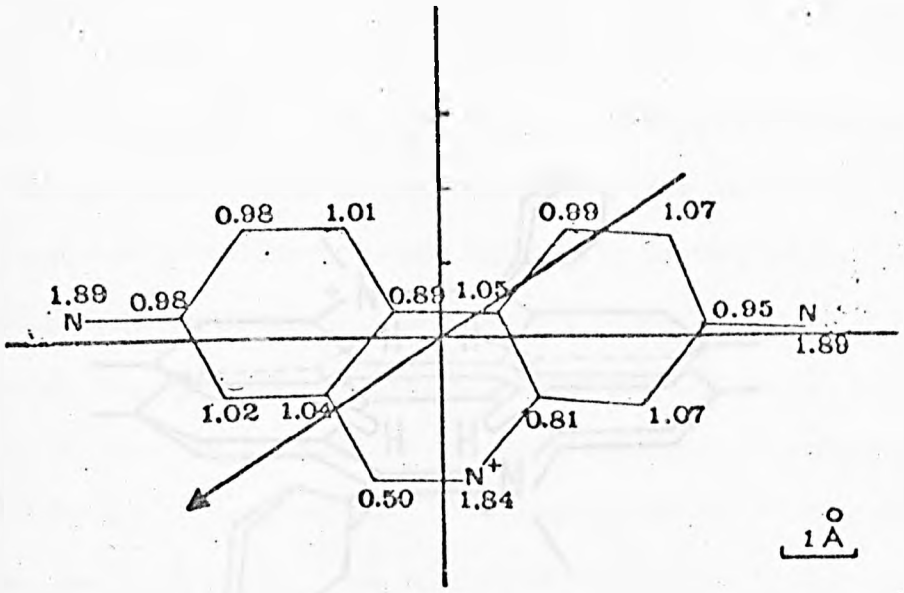

Figure 4.1 The planar geometry and charge distribution of the ethidium chromophore. The numbers refer to the net electronic distribution on single atoms. The arrow shows the direction of the first transition moment (after Giacomoni and Le Bret, 1973).

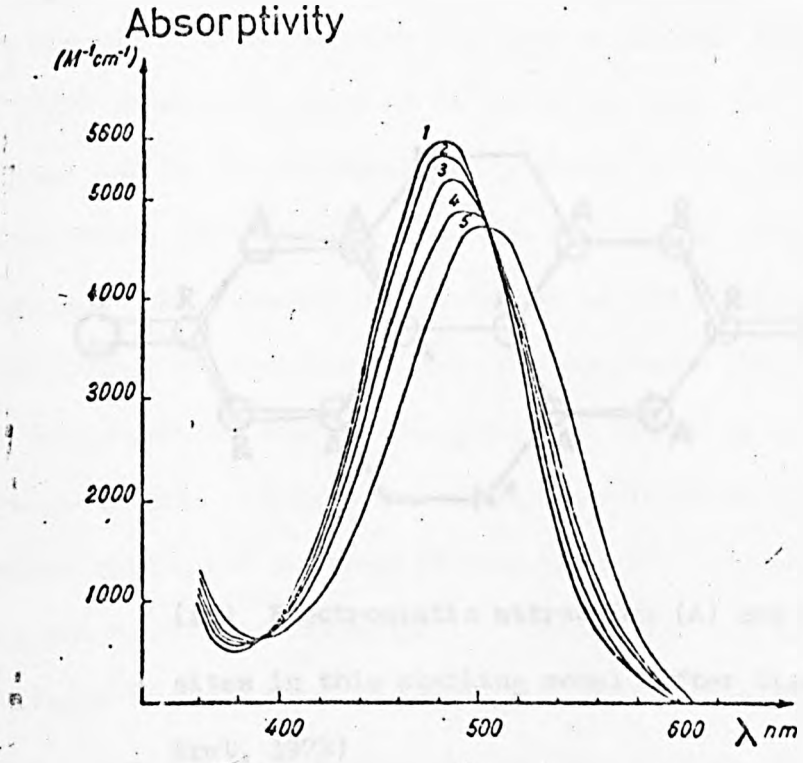

Figure 4.2 Absorption spectra of ethidium bromide in acqueous solution. The concentrations are (1) 10^{-3}M, (2) 2 x 10^{-3}M; (3) 5 x 10^{-3}M, (4) 10^{-2}M, (5) 10^{-1}M (after Thomas and Roques, 1972).

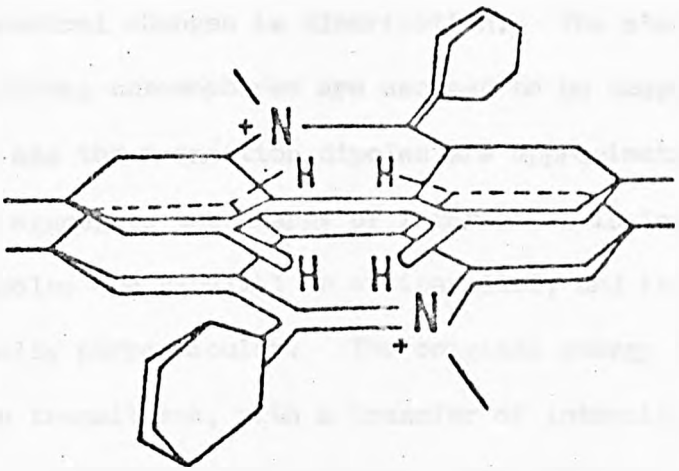

Figure 4.3 (i) Possible structure of a stacked complex between two ethidium bromide molecules (after Thomas and Roques, 1972).

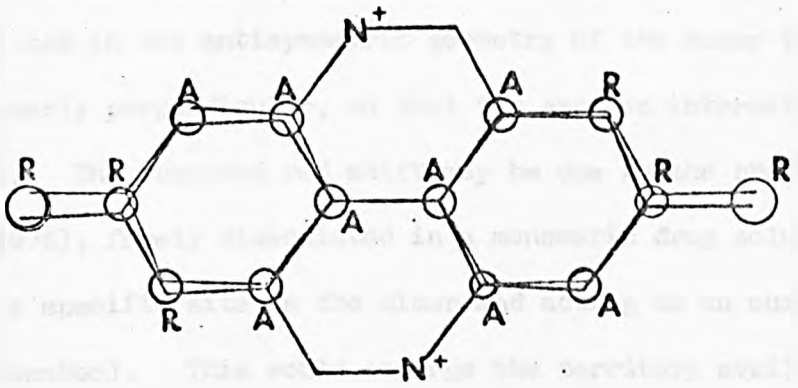

(ii) Electrostatic attraction (A) and repulsion (R) sites in this stacking model (after Giacomoni and Le Bret, 1973)

The exciton interaction theory (Philpott, 1970) has been used to explain the spectral changes in dimerisation. The electronic transitions in the neighbouring chromophores are assumed to be coupled by Coulombic interactions, and the transition dipoles are approximated to point dipoles. For a stacked aggregate the energy of interaction is largest when the transition dipoles are parallel or antiparallel, and it becomes zero when they are mutually perpendicular. The original energy of the transition is split into two transitions, with a transfer of intensity (i.e. a higher oscillator strength) to the higher energy transition, and the resulting spectrum is thus blue shifted.

The theory is successful in explaining the blue shift displayed on stacking by the acridines (whose dipoles are arranged antiparallel to each other in the dimer) but it cannot explain the red shift shown by the phenanthridines. In fact, the transition dipole of the visible transition of the ring in ethidium bromide has been calculated (Giacomoni and Le Bret, 1973) to make an angle of 34^{o} with the line joining the amino groups (Fig. 4.1) and in the antisymmetric geometry of the dimer the dipoles would be nearly perpendicular, so that the exciton interaction would be very small. The observed red shift may be due to the bromide ion, (Porumb, 1976), freely dissociated in a monomeric drug solution, attaching itself to a specific site in the dimer and acting as an auxochrome (i.e. an electron-donator). This would enlarge the territory available to the -electron system and consequently increase the wavelength of (i.e. 'red shift') the electronic transition. It is suggested that the bromine ion would attach to one of the chromophores in the positively charged area of the N_5^+ and C_6 atoms, a site protected from the acqueous environment and not available in the monomer. An increase in the ionic strength of the solution is expected to facilitate dimerisation since the anions of the salt will electrostatically shield the charged nitrogens of each ring. Although no significant effect was detected for dimidium (compare the free drug spectra

in Fig. 4.18(i) with that of Fig. 4.21(i)) and for ethidium (compare Fig. 4.9(i) with Fig. 4.13(i)) a small shift was noticed for prothidium (di)bromide, which is doubly charged in solution (compare Fig. 4.24 with Fig. 4.26(i)).

4.2 The Absorption Spectra of the DNA-Drug Complexes

Acridines and phenanthridines bind readily to DNA *in vitro*. The complexes formed are metachromatic viz. the absorption spectrum of the drug is shifted to longer wavelengths (bathochromism) and the maximum absorptivity is depressed (hypochromism). These spectral changes provide a convenient means of studying the parameters of the binding process, according to the analysis described in Chapter 3. The spectral changes can be explained on the basis of exciton interaction between the transition dipole corresponding to the visible band of the drug and that associated with the UV band of a DNA base (Philpott, 1970). According to this theory, the shifted transition energies will diverge - in particular, that associated with the visible band of the drug will be red shifted.

Spectral series were taken, as described in Section 2.3.1(b), for the three drugs complexed with different DNA types. Within each series there is a progressive shift in the absorbance maximum to longer wavelengths with increasing DNA content. For the three drugs considered here (with the exception of prothidium at low ionic concentration and low binding ratios) all the spectra in a series pass through a common point, called an isosbestic point. The most common circumstance under which this obtains is when there are only two forms of the drug, in this case "free" and "bound" components. If these have the same absorptivity at some wavelength, then shifts in the relative proportions of each will produce no change in absorbance, for a constant total drug concentration, at that wavelength (if the DNA has negligible absorptivity in this wavelength region). However, the existence of isosbestism is not proof that only two forms are present. There could be more than one form of bound drug (e.g. intercalated and externally bound) having different spectra, but if these are always present in the same ratio an isosbestic point will be observed. Alternatively, two bound species may be present each producing shifted spectra so similar that they are

indistinguishable within experimental error.

The converse behaviour allows a more definite conclusion. If there is not an isosbestic point, even though the spectra of complex and free drug cross, then there must be more than one form of binding. This is the case for proflavine (Blake and Peacocke, 1968), where it is interpreted as demonstrating intercalative binding at low binding ratios and additional external stacking on the sugar-phosphate backbone when the drug concentration is high.

4.3 Theory of the Spectroscopic Analysis

Fig. 4.4 shows schematically a two-component case (i.e. a free and a single bound species) in which the free drug spectrum is denoted "library 1", the bound spectrum (Section 2.3.1(b)) is called "library 2", and spectra taken at intermediate values of r are the "mixture" spectra.

At any wavelength λ,

$$A = a_1c_1 + a_2c_2 \qquad (4.1)$$

where A is the absorbance of the mixture, a_1, a_2 are the absorptivities of the free and bound drugs and c_1, c_2 are the concentrations of free and bound components in the mixture. The concentrations c_1 and c_2 can be found by considering the spectra at any one wavelength, λ (Peacocke and Skerrett, 1956), since the total drug concentrations, c, is constant and known.

By proportions,

$$\text{the fraction bound } \left(= \frac{c_2}{c}\right) = \frac{|A_1 - A|}{|A_1 - A_2|} \qquad (4.2)$$

where A_1, A_2 and A are the absorbances of library 1, library 2 and the mixture spectrum respectively, at that wavelength. The best wavelength at which to perform these measurements would be where A_1 and A_2 differ by the greatest amount, since this will minimise the effect of experimental error. The computation will be most reliable for the mixture that is located midway between the two library spectra, since in that case the numerator and denominator of Equation (4.2) will be of similar magnitude.

An extension of this analysis would be to use the entire spectra, rather than readings at just one wavelength, to improve the precision of the values of c_1 and c_2.

Thus, using m wavelengths,*

---

* Note that a reading at the isosbestic wavelength gives no information on c_1, c_2 since

$$a_{1i} = a_{2i}$$
$$A(\lambda 1) = a_{1i}(c_1 + c_2)$$
$$= a_{1i}c$$

Fig. 4.4 Schematic representation of a mixture spectrum in terms of two library spectra

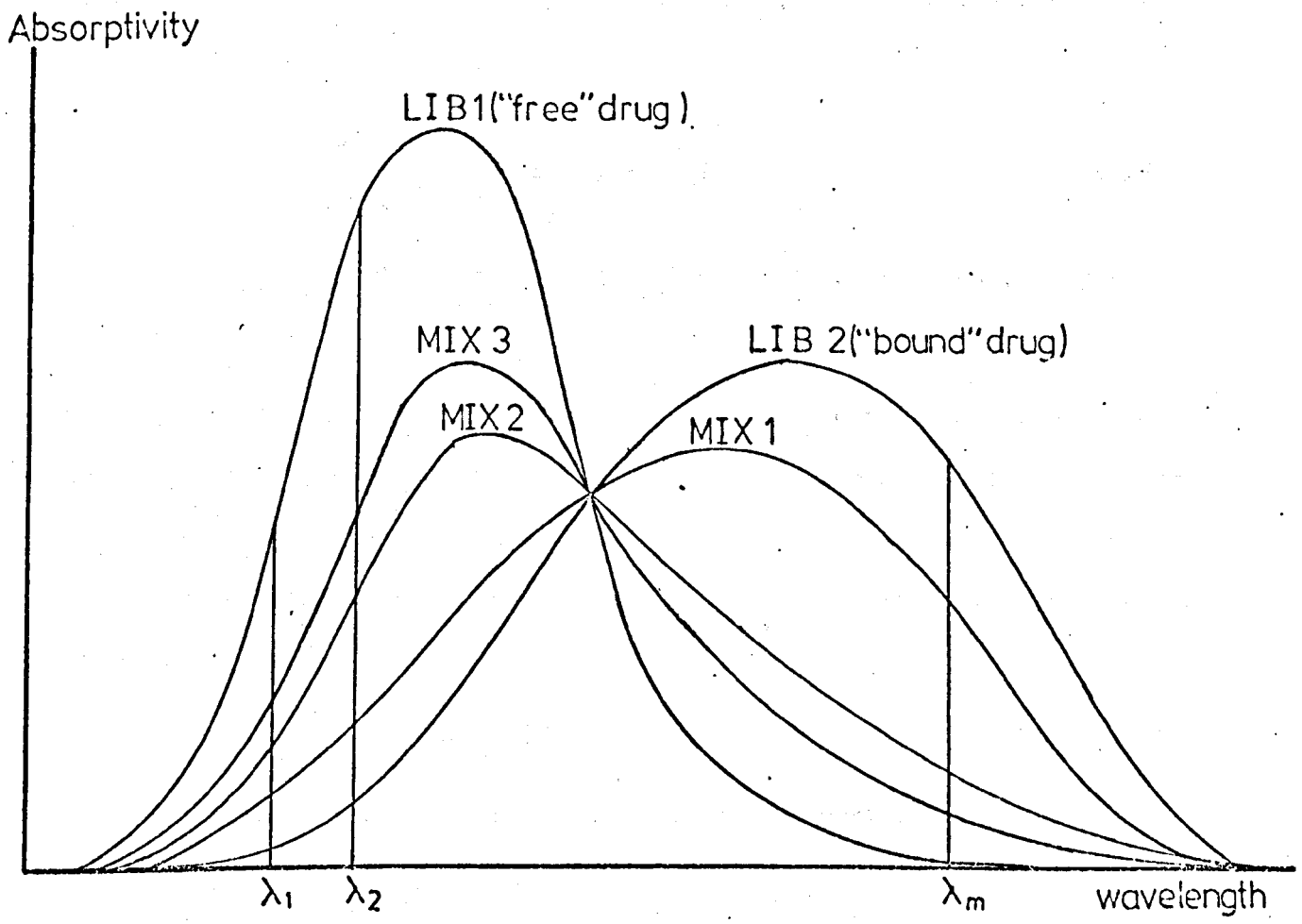

$$A^o(\lambda_1) = a_{11}c_1 + a_{21}c_2 + \delta_1$$

$$A^o(\lambda_2) = a_{12}c_1 + a_{22}c_2 + \delta_2$$

$$A^o(\lambda_m) = a_{1m}c_1 + a_{2m}c_2 + \delta_m \qquad (4.3)$$

where $\delta_1, \delta_2 \ldots \delta_m$ are the experimental errors and the superscript "o" denotes "observed" (i.e. experimental) absorbances. The problem becomes one of selecting the best values for c_1 and c_2, and the criterion adopted is to minimise

$$\phi = \sum_{j=1}^{m} \delta_j^2 = \sum_{j=1}^{m} (A^o_j - A^c_j)^2 \qquad (4.4)$$

where the superscript "c" refers to "calculated" absorbances (using the formula $A^c_j = a_{1j}c_1 + a_{2j}c_2$).

As mentioned previously, values of c_1 and c_2 derived at wavelengths where the two library spectra are different by a large amount will be more reliable so that, in this generalised scheme, it is judicious to weight contributions to the final solution by a term proportional to the magnitude of this difference,

$$w_j = |a_{1j} - a_{2j}|^N \qquad (4.5)$$

A first-order dependence was considered appropriate i.e.

$$w_j = |a_{1j} - a_{2j}| \qquad (4.5a)$$

because of the form of the dependence of the concentrations on the absorptivities (Equation 4.2), and because there is an approximately constant random error* associated with each observed absorbance.

A standard least-squares minimisation treatment results in the following solution

---

* This is a combination of the precision of measurement of the Cary 118C spectrophotometer and the resolution (0.02mm) of the D-mac pencil follower used in digitising the plots.

$$c_1 = \frac{(\sum_{j=1}^{m} w_j A_j a_{1j})(\sum_{j=1}^{m} w_j a_{2j}^2) - (\sum_{j=1}^{m} w_j a_{1j} a_{2j})(\sum_{j=1}^{m} w_j A_j a_{2j})}{\Delta} \qquad (4.6)$$

$$c_2 = \frac{(\Sigma w_j a_{1j}^2)(\Sigma w_j A_j a_{2j}) - (\Sigma w_j A_j a_{ij})(\Sigma w_j a_{ij} a_{2j})}{\Delta} \qquad (4.7)$$

where $\Delta = (\Sigma w_j a_{1j}^2)(\Sigma w_j a_{2j}^2) - (\Sigma w_j a_{1j} a_{2j})^2$

A computer program "SOLVE" was used to find c_1 and c_2, with the libraries and the mixture spectra (labelled 1, 2, ...M) digitised by a D-mac pencil follower. The program is an extension of one used by Porumb (1976), with added options including weighting of the data and computer graphic output.

4.3.1 The Program "SOLVE"

The input data to the program consists of the digitised spectra, values for the total drug concentration (a constant for each spectrum (Section 2.3.1(b)) obtained from the free drug spectrum) and the DNA concentration appropriate to each spectrum. The program plots the digitised spectra (e.g. Figs. 4.6, 4.7 and 4.8), and determines the concentrations, c_1 and c_2, for each mixture. An option is available to weight the equations comprising Equation (4.3) according to the weighting scheme of Equation (4.5), where N is an integer. Results can be obtained by utilising the entire wavelength range, or a selected part of it. The difference between the total drug concentration, c, and the sum of the computed concentrations, $c_1 + c_2$, will reflect the total experimental errors. The discrepancies, $\Delta A (= A^o_j - A^c_j)$, for each mixture spectrum are plotted against wavelength. Inspection of these plots can be used to

detect the presence of a base-line shift (i.e. a systematic error) in the mixture spectra (Ellis and Duggleby, 1978). The presence of an additional species in the system (either a second bound mode, or a contribution from DNA absorption) would be evident from persistent systematic effects in a spectral series in the wavelength region where this species absorbs.

Several other graphs are produced by the program. A plot of r vs. c_1 will typically have the form of Fig. 3.2, with r increasing to a maximum (in the case of a single binding mode) approaching $\frac{1}{n}$ (Section 3.4.2), and the free drug concentration, c_1, increasing as the mixtures 1 to M are considered sequentially. The quantity r rises as the bound drug occupies sites on the DNA (whose concentration is decreasing due to the pipetting scheme (Section 2.3.1(b)). Eventually this increase slows up and approaches a limit, as all the available binding sites on the DNA become filled. The estimation of c_1 will tend to be inaccurate when it is small i.e. for mixture spectra which are difficult to differentiate from library 2 (viz. at small M). Similarly c_2 (and hence r) is more inaccurate for mixtures that are close to library 1 (viz. at large M).

A Scatchard plot is produced, and this would typically be of the form depicted in Fig. 4.5. Both r and c_1 increase progressively through the mixtures 1 to M, but r increases at a slower rate than c_1 (due to the kinetics of binding) so that the quotient $\frac{r}{c_1}$ falls as the mixtures 1 to M are considered. According to the model of McGhee and Von Hippel (Section 3.4), the binding ratio r would increase to a saturation value equivalent to $\frac{1}{n}$, where n is the binding site size. At low binding, errors in $\frac{r}{c_1}$ will be prominent and at high binding errors in r are more important. Experimentally, a lot of points are required at the extremities of the plot if accurate values of the association constant, k, and the site size, n, are to be determined.

Fig. 4.5 Schematic Scatchard plot, showing the typical error bars (exaggerated in length) arising at the extremities of the ranges

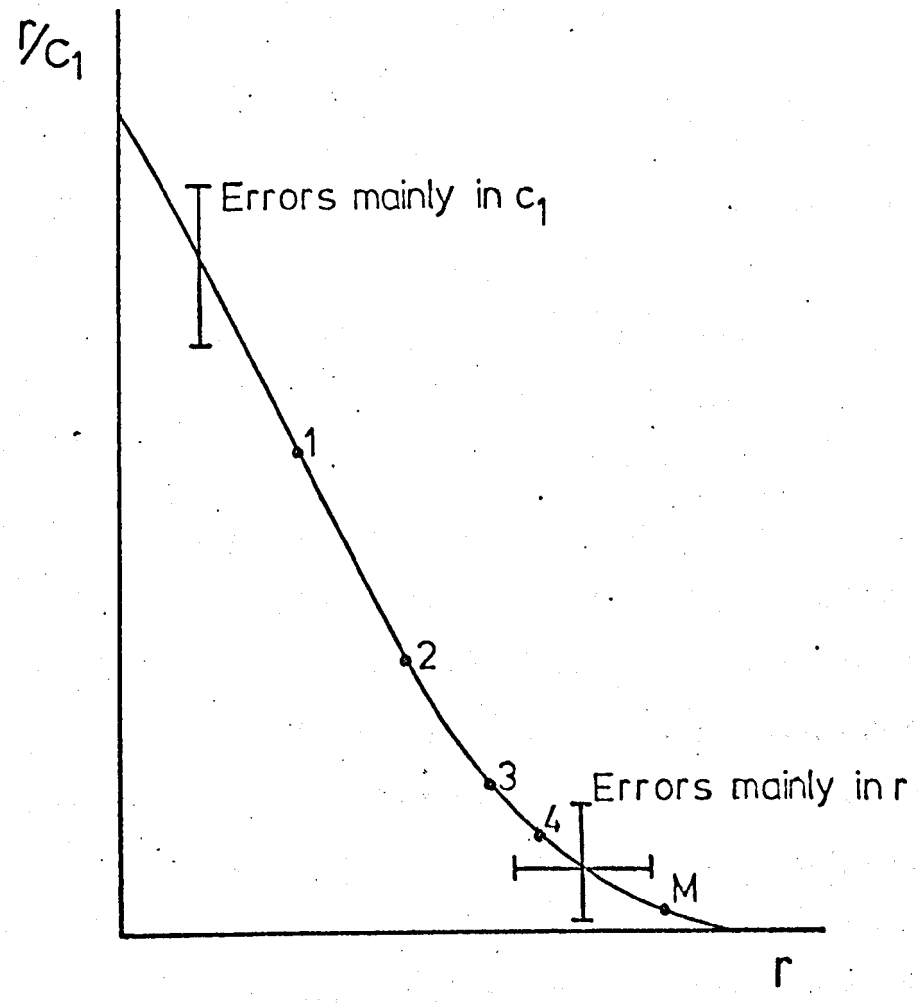

4.3.2 Testing the Program

An additional subroutine was used to generate two gaussian library spectra, and three mixture spectra by combining the library spectra in the ratios ⅓ : ⅔, ½ : ½ and ⅔ : ⅓ such that the total drug concentration was unity. Baseline errors and random noise (using a random number generating subroutine) were added to the mixtures to simulate experimental conditions, and their effects were monitored.

Five cases were considered

(i) no random or baseline errors.

(ii) a 5% random error (i.e. at each wavelength of each mixture spectrum an amount of up to 5% of that particular absorbance reading was either added or subtracted), and no baseline error.

(iii) no random errors, but baseline shifts of +5%, -5% and +10% of the respective peak absorbances were added to the mixture spectra.

(iv) a 5% random error, plus baseline shifts of +5%, -5% and +10%.

(v) a 1% random error, plus baseline shifts of +5%, -5% and +10%.

The graphs generated for examples (i), (ii) and (v), together with a typical discrepancy plot for each, are shown in Figs. 4.6, 4.7 and 4.8. In the cases where a large portion of the error was systematic the ΔA plot approximates to the shape of the original spectrum (Fig. 4.8(ii)). Where the error is largely random, ΔA fluctuates randomly about zero (Figs. 4.6(ii) and 4.7(ii)). Thus, discrepancy plots are useful in distinguishing base-line errors in an experimental situation.

The values calculated for c_1 and c_2 and their sum $(c_1 + c_2)$ (which should equal unity for the test curves), and the root - mean - square discrepancy (averaged over the mixtures for the complete wavelength range) in each of the cases (i) to (v) - for both an unweighted scheme, and one which weights according to $|A_{1j} - A_{2j}|$ - are shown in Table 4.1. Although the differences are small the weighted scheme appears to deal with random errors slightly better, and baseline (systematic) errors a little worse than

Fig. 4.6 (i) Generated gaussian library and mixture spectra as described in Section 4.3.2 (Case (i))

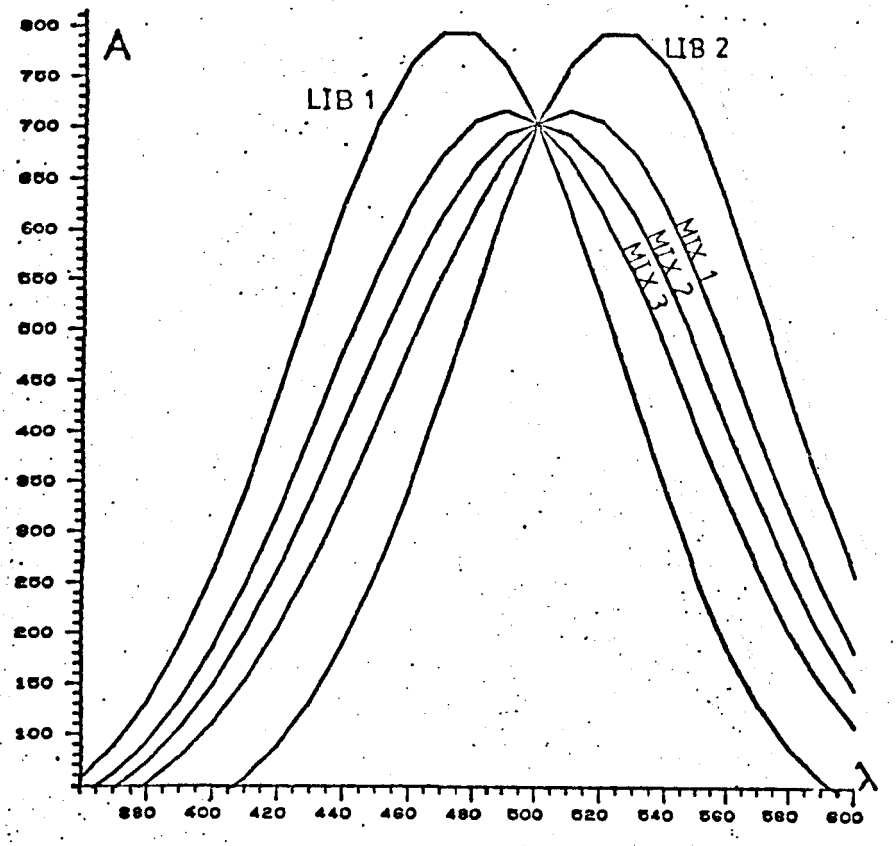

(ii) A discrepancy plot, ΔA vs. λ, obtained for the spectra shown above

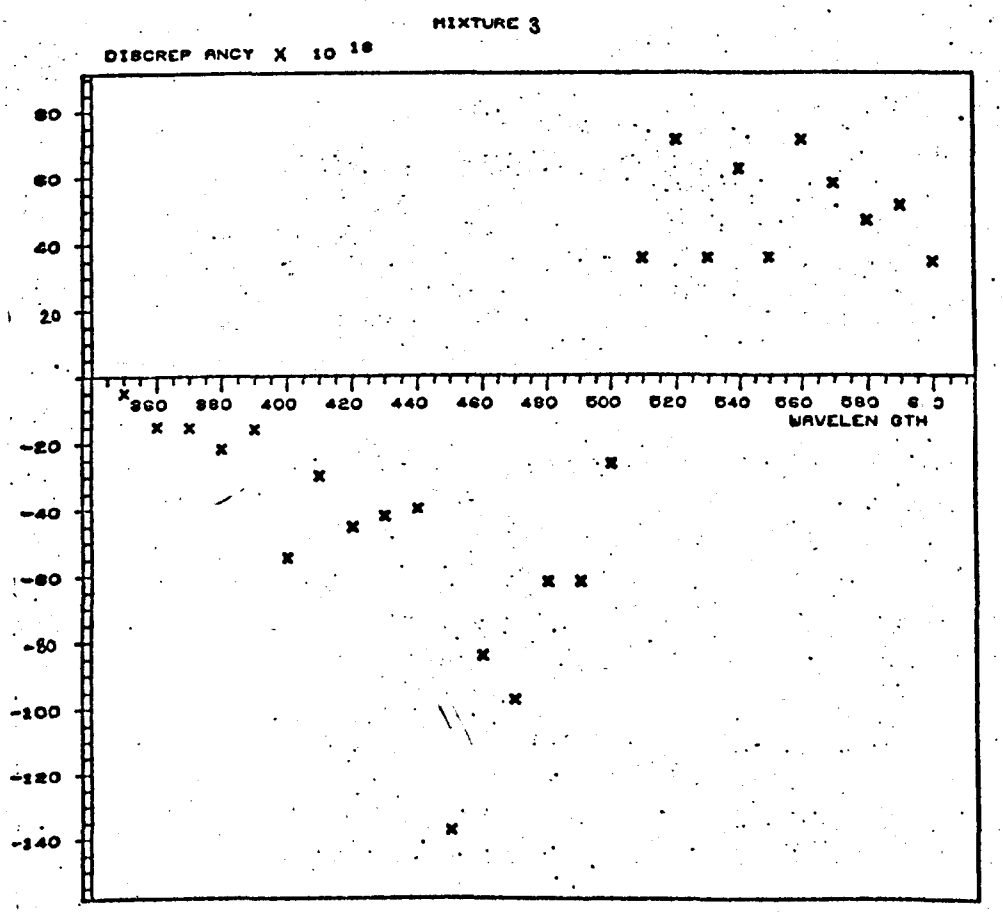

Fig. 4.7 (i) Generated gaussian library and mixture spectra

(Case (ii) in Section 4.3.2)

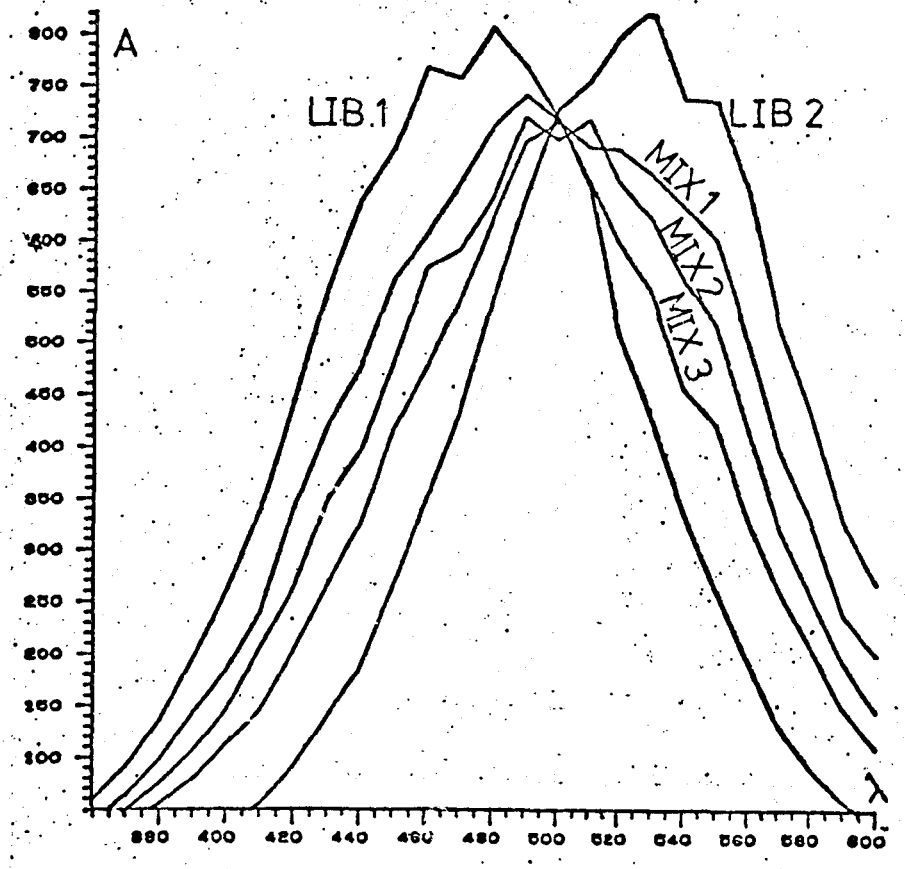

(ii) A discrepancy plot, ΔA vs. λ; for the spectra shown above

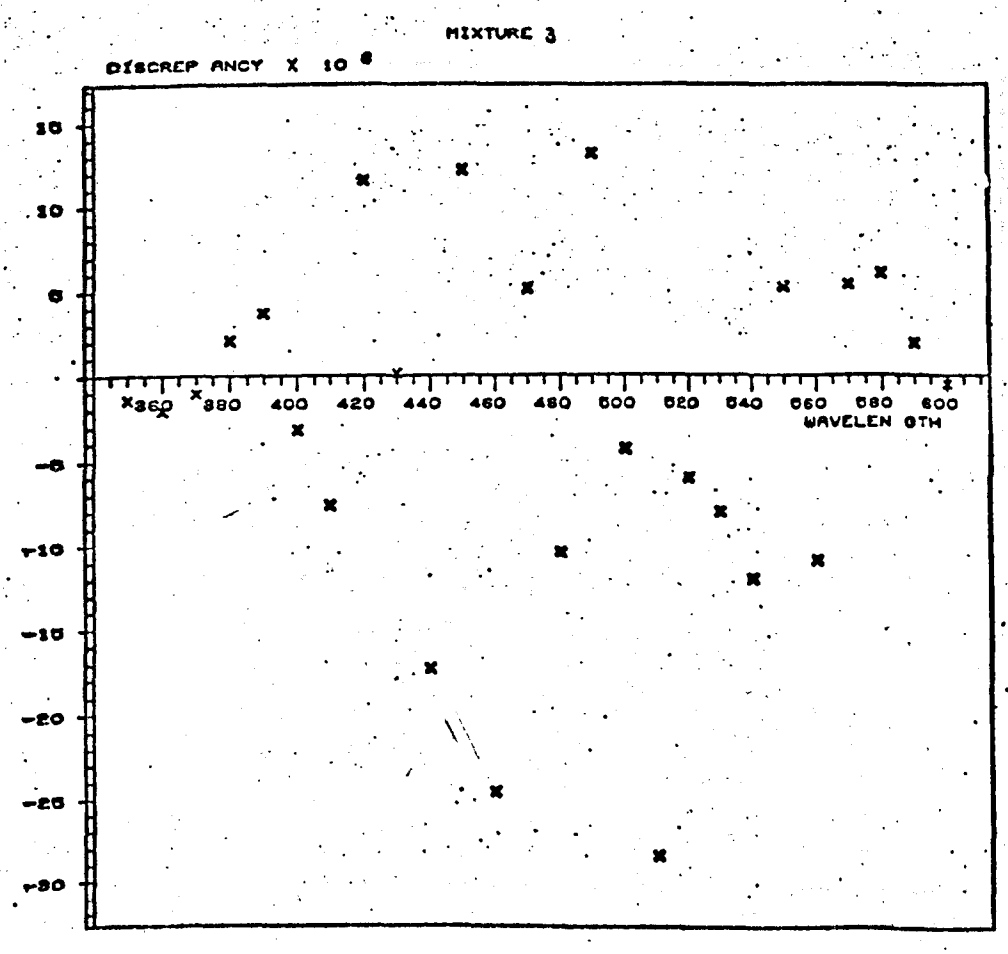

Fig. 4.8 (i) Generated gaussian and mixture spectra (Case (v) in Section 4.3.2)

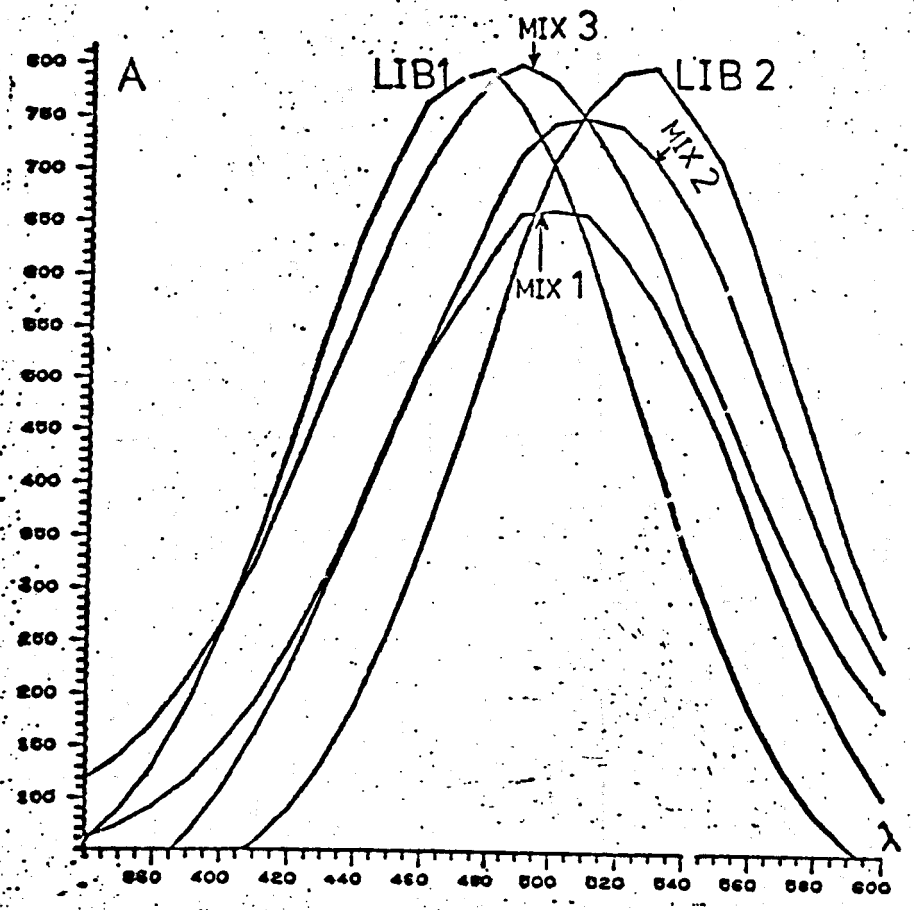

(ii) A discrepancy plot, ΔA vs. λ, for the spectra shown above

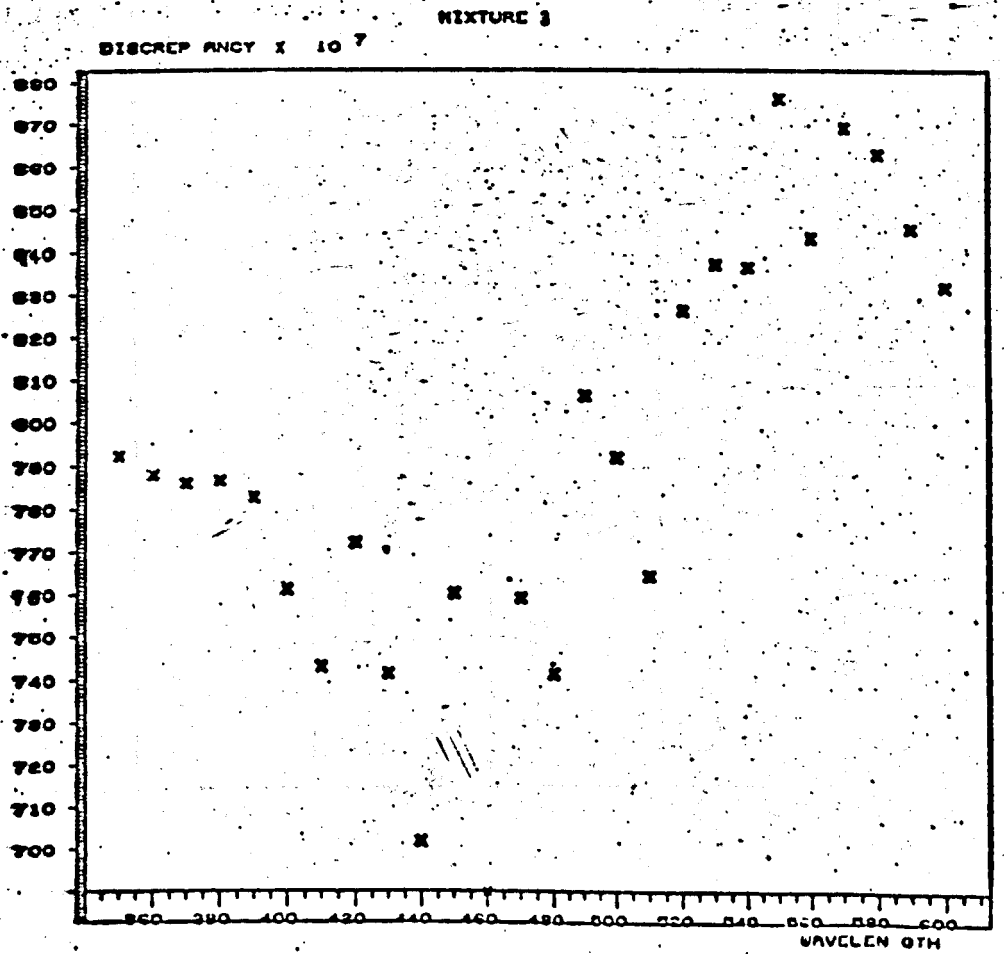

TABLE 4.1

Results Obtained in Testing "SOLVE" (see Section 4.3.2)

		No Weighting				Weighting $\propto \lvert A1 - A2 \rvert$			
		C_1	C_2	(C_1+C_2)	rms discrepancy	C_1	C_2	(C_1+C_2)	rms discrepancy
Case (i)	MIX 1	0.333	0.667	1.000	0.140×10^{-13}	0.333	0.667	1.000	0.874×10^{-14}
	MIX 2	0.500	0.500	1.000	0.117×10^{-13}	0.500	0.500	1.000	0.635×10^{-14}
	MIX 3	0.667	0.333	1.000	0.913×10^{-14}	0.667	0.333	1.000	0.135×10^{-13}
Case (ii)	MIX 1	0.318	0.676	0.994	0.125×10^{-4}	0.317	0.681	0.998	0.126×10^{-4}
	MIX 2	0.492	0.508	1.000	0.117×10^{-4}	0.494	0.510	1.004	0.118×10^{-4}
	MIX 3	0.671	0.320	0.991	0.977×10^{-5}	0.669	0.322	0.991	0.979×10^{-5}
Case (iii)	MIX 1	0.378	0.699	1.077	0.210×10^{-4}	0.376	0.706	1.082	0.212×10^{-4}
	MIX 2	0.455	0.468	0.923	0.210×10^{-4}	0.457	0.461	0.918	0.212×10^{-4}
	MIX 3	0.757	0.398	1.155	0.421×10^{-4}	0.752	0.411	1.163	0.423×10^{-4}
Case (iv)	MIX 1	0.384	0.699	1.083	0.232×10^{-4}	0.372	0.710	1.082	0.240×10^{-4}
	MIX 2	0.452	0.473	0.925	0.245×10^{-4}	0.460	0.441	0.901	0.236×10^{-4}
	MIX 3	0.759	0.403	1.162	0.432×10^{-4}	0.759	0.400	1.159	0.457×10^{-4}
Case (v)	MIX 1	0.376	0.701	1.077	0.217×10^{-4}	0.376	0.705	1.081	0.213×10^{-4}
	MIX 2	0.453	0.469	0.722	0.212×10^{-4}	0.457	0.461	0.918	0.214×10^{-4}
	MIX 3	0.758	0.395	1.153	0.423×10^{-4}	0.750	0.411	1.161	0.431×10^{-4}

the unweighted scheme. Since baseline errors can be recognised from the discrepancy plots and compensated for if necessary, the weighted program was adopted in all further work.

4.4 The Spectra for the DNA-Phenanthridine Complexes

The absorption spectra of the three phenanthridine drugs under consideration were measured when bound to three naturally occurring DNA types of differing G-C content (Section 2.1.1), and these results were repeated using low and high ionic concentrations (Section 2.1.2). Although binding studies of DNA-ethidium complexes have been reported previously (e.g. Waring, 1965; Paoletti and Le Pecq, 1971; Plumbridge and Brown, 1977), none of these have investigated the binding in such detail. The scheme adopted here ensures a large number of data points on the Scatchard plot for each spectral series. Analysis using the excluded site model of McGhee and Von Hippel (1974) is shown to provide a better fit to the data than the classical analysis used in the earlier studies, and a detailed consideration of the binding specificity has been made possible by analysing the binding to several DNA types. The binding of dimidium and prothidium has not been reported previously, and a similarly detailed analysis has been performed for these drugs.

The mixing scheme employed (Section 2.3.1(b)) ensured that the results within each spectral series were self-consistent. Several of the series were repeated to check on the reproducibility of the results. In all cases, the values of the binding parameters obtained from the Scatchard plot with the repeated series agreed to within 2% of the values obtained with the corresponding initial series.

The spectroscopic results (marked with a '+') are displayed as a Scatchard plot for each spectral series, and they are supplemented by results obtained from equilibrium dialysis (marked with a 'X').

4.4.1 Ethidium Bromide

4.4.1(a) The Results

The metachromatic shift of the absorption spectrum of ethidium bromide in the presence of DNA is shown in Figs. 4.9(i) and 4.13(i), for a series

of binding ratios r. Minor differences were evident between the shifts produced by the different DNA's, but the general effect was the same. The absorption spectrum was shifted from 478nm to 519nm with calf thymal DNA, and to 515-6nm for Cl. perfringens and M. lysodeikticus DNA's. Good isosbestic points were obtained for all three DNA types - at 510nm for calf thymal DNA, and at 506nm* for the other two DNA's, suggesting the existence of only one (spectroscopically distinct) bound mode. The effect of binding was visible as a change in colour, from yellow-orange (free drug) to bright pink (bound drug). The binding appeared to be almost instantaneous, as judged from the change in colour. Nevertheless, the protocol described in Section 2.3.1(b) was adhered to, so as to put all the readings on the same basis.

Similar spectral series were obtained at both low and high ionic concentration; good isosbestism was evident in both instances, and at the same wavelength, for the same variety of DNA. At low binding ratios the absorption spectra for the two cases are identical, but at a high degree of binding ($r \gtrsim 0.2$) the spectra at high ionic concentration are shifted towards the blue and are more intense than those taken at low salt concentration. This effect will be apparent as giving rise to smaller values of r_{max}, the saturation binding level, and consequently to larger values of n_{app}, the apparent binding site size.

Each spectral series was analysed to determine the concentrations of the free and bound components at each binding ratio. The analysis in terms of one bound species, instead of two, was justified by the existence of a well-defined isosbestic point in each case. Examples of the binding curves (r vs. c) are shown in Figs. 4.9(ii) and 4.13(ii). In each case, the value of r rises sharply with c, and then assumes a steady value within

---

* The lower wavelength values for the shifted library 2 spectra and for the isosbestic points, for Cl. perfringens and M. lysodeikticus, may reflect the lower wavelength at which maximum absorbance was found to occur for these DNA types (Section 2.1.1).

Fig. 4.9 (i) Absorption spectra for ethidium bromide binding to calf thymal DNA at low ionic concentration

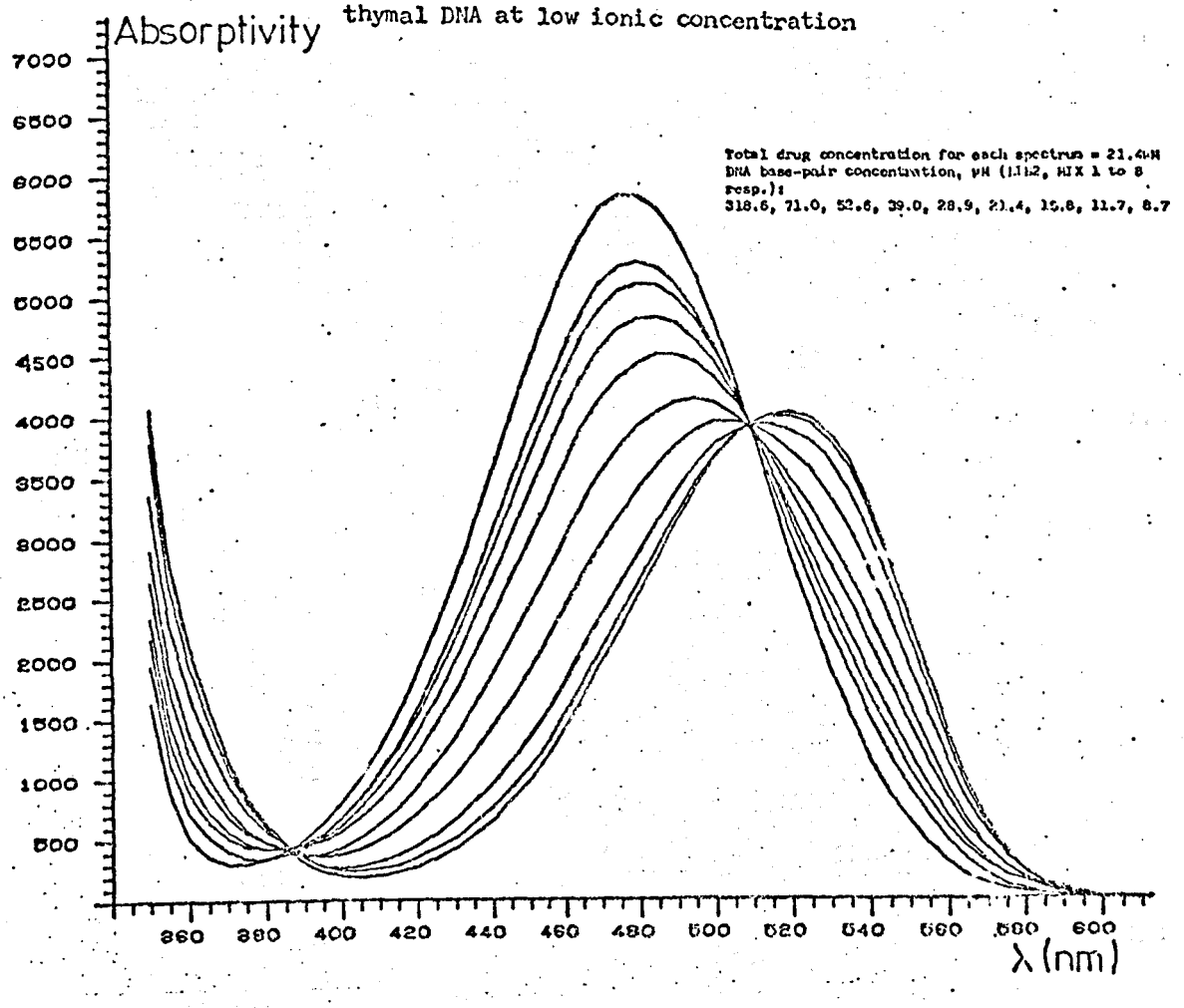

(ii) The binding curve, r vs. c, for the spectra shown above

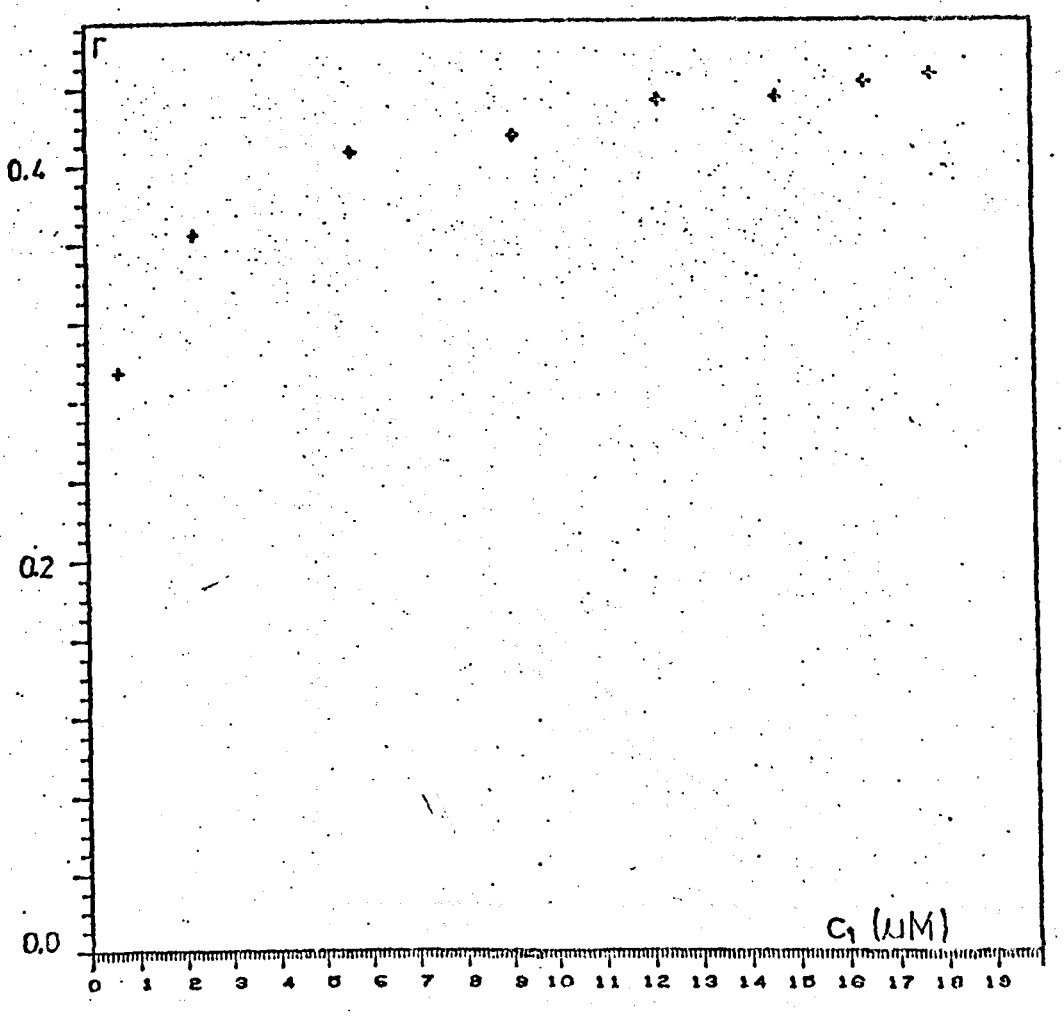

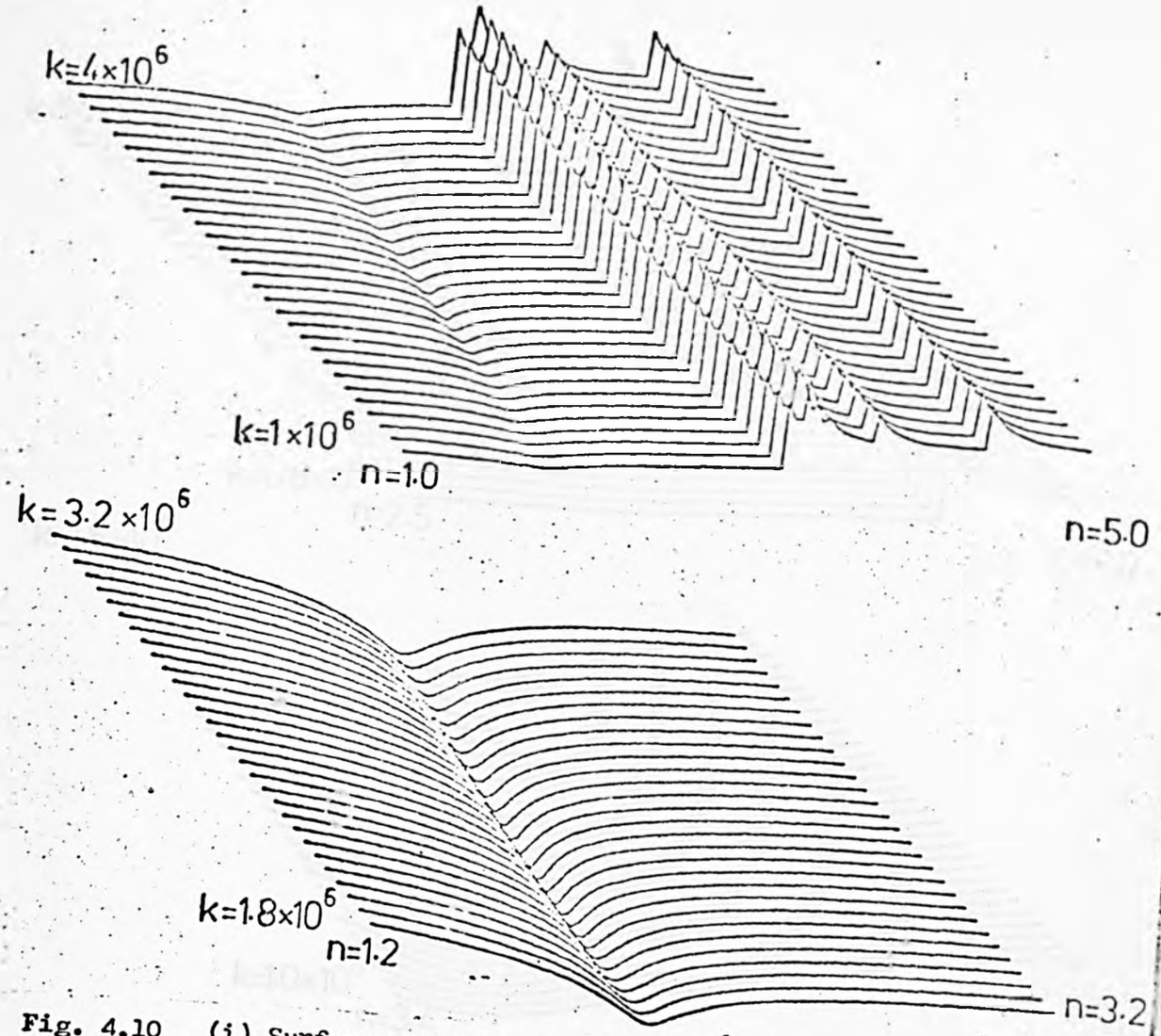

Fig. 4.10 (i) Surface plots for ethidium bromide binding to calf thymal DNA at low ionic concentration

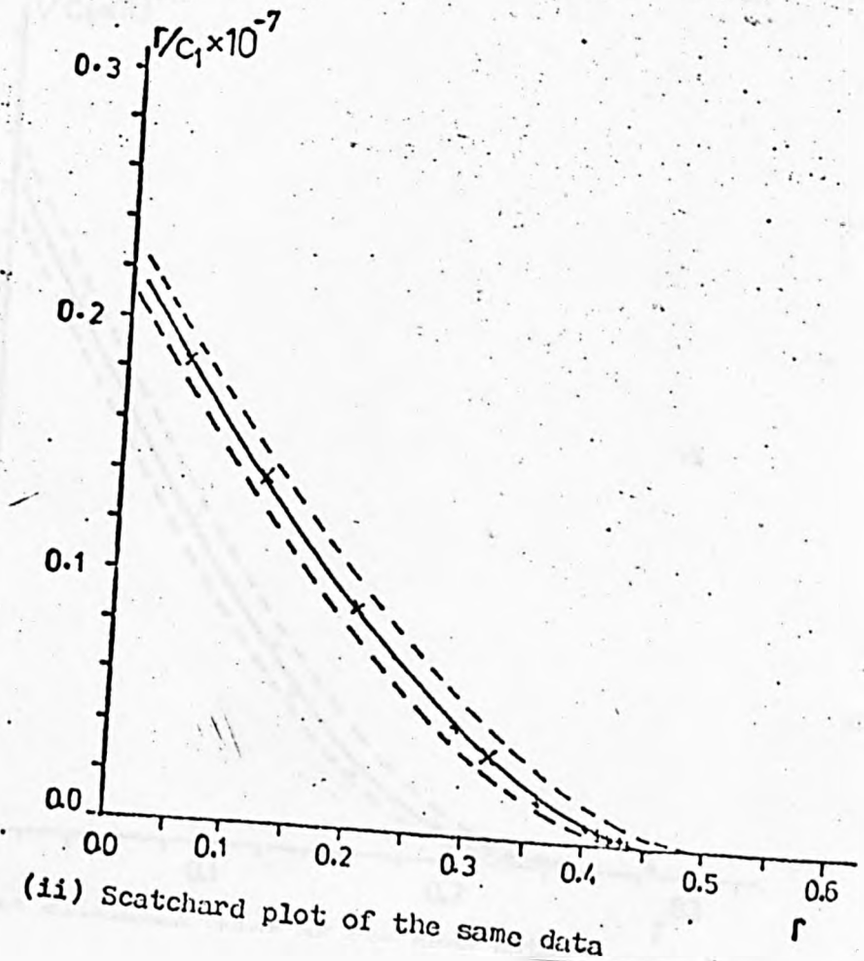

(ii) Scatchard plot of the same data

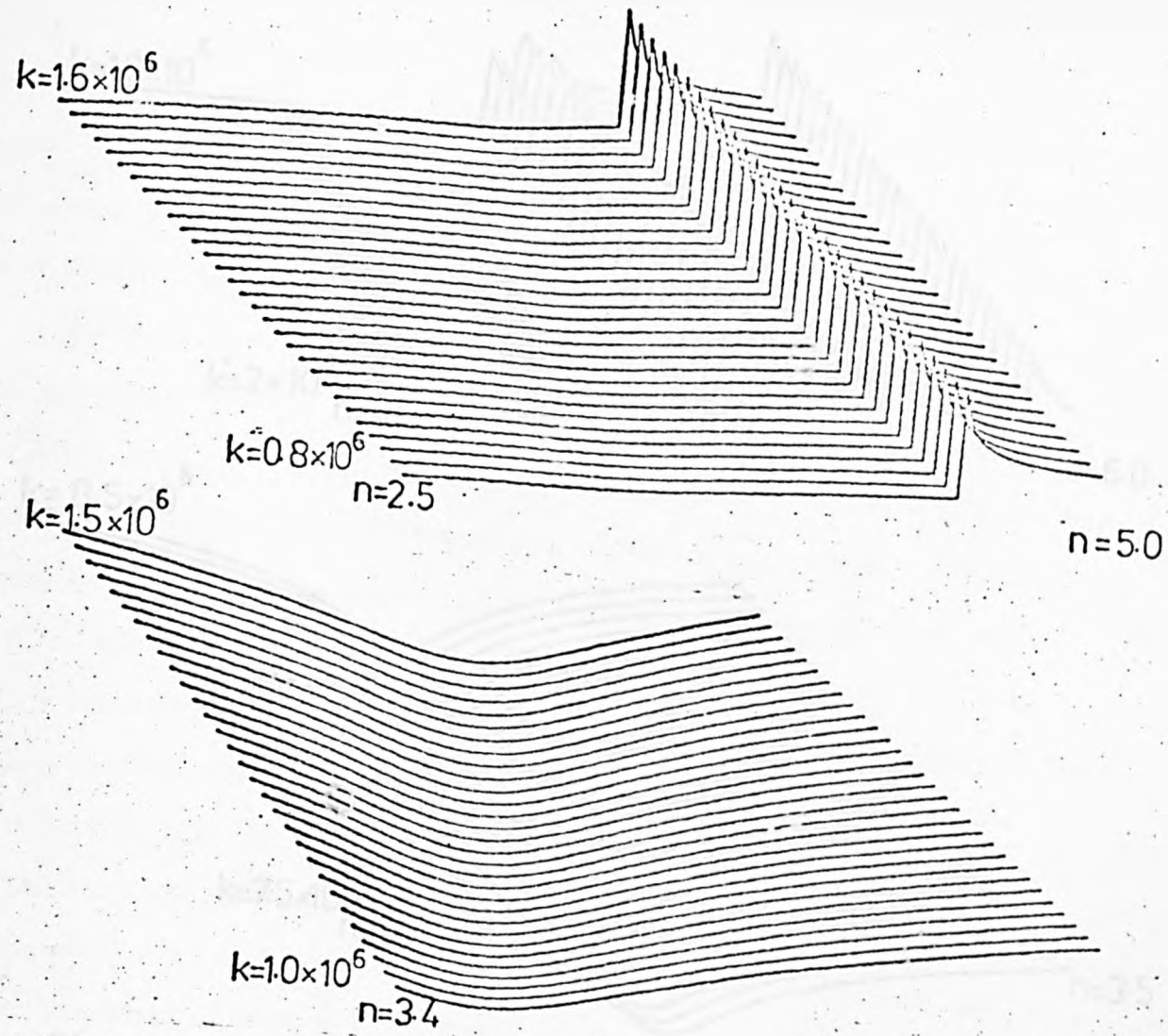

Fig. 4.11 (i) Surface plots for ethidium bromide binding to Cl. perfringens DNA at low ionic concentration

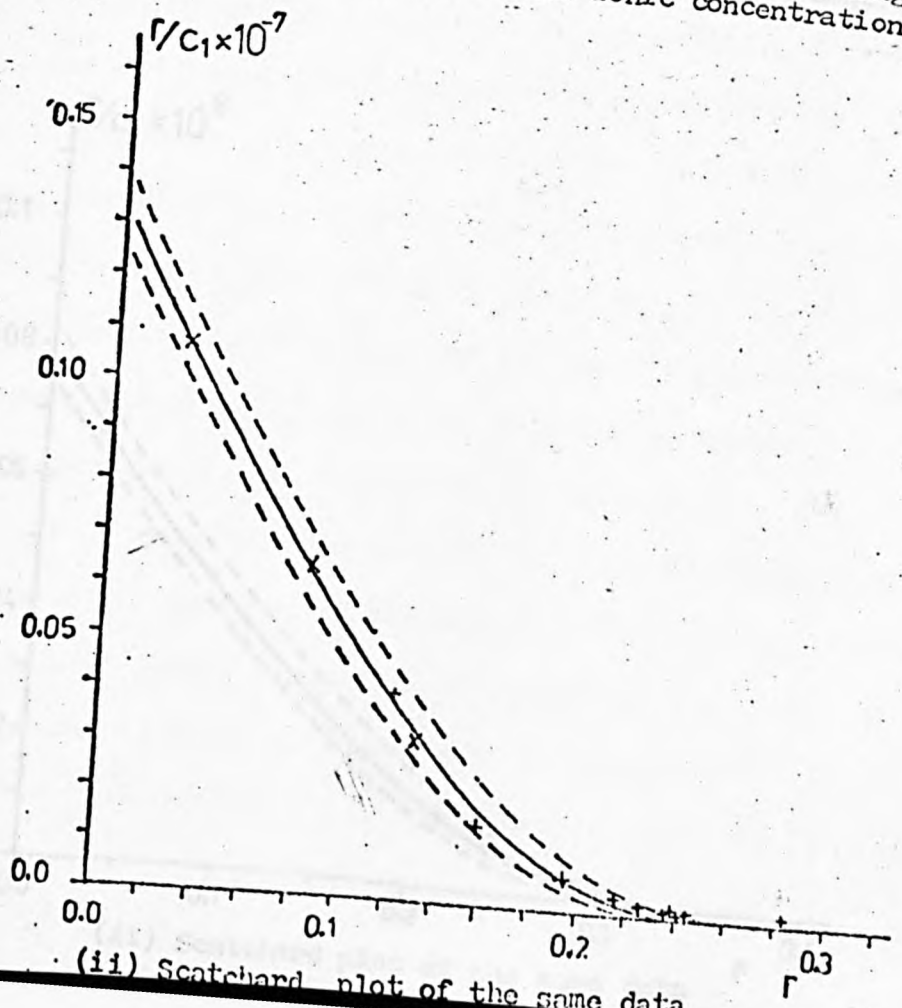

(ii) Scatchard plot of the same data

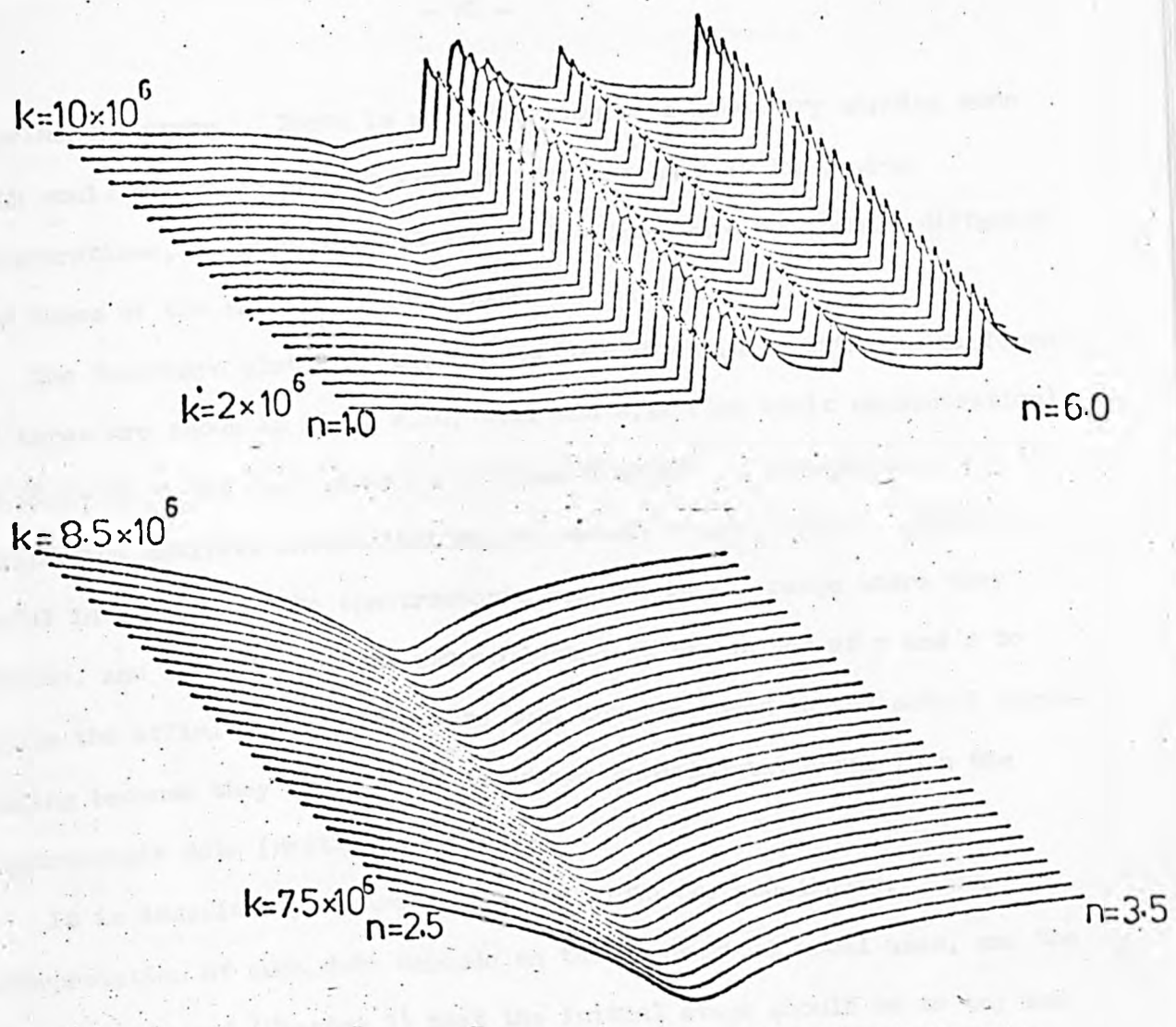

Fig. 4.12 (i) Surface plots for ethidium bromide binding to M. lysodeikticus DNA at low ionic concentration

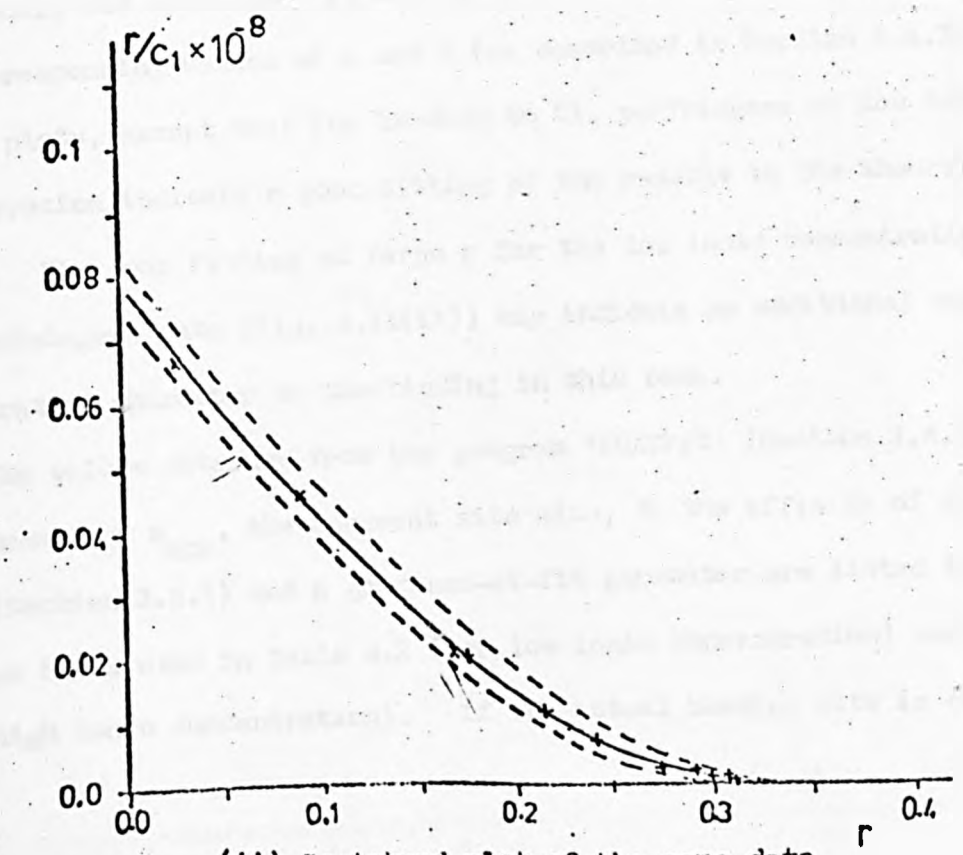

(ii) Scatchard plot of the same data

experimental error. There is no indication of a secondary binding mode which would have been evident from an increase in r at large drug concentrations, c, provided that its n, k values were reasonable different from those of the primary binding mode.

The Scatchard plots for the interaction of ethidium with the different DNA types are shown in Figs. 4.10, 4.11 and 4.12 (low ionic concentration) and Figs. 4.14 and 4.15 (high ionic concentration). The results from the equilibrium dialysis investigations are marked on each graph. They are useful in confirming the spectroscopic results in the range where they overlap, and in verifying the extrapolation at low values of r and c to obtain the affinity, α. They were not, however, used in the actual curve-fitting because they are subject to larger experimental error than the spectroscopic data (Section 2.3.2(b)).

It is immediately apparent that the plots are non-linear. The interpretation of such data depends on the theoretical model used, and the author has argued (Chapter 3) that the initial stage should be to try and fit the data to an excluded site model using Equation (3.6). The full lines superimposed on each plot represent the best-fitting of the data to this model, and the dashed lines represent the effect of 5% deviations in the corresponding values of n and k (as described in Section 3.4.3). All of the plots, except that for binding to Cl. perfringens at low ionic concentration indicate a good fitting of the results to the theoretical model. The poor fitting at large r for the low ionic concentration Cl. perfringens data (Fig. 4.11(ii)) may indicate an additional anti-co-operative character to the binding in this case.

The values obtained from the program 'SCATFIT' (Section 3.4.3) for the parameters n_{app}, the apparent site size, α, the affinity of an isolated site (Section 3.5.1) and a goodness-of-fit parameter are listed for the various DNA's used in Table 4.2 (for low ionic concentration) and Table 4.3 (for high ionic concentration). If the actual binding site is determined

Fig. 4.13 (i) Absorption spectra for ethidium bromide binding to calf thymal DNA at high ionic concentration

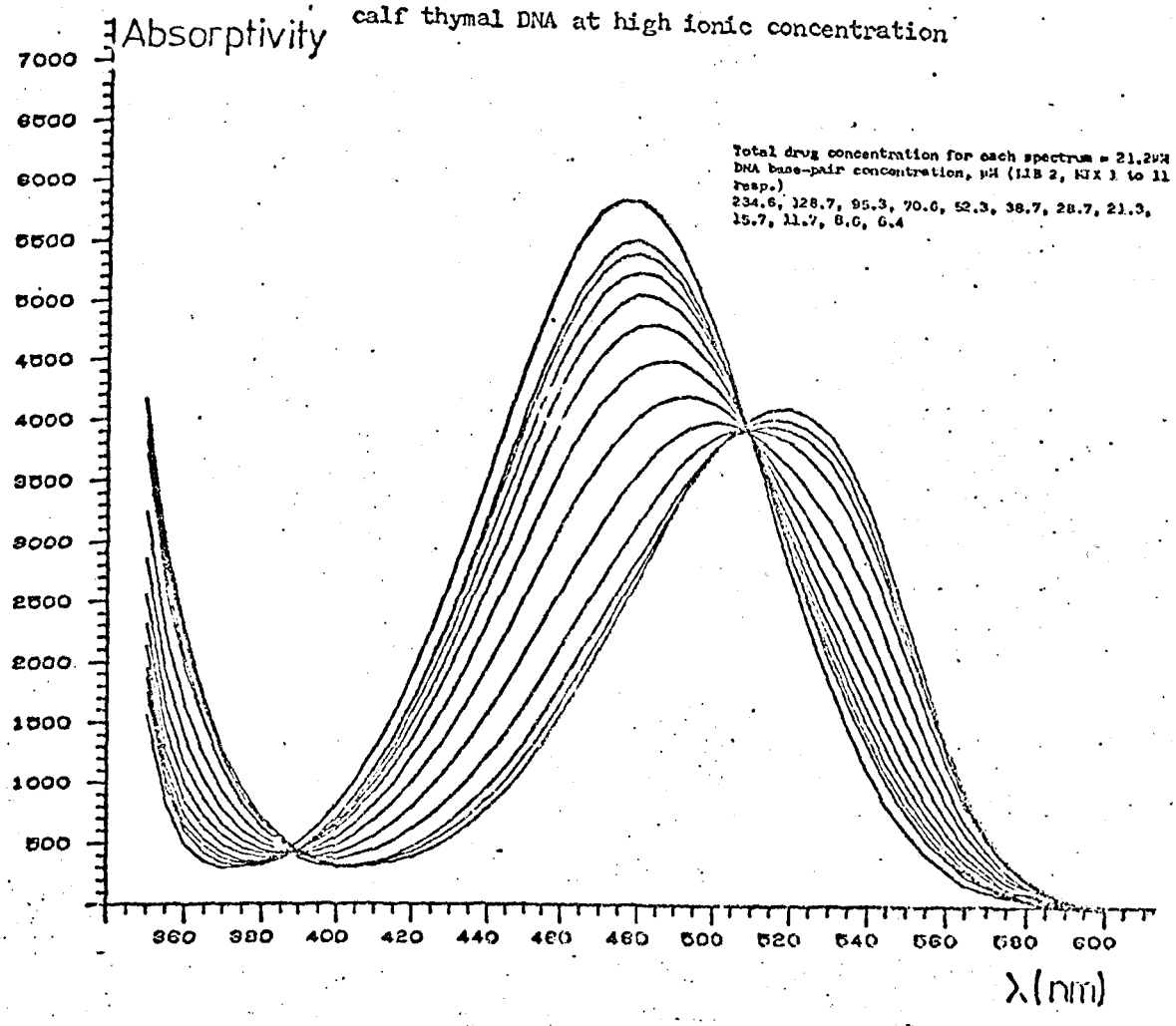

(ii) The binding curve, r vs. c_f, for the spectra shown above

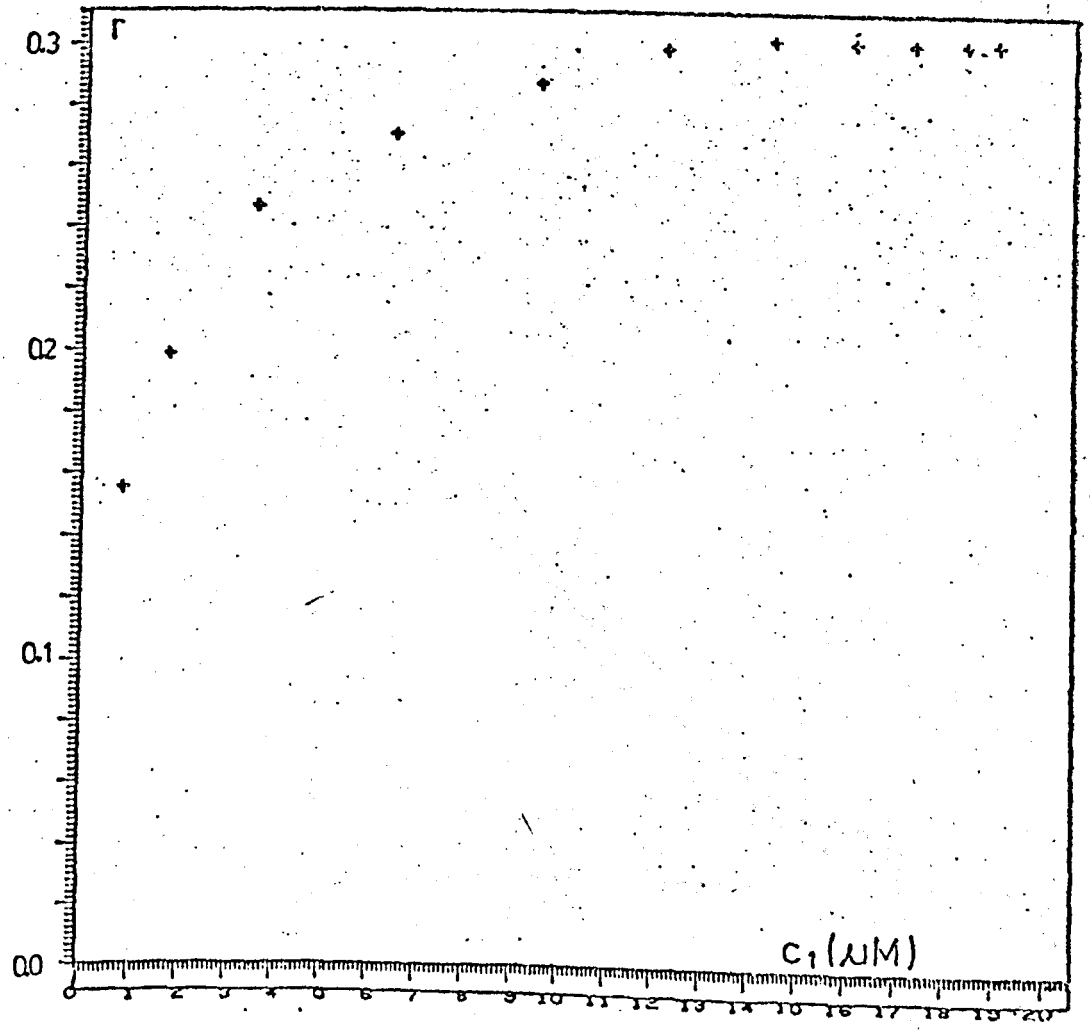

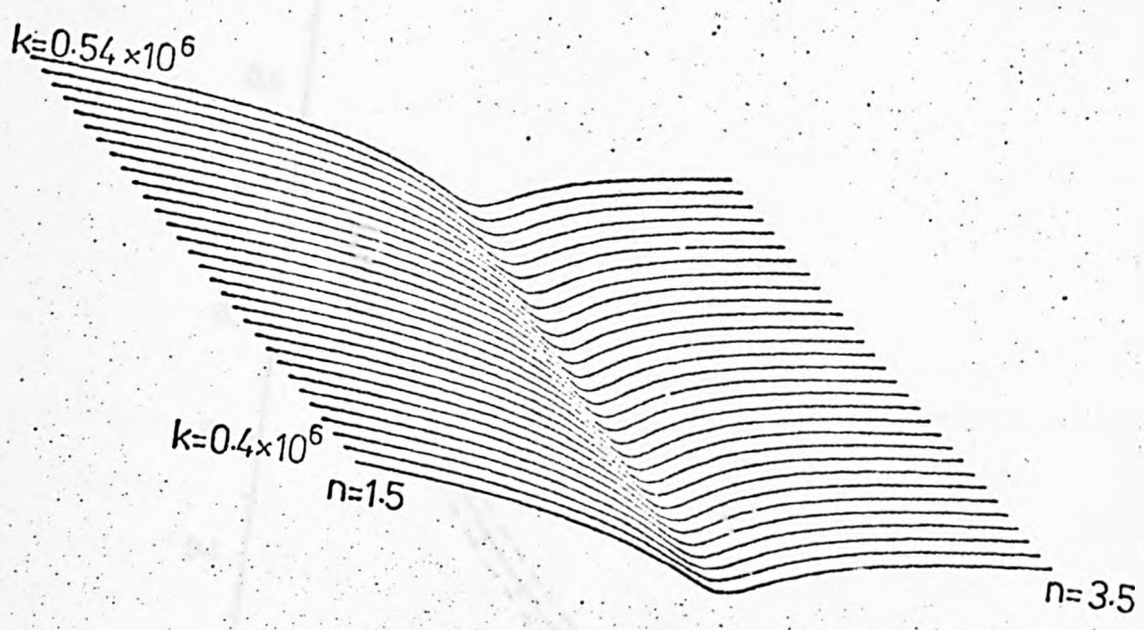

Fig. 4.14 (i) A surface plot for ethidium bromide binding to calf thymal DNA at high ionic concentration

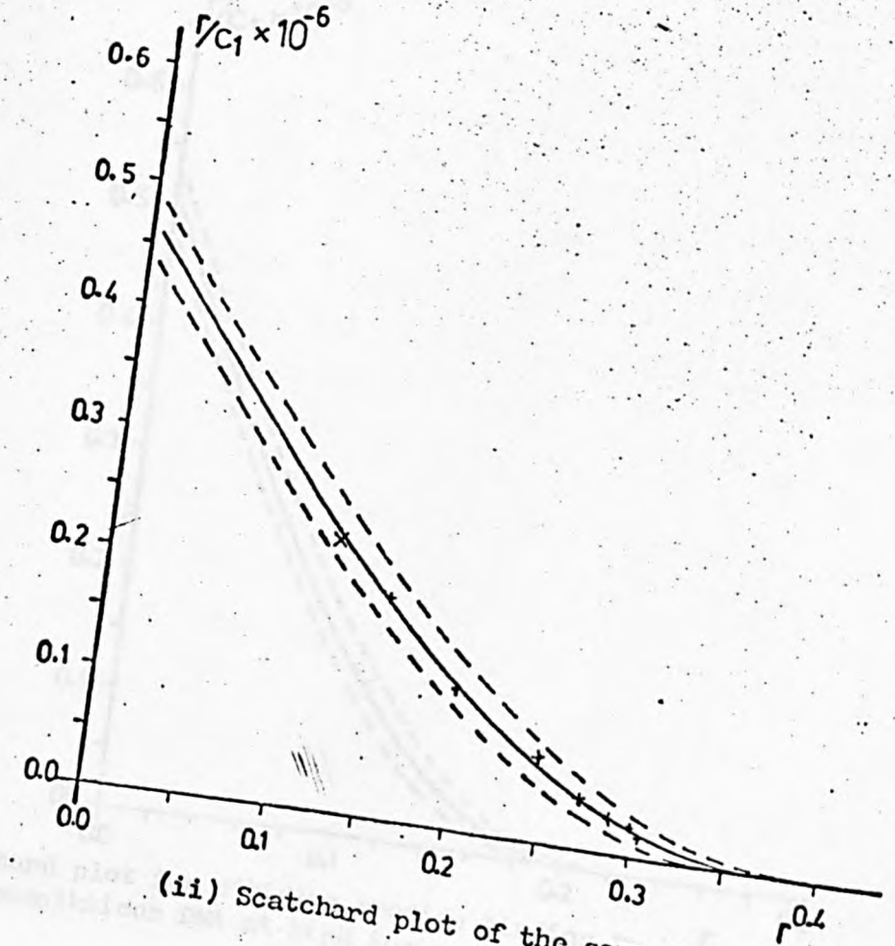

(ii) Scatchard plot of the same data

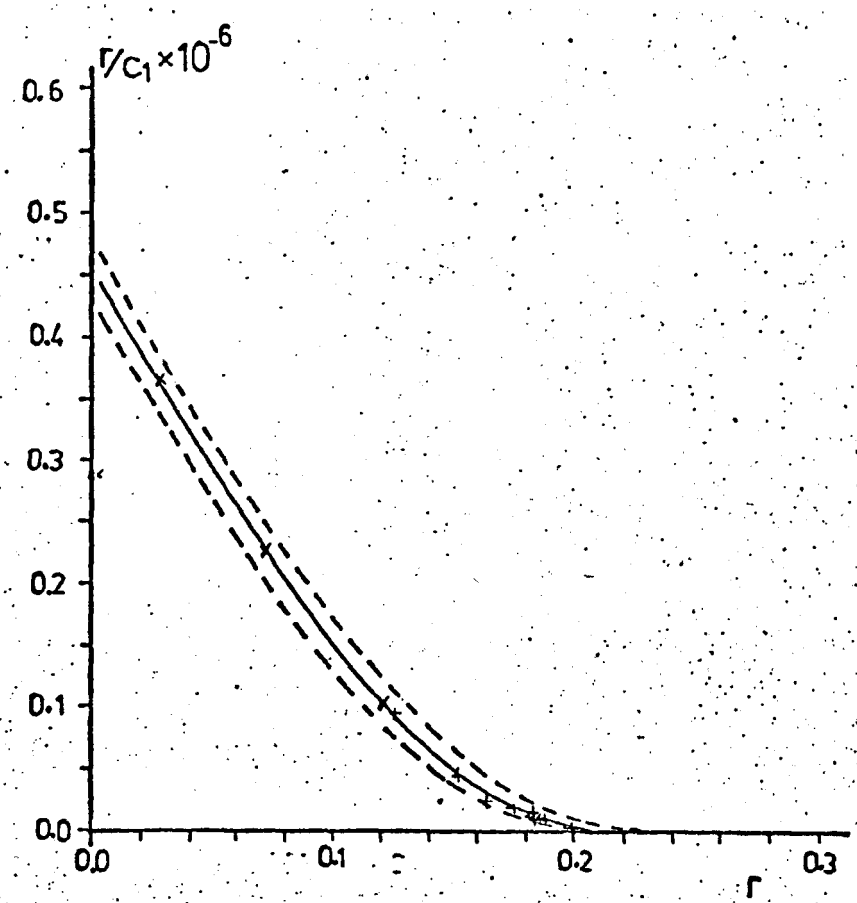

Fig. 4.15 (i) Scatchard plot for ethidium bromide binding to Cl. perfringens DNA at high ionic concentration

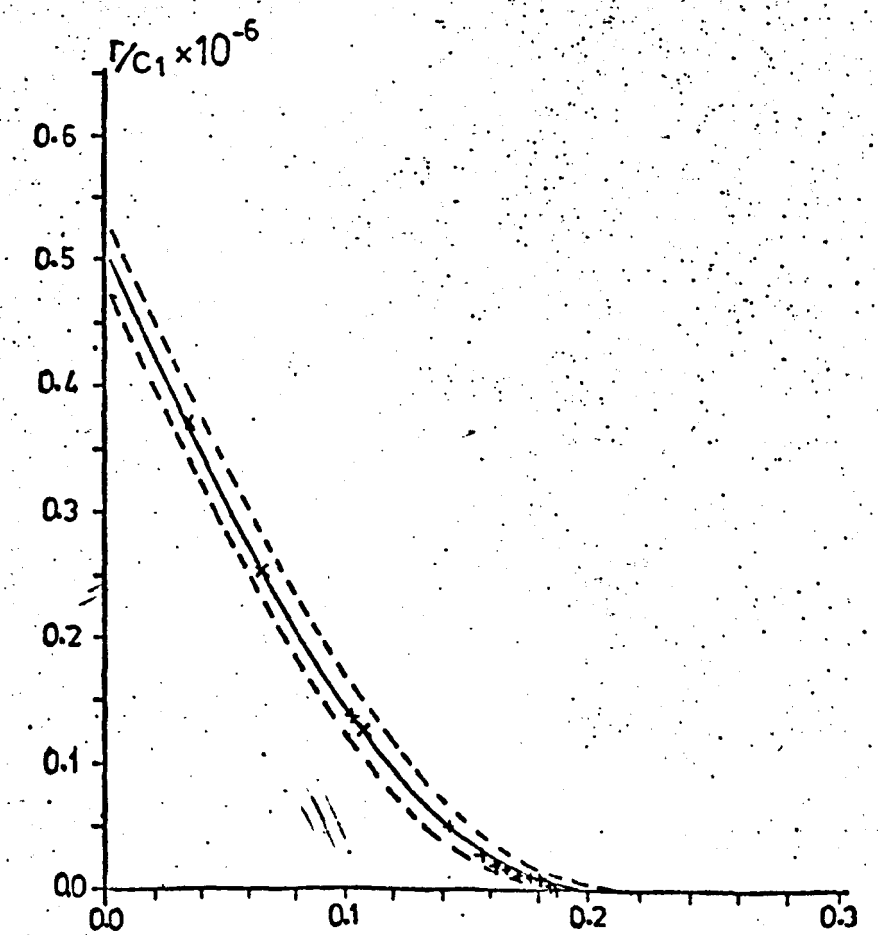

(ii) Scatchard plot for ethidium bromide binding to M. lysodeikticus DNA at high ionic concentration

TABLE 4.2

Best-Fit Parameters for Ethidium Bromide binding to DNA at low ionic concentration: f is the fractional G-C content

DNA type	n_{app}	Affinity, α (= P.k)	Goodness-of-fit parameter
Cl. perfringens (f=0.30)	3.86	1.33×10^6	0.125
Calf thymus (f=0.42)	2.13	2.20×10^6	0.010
M. lysodeikticus (f=0.72)	2.97	7.90×10^6	0.049

TABLE 4.3

Best-Fit Parameters for Ethidium Bromide binding to DNA at high ionic concentration

DNA type	n_{app}	Affinity, α (= P.k)	Goodness-of-fit parameter
Cl. perfringens (f=0.30)	4.33	4.54×10^5	0.007
Calf thymus (f=0.42)	2.74	4.77×10^5	0.170
M. lysodeikticus (f=0.72)	4.64	5.10×10^5	0.001

by a number of specific bases then, in a heteropolymer such as DNA, r_{app} (the apparent size of a binding site) will be larger than n (the actual site size) since it will also account for the bases to which the drug does not bind. For example, if a drug were to show an outright specificity for a G-C base-pair n_{app} would be much larger than two for Cl. perfringens DNA since there is a 40% likelihood that a second G-C base-pair will be located further than two base-pairs away from the first G-C. In fact, application of Equation (3.9) would indicate a value of about four for n_{app} in this example.

4.4.1(b) Discussion of Results

The values for α are in agreement with those of the previous, more limited binding studies of Waring (1965), Paoletti and Le Pecq (1967) and Plumbridge and Brown (1977). The n_{app} values are generally lower than those obtained previously, but this reflects the method of analysis used here. If an attempt was made to fit data presented here to the classical analysis, by fitting a straight line to the data at low r, a lower intercept (r_{max}) and hence a larger value for n_{app} would result. The values obtained for n_{app} and α are mean binding parameters, averaged over the microscopic binding constants for all possible sites, since Equation (3.6) considers the DNA as a homogenous one-dimensional lattice of possible binding sites. The values for n_{app} and α may be expected to reflect, albeit crudely, the relative abundances of the ten different binding sites available in an heterogeneous DNA molecule (Section 3.5).

The values of the affinity α, show a correlation with G-C content. In particular, the binding appears to be tighter (i.e. the association constant is larger) with species rich in G-C. This specificity is much more marked at low ionic strength, where there is a factor of nearly 6 between the values for M. lysodeickticus and those for Cl. perfringens. At high ionic strength, this factor is only 1.12, and the association constants are all lower than those obtained at low ionic strength.

At high ionic strength the binding saturates at a lower binding level e.g. with calf thymal DNA, binding saturates at $r \approx 0.3$ at high ionic concentration, whereas it continues to $r \approx 0.45$ at low ionic concentration. This reduction in binding with increased ionic strength has been reported previously (Waring, 1965; Le Pecq and Paoletti, 1967; Porumb, 1976), and can be explained in terms of the positive charge on ethidium at this pH due to its quaternised nitrogen at position 5 (Fig. 1.3). If the binding has an electrostatic character (i.e. there is either a distinct electrostatically bound species, or there is an electrostatically bound stage en route to the finally bound species), competition with the sodium cations of the buffer will affect the drug binding. In particular, at high ionic concentration more phosphate anions will be screened by the sodium cations and binding of the charged drug will be inhibited. The lower values of k at high ionic concentration indicate a less stable DNA-drug complex at high salt content.

The nature of the G-C preference can be investigated by plotting the affinities for various DNA types as a function of the fractional G-C content (Fig. 4.16). At low ionic strength, the variation of α with f is faster than linear and resembles an f^2 variation (Fig. 3.18). The ratios of the experimental affinities correlate best with the theoretical ratios assuming an f^2 variation (Table 4.4). A plot of log α against log f (Fig. 4.17) shows that the data could be fitted to a straight line of gradient 2.03 ± 0.05, which is a strong indication of the f^2 dependence. Thus it appears that ethidium prefers to bind at low ionic strength to a sequence of two G-C pairs, although the precise nature of this sequence specificity cannot be ascertained (viz. whether GpC, CpG, GpG or CpC).

At high ionic strength, the results are more difficult to interpret. Fig. 4.16 indicates that the variation of α with f may be according to $(2f - f^2)$, but Table 4.4 indicates that the variation in α is much less than required for this model. It would appear that the specificity for

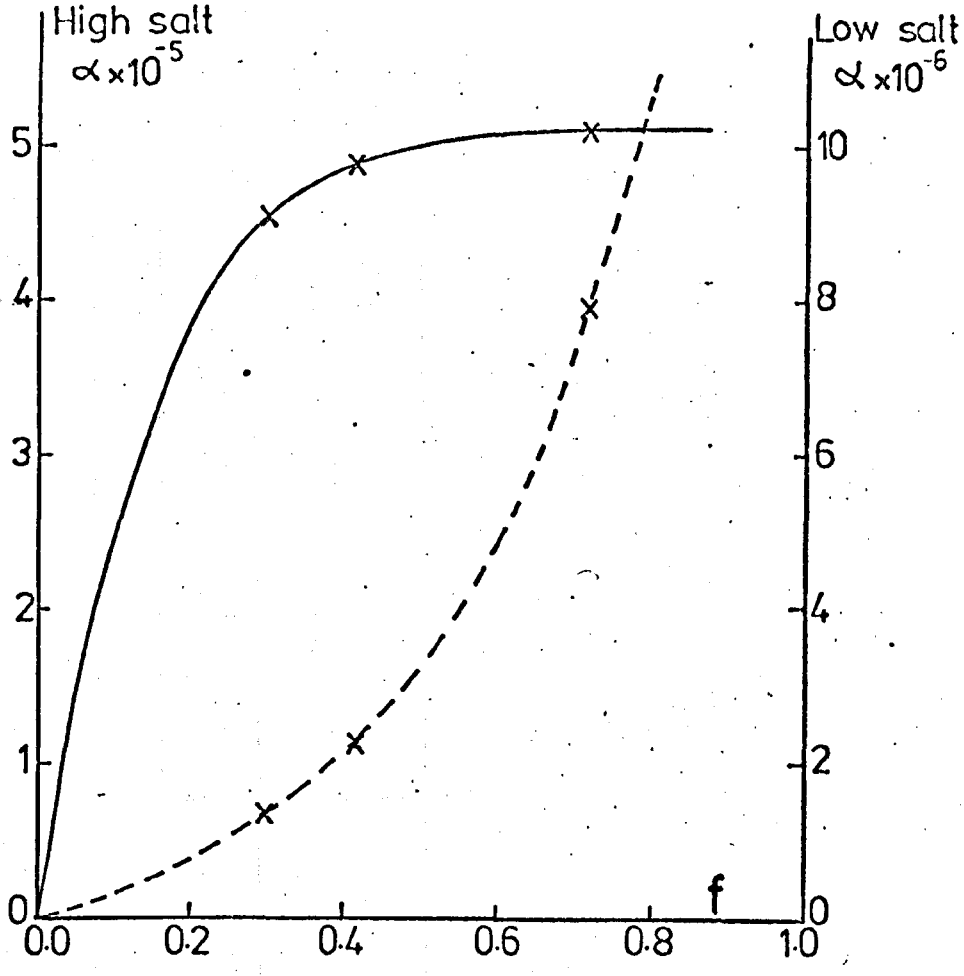

Figure 4.16 The affinity, α, as a function of the fractional G-C content, f, for ethidium bromide binding to DNA. The full curve indicates the results at high ionic concentration, and the broken curve shows the results at low ionic conc.

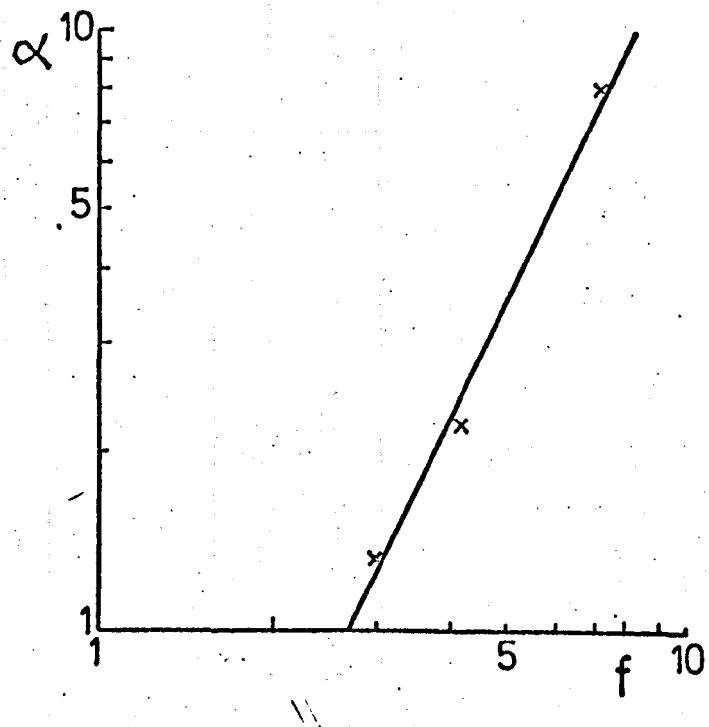

Figure 4.17 α vs. f plotted on a logarithmic scale, for ethidium binding to DNA at high ionic concentration

TABLE 4.4

A Comparison of the Ratios of the Theoretical Affinities for Binding to Different DNA Types with those Obtained Experimentally using Ethidium Bromide

	Theoretical			Experimental	
	$P=f$	$P=f^2$	$P=2f-f^2$	At low salt Concentration	At high salt Concentration
M.lysodeikticus/Calf thymus	1.71	2.94	1.39	3.59	1.07
M.lysodeikticus/Cl. perfringens	2.40	5.76	1.81	5.94	1.12

G-C base-pairs at this ionic concentration is only slight, and that binding probably occurs to both G-C and A-T pairs with only marginally differing association constants. It could be that at low ionic strengths, when competition with the sodium ions for binding is not so severe, ethidium has sufficient binding sites available (at least at low binding ratios) for it to exercise its sequence specificity for two G-C pairs; but at higher ionic strengths, so many phosphate groups are screened by sodium cations that the drug cannot find its preferred binding site (viz. two G-C's) and binds to those which it finds a little less favourable.

The variation of the experimentally determined values of n_{app} with the fractional G-C content should reflect this specificity, although the relationship is more complicated especially when n (the value of n_{app} for f = 1.0) is more than two (Section 3.5.1). The fact that n_{app} does not vary monotonically with f at either low or high salt concentration is of some concern, although similar variations to those obtained here have been reported for the binding of the peptide antibiotic echinomycin (Wakelin and Waring, 1976). The variation in n_{app} amongst the DNA varieties considered here is much less than the variation in k within the group, and values for the intercept r_{max} (from which the n_{app} values have been obtained) are notoriously inaccurate even when a large number of data points are taken at high values of r, because of the curvature of the Scatchard plot in this region. The value for Cl. perfringens at low ionic strength may also be affected by additional anti-co-operative effects, which could be due to repulsion between a bound drug molecule and a prospective binding molecule.

Another factor to be taken into account is the values taken for the maximum absorptivities of the three DNA types. A value of $6600 M^{-1} cm^{-1}$ has been assumed by the author for all three varieties. Various studies have reported a difference in absorptivity amongst DNA's of different type, but unfortunately there is no unanimity in their findings (Table 2.1.1). Müller and Crothers (1975) have suggested that the value should be higher

for M. lysodeikticus and lower for Cl. perfringens. If this were the case, the values of r (and therefore $\frac{r}{c_l}$) would be systematically shifted leading to an error in the determination of n_{app}. (The effect on k is not so great, since both r and $\frac{r}{c_l}$ values on the Scatchard plot are systematically shifted). However, the changes in the absorptivities suggested by Müller and Crothers (1975), if implemented, are only about 5% resulting in a shift of around 5% in n_{app}. This would not account for the strange variation in n_{app} with f reported here. It seems likely that, because the binding is more complicated than merely an absolute specificity for C-C, the theory adopted to explain the variation of n_{app} (or r_{max}) with f is inadequate. The more straightforward theoretical fluctuation of the affinity, α, with f, and the ability to determine α more accurately than n_{app}, would point towards the variation of α with f being a more reliable indicator of the binding specificity. The observation that n_{app} is appreciably increased, for all DNA types, at higher ionic concentration indicates an increased exclusion effect. This is probably due to the sodium cations occupying more of the phosphate sites and precluding binding at these sites, although it may also reflect conformational changes in the DNA at high ionic concentration which make the binding sterically less favourable.

4.4.2 Dimidium Bromide

4.4.2(a) The Results

The spectra obtained with dimidium bromide (e.g. Figs. 4.18(i) and 4.21(i)) are very similar to those recorded for ethidium bromide, as expected from their very similar chemical structures. Good isosbestic behaviour was observed, with the isosbestic points occuring at similar wavelengths (508 - 512nm) to those for ethidium. A similar trend to that obtained with ethidium was observed as the ionic concentration was increased. The spectra for large values of r at high ionic concentration were noticeably

Fig. 4.18 (i) Absorption spectra for dimidium bromide binding to calf thymal DNA at low ionic concentration

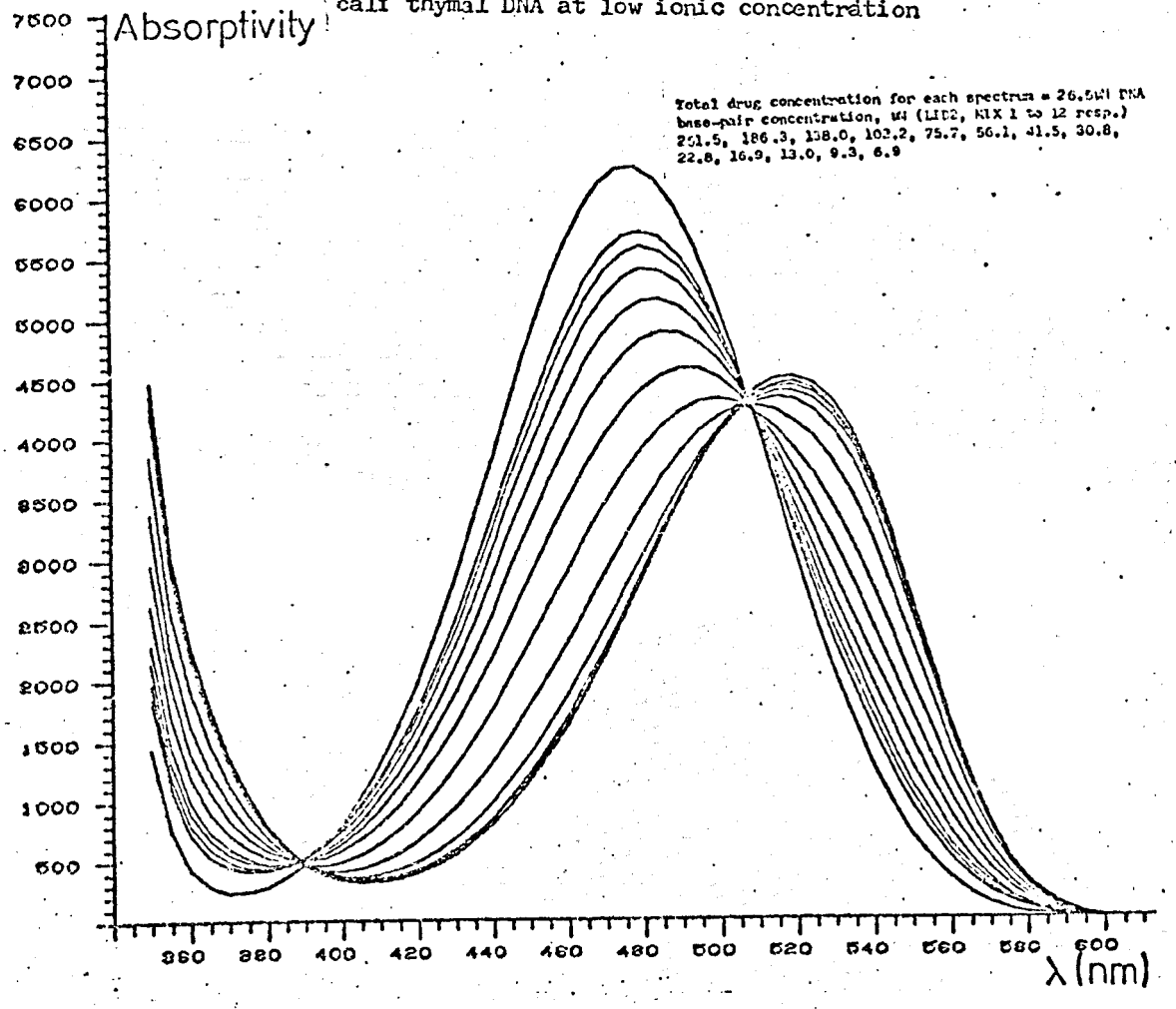

(ii) The binding curve, r vs. c, for the spectra shown above

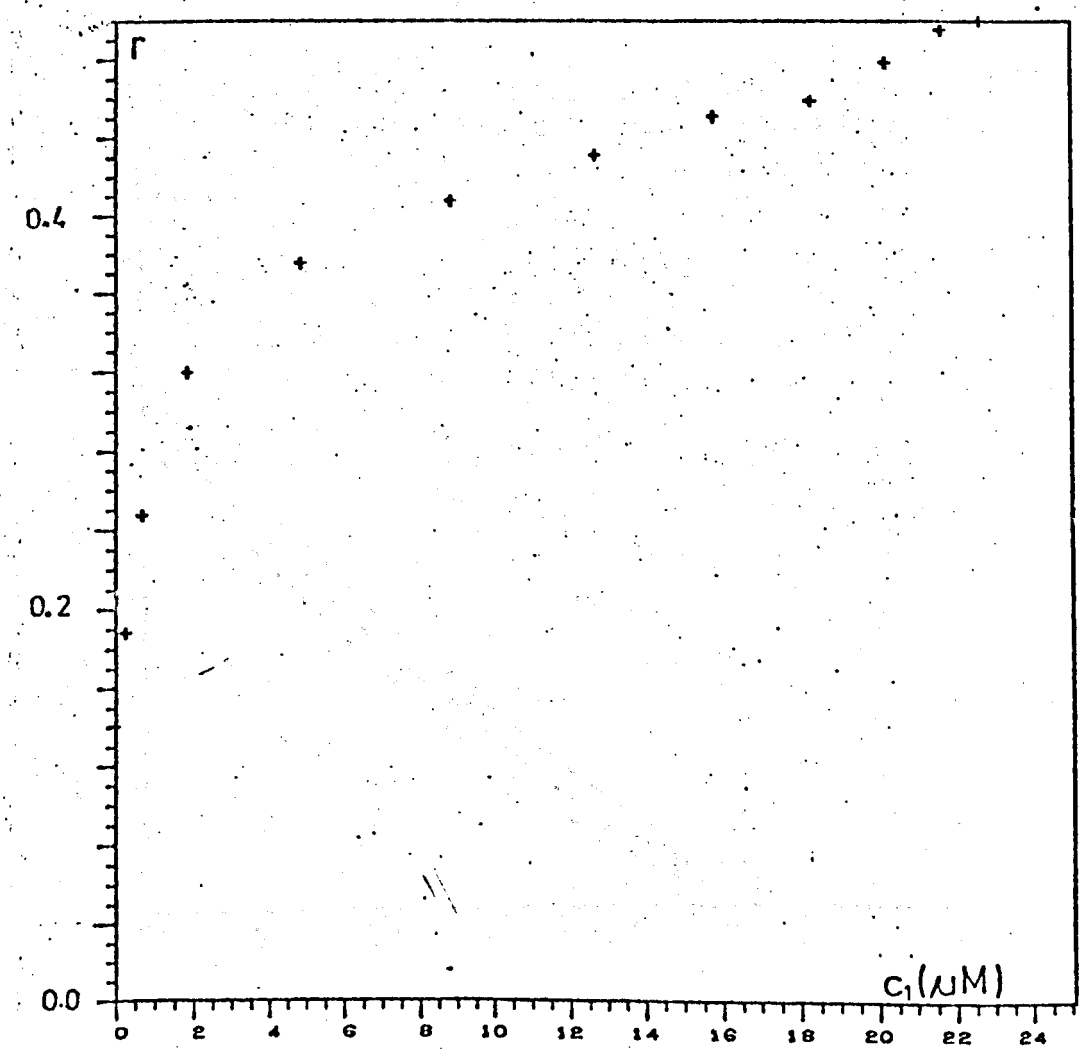

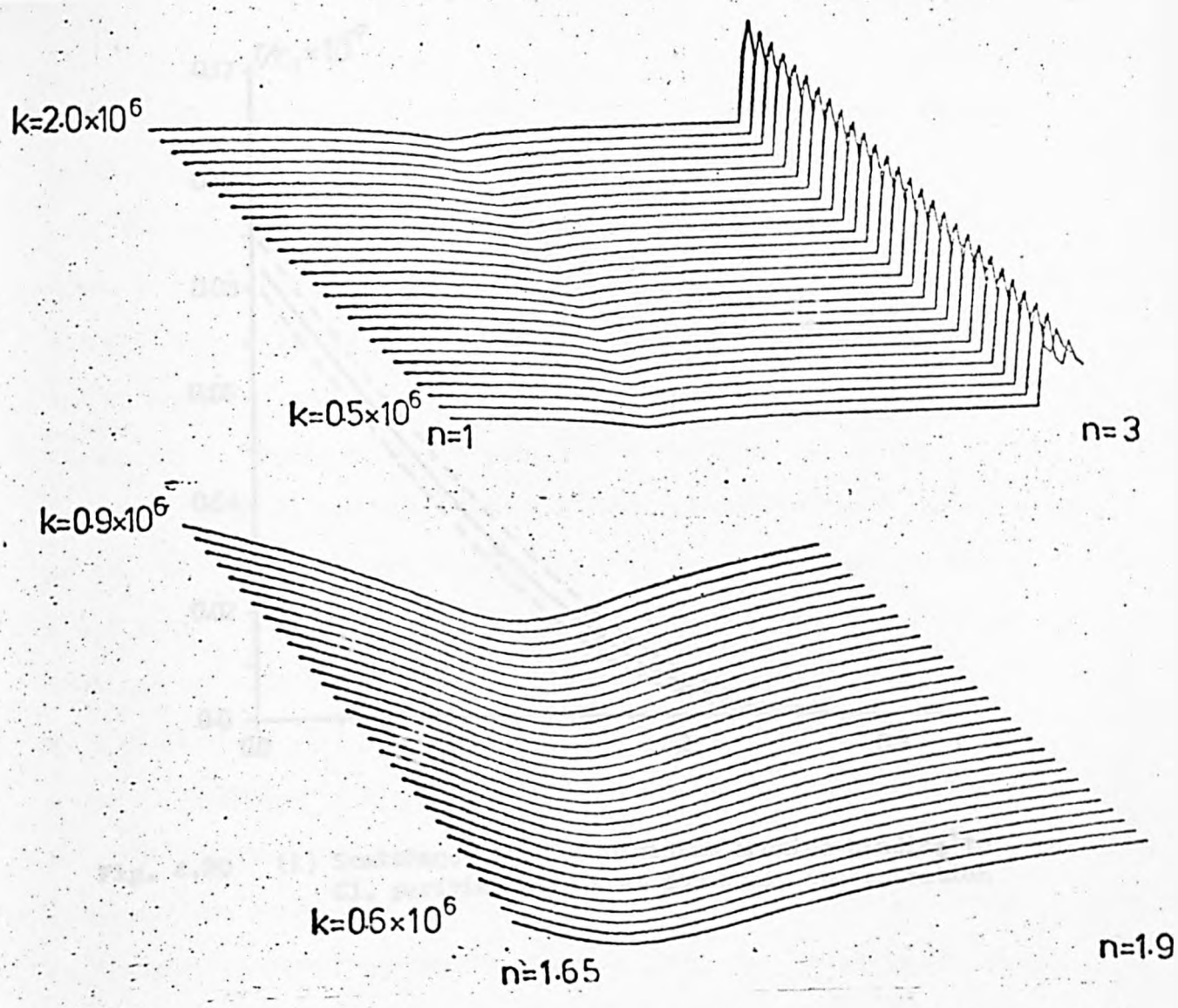

Fig. 4.19 (i) Surface plots for dimidium bromide binding to calf thymal DNA at low ionic concentration

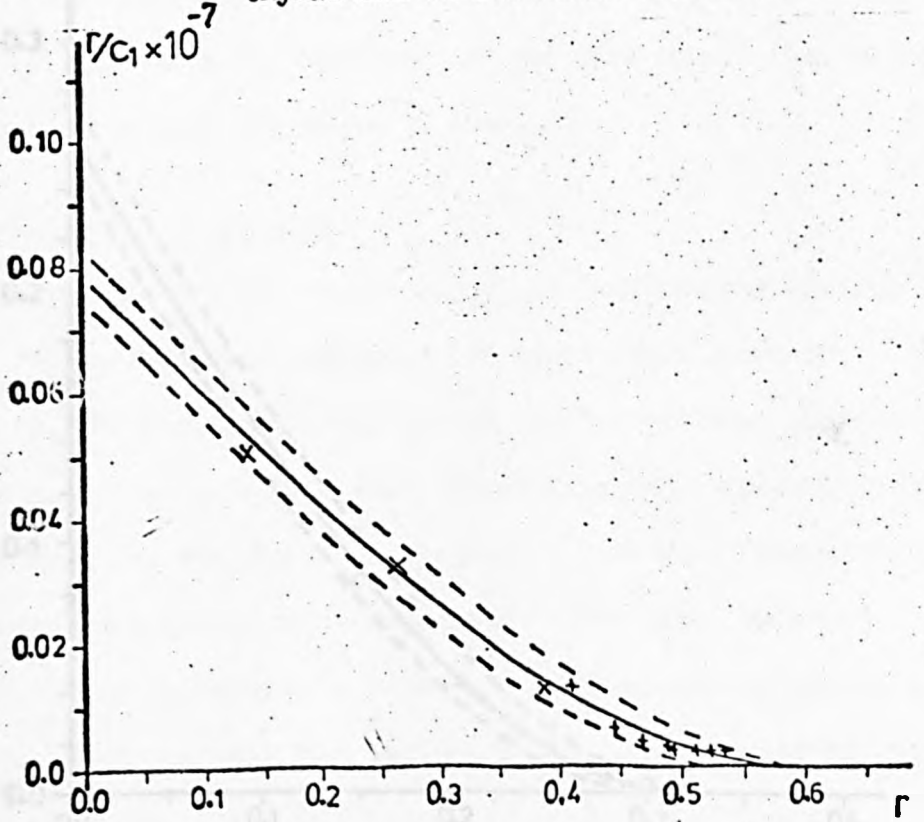

(ii) Scatchard plot of the same data

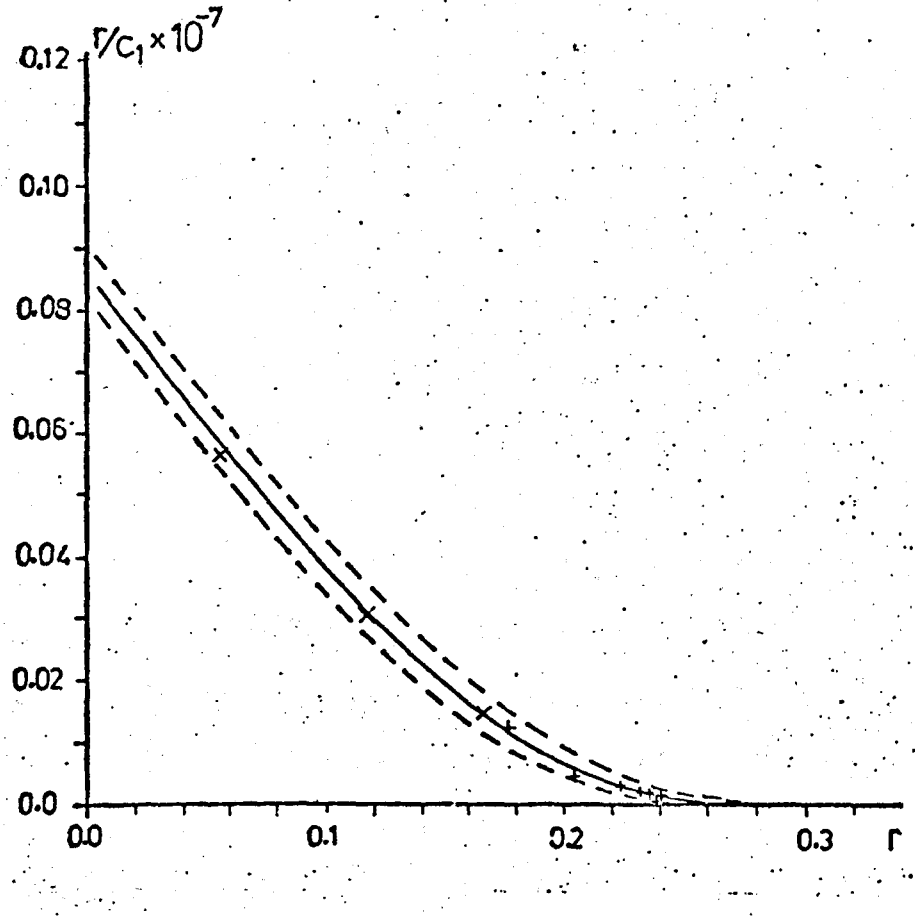

Fig. 4.20 (i) Scatchard plot for dimidium bromide binding to Cl. perfringens DNA at low ionic concentration

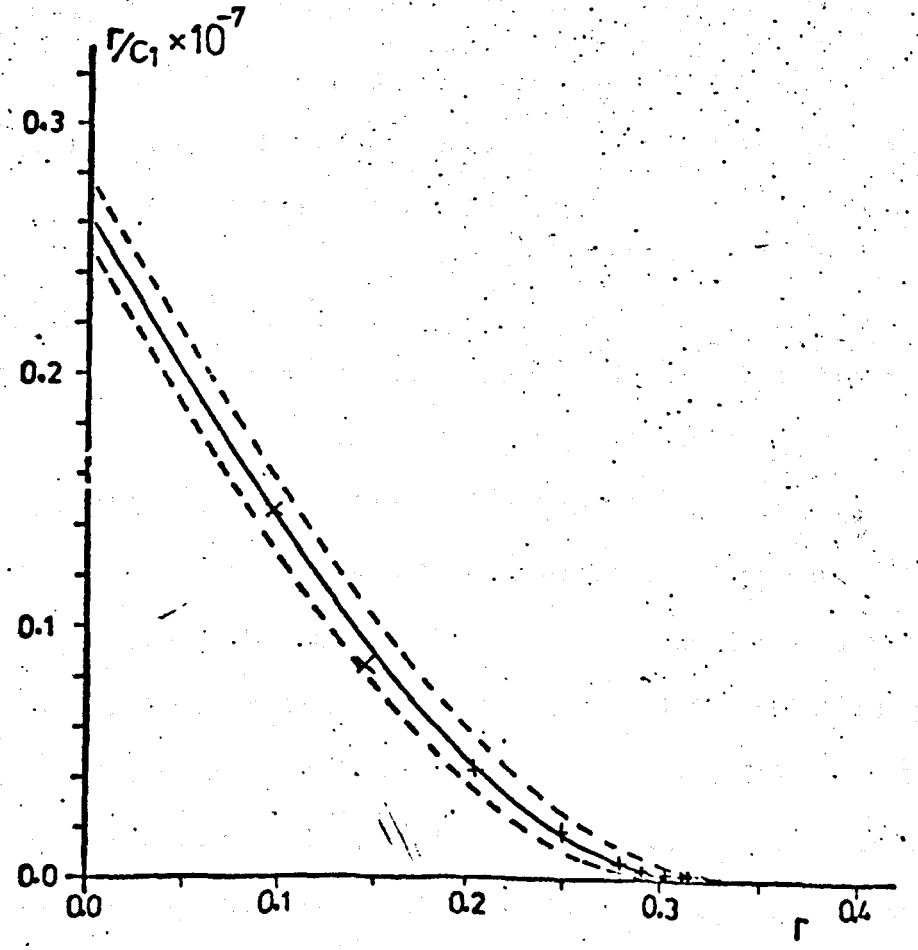

(ii) Scatchard plot for dimidium bromide binding to M. lysodeikticus DNA at low ionic concentration

blue-shifted and more intense than those at low ionic concentration, indicating reduced binding with increased salt content.

The spectral series were analysed in terms of a free and a single bound drug species, and examples of the binding curves are shown in Figs. 4.18(ii) and 4.21(ii). Except for the case of binding to calf thymal DNA at low salt concentration, the binding level increased sharply to a steady value, providing no evidence of the existence of a second binding species. For the low salt binding to calf thymal DNA there was evidence of some secondary (weaker) binding for free drug concentrations above about 17μM. The levels of saturation binding were higher than those obtained for ethidium (leading to smaller values of n_{app}) except for M. lysodeikticus at low ionic concentration which displayed a similar level of binding as with ethidium.

The Scatchard plots are shown in Figs. 4.19(ii), 4.20, 4.22(ii) and 4.23, and the parameters n_{app} and α obtained from data-fitting to the excluded site model described by Equation (3.6) are listed in Tables 4.5 and 4.6. The experimental results were a good fit to the theoretical expression, except for binding to calf thymal DNA at low ionic concentration (Fig. 4.19(ii)) but even in this case all the data points fell within the 5% limits on either side of the best-fit line.

4.4.2(b) Discussion of results

The binding of dimidium to DNA is not so tight as the binding of ethidium. The association constants are appreciably lower than those obtained with ethidium, especially at low ionic strength. However, the affinity of dimidium for calf thymal DNA at high ionic concentration is larger than that for ethidium, and slightly larger even than its affinity for calf thymal DNA at low ionic strength. This later point is particularly puzzling especially since the goodness-of-fit parameter at high ionic strength is very low, indicating that the results fit the theoretical excluded site model well. It is probable that the value at

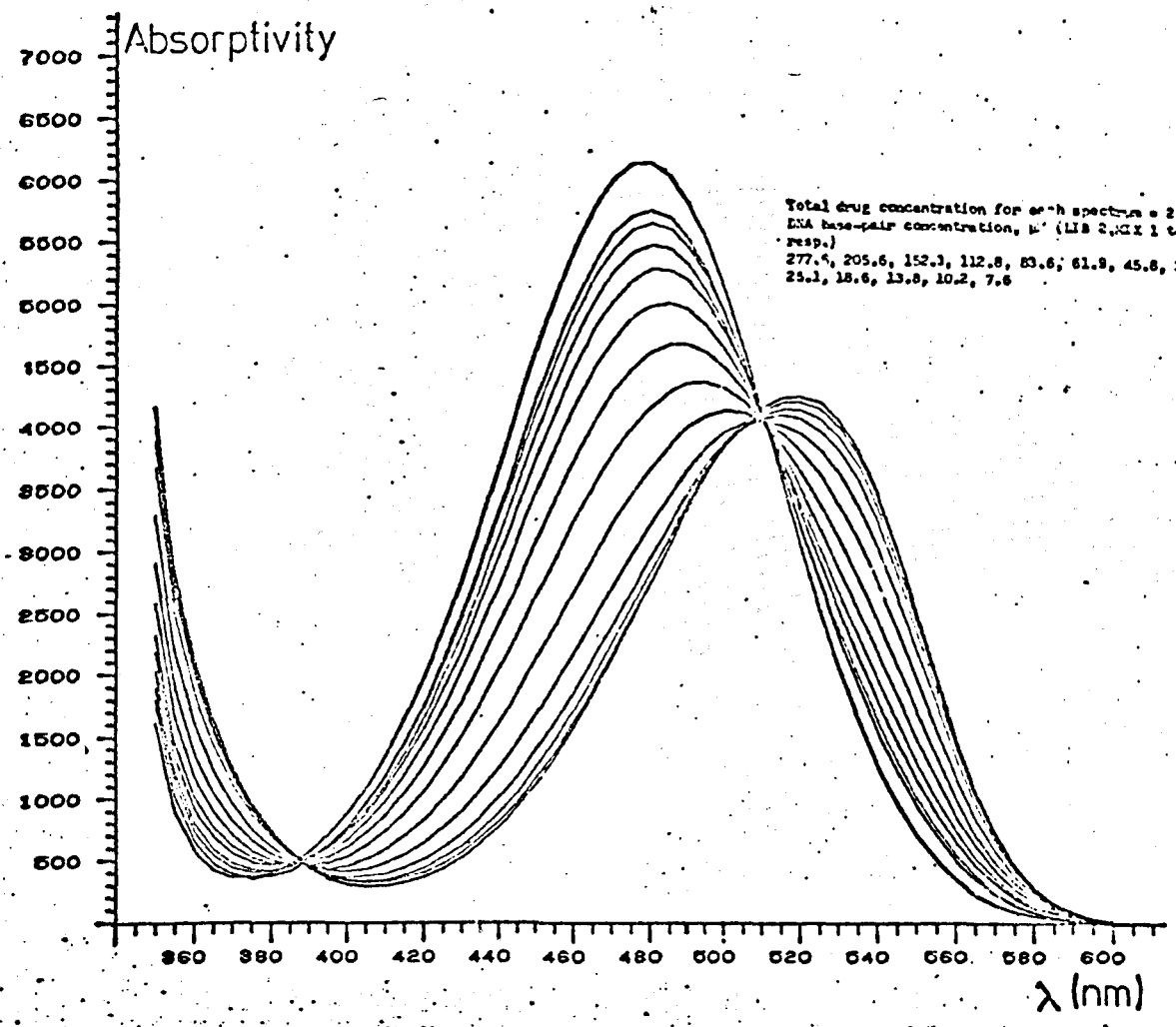

Fig. 4.21 (i) Absorption spectra for dimidium bromide binding to calf thymal DNA at high ionic concentration

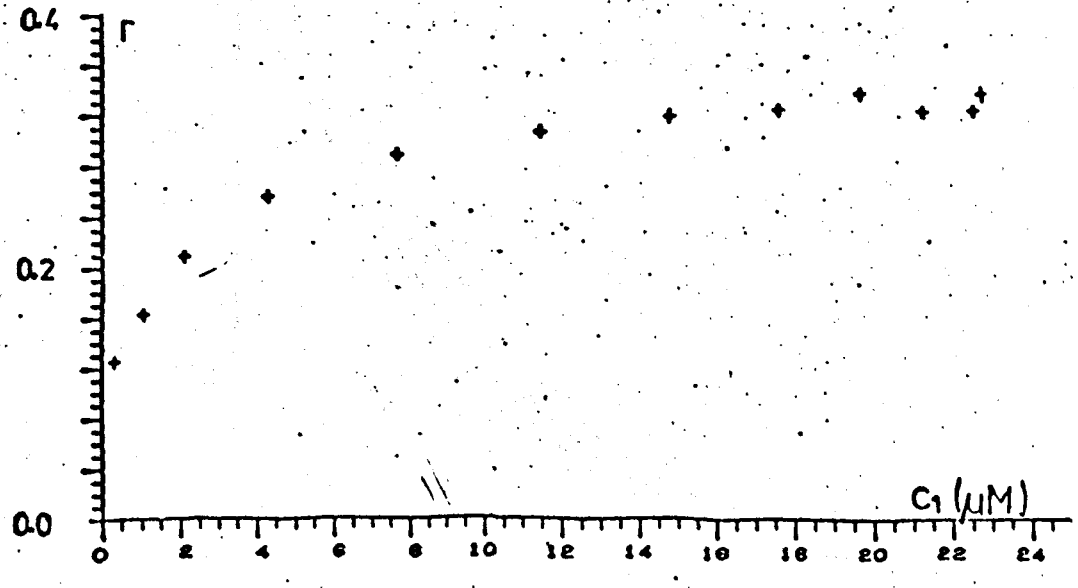

(ii) The binding curve, r vs. c, for the spectra shown above

Fig. 4.22 (i) A surface plot for dimidium binding to calf thymal DNA at high ionic concentration

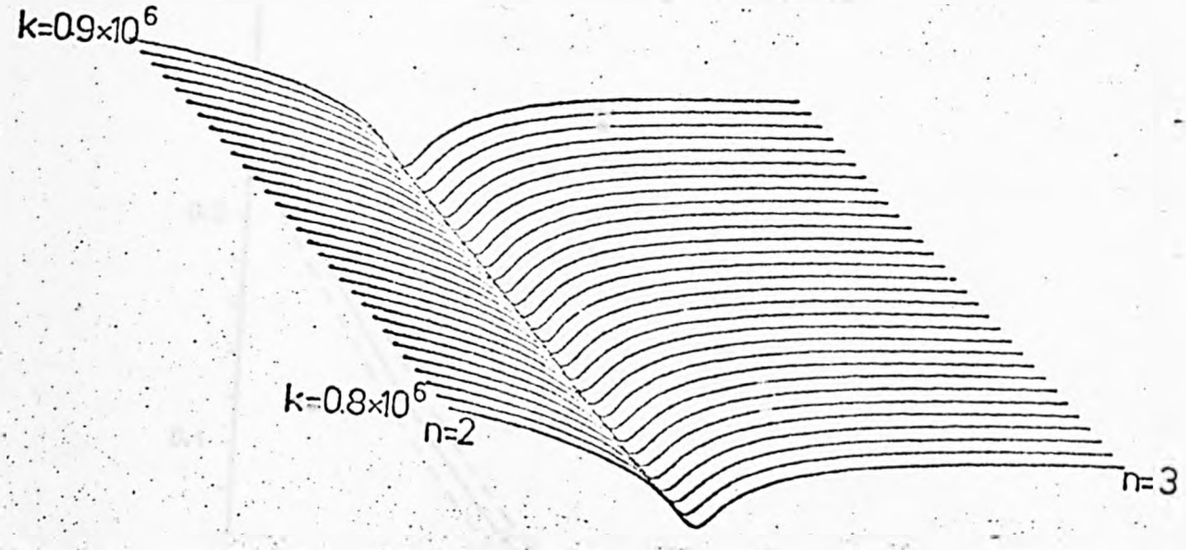

(ii) Scatchard plot of the same data

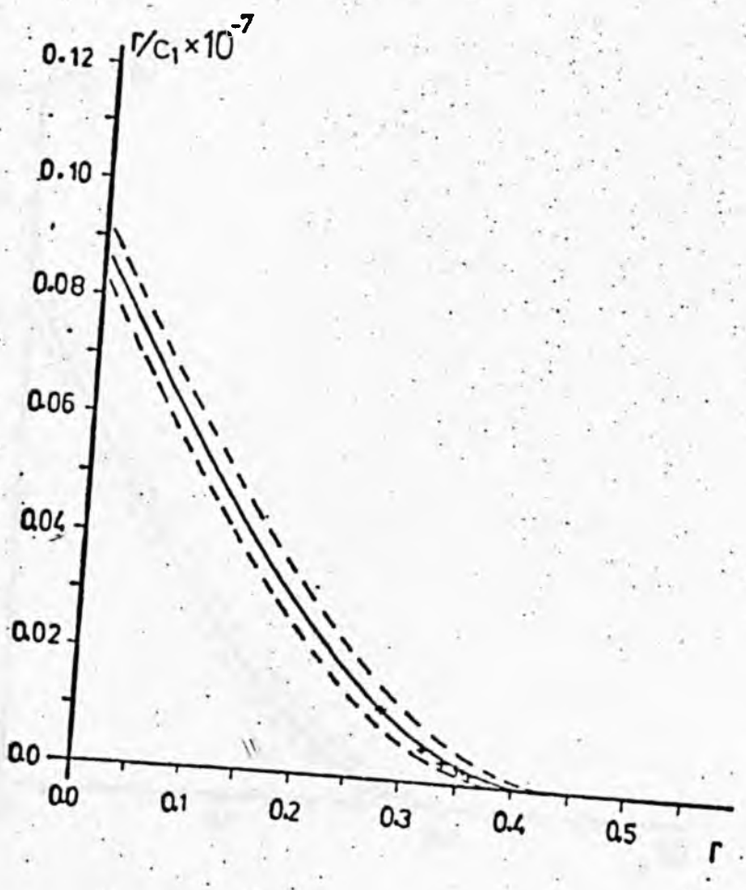

Fig. 4.23 (i) Scatchard plot for dimidium bromide binding to DNA from Cl. perfringens at high ionic concentration

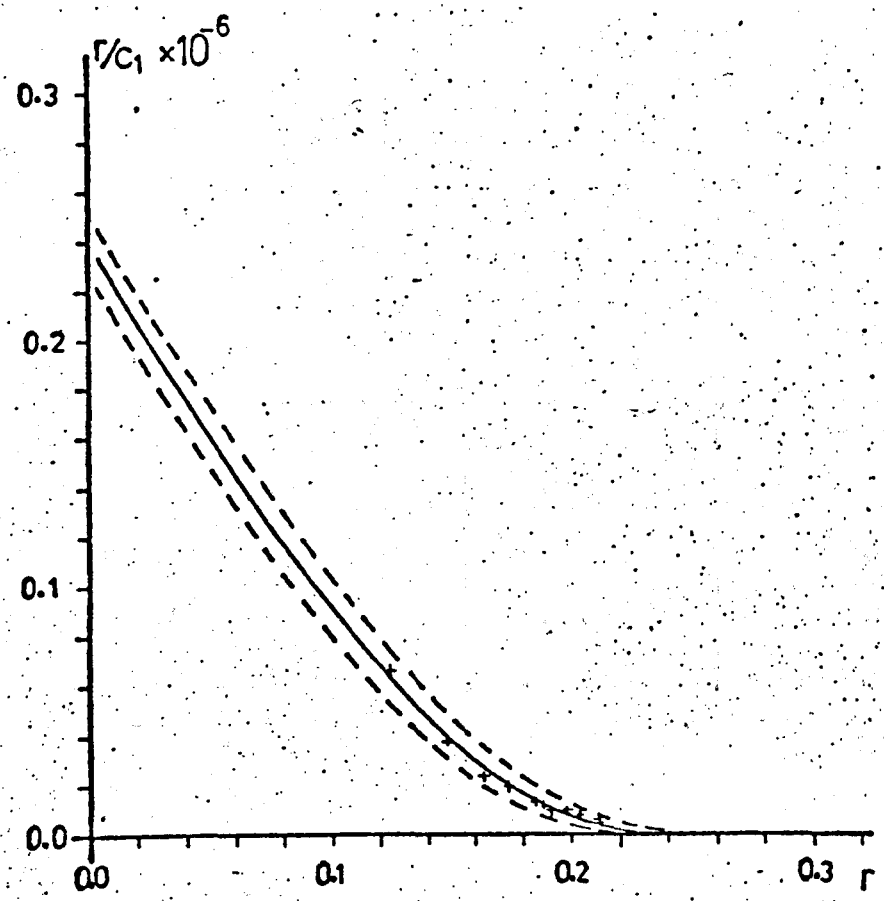

(ii) Scatchard plot for dimidium bromide binding to DNA from M. lysodeikticus at high ionic concentration

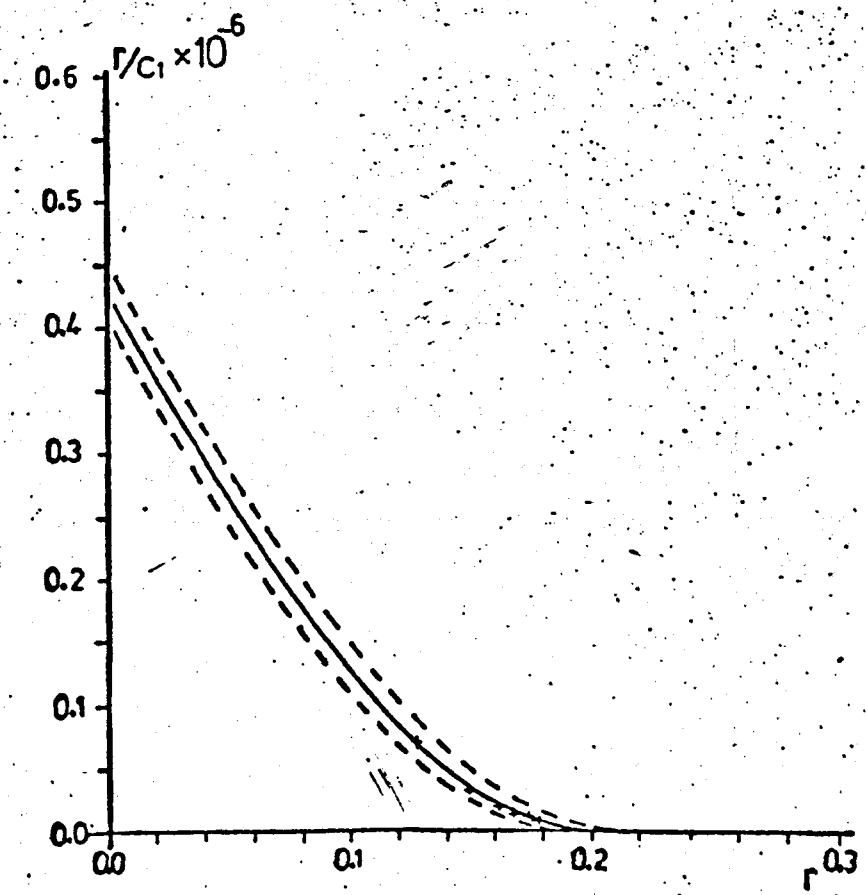

TABLE 4.5

Best-Fit Parameters for Dimidium Bromide binding to DNA at low ionic concentration

DNA type	n_{app}	Affinity, α (= P.k)	Goodness-of-fit parameter
Cl. perfringens (f=0.30)	3.59	0.86×10^6	0.038
Calf thymus (f=0.42)	1.76	0.79×10^6	0.016
M. lysodeikticus (f=0.72)	3.00	2.65×10^6	0.001

TABLE 4.6

Best-Fit Parameters for Dimidium Bromide binding to DNA at high ionic concentration

DNA type	n_{app}	Affinity, α (= P.k)	Goodness-of-fit parameter
Cl. perfringens (f=0.30)	3.99	2.4×10^5	0.014
Calf thymus (f=0.42)	2.41	8.8×10^5	0.005
M. lysodeikticus (f=0.72)	4.57	4.3×10^5	0.001

low ionic strength is a little low, since its goodness-of-fit parameter is higher, and that there is no statistical difference between the two association constants for calf thymal DNA. Apart from this one result, the overall trend for dimidium is for lower association constants than ethidium, indicating a less stable complex with DNA.

The specificity for G-C base-pairs appears less marked, with the difference in affinities at low salt concentration between Cl. perfringens and M. lysodeikticus DNA indicating a probable preference for a single G-C pair (i.e. α is proportional to f). At high ionic strength the difference between the affinities for Cl. perfringens and M. lysodeikticus is less significant, indicating that the specificity for G-C is only slight. It is probable that at higher ionic concentrations, relatively more binding takes place to A-T pairs since many of the sites will be screened to some degree by the additional sodium ions present.

The values for n_{app}, the apparent binding site size, are lower than those obtained with ethidium, indicating that dimidium molecules can be bound more closely together along a DNA helix. It is unlikely that the significantly smaller values obtained with dimidium reflect the slightly smaller overall dimensions of the drug (which contains a $-CH_3$ group in place of a $-C_2H_5$ group in ethidium). It is probable that dimidium shows a relatively higher affinity for A-T pairs than does ethidium, so that binding is not limited to the presence of G-C base-pairs to such a degree. It is possible that the binding of ethidium and dimidium distorts the DNA secondary structure and this tends to inhibit further binding, but that the effect of dimidium is smaller and so binding continues to a higher level. There was some evidence at low ionic concentration that a secondary binding mode may operate in the dimidium binding at larger binding ratios. Binding could continue to high binding levels if it were to bind by a mechanism which caused very little disturbance of the DNA secondary structure, and this would account for the lower values for n_{app} obtained with dimidium.

The variation of n_{app} with G-C content is similar to the variation observed in ethidium. Since the variation is not monotonic, it is difficult to fit the findings to one of the specificity models considered in Section 3.5. In any case, consideration of the affinities for dimidium has indicated that simple specificity for a G-C base-pair is scarcely adequate to explain those results. It is more likely that the binding scheme is more complicated, with association constants for binding to both G-C and A-T base-pairs which are not far removed from each other in magnitude.

The values of n_{app} for calf thymal DNA are significantly lower than for the other DNA types for both dimidium and ethidium binding at the two ionic concentrations considered here. It is likely that this reflects small conformational differences in the native DNA's. Bram and Tougard (1972) have claimed two new conformations, the P and T forms, for Cl. perfringens DNA in the fibre state, based on fibre X-ray diffraction patterns. A later paper (Bram, 1973) has reported a progressive decrease in the intensity of the second layer line as the fractional G-C content decreases, with an approximately three fold decrease being observed between diffraction patterns from Sarcina lutea DNA (f = 0.72) and those from yeast mitochondrial DNA (f = 0.18). Whether the same conformational differences with varying G-C content are present in solution is more difficult to ascertain, since solutions are more disordered than fibres and this disorder degrades the diffraction data. Bram (1972) has reported that high-angle X-ray diffraction data from Cl. perfringens DNA in solution suggests that the structure is not that of the B form and is different from DNA's having a higher G-C content ($f \gtrsim 0.4$). The change is relatively slight, and at present has not been fully explained in terms of a modification to the DNA structure. It appears possible, however, that conformations observed in solution may vary at least in the turn angle per residue, and that this variation may be dependent upon base composition. Calculations by Levitt

(1978) have suggested that in solution complementary bases in DNA are not coplanar, each being propellor-twisted with respect to the other by about 35° to give a DNA structure with an average base twist of 17°. These variations in the DNA conformation with ionic concentration, and conformational changes induced by drug binding, may account for the variation of n_{app}.

4.4.3 Prothidium (Di)bromide

4.4.3(a) Results

Prothidium (di) bromide appears to form stacked aggregates in solution, as evidenced by a red shifting of its spectrum with increasing drug concentrations, at lower concentrations than for ethidium and dimidium. There is little doubt that the large hydrophobic ring surfaces are the main cause of this stacking. Solutions of around 0.05mM concentration have a maximum absorptivity at 460nm, and at a concentration of 0.25mM the maximum has shifted to around 465nm. Increasing ionic strength appears to cause slight red shifting of the spectrum as well, though this effect is slight ($\sim$1-2nm). By analogy with ethidium bromide, the red shifting may be explained by the bromine ions acting as auxochromes at specific sites on the asymmetric dimer when the concentration is raised. The most probable sites for attachment would be in the positively charged areas around the N_5^+ of the chromophore and the N_1^+ of the pyrimidyl moiety. The N_3 nitrogen of the pyrimidyl ring has a lone pair of electrons. It could either act as a H-bond acceptor or it could be protonated and electrostatically attract a bromine anion. The observation that red shifting of the prothidium spectrum becomes evident at lower concentrations than for ethidium and dimidium may be related to the fact that there are two bromine ions for every drug molecule. Increased ionic strength is expected to facilitate dimerisation, resulting in the observed shift of the spectrum to longer wavelengths at high ionic concentration.

The spectra for the binding of prothidium to DNA (Figs. 4.24, 4.25 and 4.26) differ from those for ethidium and dimidium providing a direct indication that the type of binding may be significantly different. At low ionic strength, for each DNA type, the spectra show a red shift from the free drug spectrum for all mixtures, but at lower drug/base-pair values ($\lesssim$ 1.0) a hyperchromic effect is evident accompanied by a slight blue shifting. In fact each spectral series can be split into two sub-series-one (series B) consisting of the spectra with drug/base-pair ratios greater than or about unity, and the other (series A) comprising the spectra with drug/base-pair values less than or about unity. Each series shows isosbestic behaviour within itself. Series A has isosbestic points at about 455nm and around 520nm, and series B has isosbestic points at 410-415nm and 485-490nm. At high ionic strength, this rather complicated behaviour is less apparent and all the spectra appear to belong to a single series, with isosbestic behaviour at 400-405nm and 485nm. It seems likely that the binding operating at high salt concentration is similar to the type predominating at large drug/base-pair ratios (viz. series B) when the salt concentration is low. There is little variation in the spectra when different DNA types are used.

Since fairly good isosbestism was obtained at high ionic strength these results were analysed in terms of a single binding species using the excluded site model. Binding curves and Scatchard plots are shown in Figs. 4.26 to 4.29. This analysis was not carried out on the binding spectra obtained at low salt concentration, since it is inappropriate to a case that does not show a single isosbestism throughout the range of mixing ratios.

4.4.3(b) Discussion of Results

The library '1' spectra corresponds to a drug concentration of about 20μM, which is below the concentration at which stacking of the free drug

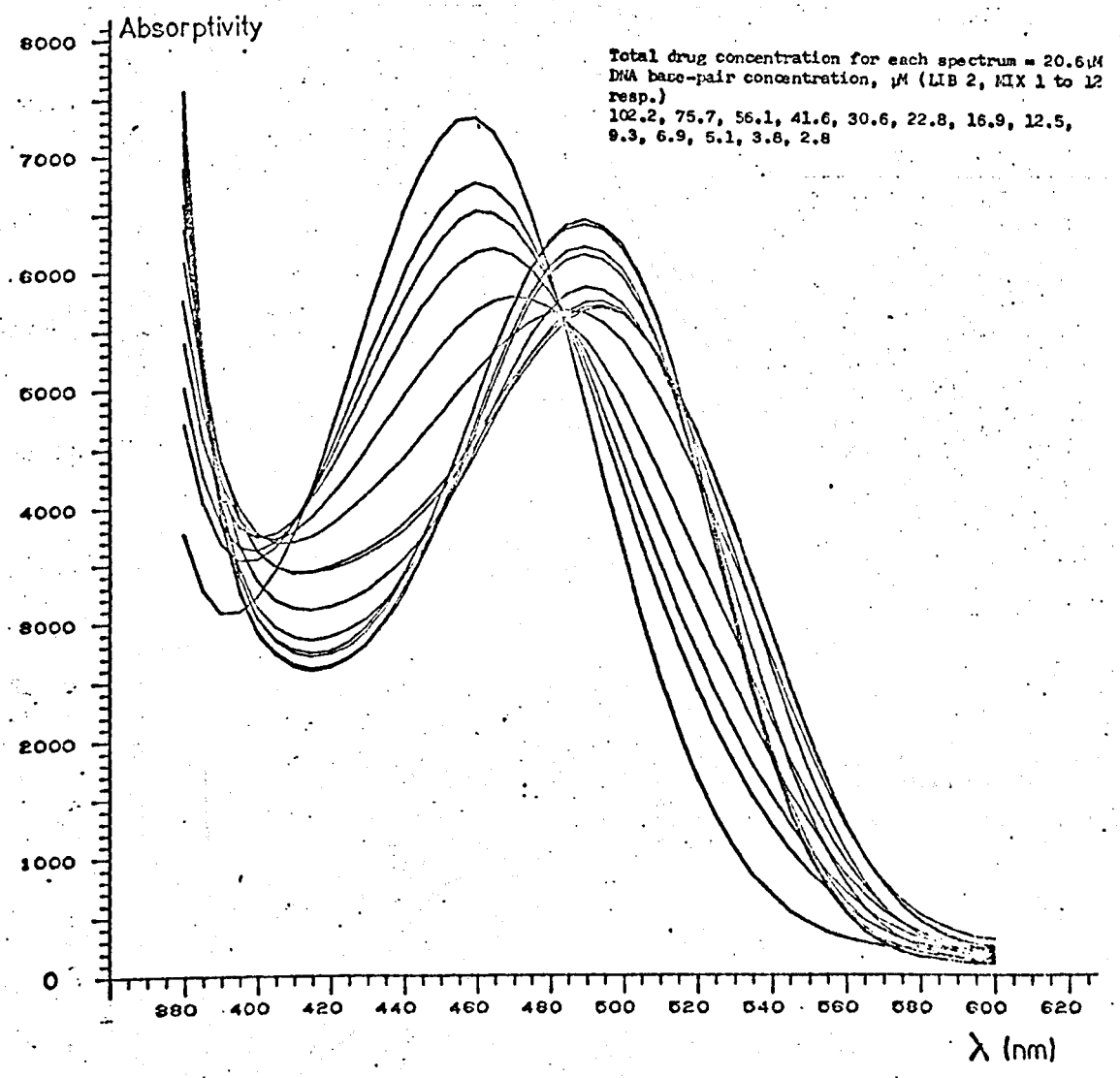

Fig. 4.24 Absorption spectra for prothidium (di)bromide binding to calf thymal DNA at low ionic concentration

Fig. 4.25 (i) Absorption spectra for prothidium (di) bromide binding to Cl. perfringens DNA at low ionic concentration

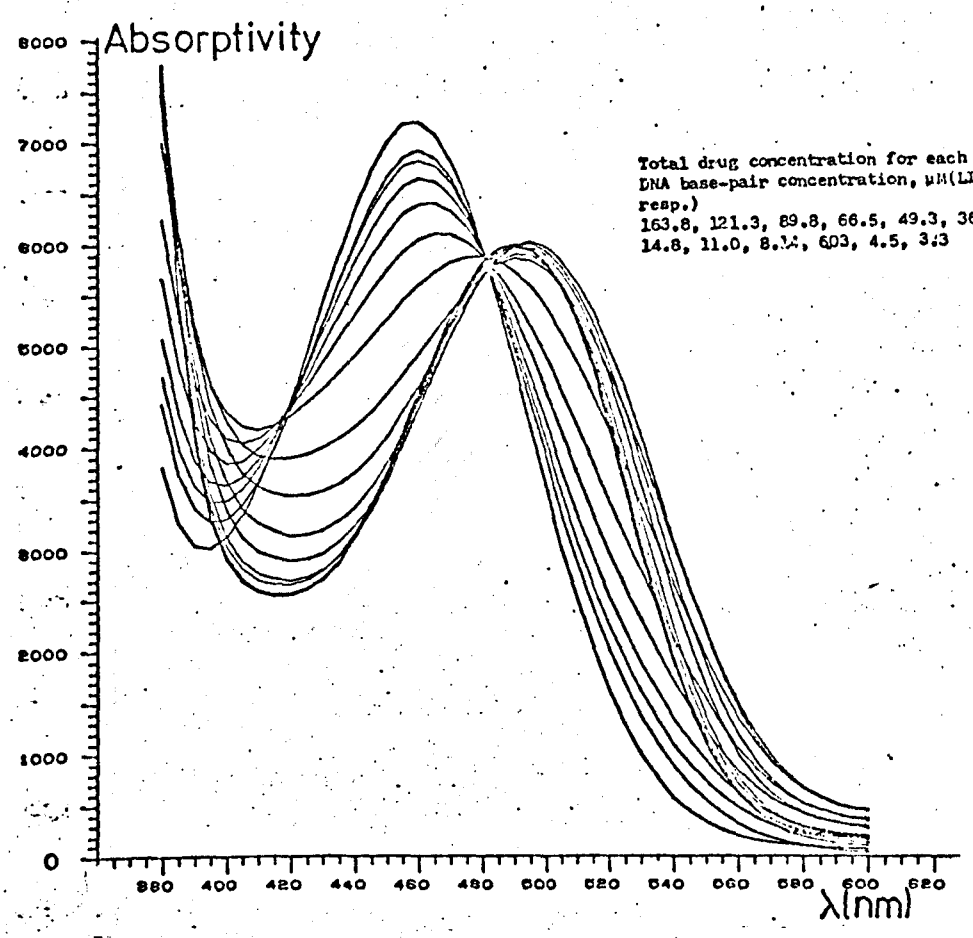

(ii) Absorption spectra for prothidium (di)bromide binding to M. lysodeikticus DNA at low ionic concentration

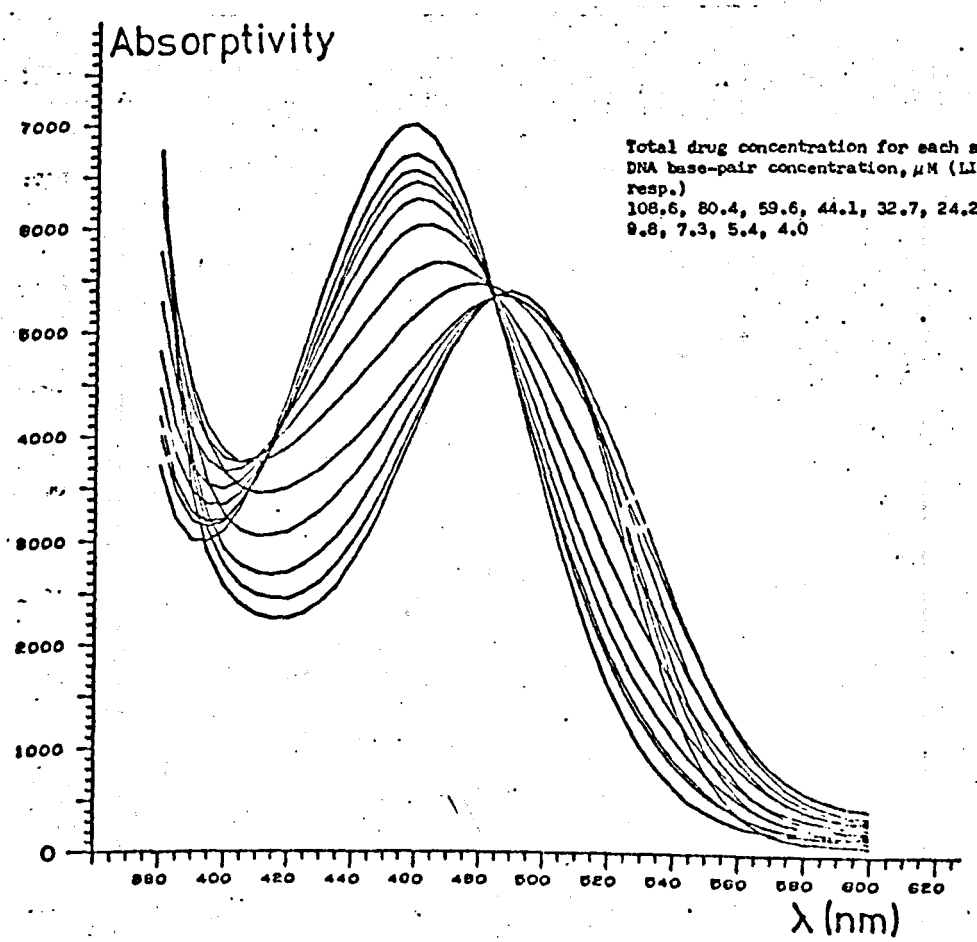

Fig. 4.26 (i) Absorption spectra for prothidium (di)bromide binding to calf thymal DNA at high ionic concentration

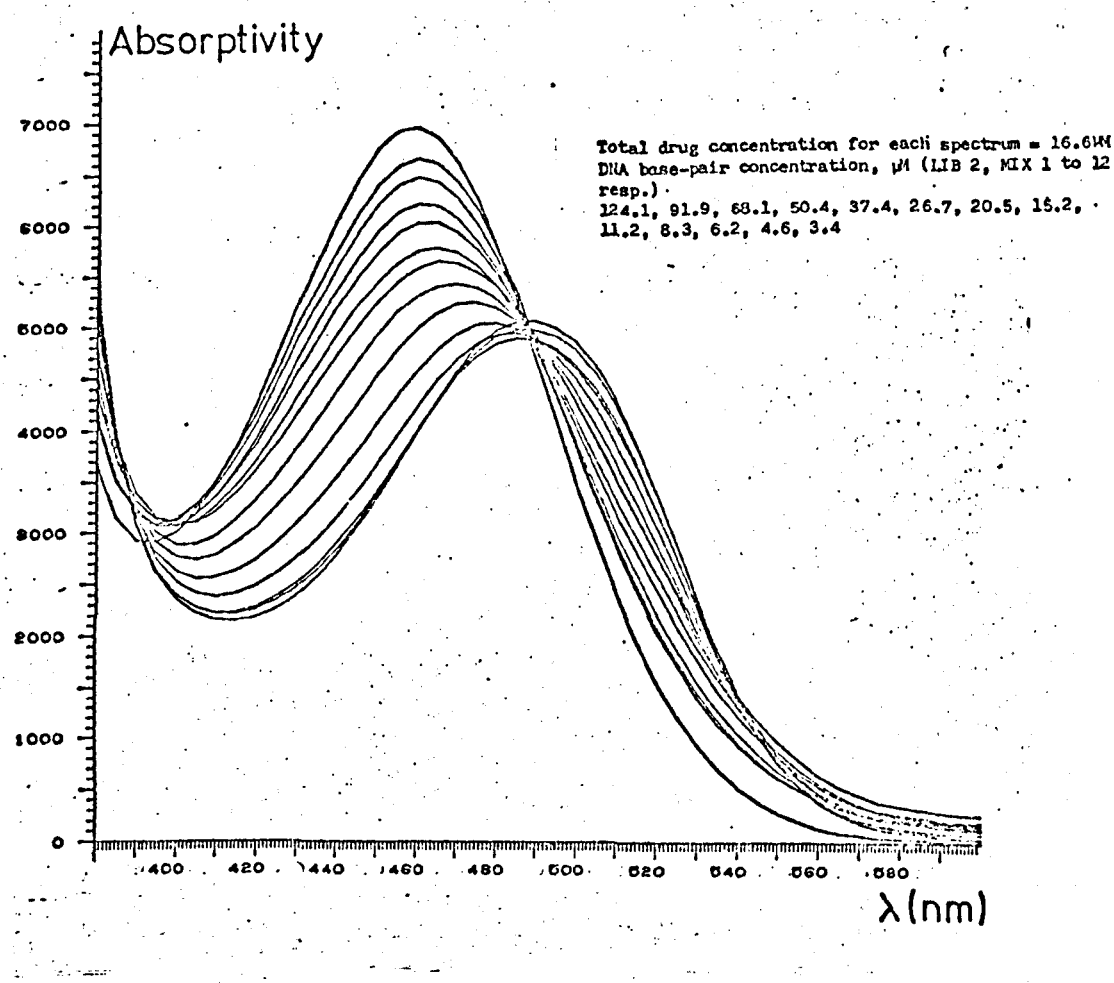

(ii) The binding curve, r vs. c, for the spectra shown above

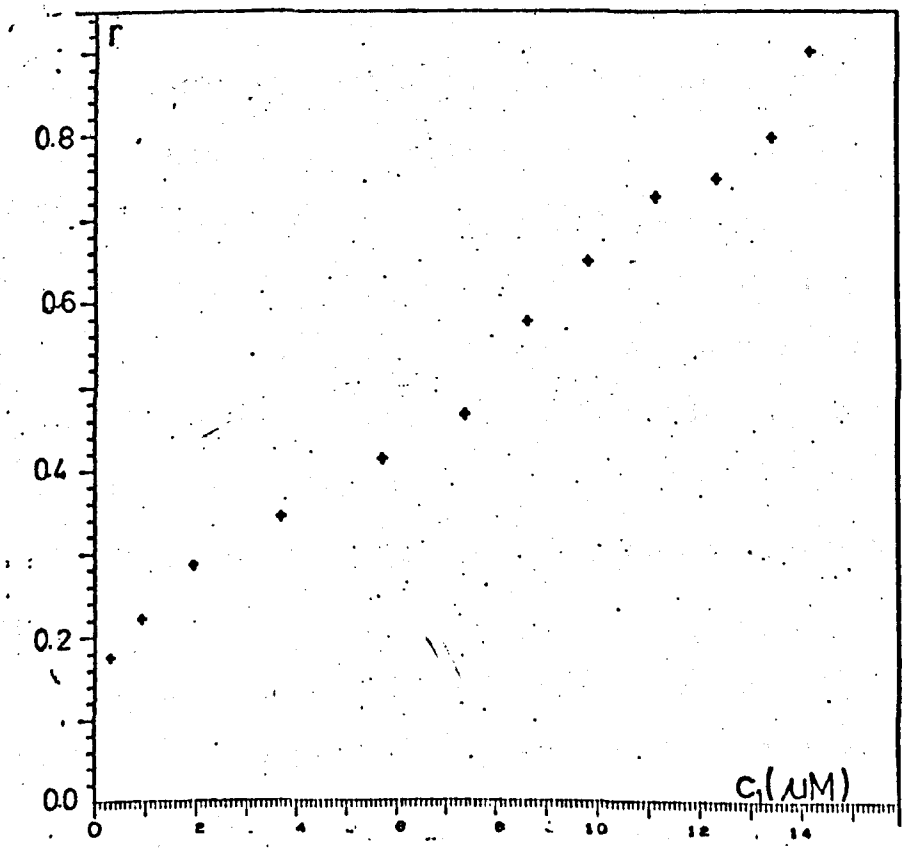

occurs. The binding curves at high ionic strength for Cl. perfringens and calf thymus DNA rise steeply at low values of r and c, indicating tight binding (mode I binding), and then they rise less steeply at around 0.4 - 0.5 (mode II binding). The transition between the two regions is gradual, but a change in the slope of the binding curve is apparent. The appearance of the two regions indicates that there are at least two binding species. The observation that they are not well separated may be due to the two species having similar association constants, so that they both occur together in significant proportions at all binding ratios, or, indeed, there may be more than two binding species. For binding to M. lysodeikticus DNA, the binding curve approaches asymptotically the value r = 0.45 at large c_1 values and there is no further increase in r. This shows either that there is only one binding species in this instance or, more likely, that the two (or more) binding species are so similar spectroscopically and have so similar n and k values that their effects are indistinguishable. It may be that these species correspond to binding to A-T and G-C pairs by a similar mechanism, although if this is the case it is difficult to explain why binding does not continue above an r value of 0.45.

The Scatchard plots show that the data for binding to M. lysodeikticus DNA can be fitted fairly well to the single binding species, excluded site model. For binding to Cl. perfringens and calf thymus DNA the fitting is inadequate at large values of r, and this is probably due to the effects of other modes of binding. The binding constants to M. lysodeikticus DNA, and the constants for the binding at low r values (mode I binding) to the Cl. perfringens and calf thymal DNA, are listed in Table 4.7. There is no evidence of G-C specificity in the binding. The values for n_{app} are similar for the three types, and there is very little variation amongst the affinity values.

The binding constants are all significantly higher than those obtained with ethidium bromide, indicating that the interaction with the DNA's is

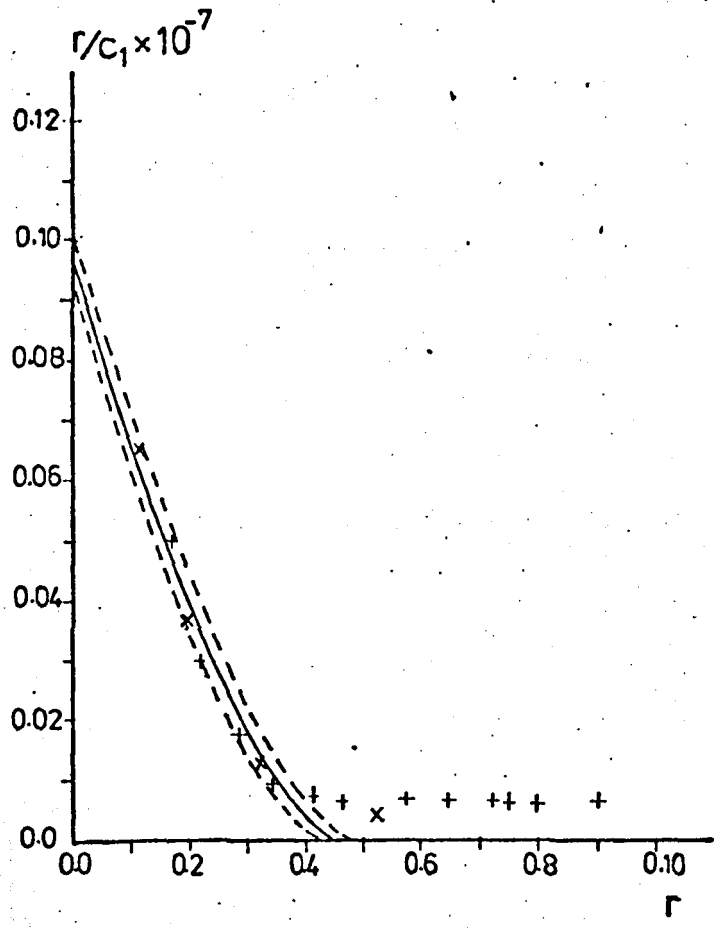

Figure 4.27 Scatchard plot for the binding of prothidium di(bromide) to calf thymal DNA at high ionic concentration.

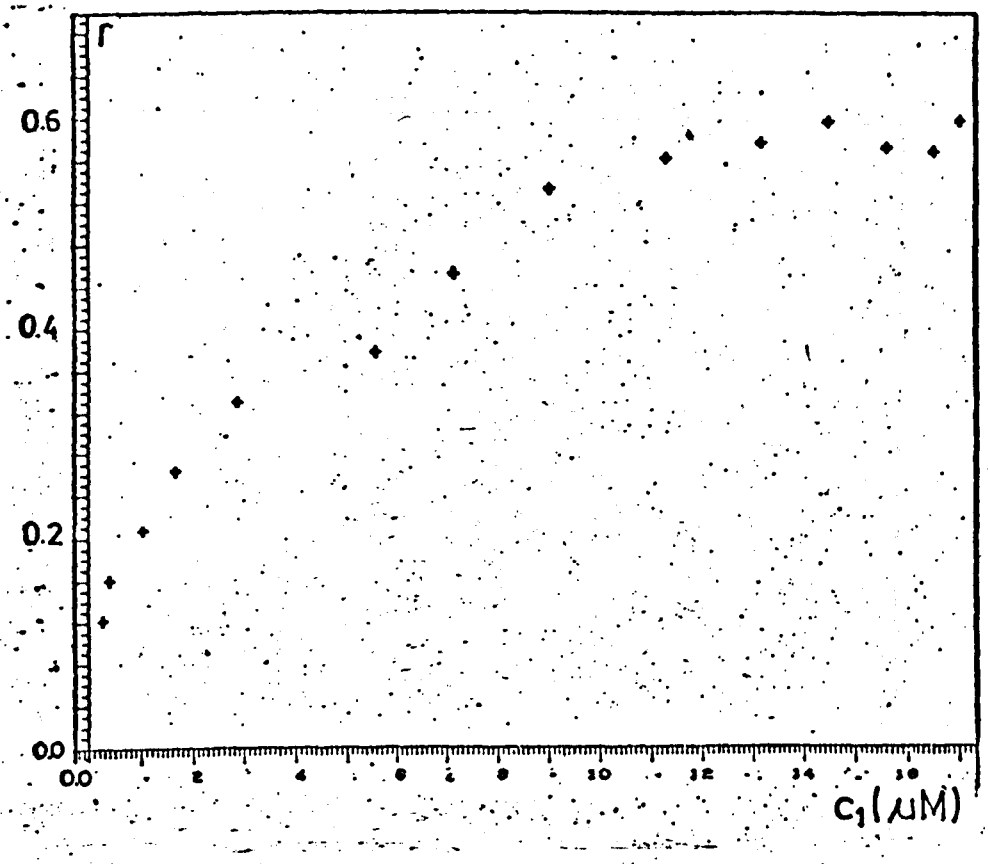

Fig. 4.28 (i) The binding curve, r vs. c, for prothidium (di) bromide binding to Cl. perfringens DNA at high ionic concentration

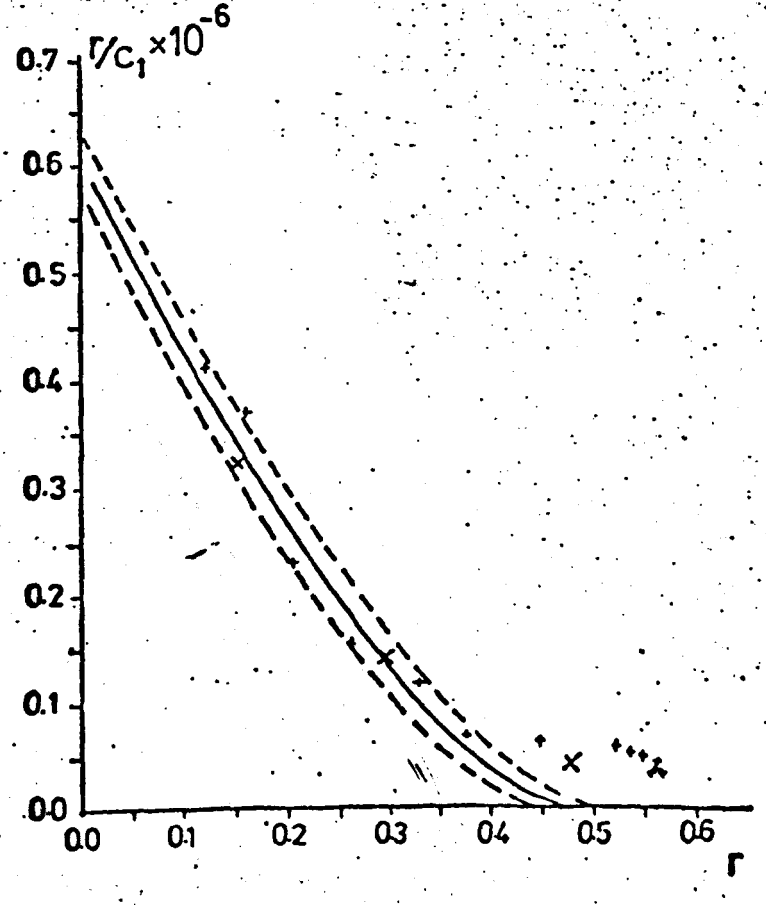

(ii) Scatchard plot of the data shown above

Fig. 4.29 (i) The binding curve r vs. c, for prothidium (di)bromide binding to M. lysodeikticus DNA at high ionic concentration

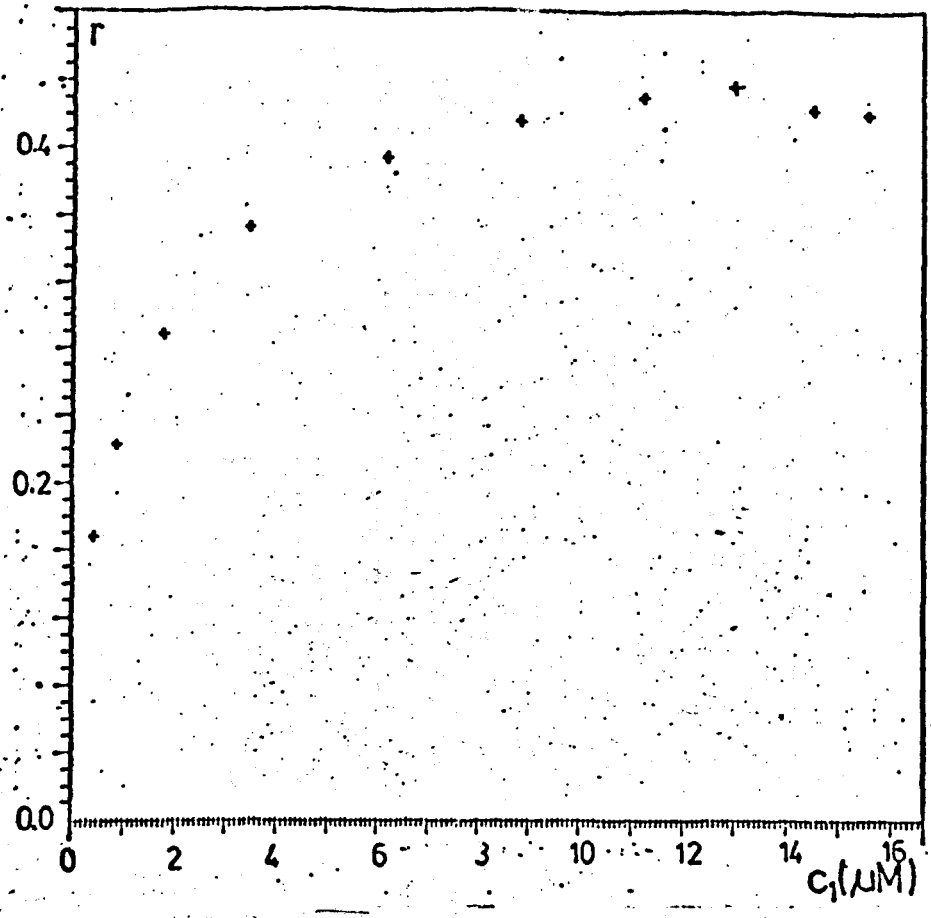

(ii) Scatchard plot of the data shown above

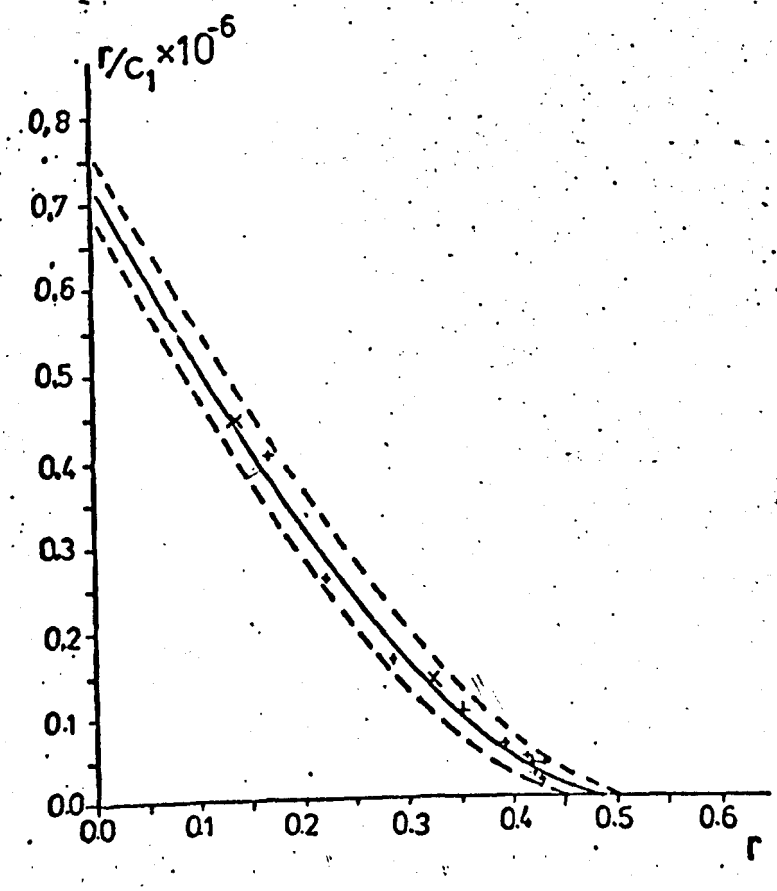

TABLE 4.7

Best-Fit Parameters for Prothidium (Di)bromide binding to DNA at high ionic concentration

DNA type	n_{app}	Affinity, α (= P.k)	Goodness-of-fit parameter
Cl. perfringens (f=0.30)	2.03	6.06×10^5	0.606
Calf thymus (f=0.42)	2.11	9.72×10^5	1.508
M. lysodeikticus (f=0.72)	2.01	7.24×10^5	0.059

stronger. This could be related to the doubly-charged nature of prothidium, which renders it strongly attracted to the negative phosphate ions of the DNA backbone. The charge separation in prothidium is 8.0Å (Cain et al., 1969), which is the approximate distance separating phosphate groups along either strand of the DNA double helix. Each prothidium molecule has three amino groups and a lone-pair nitrogen, all of which are likely to form hydrogen bonds - the amino groups as donors, and the N_3 of the pyrimidyl moiety as an acceptor. The distance between the amino groups are such that hydrogen bonds could be formed to phosphate oxygens located either along the same strand, or on opposite strands (across either a narrow or a wide groove). The hydrogen binding would be expected to be less strong than the electrostatic binding, although it may be mediated by a strong electrostatic character due to charge delocalisation around the aromatic rings.

Since prothidium possesses so many groups capable of providing strong interactions, in several different ways, with DNA it is likely that some or all of these binding types will be present simultaneously. The spectra of the drugs bound by these different mechanisms may be very similar, and the binding parameters describing the different species may not be very different. This would account for the fairly good isosbestism observed, and the findings that the binding curves each show two rather poorly separated regions and the Scatchard plots indicate more than one binding species.

Binding mode I appears to saturate, to some extent at least, at a binding ratio of about 0.5 i.e. at one bound drug molecule for every two base-pairs. This results in n_{app} values of around 2.0, and these are insensitive to the G-C content. Further binding to Cl. perfringens and calf thymus DNA can occur, approaching r values of unity with calf thymal DNA. The saturation of the initial stronger binding occurs at around the value for total binding saturation for ethidium and dimidium. Prothidium is a significantly larger molecule than ethidium and dimidium. It seems

likely that binding mode I in prothidium differs in type from the binding operating with the other two drugs. If ethidium and dimidium bind primarily by intercalation and this mode were considered for prothidium, the increased steric hindrance (Chapter 8) due to its larger size would be expected to result in a lower value for binding saturation and therefore in a larger value for n_{app} for mode I binding. In addition, the fact that further binding can continue past this level suggests that the initial mode I binding has not markedly changed the DNA conformation by, for example, unwinding the helix.

High k values are a perennial source of problems with the analysis of DNA-phenanthridine spectra since they mean that data at low free drug concentrations, c_1, are difficult to obtain. At low ionic strength the association constants are even larger, because of the reduced competition with Na^+ ions, and the analysis is even more difficult than for the series at high ionic concentration. At moderate to high ionic concentrations, results from equilibrium dialysis may be used to supplement the spectrophotometrically determined data but at low ionic concentration these too become suspect (Section 2.3.2(a)). For prothidium at low salt concentration, it is thought that the same binding schemes are operating as at high salt concentration, although the electrostatic character to the binding will be enhanced because the phosphates will not be shielded by the sodium cations to any great extent.

A plausible rationale for the anomalous shifting of the spectra at low ionic strengths is that, at low binding ratios, initial binding (proposed as being strongly electrostatic) causes a red shifting relative to the free drug spectrum. By analogy with the formation of dimers in a free drug solution at high concentrations, as more drug is bound some of it may form antisymmetric dimers with the already bound drug to cause a further shift towards long wavelengths. At still higher drug/base-pair ratios some drug will remain unbound in solution causing the spectra to shift towards the

spectrum of the completely free drug. It is not clear, however, why the formation of bound dimers would be inhibited at high ionic concentration.

The spectra at low ionic concentration have not been analysed according to a single species, excluded site binding model since it is obviously inadequate to describe the observed spectral data. The author has decided not to analyse the results according to a different scheme because of the computational difficulties, and because of the uncertainties in the interpretation of the binding modes in operation. Careful equilibrium dialysis measurements in the future at moderate ionic strengths may elucidate the nature of the binding interactions. For the present, however, only the data at high ionic strength appears amenable to quantifying the nature of the binding.

4.5 A Summary

The binding of dimidium is very similar to that of ethidium, as is expected from their similar chemical structures. The electron-donating power of the methyl group to the triple aromatic ring is greater than that of an ethyl group. This difference can be expected to affect the electron density and hence the dipole moment of the chromophore. If the binding were primarily intercalative, a strong base-pair specificity in the binding would require that the dipole moment of the preferred base-pair should match that of the bound drug. Charge displacement would result in changes in the direction of the transition dipole moment in the drug and may result in a less favourable alignment of the drug and base-pair dipole moments, resulting in the reduced specificity observed for dimidium bromide. More information on the precise nature of the specificity could be obtained with synthetic polynucleotides of known sequence, especially if the small conformational changes thought to occur with different base sequences were known more quantitatively.

The binding of both of these drugs appears to be mainly by a single mode, although this does not rule out the possibility that the binding may occur via several stages. Any model proposed for this binding mode must be able to explain satisfactorily the observed saturation of the binding at around one bound drug for every two base-pairs (see Chapter 8).

The spectral series for prothidium binding is very different to those for ethidium and dimidium, indicating that a different binding mechanism may be operating. In particular, the binding cannot be successfully explained in terms of a single bound species. The higher levels of binding observed is further evidence that there is a different binding scheme than for ethidium and dimidium. Prothidium has been observed to remove and reverse the supercoiling of closed circular duplex DNA (Wakelin and Waring, 1974), indicating that some unwinding of the helix must occur on binding. However the result is not diagnostic for intercalative binding,

since known non-intercalators, such as the steroidal diamines, are known to unwind closed circular DNA. Binding models will be discussed in detail in Chapter 8 but the differences in the spectroscopic behaviour of prothidium compared to ethidium and dimidium suggest that more than one binding mechanism is involved, and that probably none of them correspond to the mechanism operating with ethidium and dimidium. The presence of a double positive charge and the three amino groups in prothidium suggest that electrostatic and hydrogen-bonding interactions are prominent in its binding to DNA, and steric hindrance due to the pyrimidyl moiety can be expected to be a important factor in any binding scheme.

CHAPTER 5

X-Ray Diffraction from DNA-Drug Fibres

5.1 Introduction

The scattering of X-rays by a molecule is described by its Fourier transform and this in turn depends on the positions of the constituent atoms and on their Fourier transforms, known as atomic scattering factors. If the molecule is part of a regular crystalline lattice then diffraction will occur only at specific angles which are related to the size and shape of the unit cell of the crystal. The Fourier transform of the molecule is 'sampled' by the reciprocal lattice of the crystal and the diffraction pattern shows discrete spots, or reflections, instead of a continuous variation in intensity. The spacings of reflections in a diffraction pattern bear a reciprocal relation to spacings in the real structure.

In a non-crystalline DNA fibre, although there is normally some degree of regular often hexagonal packing, there is no azimuthal correlation between the molecules. Such fibres give diffraction patterns consisting of continuous intensity streaks along each layer line, which essentially represent the diffraction from a single molecule. In principle such data allows more information to be obtained from the diffraction pattern along each layer line since, unlike the case of a crystalline fibre, the intensity is not merely sampled at discrete points. However, because the diffracted intensities from each molecule are spread out over a large sampling region, they are less easy to distinguish from the background (due to diffraction from water and amorphous DNA) and accurate measurements are more difficult. An intermediate situation occurs for semi-crystalline fibres. If the molecules are considered as smooth helices then they are packed in a crystalline lattice, but if the atomic detail is considered then the molecules have a random screw displacement. This gives rise to

fairly sharp crystalline reflections in the centre of the pattern, but a non-crystalline pattern at higher angles.

Cochran et al. (1952) have shown that the Fourier transform of a right handed, infinitely long, helical molecule is given by -

$$F(\xi,\psi,\zeta) = \sum_n \sum_j f_j J_n(2\pi\xi r_j) \exp i[n(\psi-\phi_j+\tfrac{\pi}{2}) + 2\pi\zeta Z_j] \qquad (5.1)$$

where

r_j, ϕ_j, Z_j = the real space cylindrical polar co-ordinates of the j^{th} atom.

ξ, ψ, ζ = the reciprocal space cylindrical polar co-ordinates (Fig. 5.1).

J_n = a Bessel function of the first kind of order n.

and f_j = the atomic scattering factor of the j^{th} atom.

This describes a three dimensional transform which is observed on a two dimensional plane. It is zero everywhere except on a series of planes observed as layer lines. On any particular layer line, l, the orders of Bessel functions contributing to the resulting transform are given by the following selection rule -

$$n = \frac{l - mN}{K} \qquad (5.2)$$

where n = Bessel function order

m = an integer

K is the minimum number of complete turns of the helix necessary to incorporate an integral number of residues,

and N is the number of residues in this repeat distance.

The first maxima of Bessel functions occur at increasing values of the argument as n increases, and only a $zero^{th}$ order Bessel function has a non-zero value when the argument is zero (Fig. 5.2). If the helix is integral (K = 1), then n = l when m = 0 so that an l^{th} order Bessel function occurs on the l^{th} layer line (Fig. 5.3). This arrangement, repeated in the four quadrants of a diffraction pattern, produces the cross-like pattern

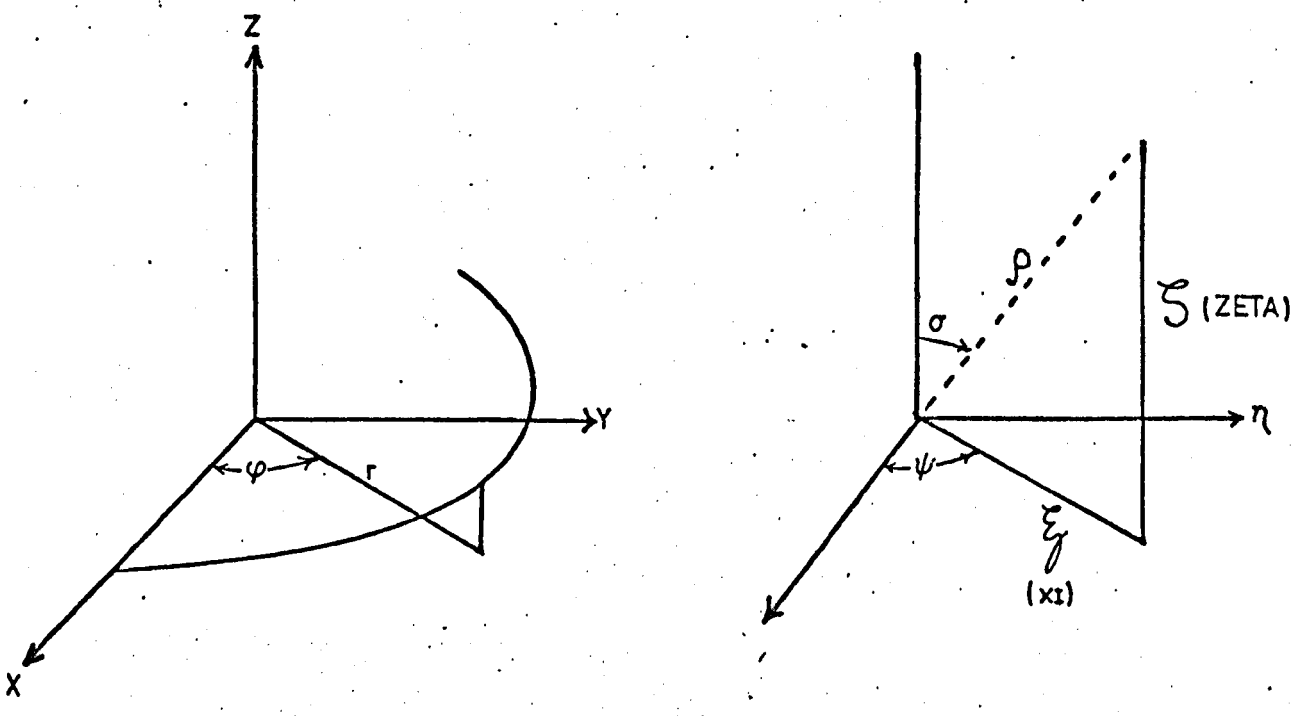

Figure 5.1 The real-space and reciprocal space co-ordinates used to define a helix.

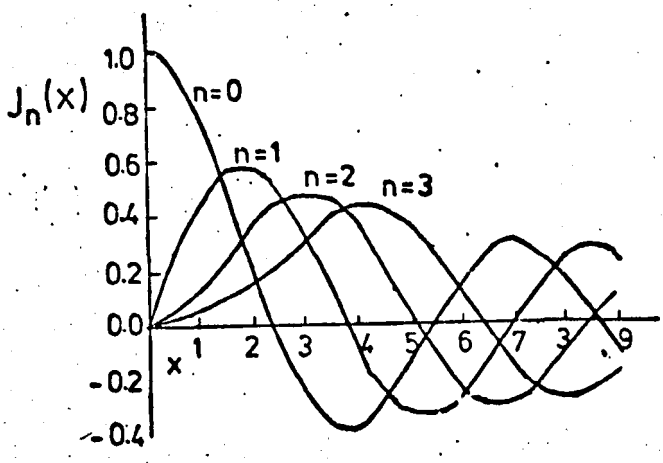

Figure 5.2 Bessel functions, $J_n(x)$, from zeroth to third order.

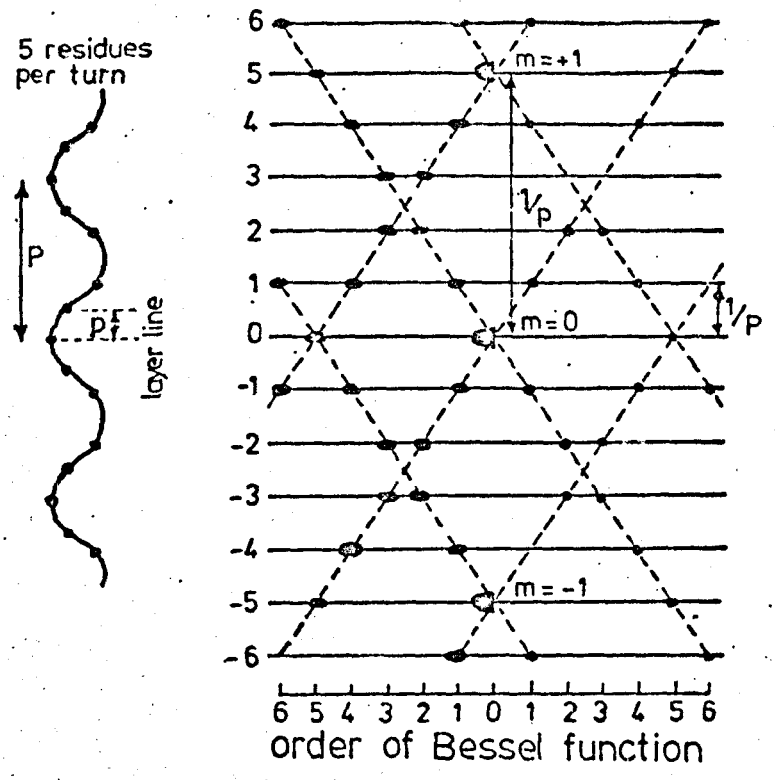

Figure 5.3 Calculated diffraction pattern for a discontinuous helix with 5 residues per turn (after Wilson (1966))

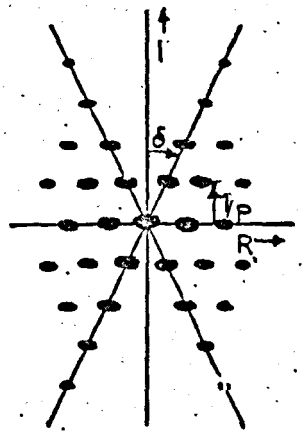

Figure 5.4 Diffraction pattern from a continuous helix

characteristic of diffraction from a helix (Fig. 5.4).

The DNA molecule has two periodicities along its length - the pitch, and the translation per residue. The ζ spacing of the layer lines depends on the helix pitch and whether or not the helix is integral. The layer line with $l = 0$ is known as the equator and the line perpendicular to it and passing through the centre of the pattern is known as the meridian. The magnitude of the Fourier transform at $\xi = 0$ must be zero except when zeroth order Bessel functions occur on a particular layer line. For B-DNA ($N = 10$, $K = 1$) Equation (5.2) predicts that a zeroth order Bessel function will occur on the 10th layer line when $m = 1$. Because the base pairs are approximately perpendicular to the helix axis, diffraction is observed as a very strong meridional corresponding to a 3.4Å residue repeat distance. Equatorial reflections ($l = 0$, $m = 0$) correspond to a projection along the helix axis, and provide information on the packing of the helices. For a diffraction pattern from A-DNA the resulting crystalline reflections can be indexed enabling the unit cell dimensions to be calculated. For semi-crystalline B-DNA patterns the equatorial reflection enables the intermolecular separation, IMS, of the helices to be obtained.

If there is a distribution in the orientation of the helix axes within a fibre, the observed pattern is a convolution of the molecular intensity transform and the orientation probability function $P(\theta_1, \phi_1)$ defined in Section 6.3.1. This has the effect of spreading out the diffracted intensity along an arc centred on the centre of the diffraction pattern (Fig. 5.5(i)). A simple geometric explanation of this is illustrated in Fig. 5.5(ii)). Holmes and Barrington-Leigh (1974) have shown that for a gaussian disorientation function the intensity is gaussian along the arc, provided the arc is not close to the meridian. Deconvolution schemes have been proposed by which the molecular transform itself may be extracted from such diffraction patterns (Cella et al., 1970; Holmes and

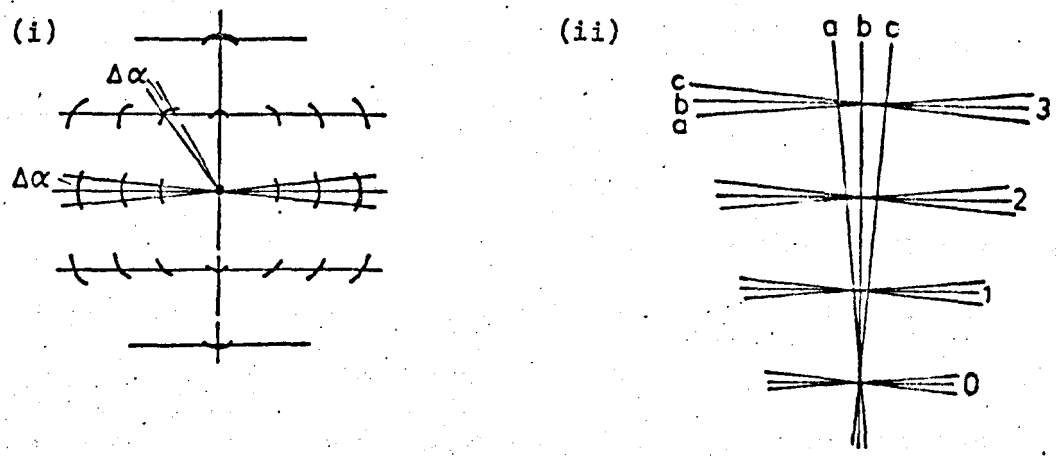

Figure 5.5 (i) The arcing of reflections on a diffraction pattern due to disorientation.

(ii) The disorientation along a layer line is approximately proportional to the distance from the meridian. The axes of three helices a, b and c are shown together with the disorientated layer lines (l=0,1,2,3) they produce. (After Holmes and Barrington;Leigh, 1974)

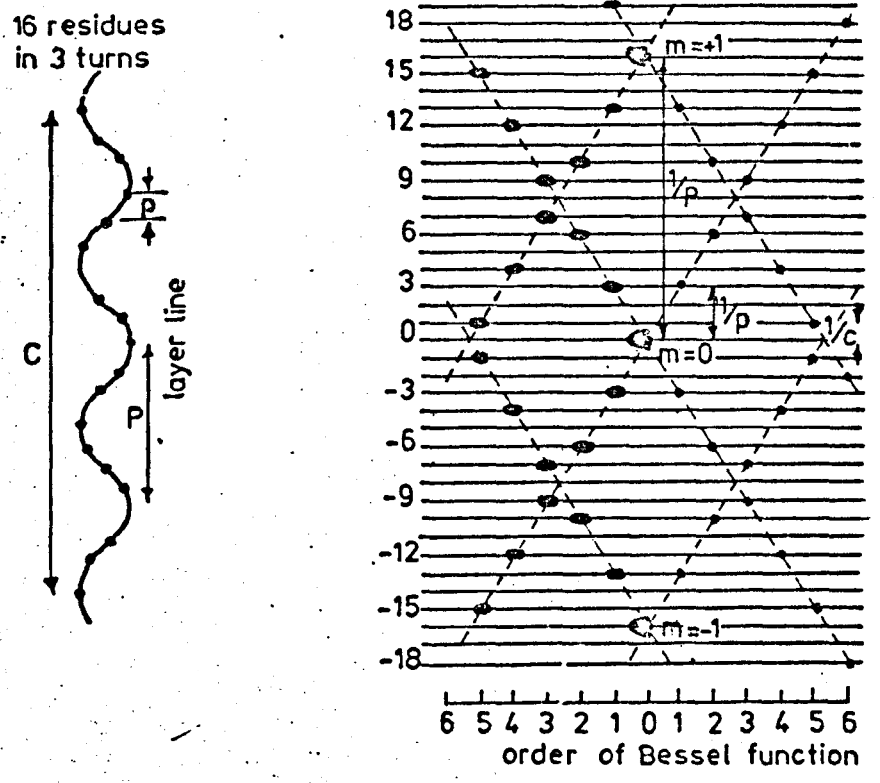

Figure 5.6 Calculated diffraction pattern from a discontinuous non-integral helix (after Wilson (1966))

Barrington-Leigh, 1974; Stubbs, 1974).

The situation is further complicated in the case of DNA molecules possessing a non-integral number of residues per turn (e.g. C-DNA N = 28, K = 3) as this results in splitting of the layer lines (Fig. 5.6). This causes an increase in the apparent angular half-width of reflections if the split layer lines are not resolved (Franklin and Klug, 1955). In DNA-drug fibres the regularity of the molecule is itself disturbed by the random attachment of drug molecules along the helix. At low drug content the complex can be considered as a more-or-less regular backbone structure with a non-integral number of residues per turn, so long as the drug molecule resembles a base-pair in its scattering characteristics. The X-ray beam will impinge on an area corresponding to many repeats of the helical complex, and the diffraction pattern will show new, average helix parameters. As the proportion of drug is raised the increased disorder results in a deterioration of the pattern and a consequent loss of readily interpretable information.

5.2 Previous X-ray Diffraction Studies

X-ray diffraction experiments on oriented DNA-drug fibres have been reported for the drugs proflavine (Lerman, 1961; Neville and Davies, 1966), ethidium bromide (Fuller and Waring, 1964), daunomycin (Pigram 1968, Pigram et al., 1972), adriamycin (Porumb, 1976)and steffimycin (Al-Jubory, 1978). The results of these studies have varied in their details but, in general, the binding of the drug to DNA resulted in a disordered pattern as seen by the diffuseness of the layer lines. The amount of disorder was seen to depend on the nature of the drug, the drug content within the fibre and the relative humidity. An increase in the observed pitch with increasing drug content, together with a retention of the 3.4Å meridional, was interpreted as indicating intercalative binding.

Neville and Davies (1966) reported a systematic examination of the diffraction patterns observed for DNA-acridine fibres. At high humidity the patterns revealed a significant increase in the pitch of the fibres compared to the pitch of B-DNA. This increase could arise from an unwinding of the helix either by intercalation or by an external binding mode. However, external binding models could not successfully explain the length increases found by a number of measurements on solutions of the complex (Luzzati et al., 1961; Cairns, 1962). Consequently, Neville and Davies proposed that the acridines bound to DNA primarily by intercalation, although some of it was in an externally bound state. A variation in the equilibrium between these two binding modes would explain the observed change in layer line spacing as the relative humidity was changed.

A similar X-ray fibre diffraction study was performed on the interaction between daunomycin and DNA (Pigram, 1968; Pigram et al., 1972). These authors observed a pitch increase and a reduction in the intermolecular separation of adjacent DNA molecules. The observed changes in DNA parameters at 92% and 98% R.H., in combination with computer model building studies, supported an intercalation model. Experimental data suggested

agreement with the earlier result for ethidium (Fuller and Waring, 1964), so that the DNA helix untwists locally by 12° in order to intercalate one daunomycin molecule.

Porumb (1976) has reported a significant difference in the binding of the anthracyclines adriamycin and daunomycin to DNA as the humidity is lowered. This has direct relevance to the understanding of the difference in their biological activity. Both drugs are characterised by a marked antitumour activity, and from the chemotherapeutic point of view adriamycin appears to be more effective than daunomycin. In living cells, the presence of nucleoprotein and enzyme systems complexed with DNA is likely to create an environment devoid of water, similar to the environment existing in fibres at low relative humidity. It appears that adriamycin is a more effective drug because of its ability to remain intercalated even under conditions of low humidity.

The interpretation of DNA-drug diffraction results is difficult because of the uncertainty of the unwinding caused by intercalation, and because the fraction of drugs intercalated at a given humidity is generally unknown. Controversy still surrounds the value for the unwinding angle. The value of 12° for ethidium (Fuller and Waring, 1964) has been challenged and a value of 26° has been proposed (Wang, 1974). The chemical and enzymatic studies of Pulleyblank and Morgan (1975) have also predicted that the untwisting angle is between two and three times as high as the previously accepted value of 12°, and experiments using electron microscopy (Liu and Wang, 1975) and gel electrophoresis (Keller, 1975) have supported the 26° estimate. Tsai et al. (1977) have co-crystallised ethidium with both the dinucleoside monophosphates adenosine (5' - 3') 5-iodouridylyl and guanosine (5' - 3') 5-iodocytidylyl, and have solved the crystal structures to atomic resolution. The phenyl and ethyl groups of the intercalated ethidium molecule lie in the narrow groove of the miniature double-helices, and there is an unwinding of the helices by 28°. It

should be noted, however, that there is no evidence for the intercalative binding of ethidium to double-helical RNA. The fact that intercalation has been visualised in an RNA fragment (A (5' - 3') iodoU) may illustrate the limitation of studying the intercalative binding of drugs to nucleic acid duplexes by extrapolation from data obtained from binding to oligonucleotides. In principle, with DNA-drug patterns it should be possible to identify a peak on the equator, the position of which is independent of the DNA/drug ratio, from which the degree of untwisting at the intercalation site could be determined (Goodwin, 1977). Unfortunately, such a peak would correspond to a Bessel function of very high order (n = 30 if the untwisting angle were 12^{o}). Such peaks occur far out in reciprocal space and are not easily recorded.

Relaxation kinetic measurements (Li and Crothers, 1969) show that even in solution, several percent of the bound proflavine is attached externally to DNA. The balance between intercalation and external binding is a delicate one, readily influenced by environmental conditions. The interpretation of X-ray results has been limited due to a lack of knowledge of the fraction of bound drug actually intercalated in a fibre, under given ionic and humidity conditions and for a certain drug loading in the fibre. Measurements of the dichroic ratio, taken in parallel with the X-ray diffraction measurements, can help to resolve this difficulty and the two sets of data will be discussed together in Chapter 7 with a view to clarifying this situation.

The question of the biological significance of intercalation remains open. The diverse biological activities which have been attributed to intercalative modes of binding may be due to differences in the stereochemistry of intercalation for different drugs, and to differences in the equilibrium between intercalative and external binding.

5.3 The Program 'FFILM'

The program 'FFILM' performs three tasks -

(i) It finds the centre of the diffraction pattern and scales the pattern. Diffraction from the aragonite powder (Section 2.3.3.2), with which each fibre had been sprayed, produces a ring centred on the centre of the pattern. If the corresponding spacing in real space is known, then the ring may be used to find the centre of the pattern and the specimen-to-film distance, D. The best values of these quantities may be obtained by application of the formula

$$\frac{1}{d} = \frac{2}{\lambda} \sin(\tfrac{1}{2} \tan^{-1} \frac{E}{D}) \qquad (5.3)$$

where λ is 1.5418Å, the wavelength of the copper K_α radiation used in this work, E is the radius of the ring and d is the corresponding distance in real space.

The program incorporates a subroutine 'CENTRE', written by Dr. W.J. Pigram, which obtains the best values of the centre co-ordinates and specimen-to-film distance by using a least-squares minimisation algorithm.

(ii) It obtains the reciprocal space co-ordinates (and the corresponding real space values) for points in a diffraction pattern. The measured film co-ordinates (X, Y) of an elongated spot on the pattern are converted to (cylindrical) reciprocal space co-ordinates, using the relations

$$\zeta = \frac{Y}{\lambda(D^2 + X^2 + Y^2)^{1/2}} \qquad (5.4)$$

$$\xi = \frac{1}{\lambda} \left[2 - \lambda^2\zeta^2 - \frac{2(1-\lambda^2\zeta^2)^{1/2} D}{(D^2+X^2)^{1/2}}\right]^{1/2} \qquad (5.5)$$

$$\rho^2 = \zeta^2 + \xi^2 \qquad (5.6)$$

where the quantities ρ, ξ and ζ are defined in Fig. 5.1. The reciprocal of ζ is also given, except for points on the equator,

since this value is usually equal, or proportional, to either the helix pitch or the translation per residue along the helix axis.

For B-DNA and complexes of DNA with an intercalated drug the packing of the helices usually conforms to a hexagonal pattern. In this case, the intermolecular separation, IMS, is given by

$$IMS = \frac{2}{\sqrt{3}} \frac{1}{\xi_{110}} \qquad (5.7)$$

where ξ_{110} is the value calculated for the strong (innermost) equatorial spot, taken as the (110) reflection.

(iii) It calculates a value for the disorientation, δ, of the molecules within the fibre.

For spots remote from the meridian, Fraser et al. (1976) have shown that the following formula holds well.

$$Q = \frac{1}{\pi^2 p^2 X^2} + 2\delta^2 \qquad (5.8)$$

where $Q = \frac{(\Delta\alpha)^2}{\ln 2}$

$\Delta\alpha$ = the angular half-width of the spot on the photograph, taken as the angular distance between the peak intensity point and a half-intensity point.

p = the coherent particle length, which determines the sharpness of the layer lines in the ζ-direction.

X = the X co-ordinate of the spot.

and δ = the half-angle of the gaussian disorientation (defined in Section 6.3.1).

The intercept of a plot of Q against $\frac{1}{X^2}$ will give $2\delta^2$.

The half-width of a reflection is measured from a microdensitometer trace tangential to the arc (Fig. 5.7). The program calculates the corresponding angular half-width, $\Delta\alpha$, given the pantograph ratio of the microdensitometer arm and the distance of the reflection from the centre of

(i) From an A-DNA pattern

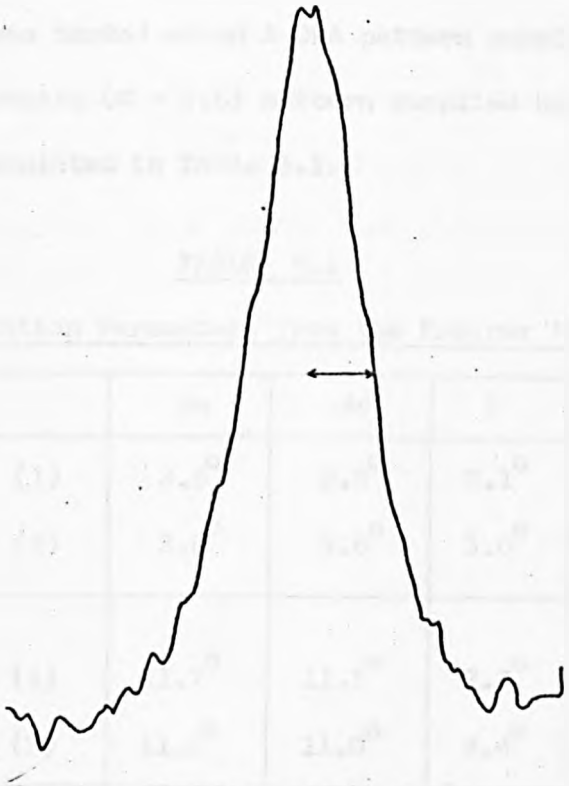

(ii) From a DNA-daunomycin (M = 2.5) pattern

Figure 5.7 Typical densitometer traces used to test the program 'FFILM' (see text for details)

the pattern. The angular half-width in 3-dimensional reciprocal space, $\Delta\sigma$, is output, along with values for Q and $\frac{1}{X2}$ from which δ may be obtained. A facility exists to input uncertainties in the microdensitometer half-widths and obtain corresponding uncertainties in Q.

The parameter p, determined from the gradient, will not have as much significance for a DNA-drug fibre as for a pure DNA fibre because the helices are irregular, but it should still give some idea of the distance over which a semblance of regularity persists. Its value would be expected to decrease as the proportion of drug in a fibre is increased. The value of δ obtained will be an overestimate of the gaussian disorientation since other factors (such as the limited crystallinity of the fibre, lack of collimation of the X-ray beam and, in the case of a non-integral helix, layer line splitting) will have contributed to the arcing of the spots.

The program was tested on an A-DNA pattern supplied by Dr. C. Nave, and on a DNA-daunomycin (M = 2.5) pattern supplied by Dr. W.J. Pigram. The results are tabulated in Table 5.1.

TABLE 5.1

Disorientation Parameters from the Program 'FFILM'

		$\Delta\alpha$	$\Delta\sigma$	δ	p(Å)
A-DNA	(1)	3.6°	3.6°	3.1°	1000
	(2)	3.6°	3.6°	3.0°	500
DNA-daunomycin	(1)	11.7°	11.5°	7.7°	91
	(2)	11.2°	11.0°	8.4°	167

The readings marked (1) were obtained using a 2-dimensional travelling microscope to measure the reflection co-ordinates; those marked (2) employed a DMac digitiser. The good agreement for corresponding cases

indicates that both methods are equally reliable.

The large values obtained for the coherence length of A-DNA indicate that regularity persists over a considerable distance. The values themselves, however, are imprecise because the gradient of the graph of Q vs. $\frac{1}{X^2}$ is so small that it is almost horizontal. Relatively small uncertainties in the densitometer half-widths result in large uncertainties in the slope of the best-fitted lines, and hence in the value of p. For the DNA-daunomycin fibre at M = 2.5 regularity seems to persist over 3 to 5 base-pairs which is comparable to or slightly more than the distance between the drugs if they had been bound regularly.

The values of δ are slightly lower than those for $\Delta\alpha$ and $\Delta\sigma$, although they correlate well. The disorientation half-angle, δ, is expected to show this trend since the total arcing, described by the half-angles $\Delta\alpha$ and $\Delta\sigma$, will be due to other factors in addition to the disorientation of the helices. For the further work in this Chapter, the disorientation δ has either been computed using measurements from a tangential microdensitometer trace, or it has been assigned a value equal to 70% of the value of $\Delta\alpha$ estimated geometrically from a diffraction photograph.

5.4 Aims of the Diffraction Study

The details of fibre making are given in Section 2.2. All the fibres used in this study were made using the low ionic concentration buffer (Section 2.1). At this ionic strength, a DNA fibre would normally undergo a transition from the B form to the A form at about 80% R.H.. For some of the discussion of the experimental results of this chapter, it will be more convenient to specify the bound drug content of a fibre by its base-pair/bound drug ratio, M. This is obtained by measuring both the UV and visible absorbances of the complex in solution and its corresponding supernatant after centrifugation. Subtraction of the values obtained will give the concentrations of bound drug and DNA in the gel, and hence in the fibre, assuming that all the drug molecules bound to the DNA in solution remain bound during sedimentation and the subsequent drying down of the gel to form a fibre. The ratio M is equivalent to the inverse of the binding ratio, r, which has been used exclusively up until this chapter as a measure of the proportion of bound drug. For each of the three drugs considered in this thesis, an extensive set of fibres (together with control DNA fibres) was prepared with M values in the range 2.8 to 19.

The purpose of this study was to determine accurately the modified DNA helix parameters from the diffraction patterns of a series of fibres as a function of the drug content and the hydration of the complexes. These parameters indicate whether or not intercalative binding takes place, and, if so, to what extent. Since intercalation is a largely hydrophobic mechanism it was anticipated that the relative humidity would affect the amount of intercalatively bound drug. An estimate of the gaussian disorientation can be obtained from the arcing of the diffraction spots. Application of some of this information is reserved for Chapter 7, where it is interpreted in conjunction with the dichroism and birefringence

measurements. These latter measurements provide information on the orientation of the drug chromophores in the fibres, and may be used to estimate the proportions of interc.latively and externally bound drug molecules for a particular set of environmental conditions.

5.5 Ethidium Bromide

5.5.1 Experimental Results

Typical X-ray diffraction patterns from the control DNA are shown in Fig. 5.8. The pattern obtained at 75% R.H. is that of the crystalline A form, and the pattern at 98% R.H. shows the semi-crystalline B form. The quality of the patterns does not match the best of the previously published DNA patterns (Langridge et al., 1960; Fuller et al., 1965; Fuller, 1961), but the previously published patterns were obtained from fibres which were formed by dissolving DNA in a droplet of water between two glass rods whereas the fibres used here were made by drying down a centrifuged gel. The patterns in Fig. 5.8 are sufficient to show that the control DNA is neither degraded nor denatured and that it is extensively free from impurities. The quality of the patterns depends on the disorientation within the fibre, and this is related to the conditions under which the fibre was pulled. From the layer line spacings the helix pitch of the B form is calculated to be 33.8Å at 92% R.H. and 34.2Å at 98% R.H., and the equatorial reflections give intermolecular separations of 25.8Å and 26.2Å respectively. The layer line spacing of the A pattern corresponds to a pitch of 28.1Å, and the spot positions agree with those of Fuller (1961) indicating that the DNA crystals are monoclinic with unit cell dimensions a = 22.24Å, b = 40.62Å, c (=Pitch) = 28.15Å and β, the angle between the a and c axes, = 97.0°.

Typical X-ray diffraction photographs from DNA-ethidium fibres are shown in Figs. 5.9 and 5.10. Those taken at 92% R.H. are all of the semi-crystalline B type, as shown by the strong meridional reflections and the distinctive intensity distribution on the layer lines. The retention of the strong 3.4Å meridional at all M values indicates that the bound drug molecules must be attached such that the 3.4Å repeat distance along the helix axis is preserved. The layer lines become more diffuse for

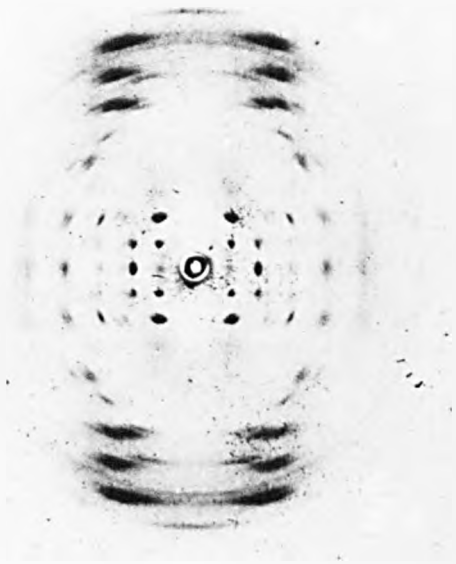

(i) A conformation, 75% R.H.

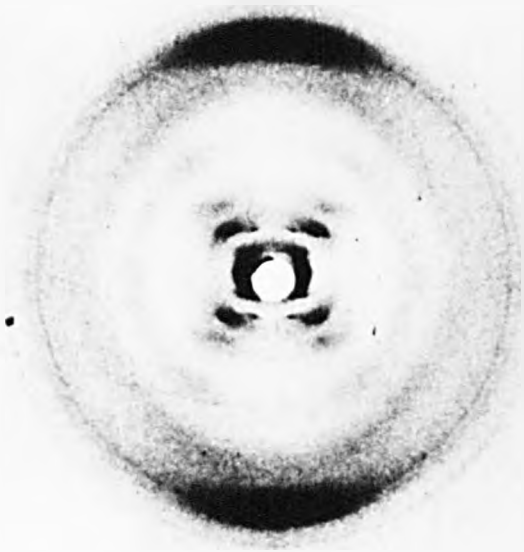

(ii) B conformation, 98% R.H.

Figure 5.8 X-ray diffraction patterns from a DNA fibre (0.01M NaCl)

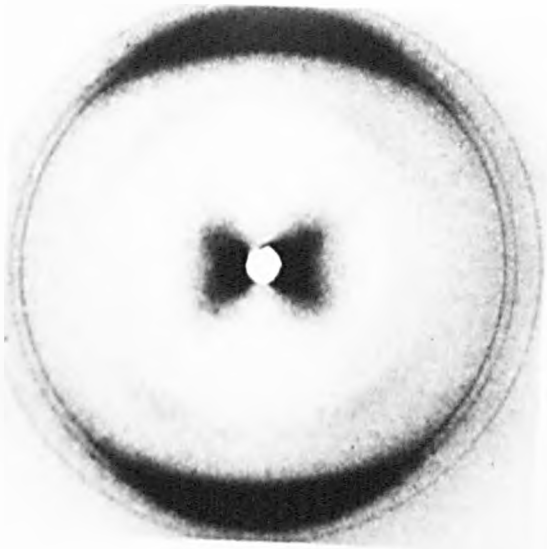

(i) M = 2.8

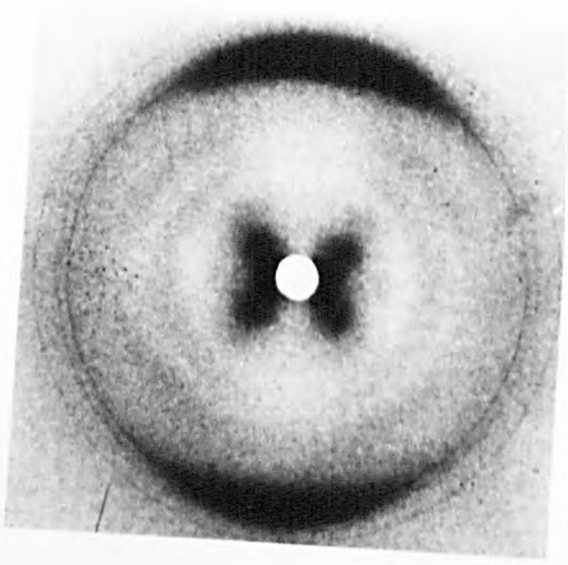

(ii) M = 4.4

(iii) M = 5.5

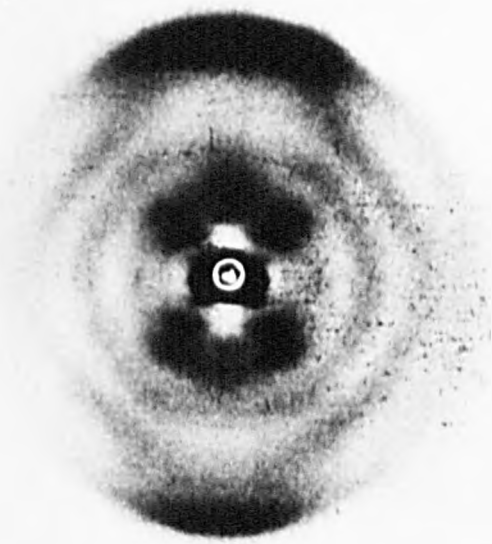

(iv) M = 12.0

Figure 5.9 X-ray diffraction patterns from DNA-ethidium fibres at 92% R.H. (0.01M NaCl)

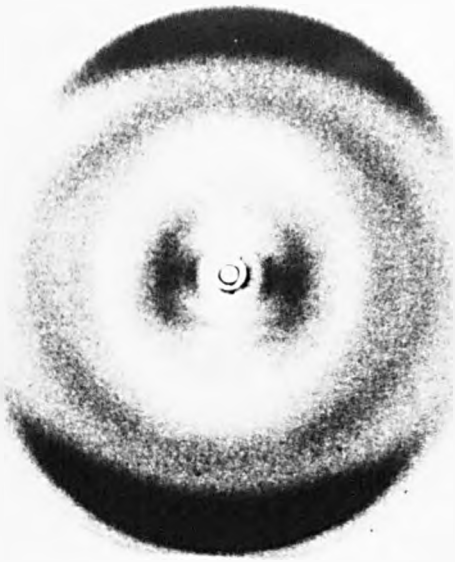

(i) M = 4.0

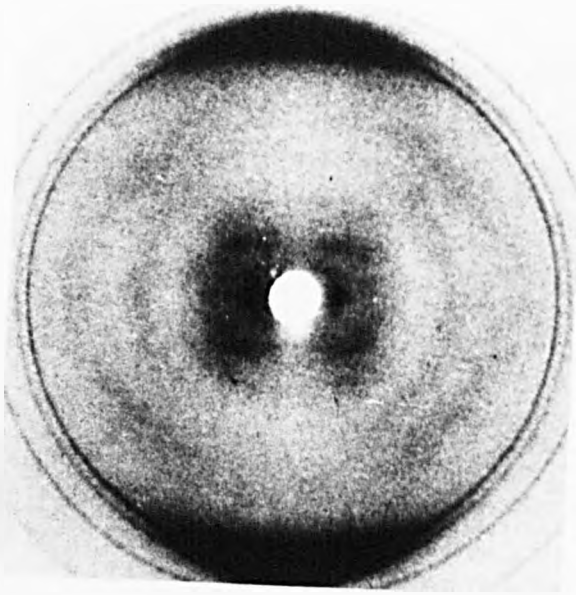

(ii) M = 5.5

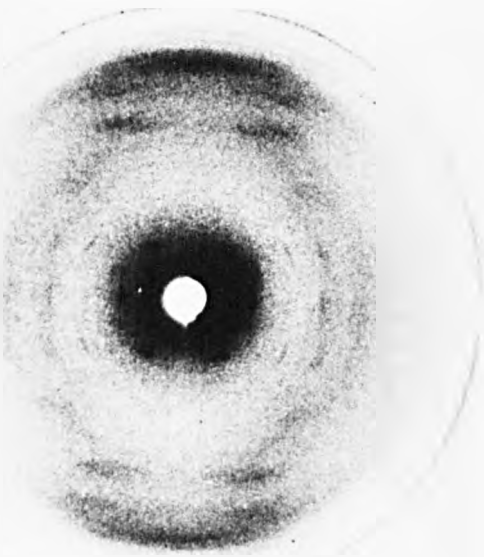

(iii) M = 8.0

(iv) M = 19.0

Figure 5.10 X-ray diffraction patterns from DNA-ethidium fibres at 75% R.H. (0.01 M NaCl)

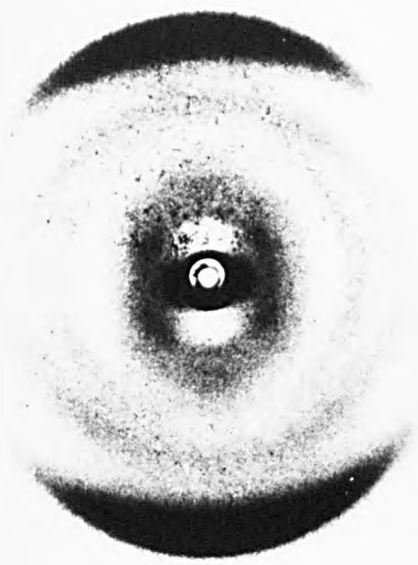

(i) M = 5.0, 92% R.H.

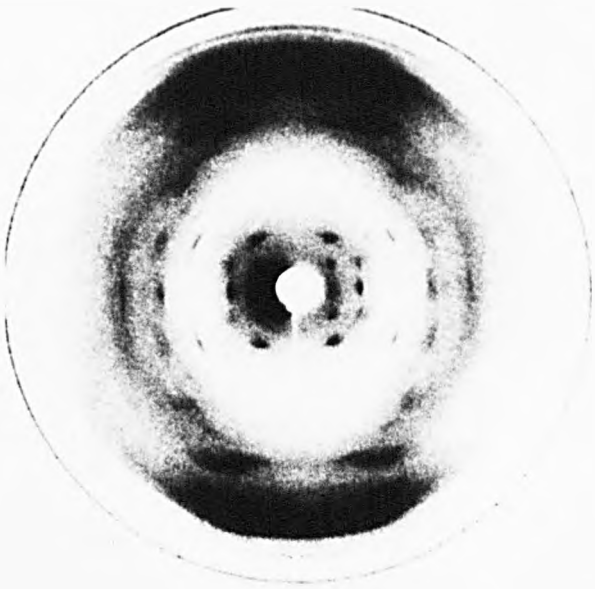

(ii) M = 8.0, 57% R.H.

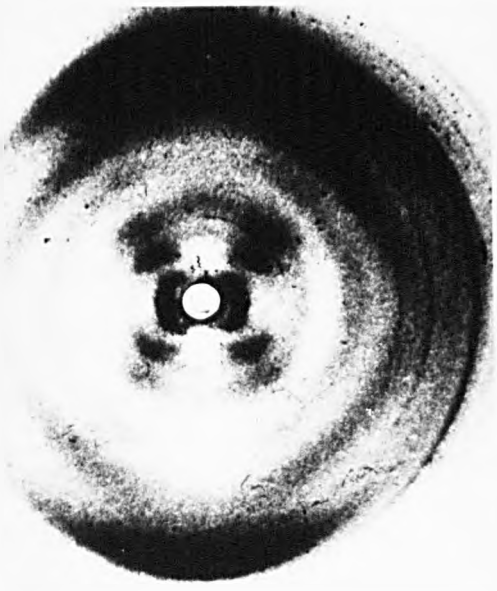

(iii) M = 8.0, 92% R.H.

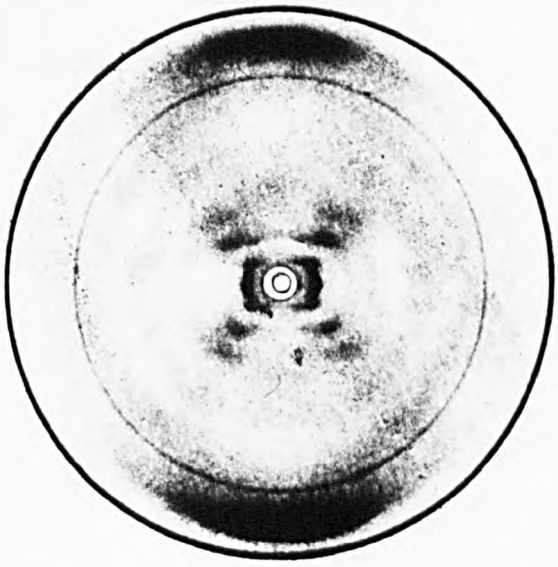

(iv) M = 19.0, 92% R.H.

Figure 5.11 X-ray diffraction patterns from DNA-dimidium fibres (0.01M NaCl)

fibres of larger drug content as expected from the increased disorder caused by binding, and reflections on the layer lines are not resolved as spots. Only the second layer line is resolvable in Fig. 5.9(i) and (ii). The first layer line is never as clear as the second layer line in B-DNA patterns, but as fibres of increasing drug content are considered the first layer line becomes more obscured by the equatorial streaks (Fig. 5.9(i), (ii) and (iii)). Repeated measurements along the second layer line produced an estimate of the pitch which agreed with estimates from the other three quadrants of the pattern to about $\pm$ 2% for most fibres.

Measurements made on the patterns showed that, at 92% R.H., ethidium causes an increase in the helix pitch from the 33.8Å value obtained with the control DNA fibres, and this increase is a monotonic function of the fractional drug content (Fig. 5.12). The intermolecular separation appears to decrease slightly when ethidium is bound in moderate proportions, but at large drug binding ratios it increases again to about the value for the control DNA (Fig. 5.13).

At 75% R.H. (Fig. 5.10) fibres of high drug content (e.g. M = 4 and M = 5.5) show a vaguely B-type pattern, whereas fibres containing only a small amount of ethidium (e.g. M = 19) exhibit an A-type pattern. Both Fig. 5.10(i) and (ii) show the very strong 3.4Å meridional, with that of Fig. 5.10(i) being arced to a large degree indicating poor orientation within the corresponding fibre. At intermediate values, sometimes an A and sometimes a B type pattern was obtained with different fibres of the same M value. In this range of M values, the variability in the conditions under which the fibre was made seems to be a greater determining factor as regards the conformation than does the actual drug proportion within the fibre. The A-type patterns all show a pitch of around 28.1Å, the pitch of the control fibre at this humidity. The measured pitches for the B-type patterns appearing at 75% R.H. are larger than 28.1Å and they increase over the range of M values as the drug content is increased. For

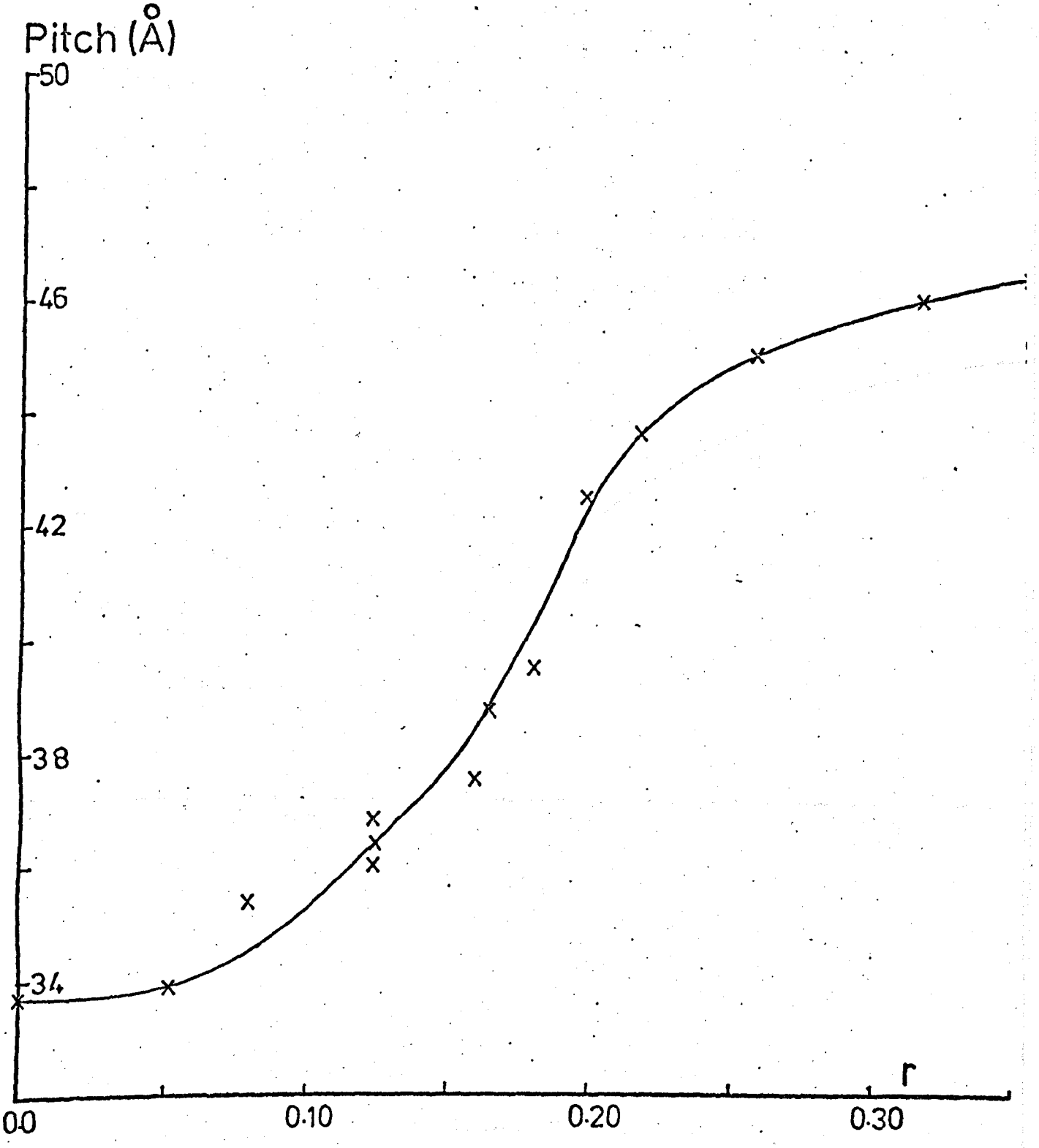

Figure 5.12 The pitch of DNA–ethidium fibres at 92% R.H. as a function of the binding ratio, r. (0.01M NaCl)

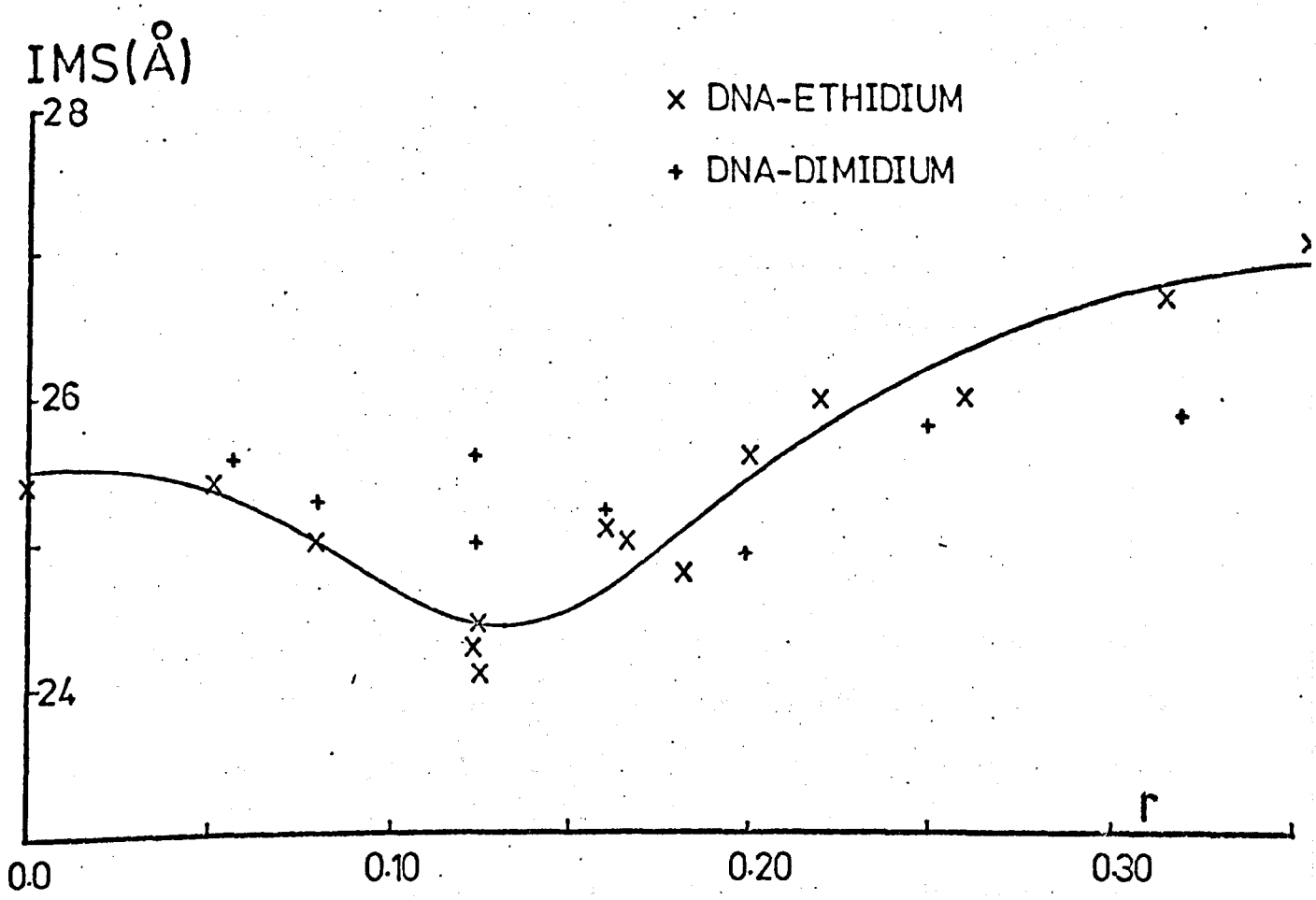

Figure 5.13 The intermolecular separation, IMS, at 92% R.H. for DNA-ethidium and DNA-dimidium fibres as a function of the binding ratio, r. (0.01M NaCl)

large M values (M = 4 and M = 5.5) the pitch has risen to around 33.5Å, comparable with the pitch of B-DNA at 92% R.H. The B-type drug patterns at 75% R.H. would appear to result from binding to a low-pitch form of B-DNA, similar to that obtained by Porumb (1976). The exact mechanism by which the low-pitch conformation arises is not known. It may be regarded as a helix containing alternating regions of A and B type DNA resulting from an indecisive B to A transition in the fibre. Pigram (1968) obtained a diffraction pattern of mixed A and B character from a DNA-ethidium fibre (M = 12.5) at 92% R.H. The two phases could be clearly identified from the low angle diffraction spots.

5.5.2 Discussion of Results

Fig. 5.12 shows a progressive increase in the pitch of the fibres at 92% R.H. with increasing proportions of bound ethidium. The increase in pitch becomes more gradual at high drug contents, and appears to approach a limit of about 47Å at M $\approx$ 2.5 (i.e. r = 0.4). This is similar to the saturation binding level deduced from the spectroscopic measurements in Section 4.4.1, and could be due to an exclusion site effect.

An increase in helix pitch with increased drug binding is not absolute proof of intercalative binding, since an external binding mechanism could be envisaged which would cause an unwinding of the helix. A larger unwinding angle per drug would be required to account for a certain increased pitch for an externally bound drug, than if the increase were due to intercalation. This is because intercalation increases the pitch by insertion of a drug molecule into the helix as well as by the consequent unwinding of the helix to relieve the tension in the sugar-phosphate backbone.

External binding of a large amount of drug would probably tend to increase the intermolecular separation of the helices since the added volume of the drugs would tend to keep the helices well separated.

Intercalation could successfully explain the observed reduction in intermolecular separation (Fig. 5.13), since intercalative drug molecules are inserted into the centre of the double helices and so there is less material to block the close approach of the helices. The unwinding of the helix by intercalation would result in the molecule becoming thinner, and hence in a reduced intermolecular spacing. However, the interpretation of the change in intermolecular separation with M is very difficult. For instance, the externally bound drug molecules would be expected to cause considerable screening of the electrostatic repulsion between the DNA helices, thus allowing the helices to pack closer together.

Intercalative binding seems to be the only realistic way to explain all the observations, and account for the retention of the 3.4Å repeat along the helix axis. An intercalated chromophore would scatter X-rays in much the same way as a base-pair and since the ethidium chromophore is about 3.4Å thick the meridionial would be almost unaltered.

The relationship between the increased pitch, P_{int}, and the amount of intercalated drug (of 3.4Å thickness) into a B-type structure is given (after Fuller, 1966) by -

$$P_{int} = \frac{P(1 + Fr)}{1 - \frac{Fr\,\phi}{36^{o}}} \qquad (5.9)$$

where P is the original pitch, before intercalation, F is the fraction of bound drug which is intercalated, ϕ is the unwinding angle at the intercalation site and r is the binding ratio as previously defined (Section 2.3.1 (a)). This relationship is shown in Fig. 5.14 with P = 34Å for various unwinding angles in the range 6^{o} and 36^{o}, and F values of 0.5, 0.7 and 1.0.

A corresponding formula for the increased pitch due to external binding P_{ext}, is given by

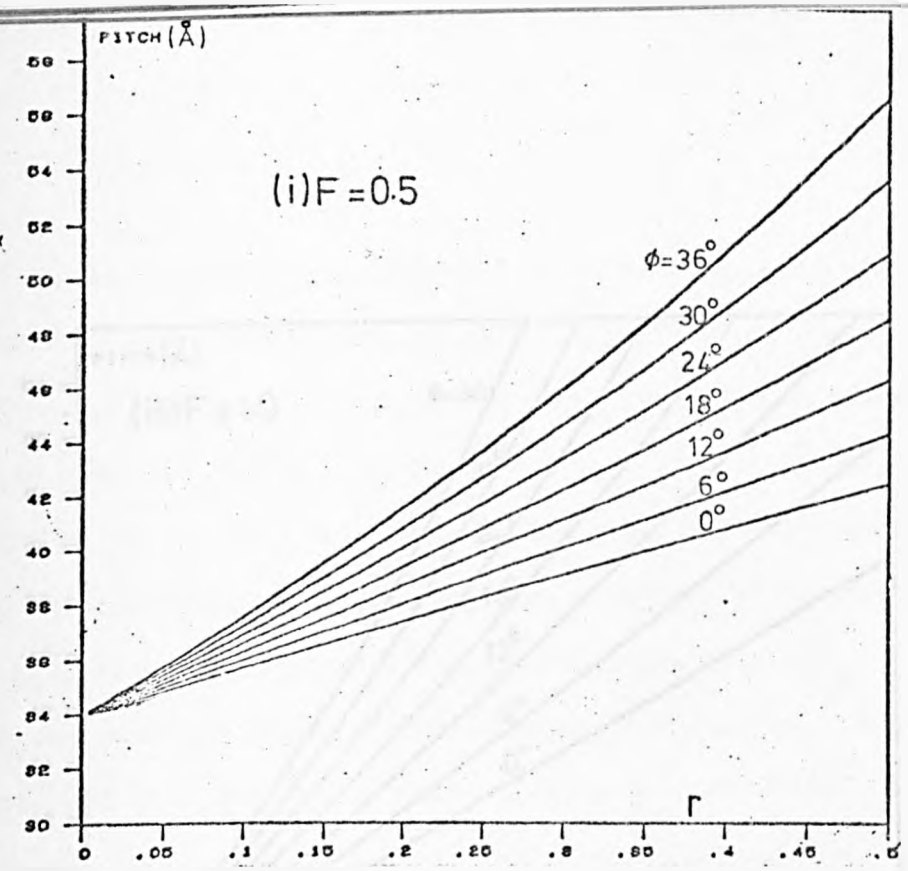

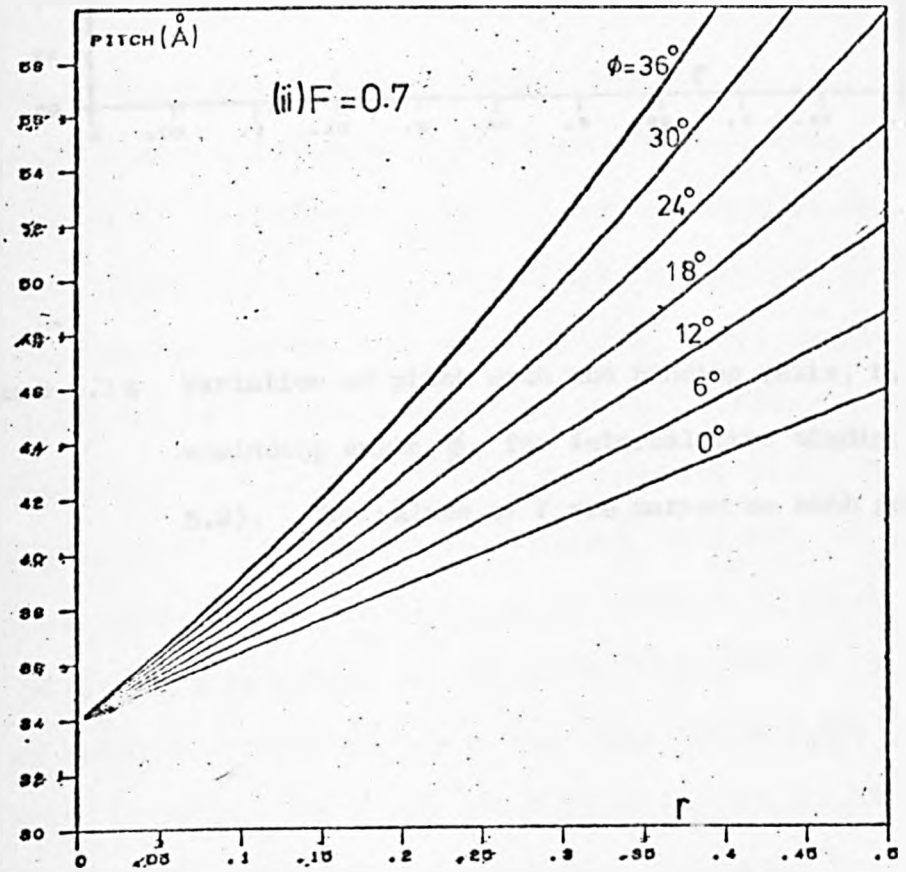

Figure 5.14

/contd.

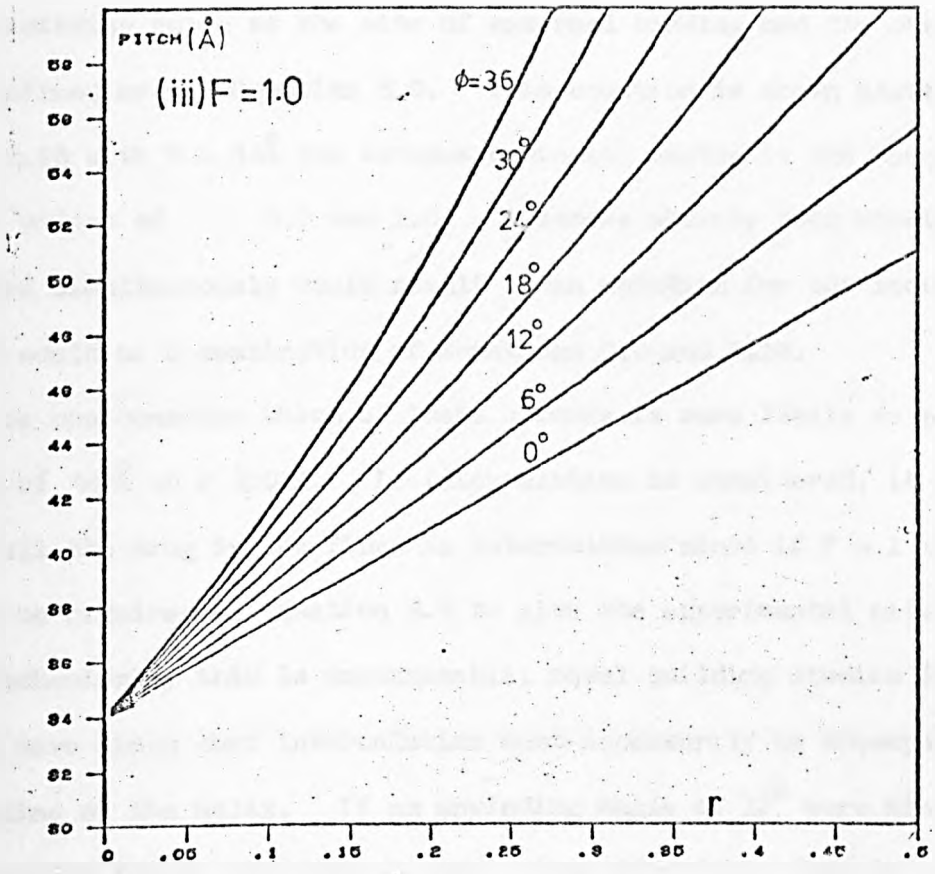

Figure 5.14 Variation of pitch with the binding ratio, r, and the unwinding angle, ϕ, for intercalative binding (Equation 5.9). The values of F are marked on each graph.

$$P_{ext} = \frac{P}{1 - \frac{F'r\phi'}{36^{o}}} \qquad (5.10)$$

where F' is the fraction of bound drug which is externally bound, ϕ' is the unwinding angle at the site of external binding and the other symbols are defined as for Equation 5.9. This equation is shown plotted in Fig. 5.15 with P = 34Å for various unwinding angles in the range 6^{o} to 36^{o}, and F values of 0.7 and 1.0. A scheme whereby both binding modes existed simultaneously would result in an equation for the increased pitch which would be a combination of Equations 5.9 and 5.10.

We can consider which of these schemes is more likely to result in a pitch of ~47Å at $r \approx 0.4$. If intercalation is considered, it is unlikely that all the drug in the fibre is intercalated since if F = 1 no unwinding would be required in Equation 5.9 to give the experimental pitch value. Stereochemically this is unreasonable; model building studies (Pigram, 1968) have shown that intercalation must necessarily be accompanied by an unwinding of the helix. If an unwinding angle of 12^{o} were assumed (as proposed by Fuller and Waring, 1964), then 67% of the drug in the fibre would need to be intercalated. If a higher unwinding is proposed, say 26^{o} (as suggested by Wang (1974)) then a smaller fraction of the drug is required to be intercalated - in this instance, 49%. Considering an external binding mode, even if all the drug in the fibre was bound externally, Equation 5.10 would require an unwinding of 25^{o} to account for the observed pitch of the fibres at high drug content. If all of the drug is not bound, higher unwinding angles would be required. For example, if 70% of the drug in a fibre is externally bound then an unwinding of 36^{o} would be required at each binding site. This latter value is unacceptably large since it would cause a very large disruption of the DNA helix, and even at fairly low drug content the diffraction patterns would lose their B-type character. Such a large unwinding angle cannot be accommodated readily into models of the DNA-drug structure (Pigram, 1968). It is difficult to

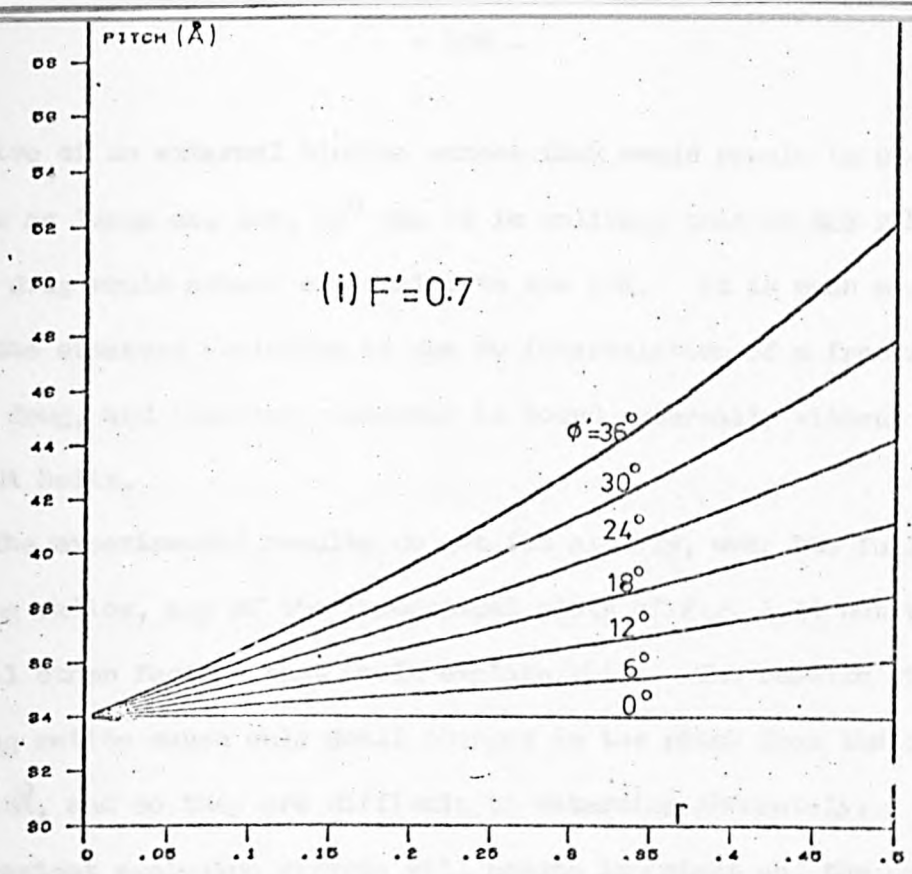

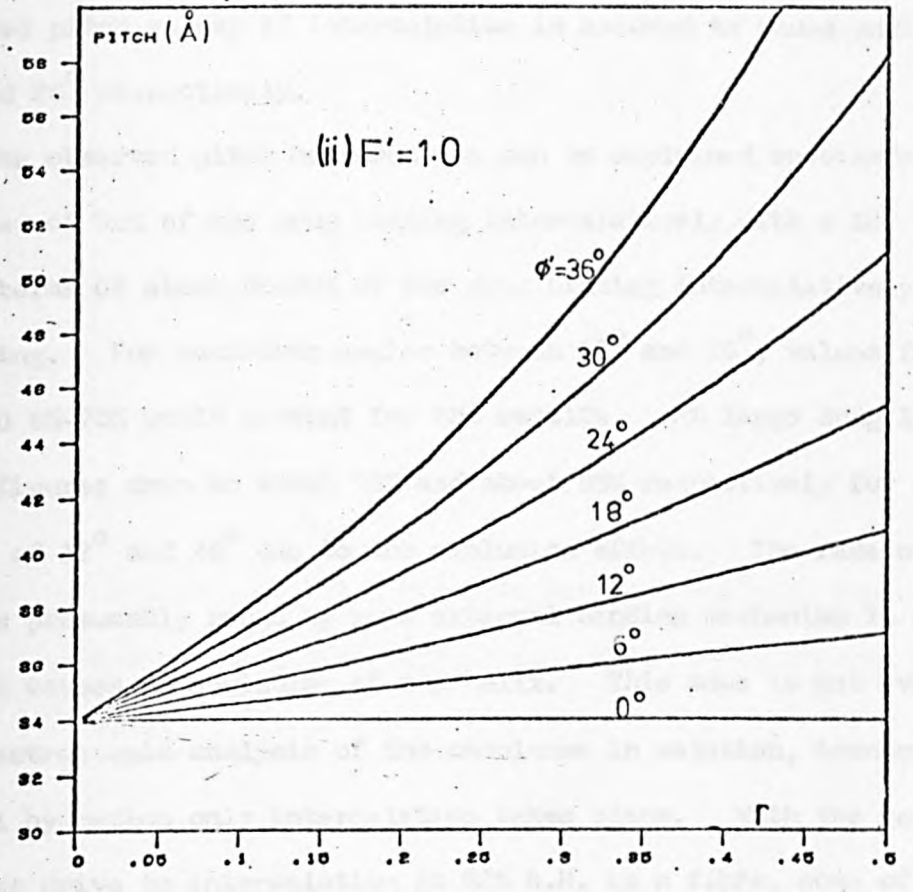

Figure 5.15 Variation of pitch with the binding ratio, r, and unwinding angle, ϕ', for external binding (Equation (5.10)). Values for F' are marked on each graph.

conceive of an external binding scheme that would result in unwinding angles as large as, say, 25° and it is unlikely that at 92% R.H. all the bound drug would attach externally to the DNA. It is much more probable that the observed unwinding is due to intercalation of a fraction of the bound drug, and that the remainder is bound externally without altering the DNA helix.

The experimental results do not fit closely, over the full range of binding ratios, any of the theoretical plots of Fig. 5.14 but there are several other factors that would explain this. The results at low binding ratios cause only small changes in the pitch from the control value of 33.8Å, and so they are difficult to determine accurately. At larger drug content exclusion effects will become important and the drug will find it increasingly difficult to find suitable binding sites. Table 5.2 shows the fraction of intercalative binding, F, required to explain the measured pitch values if intercalation is assumed to cause unwindings of 12° and 26° respectively.

The observed pitch measurements can be explained successfully either in terms of 90% of the drug binding intercalatively with a 12° unwinding, or in terms of about 65-70% of the drug binding intercalatively with a 26° unwinding. For unwinding angles between 12° and 26°, values for F between 90% and 65-70% would account for the results. At large drug loadings, these figures drop to about 75% and about 55% respectively for unwinding angles of 12° and 26° due to the exclusion effect. The remainder of the drug is presumably bound by some external binding mechanism in such a way that it causes no unwinding of the helix. This mode is not evident in the spectroscopic analysis of the complexes in solution, because presumably at full hydration only intercalation takes place. With the reduced hydrophobic drive to intercalation at 92% R.H. in a fibre, some of the drug slips out from its intercalation site and binds externally.

As the humidity is lowered the DNA-ethidium fibres adopt a conformation

TABLE 5.2

The Pitch of DNA-ethidium Fibres, P, at Various r Values, and the Fractions of Intercalatively Bound Drug Needed to Explain these Pitch Values According to Equation (5.9)

P	r	F (if $\phi = 12^{\circ}$)	F (if $\phi = 26^{\circ}$)
33.8	0	-	-
35.4	0.080	0.44	0.34
36.4	0.125	0.45	0.35
37.5	0.160	0.50	0.38
38.7	0.166	0.63	0.48
39.5	0.182	0.67	0.50
42.5	0.200	0.91	0.67
43.6	0.220	0.92	0.68
45.0	0.260	0.88	0.65
46.0	0.318	0.78	0.57
46.5	0.356	0.72	0.53

Note: The values of F for $r \leq 0.16$ are less reliable since the corresponding pitch values are close to the control DNA value.

of lower helix pitch. Intercalation is known to stabilise the B-form of DNA (Bloomfield et al., 1974 - melting temperature measurements). For fibres with a low proportion of drug (e.g. M = 19), it appears that all the intercalated drug slips out at 75% R.H. allowing the helix to adopt an A-type conformation. The drug molecules, now either externally bound or free in the fibre, are randomly orientated within the fibre and cause a degradation in the resolution of the pattern. At high drug content (M = 4 and M = 5.5) sufficient drug remains intercalated to stabilise a B-type pattern. The pitch of these patterns is around 33.5Å indicating that these complexes do not represent an unwinding of the control B-DNA appearing at 92%, but rather an unwinding of a lower pitch conformation of DNA which is similar to the B-conformation (Porumb, 1976; Goodwin, 1977). At intermediate values of M the situation is more complex, and regions of A-type and B-type DNA probably exist together within a particular fibre. For a particular value of M, the pitch at 92% R.H. is always greater than that obtained at 75% R.H., so that there is little doubt that intercalatively bound ethidium slips out of the helix as the humidity is lowered. It is not possible to assess the extent of this behaviour since patterns from the low-pitch B-type DNA, occurring at 75% R.H., have not been obtained by the author.

The patterns are generally very similar to ethidium patterns of the same drug content that have been reported previously (Pigram, 1968; Porumb, 1976). The disorientation half-angle, δ, for all the patterns is between 4^{o} and 9^{o}. There may be some correlation between the disorientation and the drug content, but it was difficult to recognise. Variations within the range 4^{o} - 9^{o} were observed with different fibres of the same M values, so it seems that the conditions operating whilst pulling an individual fibre are of prime importance. It is unlikely that variations in the disorientation within this range would have much effect on the results for the pitch and intermolecular separation, even if intercalation were to

increase the disorientation to some extent by kinking the helices (Chapter 8). Although the disorientation measurements have not been used in this discussion, they will be of value when considering the dichroic ratio values in Chapter 7.

5.6 Dimidium Bromide

5.6.1 Experimental Results

The diffraction patterns obtained with dimidium are very similar to those obtained with ethidium. A selection of them is shown in Fig. 5.11. The same features are present as with ethidium - in particular, the retention of the 3.4Å meridional and the reduction in layer line spacing, indicating an increase in pitch with increasing drug content. Generally, the patterns obtained were not as good as those obtained with ethidium, though most of the loss in detail may be attributed to a poorer orientation of the helices within the dimidium fibres (compare Fig. 5.11(i), (iii) with Fig. 5.9(i), (ii) and (iii)). By analogy with ethidium, there is no doubt that dimidium binds intercalatively. The variation of pitch with drug content at 92% R.H. is shown in Fig. 5.16, and the values for intermolecular separation are shown in Fig. 5.13 together with the results for ethidium. The values obtained for the intermolecular separation do not show clearly the drop in IMS at moderate r values, and the subsequent increase at large r values to the control value for B-DNA, that was observed with ethidium. Instead they are more-or-less randomly distributed within the range 24Å to 26Å for M values between 4 and 19.

5.6.2 Discussion of Results

The variation of helix pitch with drug content is identical to that for ethidium, at r values up to about 0.20. At higher r values, the pitch is slighter higher than for ethidium. It appears to approach a constant value of about 49Å at r = 0.4. This asymptotic behaviour at high drug content again probably reflects the exclusion character of the binding. The higher observed pitch values at large r values suggest that either exclusion effects are less prominent than with ethidium, or that

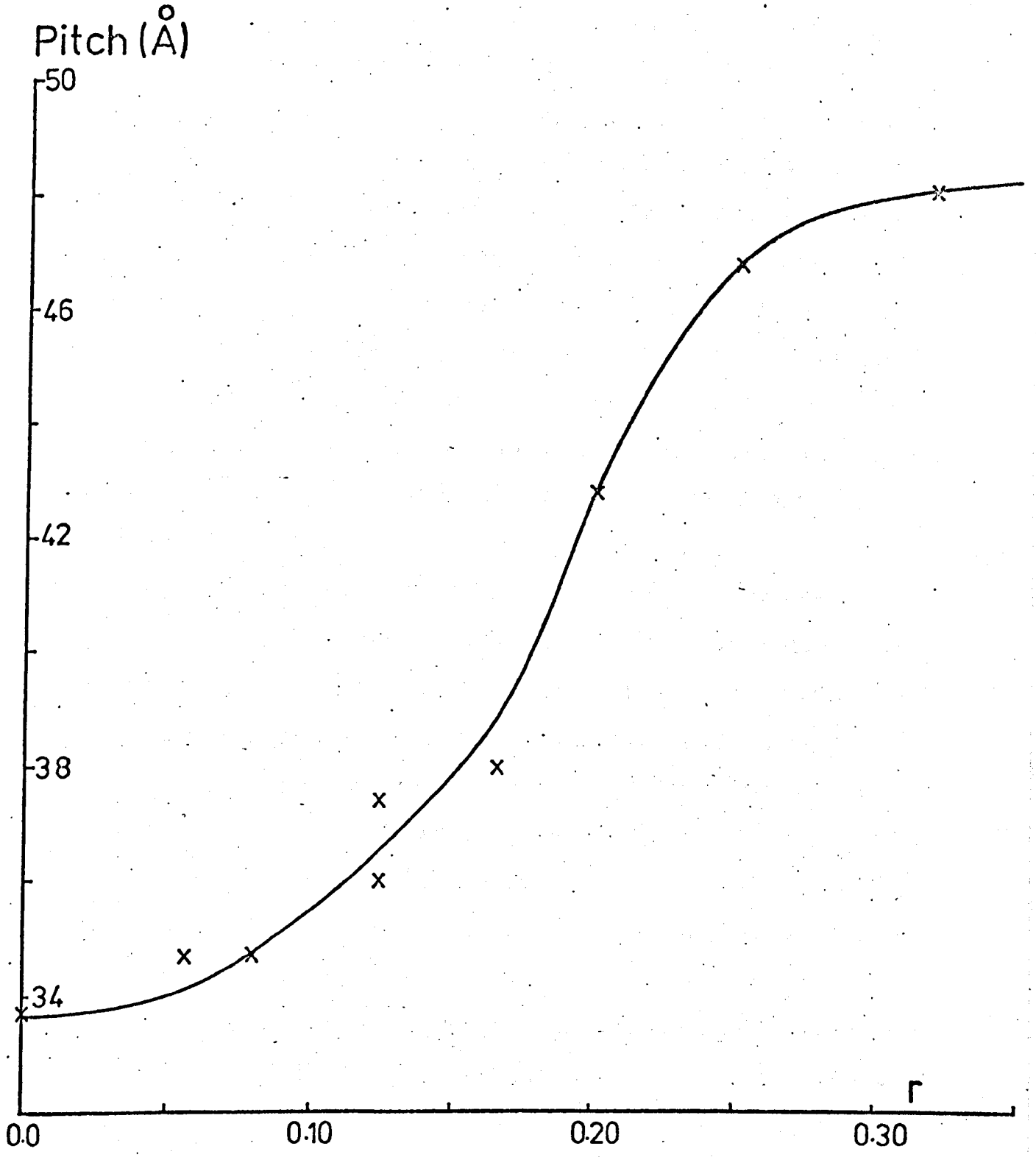

Figure 5.16 The pitch of DNA-dimidium fibres at 92% R.H. as a function of the binding ratio, r. (0.01M NaCl)

the hydrophobic drive towards intercalation is greater. This is in agreement with the findings of Chapter 4, where it was noted that the binding site size was smaller for dimidium than ethidium. A pitch of 49Å at r = 0.4 could be due to 76% of the drug in the fibre binding intercalatively with a 12° unwinding at each intercalation site. Alternatively, it could be accounted for by 55% binding with an unwinding of 26°. These values are slightly higher than the values derived for ethidium binding at high r by the same mechanisms (viz. 67% and 49% respectively), and are consistent with the smaller apparent binding site size of dimidium compared with ethidium (2.41 compared with 2.74 for binding in solution at this ionic concentration).

It is very likely that dimidium unwinds the helix by the same angle as ethidium since they are very similar molecules. This would explain the close similarity in Figs. 5.16 and 5.12 at low binding ratios. The same unwinding angle can account for the results at large r, and the higher pitch values can be explained in terms of higher fractions of intercalative binding. Wakelin and Waring (1974) estimate the unwinding angle for dimidium to be 11.5°, if a 12° unwinding is assumed for ethidium, from unwinding studies of supercoiled DNA in solution. They assumed that all the drug molecules, detected as bound by solvent partition, were actually intercalated. In the fibre state, there appears to be slightly more intercalatively bound dimidium than ethidium for a given (large) r value and this would result in the unwinding angle for dimidium appearing to be slightly lower still than for ethidium. The effect is small, however, and using the values just calculated the unwinding of dimidium would appear to be about 10.6° if the value for ethidium were 12°, and 23° if the ethidium value were 26°.

It is possible, however, that the stereochemistry of intercalation into DNA in solution is somewhat different than in the fibre state and care must be exercised in comparing the values of parameters obtained in

the two states. Hogan et al., (1979) have proposed a model for the intercalation of ethidium into a DNA molecule in solution in which the base-pairs are related to each other in a propellor-like fashion as suggested by Levitt (1978). In this scheme the complementary bases in DNA are not coplanar. Instead they are twisted with respect to each other by about 35° to give an average base twist of 17°. Hogan et al. (1979) suggest that an intercalated drug molecule unstacks the 5' pyrimidines on either side of the binding site, and that the intercalated drug is tilted by an angle between 17° and 28° from being perpendicular to the helix axis. Consequently the lengthening of the helix would be 2.7Å for each intercalated ethidium chromophore rather than 3.4Å. This scheme could not describe the situation in a fibre, since the strong meridional intensity in X-ray fibre diffraction patterns indicates that the base-pairs are nearly perpendicular to the helix axis.

There appears to be little systematic variation in the intermolecular separation of the helices with changing dimidium content (Fig. 5.13). The intermolecular separation is difficult to measure precisely on some of the patterns. The uncertainty due to the width of the equatorial spots in these patterns results in an error of up to ± 1Å, and there were less dimidium patterns measured than ethidium patterns. A large proportion of the uncertainty in the intermolecular separation may be ascribed to the variability in the drying-down of complexes involving an ionic drug (unpublished results of this research group).

5.7 Prothidium Di(bromide)

5.7.1 Experimental Results

The X-ray patterns from DNA-prothidium fibres (Fig. 5.17) are noticeably poorer in quality than those from fibres containing either ethidium or dimidium at corresponding DNA/drug ratios (e.g. compare Fig. 5.17(ii) with Fig. 5.9(iv)). A 3.4Å meridional was observed in all the patterns, indicating that at least some B-type character was retained even at 75% R.H.. For fibres of high drug content ($M \lesssim 8$), the centres of the corresponding diffraction patterns were very vague and they were no resolvable layer lines. This is evidence of a very irregular structure, but the gross features of the patterns indicate that they are based on the B-conformation. The patterns display significantly more detail as the proportion of drug is reduced. A fibre with M = 12 is shown in Fig. 5.17(i) and (ii). At 75% R.H. it exhibits a mixture of A and B-type conformations, whilst at 92% R.H. it shows the B-conformation only. Fibres of very low drug content ($M \gtrsim 17$) often retained some A-type conformation at humidites of 92% and above.

Patterns taken from different prothidium fibres of the same drug content were often variable in quality. This is thought to be largely due to the variability in the drying down of the gel. Some fibres may dry down quickly on the outside to form a skin containing a less orientated interior. Prothidium gels are very viscious, and the proportion of fibres which collapsed on drying down was much larger than with ethidium and dimidium. On occasions, particular fibres did not display reversible conformational changes as the humidity was changed.

5.7.2 Discussion of Results

The generally poor resolution of the DNA-prothidium patterns compared with patterns using the other two drugs is an early indication that the

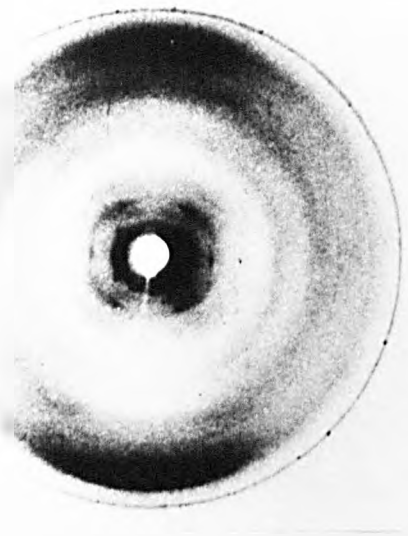

(i) M = 12.0, 75% R.H.

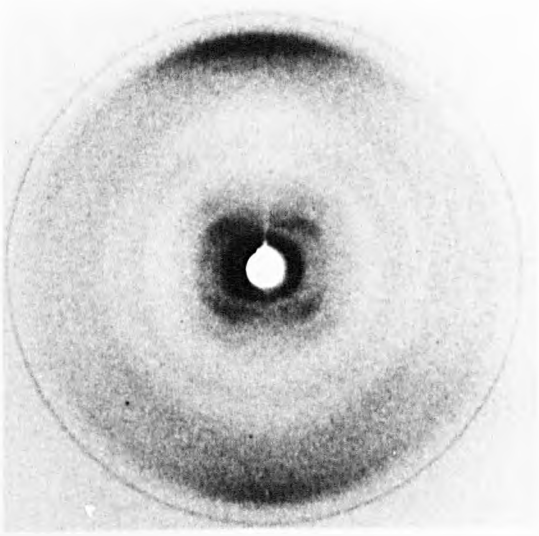

(ii) M = 12.0, 92% R.H.

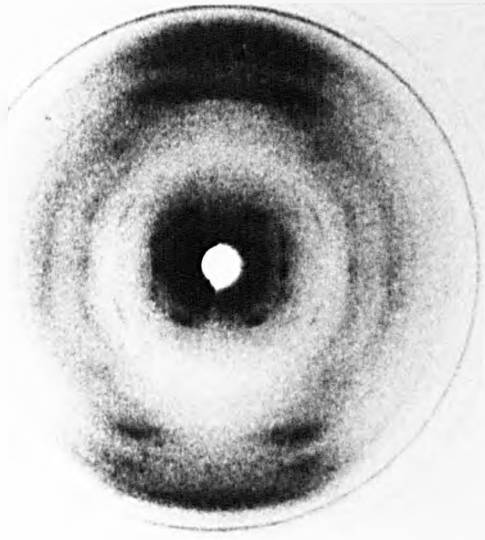

(iii) M = 17.0, 75% R.H.

(iv) M = 17.0, 92% R.H.

Figure 5.17 X-ray diffraction patterns from DNA-prothidium fibres (0.01% NaCl)

DNA is more seriously interfered with by binding prothidium to the helix, although some of the loss in detail is due to the poor orientation of many of the prothidium fibres. Some loss of resolution may be expected due to the greater size of prothidium resulting in a larger perturbation of the DNA, but the rather drastic worsening of the patterns compared with those from ethidium and dimidium suggests a much less regular character to the binding, or indeed a different mode of binding, than that operating with the other two drugs. The patterns which showed a significant proportion of A-type diffraction showed less distinct reflections than obtained in the control A-DNA patterns at angles corresponding to distances in real space of 15Å and above. This indicates a limited crystallinity within the DNA-drug structure, probably due to an increase in screw disorder as more drug is bound. There is very little detail remaining in these patterns at 3 - 10Å resolution, indicating a severe loss of regularity in the molecules at the nucleotide level.

The B-type patterns all give rise to pitch values less than or about 34Å at 75% R.H. and about 34Å at 92% R.H., which indicates no unwinding of the helix compared with the control B-DNA pattern. Porumb (1976) has obtained B-type patterns with a pitch less than 34Å using daunomycin and adriamycin at humidities around 80%R.H. This is consistent with the belief that low-pitch B-type DNA conformations may be stabilised at low humidities. The author has not obtained any low-pitch B-type DNA patterns using the control DNA fibres, with which to compare the DNA-prothidium patterns. However, the appearance of low-pitch DNA seems to require a rather delicate balance of ionic and humidity conditions (Porumb, 1976).

The intermolecular separation measured from the B-type patterns increases by 2-3Å as prothidium is bound up to M = 12, after which it is difficult to resolve the B equatorial spot. The increase indicates that binding by prothidium may result in a bulkier structure, and this could be accounted for by an external mode of binding - either along a strand of the

double helix, or across from one strand to the next. Both of these binding schemes could occur to binding levels greater than one drug for every two base-pairs (c.f. the spectroscopic results of Section 4.4.3). If both of these binding mechanisms were operating simultaneously a substantial degradation in the regularity of the structure, as revealed by X-ray diffraction, would result even at much lower binding levels. This is because the electron density of the drug, in an external binding mode, is at a radius equal to or greater than that of the sugar-phosphate backbone. The most reasonable interpretation of the B-type drug patterns is that prothidium binds to DNA by a mechanism that does not involve a substantial pitch increase, and this precludes intercalation as the major binding mode. The increased intermolecular separation at high levels of binding suggests that the mode of binding is an external attachment to the sugar-phosphate backbone.

All the vaguely A-type patterns exhibit a pitch close to 28.1Å, the pitch of the control A-DNA fibre, irrespective of the humidity at which the patterns were taken. Some patterns in which there was a substantial proportion of B-type conformation gave a slightly higher pitch value than this, but this was probably due to the interference between the two simultaneously present patterns making it difficult to measure the layer lines of the A conformation accurately. It is improbable that intercalation would occur with the A-like conformation since it was not found to occur in the B-like patterns, in which the DNA offers a stereochemically more favourable conformation. The positions of the equatorial spots on an A-DNA pattern provide information on the size of the lattice parameters a and b, and may be used to describe the separation of the helices analogous to the intermolecular separation used in discussing B-type patterns. Only one equatorial spot could be identified on the DNA-prothidium mixed A/B patterns as arising from the A-like conformation. Measurement of it indicated that there was no significant change in its position compared with

the corresponding reflection in A-DNA. The observation that an A-type character may persist even when the humidity is raised to 92% R.H., may be due to drug binding across the strands holding them rigidly in their A-conformation and resisting a conformational change to the B-type structure.

Wakelin and Waring (1974) have reported that prothidium uncoils closed circular DNA, indicating that its binding unwinds the helix. However, their results have not been quoted in detail so it is not possible to assess the magnitude of this effect. The X-ray diffraction results quoted here rule out the possibility of substantial intercalation in the fibre state. Differences in the DNA structure in solution compared with its structure in the fibre state would undoubtedly modify the binding schemes present in the two forms, and may account for the apparent change in the binding priorities. Neville and Davies (1966) have reported that in order to investigate the diffraction patterns of DNA-acridine fibres at high hydrations, it was insufficient simply to raise the humidity in the X-ray camera to 100% R.H.; the fibres had to be actually wetted. (This was in contrast to NaDNA fibres at 100% R.H., which swelled continuously without coming into direct contact with liquid water). They found that the wetting could be accompanied by exposing the fibres to a mist of water, and that the degree of hydration obtained depended on the time for which the fibre was exposed. If these considerations apply to prothidium, it is likely that the conformation of the DNA before binding is substantially different in the fibre state at 92% R.H. than it would be in solution, so that different binding mechanisms may operate in the two cases. It is possible that prothidium might intercalate in a fibre of very high humidity, but will not intercalate at 92% R.H. - a similar behaviour to the acridines.

The study of the interaction of prothidium with DNA is generally rendered very difficult because of its high binding affinity (Section 4.4.3) and the multiplity of possible binding modes (Chapter 8). The binding constant of doubly charged drugs binding electrostatically is strongly

dependent on the ionic concentration. Duane (1972) and Record et al. (1976) have shown that a straight line is obtained when the logarithm of the binding constant is plotted against the logarithm of the ionic concentration. According to Record et al. (1976) the slope of this line is $m'\psi$, where m' is the number of ion pairs formed in the interaction and ψ is a parameter equal to 0.88 for double-stranded DNA. Local variations in the ionic concentration within a DNA-prothidium fibre will greatly affect the association constants of the drug for electrostatic attachment to DNA, and would therefore affect the delicate balance between the binding modes in operation. This may be part of the reason for the greater variability in the prothidium patterns, for a particular drug content and humidity, than was observed with the singly-charged dimidium and ethidium.

5.8 Summary

The results of this chapter are best explained by intercalative mechanisms being the major binding mode to DNA for both dimidium and ethidium. It is not possible to specify the unwinding angle caused by intercalation because the fraction of bound drug actually intercalated is not known. The results are consistent with unwinding angles in the range 12° to 26°, if the corresponding fractions of intercalated drug are between about 90% and 70% respectively. No evidence of prothidium intercalating into DNA has been obtained. Some unwinding of the helix at 75% R.H. by an external binding mode cannot be precluded but since there is usually some B-type structure present as well it is more likely that the small measured pitch increase above 28Å is due to interference with the B-pattern. The doubly charged prothidium appears to bind so strongly either along the phosphate chain or between the two chains, that it is reluctant to leave this site and slip into an intercalation position even at high humidity. The optical data presented in Chapter 7 will be analysed with a view to elucidating the orientation of the bound drug molecules at their binding sites, and model-building studies in Chapter 8 will attempt to explain the differences in the binding mechanisms amongst these phenanthridines in terms of their structural features.

CHAPTER 6

Linear Dichroism and Birefringence - A Theoretical Treatment

6.1 Linear Dichroism

The absorption of visible light by a DNA-drug fibre depends on the nature of the visible absorption bands of the drug, and on the changes in these induced by binding to DNA. The DNA base-pairs do not absorb in the visible region of the spectrum. The visible absorption bands of the drug chromophores are due to $\pi - \pi^*$ transitions (Ingraham and Johansen, 1969; Giacomoni and Le Bret, 1973) which take place within the plane of the drug.

The phenomenon of linear dichroism is the result of the preferential absorption of light plane-polarised in a particular direction. As mentioned in Chapter 2, the dichroic ratio, D, can be defined as

$$D = \frac{A_\perp}{A_\parallel} \qquad (6.1)$$

where $A_\perp$, $A_\parallel$ are the absorbances for light polarised perpendicular and parallel (respectively) to the fibre axis. The absorption of polarised light depends on the square of the scalar product of the transition moment vector of the chromophore and the electric field vector of the propagating light. Therefore by making absorbance measurements with light polarised perpendicular and then parallel to the fibre axis some information will be obtained regarding the orientation of the drug chromophores. For a fibre in which the drugs are bound such that the plane of the drug chromophore is perpendicular to the DNA helix axis and in which the DNA molecules are aligned along the fibre axis, $A_\perp$ will be larger than $A_\parallel$ and the dichroic ratio will be greater than unity.

The measured dichroic ratio will reflect the anisotropy of the drug and all the factors which affect the inclination of the drug chromophore

to the fibre axis. These will include the amount of free (randomly oriented) drug in the fibre, the amounts of intercalated and externally bound drug and their respective inclinations to the helix axis, and the distribution of the helix orientations about the fibre axis.

6.2 Dichroism of Perfectly Orientated Fibres

Expressions for the dichroic ratio can be obtained either in terms of α, the angle between the transition dipole moment and the plane perpendicular to the helix axis or θ, the angle between the plane of the drug and the plane perpendicular to the helix axis. For an arbitary orientation of the transition dipole within the chromophore, α will be smaller than θ (Fig. 6.1).

Using the notation of Fig. 6.2 and considering light incident along the x-direction,

$$D = \frac{\langle (E_\perp \cos \psi)^2 \rangle}{\langle E_\parallel \cos (90-\alpha)^2 \rangle}$$

where $E_\perp$, $E_\parallel$ are the magnitudes of the electric field vector for the appropriate directions, and "< >" denotes an average taken over the azimuthal angle, ϕ. For light polarised at 45° to the fibre axis (assumed coincident with the helix axes), $E_\perp = E_\parallel$ and therefore

$$D = \frac{A_\perp}{A_\parallel}$$

$$= \frac{\langle \cos^2 \psi \rangle}{\langle \sin^2 \alpha \rangle}$$

$$= \frac{\frac{1}{2\pi} \int_0^{2\pi} \cos^2 \alpha \cos^2 \phi \, d\phi}{\frac{1}{2\pi} \int_0^{2\pi} \sin^2 \alpha \, d\phi}$$

$$= \tfrac{1}{2} \cot^2 \alpha \qquad (6.2)$$

This relationship, for a perfectly orientated fibre, is illustrated in Fig. 6.3. D varies from zero to infinity, and has a value of unity when $\alpha = 35^\circ 16'$. This result is in agreement with that of Fraser (1953), although he worked in terms of the complement of the angle α.

Fig. 6.1 The relationship between θ and α.

The arrowed line indicates the direction of the transition dipole moment

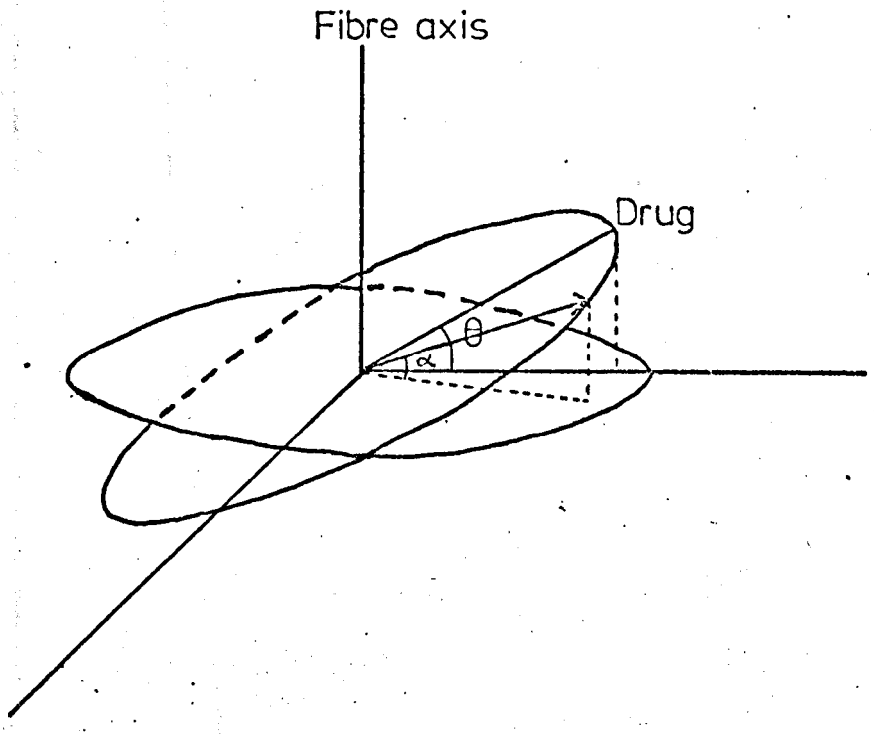

Fig. 6.2 Definition of the angles used in Section 6.2

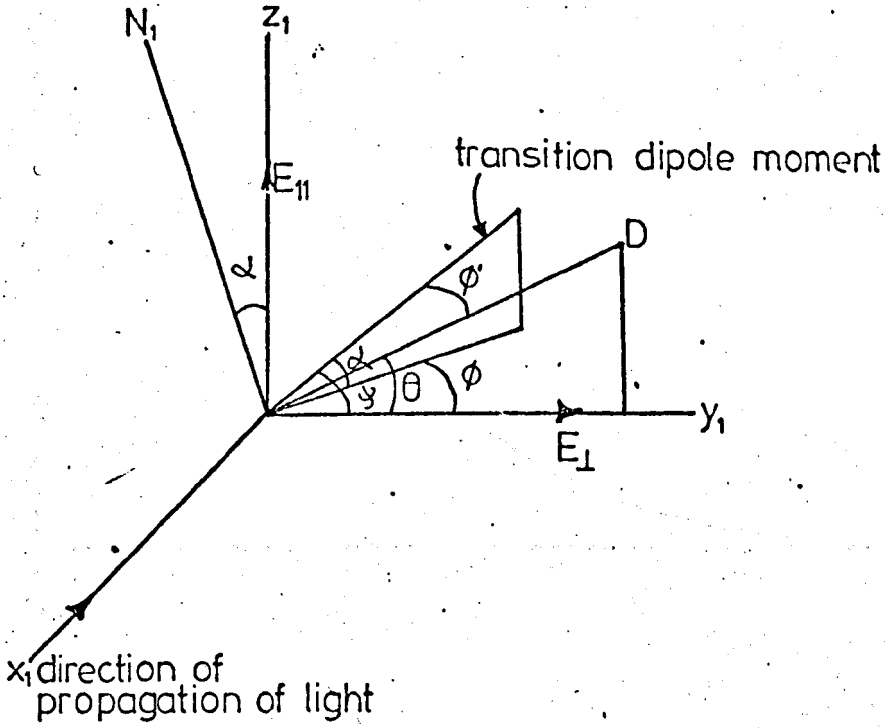

Fig. 6.3 The variation of the dichroic ratio, D, with the tilt of the transition dipole moment, α (Equation 6.2)

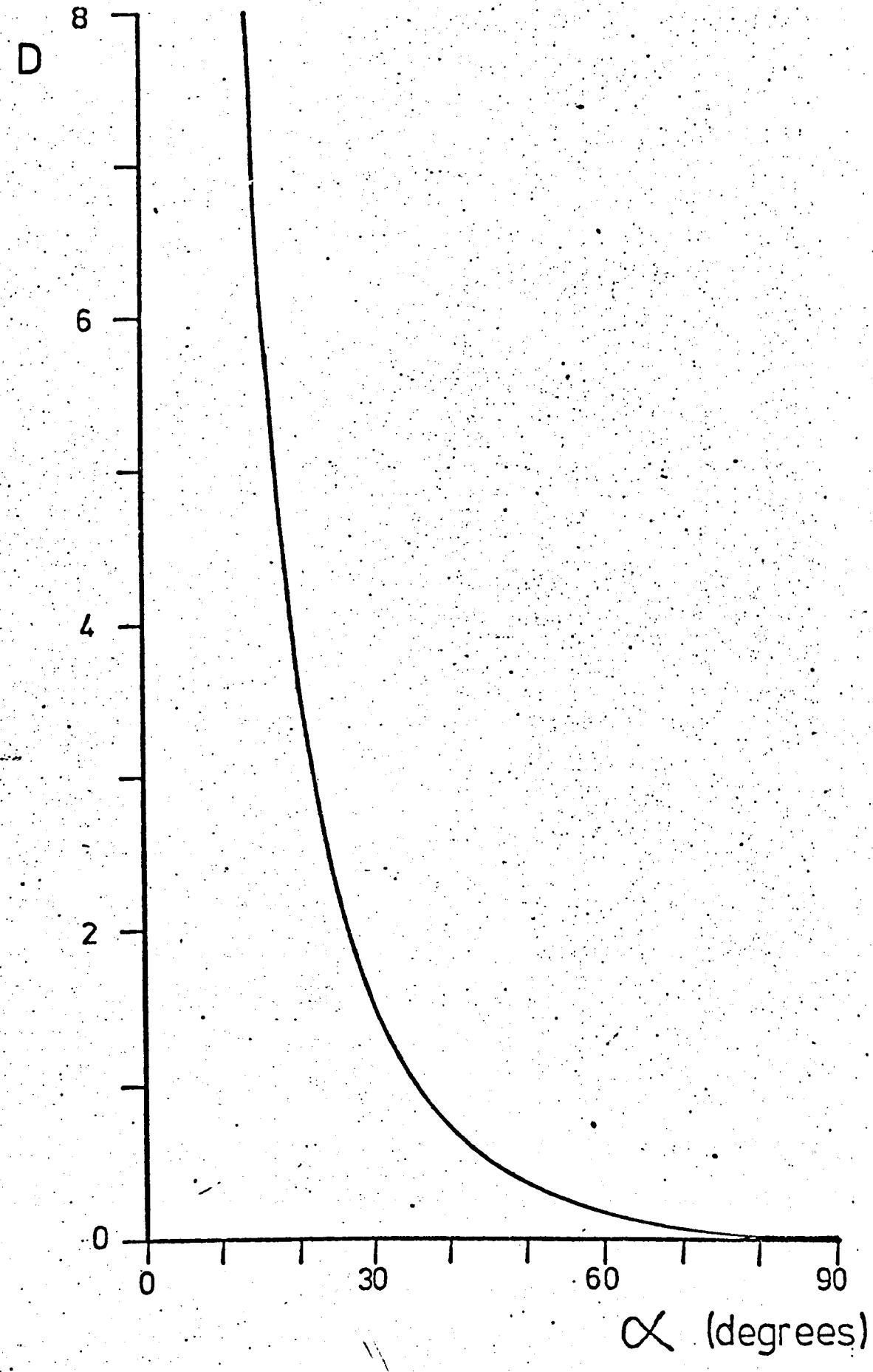

The disadvantage of this treatment is that information regarding the directions of transition dipole moments in drug molecules is very limited. In the absence of information regarding its precise orientation, the transition dipole moment may be considered as pointing isotropically within the drug chromophore. It will be seen below that for small angles of tilt of the chromophore this is a reasonable approximation.

Using the notation of Fig. 6.4,

$$D = \frac{A_\perp}{A_\parallel}$$

$$= \frac{\langle (E_\perp \cos (\Omega_\perp - 90))^2 \rangle}{\langle (E_\parallel \cos (90 - \Omega_\parallel))^2 \rangle}$$

$$= \frac{\langle \sin^2 \Omega_\perp \rangle}{\langle \sin^2 \Omega_\parallel \rangle} \qquad \text{since } E_\perp = E_\parallel$$

For a perfectly orientated fibre, $\Omega_\parallel = \theta$, and since $\cos \Omega_\perp = \sin\theta \sin\phi$ then

$$= \frac{\frac{1}{2\pi} \int_0^{2\pi} (1 - \sin^2 \theta \sin \phi)\, d\phi}{\frac{1}{2\pi} \int_0^{2\pi} \sin^2\theta \; d\phi}$$

$$= \cot^2 \theta + \tfrac{1}{2} \qquad (6.3)$$

This is equivalent to both the expression produced by Seeds (1951), who considered the dipole as being equivalent to two mutually perpendicular dipoles at any arbitrary orientation within the plane of the drug, and to the computer-simulated studies of Porumb (1976).

The variation of D with θ is shown in Fig. 6.5. The dichroic ratio varies from 0.5 to infinity, and takes the value unity when $\theta = 54^\circ 44'$. The dichroic ratio does not fall to zero when $\theta = 90^\circ$, because (unlike the situation when $\alpha = 90^\circ$) this does not correspond to zero absorbance in a plane perpendicular to the helix axis. The transition dipole is considered as isotropic in the plane of the chromophore in this case, so that even when the chromophore is aligned parallel to the helix axis a

Fig. 6.4 A trigonometric system attached to a DNA fibre

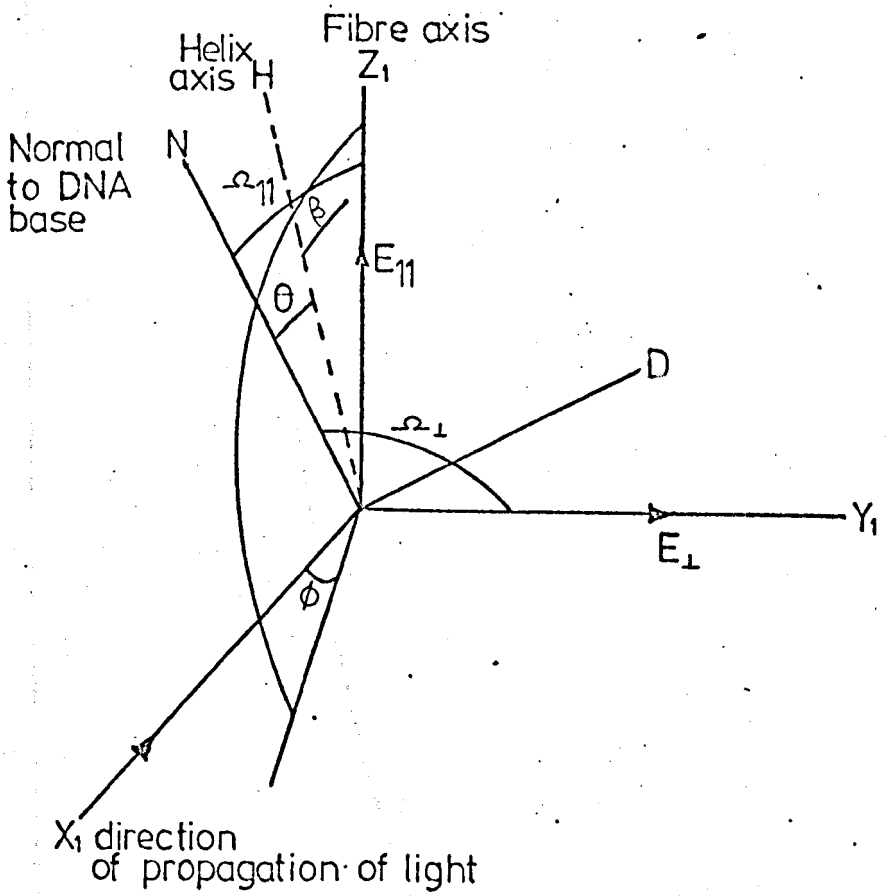

Fig. 6.5 The variation of the dichroic ratio, D, with the chromophore tilt, θ (Equation (6.3))

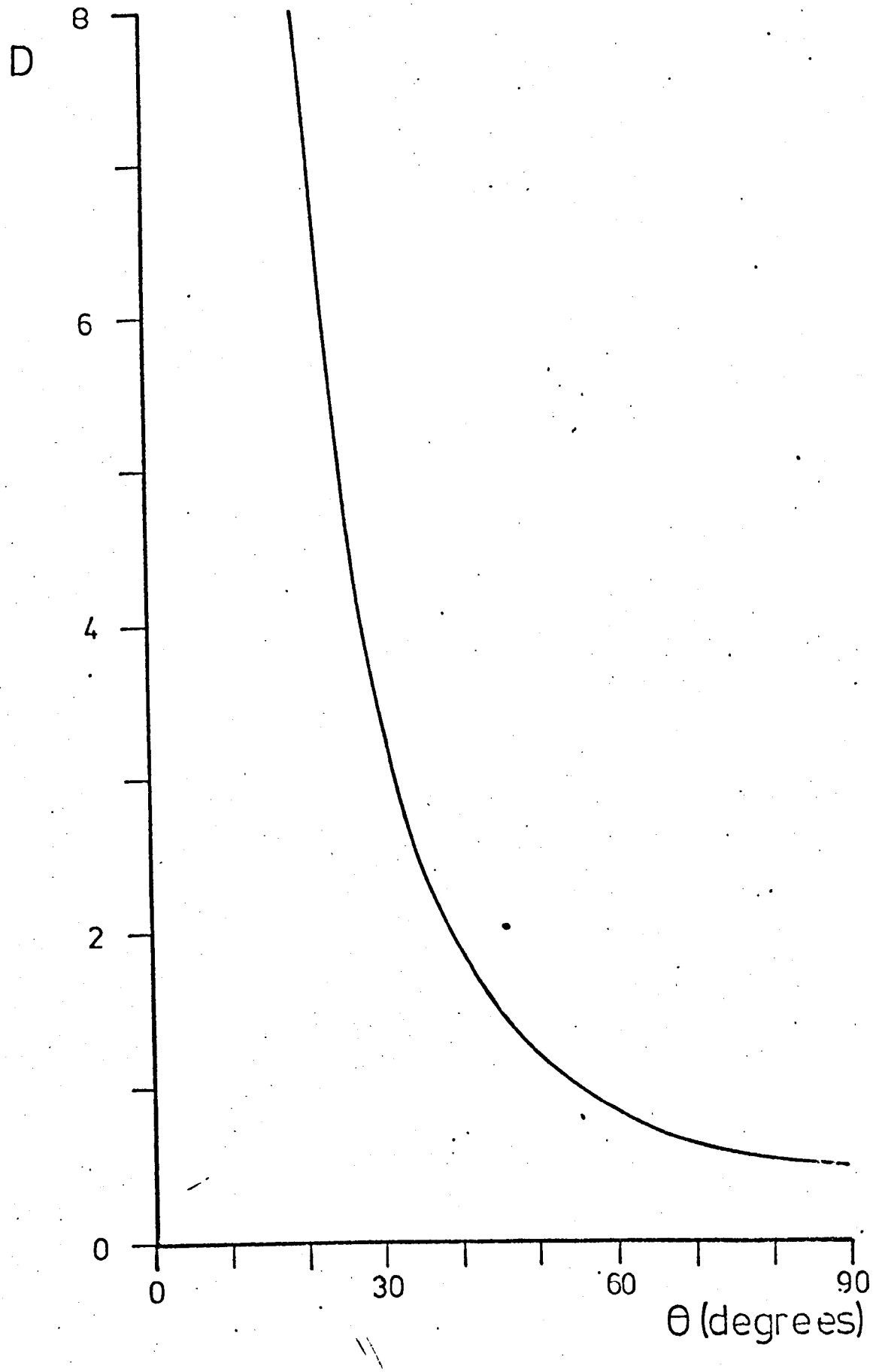

component of the isotropic dipole will contribute to absorption perpendicular to this direction. The values for D predicted on the basis of these two models are similar for small angles. In practice Equation (6.2) is less useful than Equation (6.3) since there is normally little information on the direction of the transition dipole. The angle θ, as used in Equation (6.3), can be taken as equal to the base tilt for intercalative binding and is readily obtained from X-ray diffraction patterns with reasonable accuracy. Equations (6.2) and (6.3) are identical if $\phi' = 45^{\circ}$ (Fig. 6.2). This reflects the situation that the isotropic dipole moment can be considered as two mutually perpendicular dipoles, or as their resultant (viz. one dipole at 45° to them).

6.3 Disorientated Fibres

A fibre can be considered as being comprised of a fraction of the DNA helices completely aligned to the fibre axis, with the remainder being randomly orientated (Fraser, 1953 and 1955; Pilet and Brahms, 1972 and 1973). A more realistic model is that adopted by Porumb (1976), in which the disorientation within the fibre is assumed to take the form of a gaussian spread of the helix axes about the fibre axis. The probability of a DNA helix lying along the surface of a cone of semi-angle β is proportional to $\exp\left(\frac{\beta^2}{2\delta^2}\right)$, where δ is the half-width of the distribution.

A computer program (Porumb and Slade, 1976a, 1976b and 1976c) was used to simulate this situation and gave a series of plots (Fig. 6.6 and 6.7) of the dichroic ratio against either θ or α for different disorientation half-widths, δ.

It is possible, however, to adopt the same model for the disorientation and obtain analytical expressions for the dichroic ratio, rather than resorting to the computer simulation techniques of Porumb and Slade (1976a) or the numerical integration methods of Libertini et al. (1974). These expressions, and the methods used to obtain them, are described in the following sections.

6.3.1 The Dichroic Ratio in Terms of the Chromophore Tilt

It is convenient to use the formalism of Van et al. (1974) and introduce three Cartesian frames of reference - the fibre axes (X_1, Y_1, Z_1), the DNA molecular helix axes (x_2, y_2, z_2) and axes attached to the bound drug (x, y, z).

The transformation from a given Cartesian system to another can be effected by means of three successive rotations performed in a specific sequence. These angles of rotation are called the Eulerian angles, θ, ϕ and ψ, and are defined in Fig. 6.8 using the notation* of Goldstein (1964).

* Unfortunately there is no unanimity in the literature regarding the definition of Eulerian angles; the definition adopted here is one of several.

Fig. 6.6 The dichroic ratio, D, as a function of θ for various disorientation half-widths δ. (The computer simulation results of Porumb, 1976)

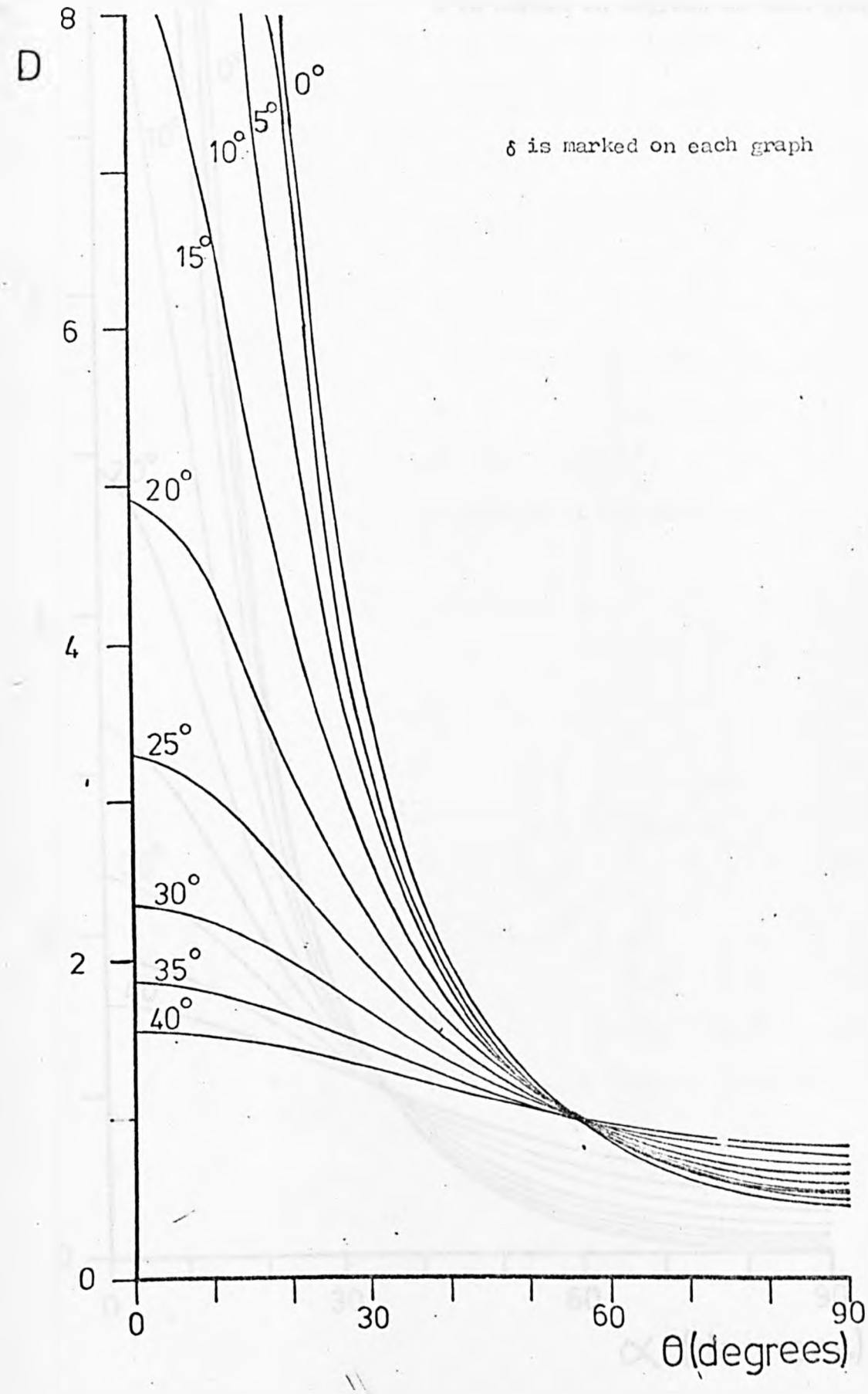

δ is marked on each graph

Fig. 6.7 The dichroic ratio, D, as a function of α for various disorientation half-widths, δ. (The computer simulation results of Porumb (1976)).

δ is marked in degrees on each graph

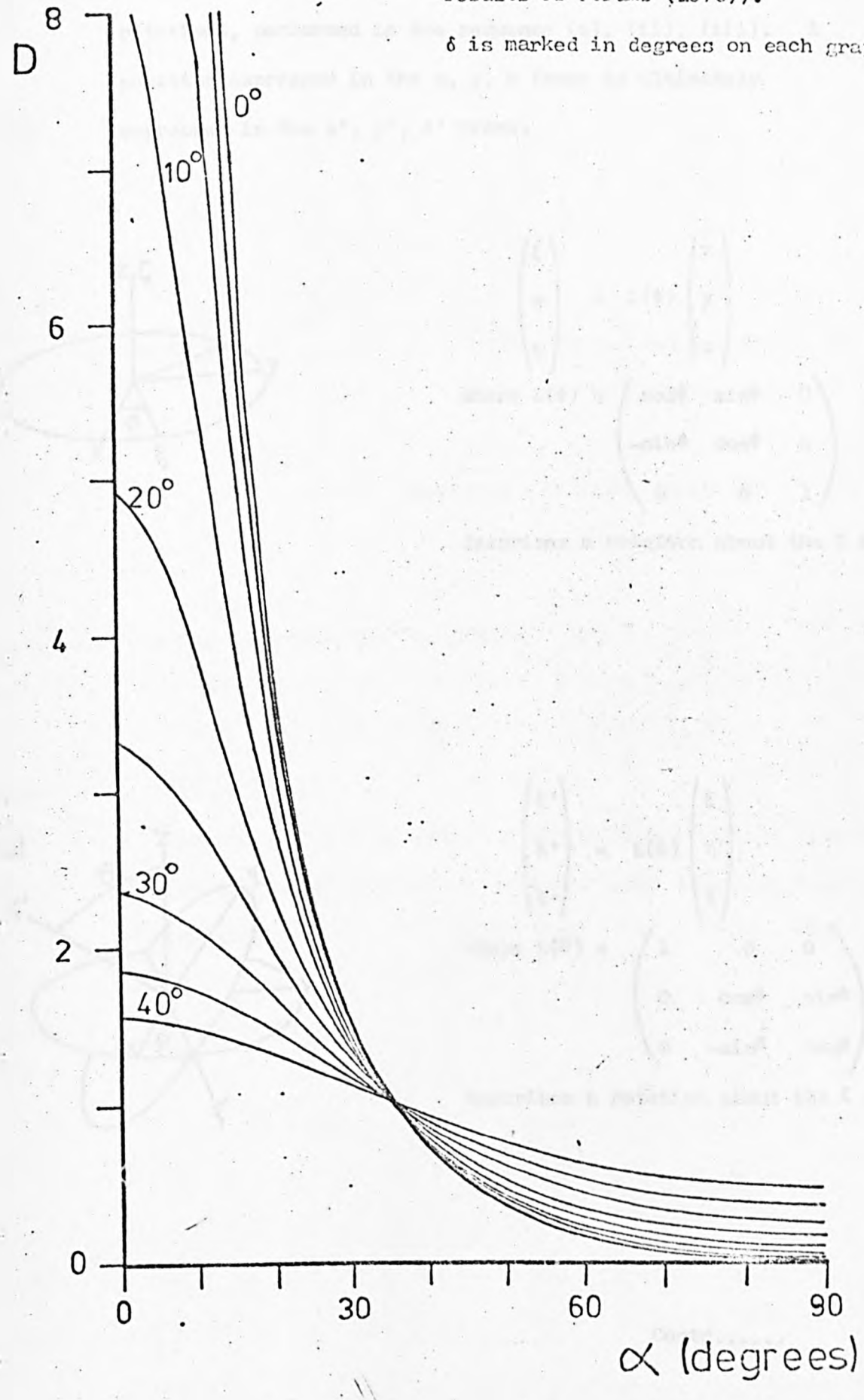

Fig. 6.8 Eulerian angles: a transformation from a given co-ordinate system to another is carried out by means of three successive rotations, performed in the sequence (i), (ii), (iii). A position expressed in the x, y, z frame is ultimately expressed in the x', y', z' frame.

(i)

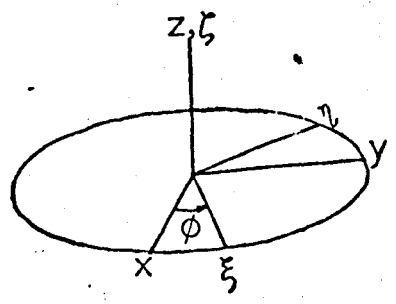

$$\begin{pmatrix} \xi \\ \eta \\ \zeta \end{pmatrix} = L(\phi) \begin{pmatrix} x \\ y \\ z \end{pmatrix}$$

where $L(\phi) = \begin{pmatrix} \cos\phi & \sin\phi & 0 \\ -\sin\phi & \cos\phi & 0 \\ 0 & 0 & 1 \end{pmatrix}$

describes a rotation about the Z axis

(ii)

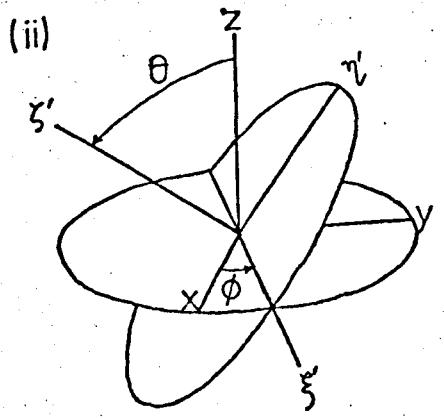

$$\begin{pmatrix} \xi' \\ \eta' \\ \zeta' \end{pmatrix} = L(\theta) \begin{pmatrix} \xi \\ \eta \\ \zeta \end{pmatrix}$$

where $L(\theta) = \begin{pmatrix} 1 & 0 & 0 \\ 0 & \cos\theta & \sin\theta \\ 0 & -\sin\theta & \cos\theta \end{pmatrix}$

describes a rotation about the ζ axis

Contd.....

Fig. 6.8 (contd.)

(iii)

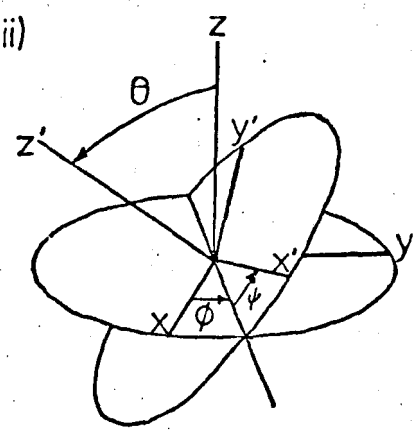

$$\begin{pmatrix} x' \\ y' \\ z' \end{pmatrix} = L(\psi) \begin{pmatrix} \xi' \\ \eta' \\ \zeta' \end{pmatrix}$$

where $L(\psi) = \begin{pmatrix} \cos\psi & \sin\psi & 0 \\ -\sin\psi & \cos\psi & 0 \\ 0 & 0 & 1 \end{pmatrix}$

describes a rotation about the ζ' axis

Hence the complete transformation is given by $\begin{pmatrix} x' \\ y' \\ z' \end{pmatrix} = L \begin{pmatrix} x \\ y \\ z \end{pmatrix}$

Where $L = L(\psi)\, L(\theta)\, L(\phi)$

$$= \begin{pmatrix} \cos\psi\cos\phi - \cos\theta\sin\phi\sin\psi, & \cos\psi\sin\phi + \cos\theta\cos\phi\sin\psi, & \sin\psi\sin\theta \\ -\sin\psi\cos\phi - \cos\theta\sin\phi\cos\psi, & -\sin\psi\sin\phi + \cos\theta\cos\phi\cos\psi, & \cos\psi\sin\theta \\ \sin\theta\sin\phi & -\sin\theta\cos\psi & \cos\theta \end{pmatrix}$$

Matrix transformations exist between these systems such that

$$\begin{pmatrix} x \\ y \\ z \end{pmatrix} = L_2 \begin{pmatrix} x_2 \\ y_2 \\ z_2 \end{pmatrix} = L_2 L_1 \begin{pmatrix} X_1 \\ Y_1 \\ Z_1 \end{pmatrix} \qquad (6.5)$$

and

$$\begin{pmatrix} X_1 \\ Y_1 \\ Z_1 \end{pmatrix} = L_1^{-1} L_2^{-1} \begin{pmatrix} x \\ y \\ z \end{pmatrix} \qquad (6.6)$$

The co-ordinates of a drug molecule relative to the DNA helix are given by

$$\begin{pmatrix} x \\ y \\ z \end{pmatrix} = L_2 \begin{pmatrix} x_2 \\ y_2 \\ z_2 \end{pmatrix}$$

where L_2 is given by

$$L_2 = L(\psi_2)\, L(\theta_2)\, L(\phi_2) \qquad (6.7)$$

and the full form of the matrix can be seen from inspection of Equation (6.4), attached to Fig. 6.8. The tilt of the drug relative to the plane perpendicular to the DNA helix axis is given by θ_2, the rotation of the drug about the DNA helix axis is given by ϕ_2 and the twist of the drug about its own axis is specified by ψ_2 (Fig. 6.9).

Similarly, the transformation from the DNA helix to the fibre co-ordinate system is accounted for by a matrix L_1, which takes the same form as L_2 with the appropriate changes in subscripts. The appropriate Eulerian angles are shown in Fig. 6.10 where θ_1 is the tilt of the DNA helix axis relative to the fibre axis (and will later be referred to in terms of the disorientation of the fibre), ϕ_1 describes the rotation of the DNA axis about the fibre axis and ψ_1 specifies the twist or rotation about the DNA helix axis. The rotation ψ_1 can be set to zero since it has already been accounted for by ϕ_2 from the previous transformation; thus

Fig. 6.9 Angles involved in the drug to DNA transformation

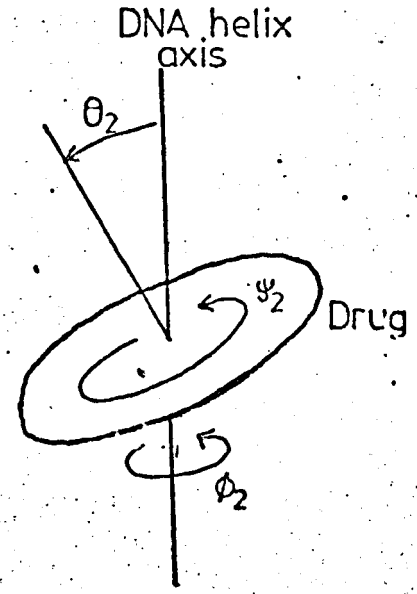

Fig. 6.10 Angles involved in the DNA to fibre transformation

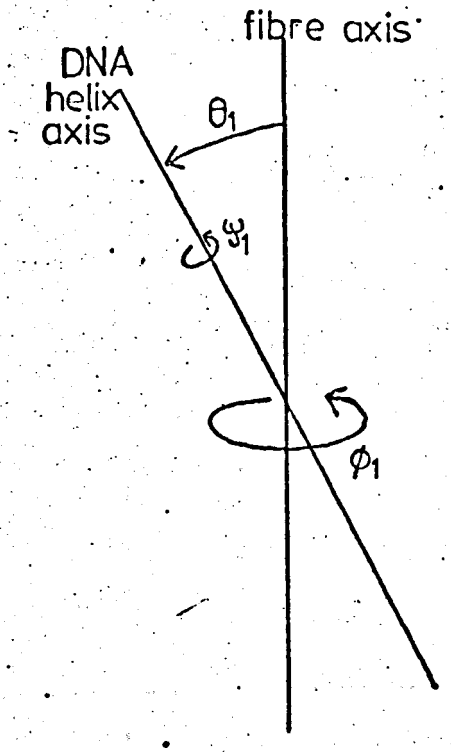

$$L_1 = \begin{pmatrix} \cos\phi_1 & -\cos\theta_1 \sin\phi_1 & \sin\theta_1 \sin\phi_1 \\ \sin\phi_1 & \cos\theta_1 \cos\phi_1 & -\sin\theta_1 \cos\phi_1 \\ 0 & \sin\theta_1 & \cos\phi_1 \end{pmatrix} \quad (6.8)$$

If the transition dipole moment in the co-ordinate system of the drug molecule is assigned an arbitrary direction $\begin{pmatrix}1\\0\\0\end{pmatrix}$, then in the fibre co-ordinate system it will be given by

$$T = L_1^{-1} L_2^{-1} \begin{pmatrix}1\\0\\0\end{pmatrix} \quad (6.9)$$

For parallel* light incident along the X_1 direction (Fig. 6.10) and polarised at 45° to the Y_1 and Z_1 axes (so that $E_\perp = E_\parallel$), the cosines of the angles between T and the Y_1 and Z_1 directions will be given by $T.\ \hat{Y}_1$ and $T.\ \hat{Z}_1$ and the dichroic ratio will be given by

$$D = \frac{\langle (T.\ \hat{Y}_1)^2 \rangle}{\langle (T.\ \hat{Z}_1)^2 \rangle} \quad (6.10)$$

where "< >" denotes that the expressions are integrated over ϕ_2 (from 0 to 2π) and ψ_2 (from 0 to π) to provide averaging at the molecular level, and over ϕ_1 (from 0 to 2π) to give averaging at the fibre level.

The resulting expression (Appendix AI) for a fibre is

$$D = \tfrac{1}{2} + \frac{2\cos^2\theta - SP}{2\sin^2\theta + SP} \quad (6.11)$$

where $P = 3\cos^2\theta - 1$ (θ is the drug tilt relative to the DNA molecule, previously subscripted as θ_2)

and S is a disorientation parameter given by

$S(\theta_1) = \langle \sin^2\theta_1 \rangle$, where θ_1 is the tilt of the DNA helix axis relative to the fibre axis.

Explicitly,

---

* In practice the light will not be exactly parallel, but the effect of divergence is small even at quite large numerical apertures. Seeds (1951) has shown that there would be an increase in absorbance of about 0.01 OD unit when a specimen of unit optical density is measured through an objective of 0.3 numerical aperture.

$$S(\theta_1) = \frac{\int_0^{\frac{\pi}{2}} \int_0^{2\pi} \sin^2\theta_1 \cdot N(\theta_1, \phi_1) \sin\theta_1 \, d\phi_1 \, d\theta_1}{\int_0^{\frac{\pi}{2}} \int_0^{2\pi} N(\theta_1, \phi_1) \sin\phi_1 \, d\phi_1 \, d\theta_1} \qquad (6.12)$$

where $N(\theta_1, \phi_1)$ is the density of states function describing the distribution of DNA helices about the fibre axis (Fig. 6.11), $\sin\theta_1$ results from the area element in spherical polar co-ordinates and the denominator normalises the expression.

A physically reasonable model for the distribution of the DNA helices about the fibre axis is to assume that a gaussian distribution of orientations exists in any cross-section of the sample (Libertini et al., 1974), thus

$$N(\theta_1, \phi_1) \propto \exp\left\{\frac{-\theta_1^2}{2\delta^2}\right\} \qquad (6.13)$$

where δ is the half-width of the distribution. This density of states function leads to a probability function

$$P(\theta_1) = \frac{1}{2\pi} \int_0^{2\pi} N(\theta_1, \phi_1) \sin\theta_1 \, d\phi_1$$

which is shown in Fig. 6.12.

When θ_1 is small, so that $\sin\theta_1 \simeq \theta_1$, the disorientation parameter S reduces simply to $2\delta^2$; but for the general case, integration of Equation (6.12) gives

$$S = \tfrac{1}{4}\left(3 - \frac{F(\frac{3\delta}{\sqrt{2}})}{F(\frac{\delta}{\sqrt{2}})}\right) \qquad (6.14)$$

where

$$F(\delta) = e^{-\delta^2} \int_0^{\delta} e^{t^2} dt$$

Fig. 6.11 Illustrating the density of states function $N(\theta_1,\phi_1)$ and the probability function $P(\theta_1)$

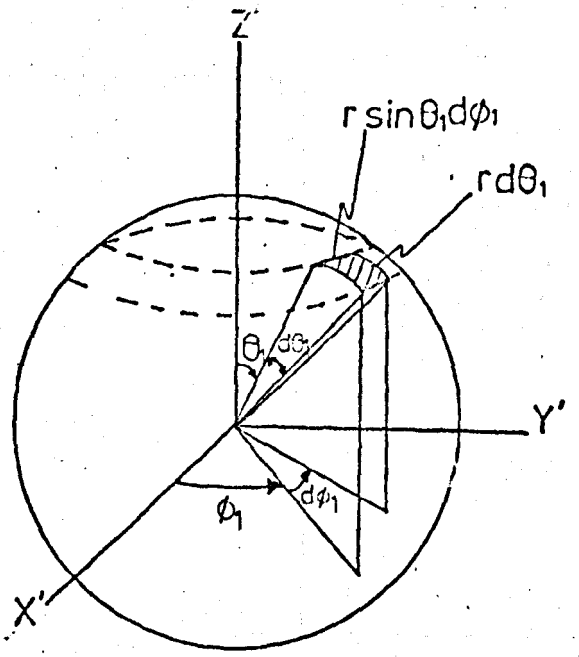

$N(\theta_1,\phi_1)$, the density of states function, is proportional to the number of DNA helices pointing into an area bounded by θ_1 and $\theta_1 + d\theta_1$, and ϕ_1 and $\phi_1 + d\phi_1$. It is assumed to have a gaussian form,

$$N(\theta_1, \phi_1) \propto \exp\left\{ \frac{-\theta^2}{2\delta^2} \right\}$$

where δ is the half-width of the function, and rotational symmetry is assumed to exist so that the function is independent of the azimuthal angle ϕ_1.

As θ_1 increases the area bounded by θ_1 and $\theta_1 + d\theta_1$ increases, and the fraction of DNA helices within this area is given by the probability function $P(\theta_1)$ where

$$P(\theta_1) = \frac{1}{2\pi} \int_0^{2\pi} N(\theta_1,\phi_1) \sin\theta_1 \, d\theta_1$$

The probability function is shown plotted against θ_1 in Fig. 6.12.

Fig. 6.12 (i) The probability function as a function of θ_1 for different disorientation half-widths, δ (after Libertini et al., 1974)

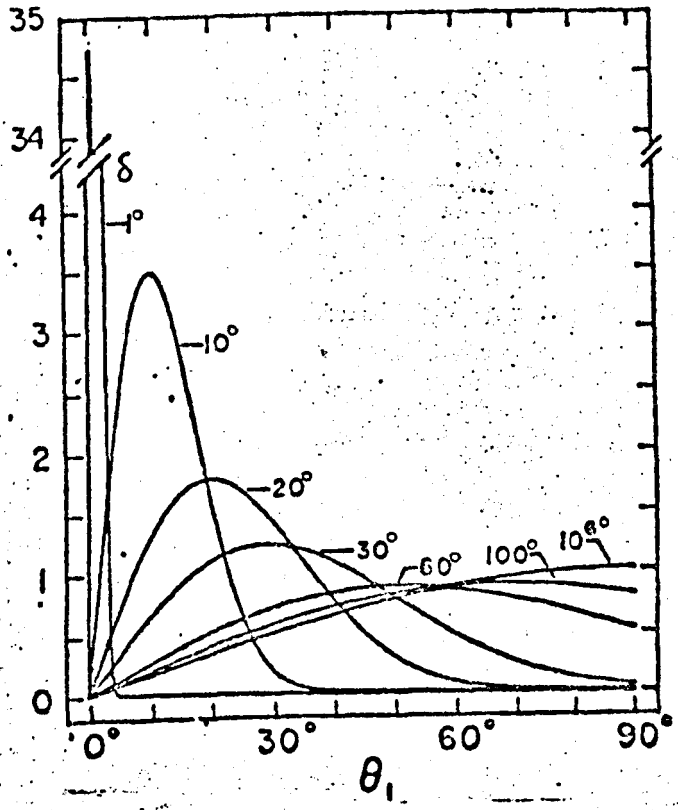

The areas under each curve are equal. At small values of δ the distribution becomes gaussian, but as δ increases the sin θ_1 term begins to dominate until at $\delta \to \infty$ the distribution becomes purely sinusoidal.

The maximum of the curve shifts from $\theta_1 = 0^\circ$ to $\theta_1 = 90^\circ$ as δ is increased from near zero (complete orientation) to infinity (complete disorientation). This does not mean that there is preferential alignment at 90°, but rather that the area element is increasing from the pole to the equator. At $\theta_1 = 0^\circ$ the probability goes to zero (because of the sine term) since the area element at the pole approaches zero. This does not cause any difficulties since contributions are always summed over a finite angle θ_1 during the integration.

(ii) Percentage of DNA helices lying within a cone of half-angle θ_1 as a function of δ (after Libertini et al., 1974)

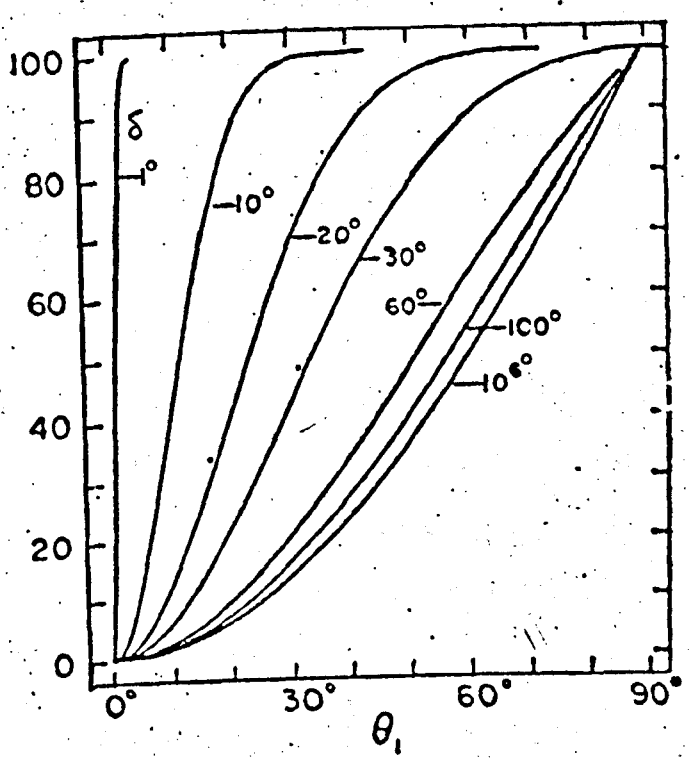

and is known as Dawson's integral (Appendix AII). This integral can be reduced to a simple series (Appendix AIII),

$$F(\delta) = \frac{\sqrt{\pi}}{2} \sum_{r=1}^{\infty} \frac{(-1)^{r+1} z^{2r-1}}{\Gamma(r + \frac{1}{2})}$$

where Γ is the Gamma function. This summation converges rapidly and can be calculated easily using a simple subroutine in a computer program. Summation to one hundred terms was found to give a result indistinguishable from summing to five hundred terms.

It is instructive to consider the expressions for the dichroic ratio, D, for several special cases -

(i) For a fibre which is perfectly orientated, S = 0 and Equation (6.11) reduces to Equation (6.3) derived for a completely orientated specimen.

(ii) For a completely disorientated fibre $N(\theta_1, \phi_1) = 1$, i.e. all all orientations of the DNA helices within the specimen are equally probable. Integrating Equation (6.12) (Appendix AIV) gives a value for the disorientation parameter S of $\frac{2}{3}$. Substituting this value into Equation (6.11) gives a value for the dichroic ratio of unity i.e. a completely disorientated fibre shows no preference for absorption in a particular direction, as is expected.

(iii) There is a unique value of the drug tilt for which the dichroic ratio is always equal to unity, irrespective of the value of the disorientation parameter S. This value is $54^{o}44'$ (i.e. $\cos^{-1}\frac{1}{\sqrt{3}} \equiv \tan^{-1}\sqrt{2}$). This is in agreement with the computer simulated results obtained for a fibre by Porumb (1976).

(iv) The dichroic ratio for zero base tilt has the simple form $D = \frac{1}{S} - \frac{1}{2}$ (6.15)

Corresponding results for orientated films are given in Appendix B. In general, for the same S value, the dichroic ratios of films will always be smaller than those for fibres, though for a given half-width δ the values for a film will be larger than those for a fibre (Figs. B.5, 6.13). This results from the different relationships between S and δ in the two cases.

6.3.2 The Dichroic Ratio in Terms of the Transition Dipole Tilt

The dichroic ratio may be expressed in terms of the transition dipole tilt, α, instead of the drug tilt, θ. A similar treatment to that described in Section 6.3.1 leads to the expression

$$D = \frac{\cos^2\alpha - \frac{SP'}{2}}{2\sin^2\alpha + SP'} \qquad (6.16)$$

where $P' = 3\cos^2\alpha - 2$

and S has the same significance as before. This expression has a similar form to Equation (6.11) which gives D in terms of θ, and it agrees with a less explicitly defined expression produced by Zbinden (1964) if appropriate notational changes are made.

Again, it is instructive to consider several special cases -

(i) For a perfectly orientated fibre, S=0 and Equation (6.16) reduces to Equation (6.2) derived less generally.

(ii) For a completely disorientated fibre, S takes the value $\frac{2}{3}$ and the expression reduces to give a value for the dichroic ratio of unity, as expected.

(iii) There is a unique value of the transition dipole tilt angle for which D=1 for any disorientation. This value is $35^{\circ}16'$ (i.e. $\cos^{-1}\sqrt{\frac{2}{3}} \equiv \sin^{-1}\sqrt{\frac{1}{3}}$), in agreement with the computer simulated results of Porumb (1976).

(iv) The values of D for zero tilt ($\alpha = 0$) are given by

Fig. 6.13 The variation of the dichroic ratio, D, of a fibre with the tilt of the drug chromophore θ, for various values of δ (Equation (6.11))

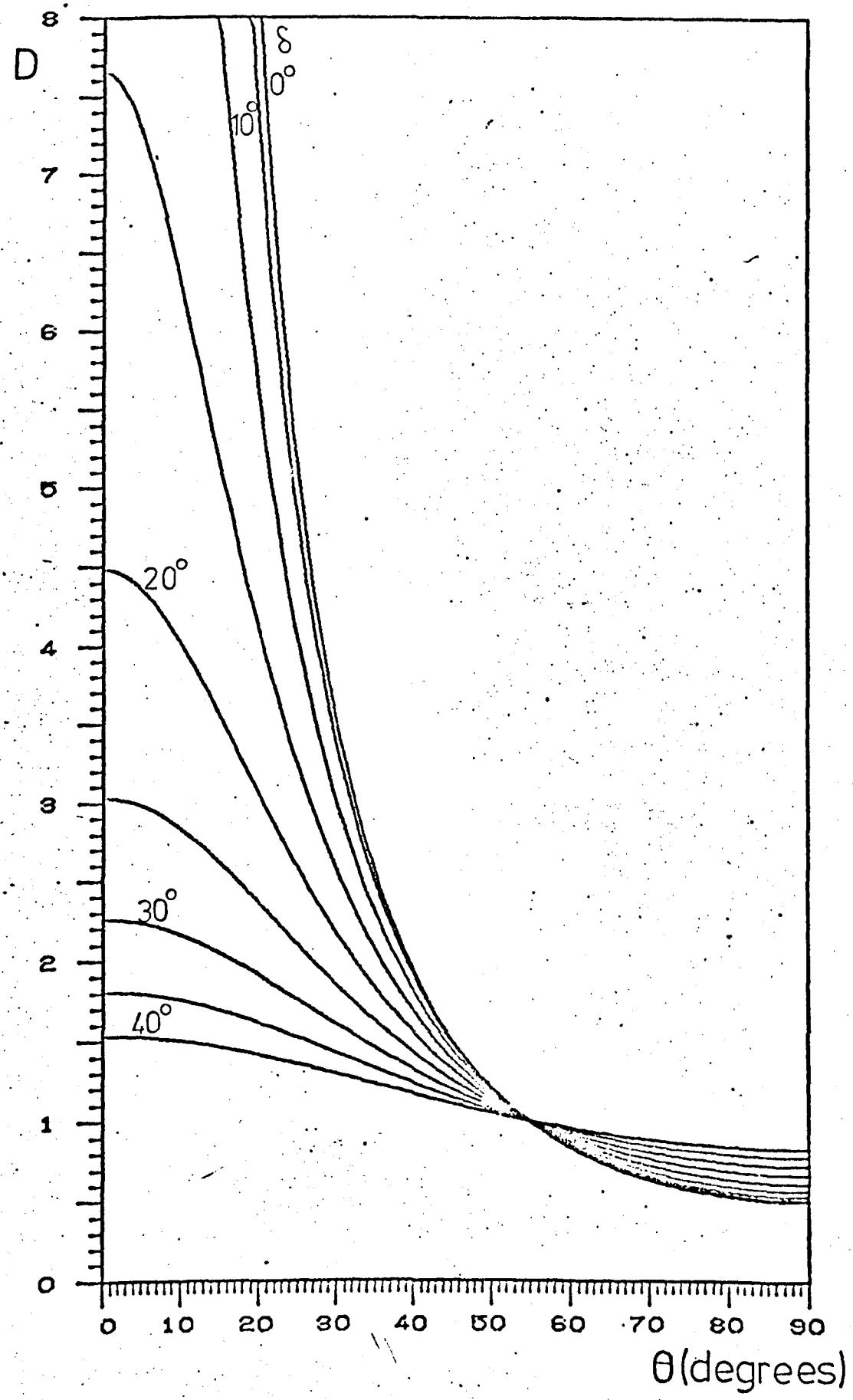

$D = \frac{1}{S} - \frac{1}{2}$. This is identical to Equation (6.15), which is as it should be. When the drug tilt, θ, is non-zero the value of α falls between zero and θ; but when θ takes the value zero, α must also drop to zero. Thus the cases when $\theta = 0$ and $\alpha = 0$ are physically the same.

It should be stressed that the cases when $\alpha = 90^{\circ}$ and $\theta = 90^{\circ}$ are not equivalent. In the former case, all the transition dipoles are constrained to point along the helix case and none point perpendicular to it. In this case, for a perfectly orientated fibre, the dichroic ratio must fall to zero. In the latter situation, the transition dipoles are not constrained to point in a certain direction within the plane of the drug, and although the drug is aligned parallel to the helix axis the dipoles may contribute to absorption in a direction perpendicular to it. For a perfectly orientated fibre, this results in the dichroic ratio dropping to 0.5, and not to zero.

In most cases of interest in this study, the drug is expected to be constrained roughly perpendicular to the helix axis so that θ and α will be small, and the values for D using either Equation (6.11) or (6.16) will be similar.

6.3.3 Comparison of the Previous Treatments

The fact that both equations (6.11) and (6.16) reduce to give the expected values of D under a number of simplified circumstances (Table 6.2), and that they are both identical if $\phi' = 45^{\circ}$ (the situation previously discussed in Section 6.2) is a strong indication that they are correct.

The expressions for D are shown plotted as a function of θ and α for various disorientation half-widths δ, in Fig. 6.13 and Fig. 6.14 respectively. Comparison with the computer simulated plots of Porumb (1976), reproduced in Figs. 6.6 and 6.7, shows that both sets of curves are similar but that the values of D currently proposed are generally less than those predicted by Porumb at the same angles of tilt (θ or α). The differences are only very slight for small gaussian half-widths ($\delta \lesssim 10^{\circ}$) and for large half-widths ($\delta \gtrsim 35^{\circ}$), but are appreciable (i.e. the differences in D approach 10%) for intermediate values of the half-width. This probably reflects the method by which Porumb performed his cylindrical averaging. Since he did not have an analytic solution to the problem, the absorbances were summed for values of ϕ_2 (in the range 0 to 2π), ϕ, (0 to 2π) and θ_1(0 to π) sampled at finite intervals. The final values for D are sensitive to the size of these intervals.

Fig. 6.14 The variation of the dichroic ratio, D, with the transition dipole moment tilt, α, for various values of δ (see Equation (6.16))

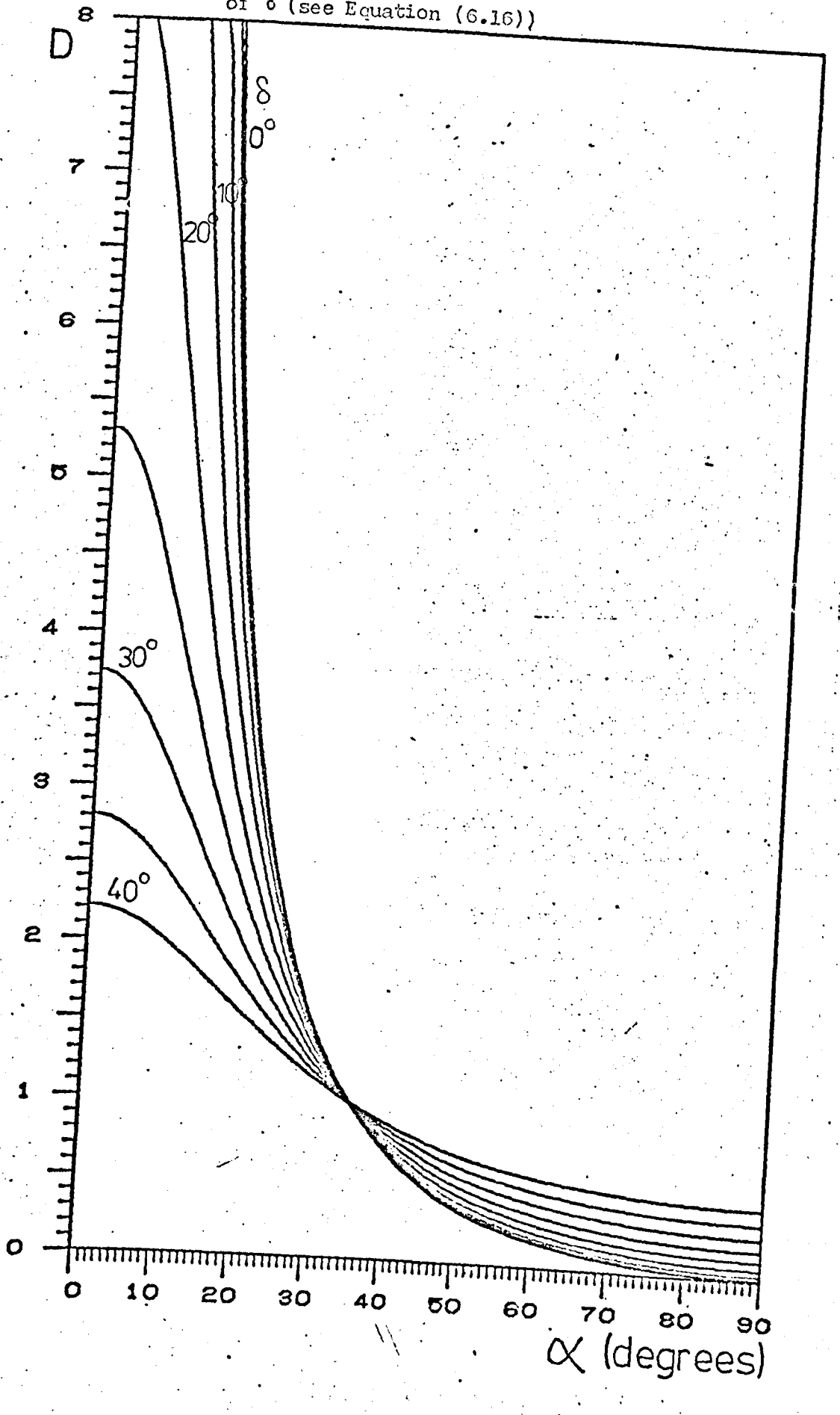

6.4 Birefringence

Birefringent (or doubly refracting) materials behave anisotropically to the passage of light through them. Light entering a birefringent material can be regarded as being comprised of two components, each polarised at right angles to the other. The two components travel through the material with different velocities (i.e. they have different refractive indices), and usually in different directions. In tetragonal, trigonal and hexagonal crystals there is one direction of propagation in which double refraction does not occur. This direction, which is the same as that of the c crystallographic axis, is called the optic axis, and such crystals are termed uniaxial. Crystals of the orthorhombic, monoclinic and triclinic systems possess two optic axes and are called biaxial. In a DNA fibre, the crystallites comprising it are orientated about the fibre axis. Only one optic axis (corresponding to the fibre axis) exists because the azimuthal orientation of the crystallites is random and, even if the crystallites themselves were biaxial, the effect would be averaged out in all directions except the fibre axis.

Uniaxial materials have two sets of wave surfaces (Fig. 6.15). One set is a series of spheres representing the behaviour of the component (called the ordinary ray) which always travels with the same speed in all directions, and the other set (for the extraordinary ray) is comprised of ellipsoids of rotation indicating that the speed varies with direction. The axis of rotation of the ellipsoid is the optic axis, and in this direction light travels with a single velocity. The ellipsoid may lie inside or outside the sphere.

For a given direction of propagation the difference in speed of the two components is given by the difference in radius of the sphere and ellipsoid. The refractive indices are inversely proportional to these radii, and their difference also increases with the separation of the two

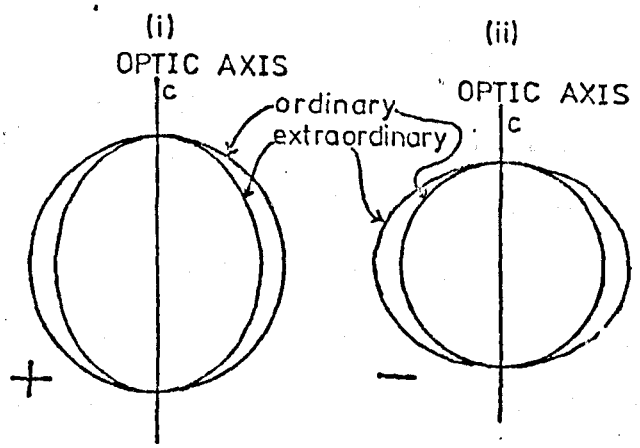

Figure 6.15. Wave surfaces of (i) a positive and (ii) a negative uniaxial material.

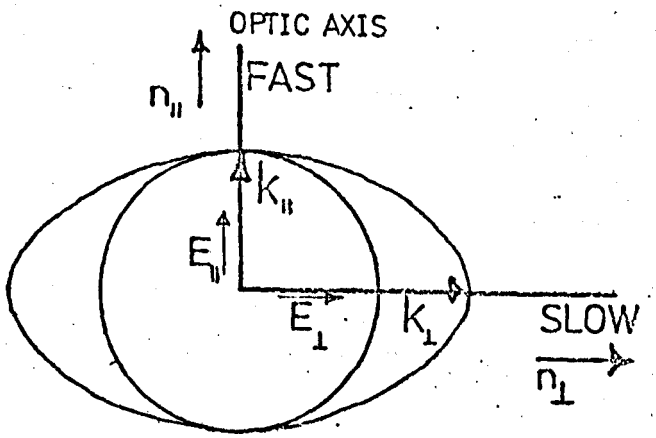

Figure 6.16. A negative uniaxial crystal, showing the components of $\underline{E}$ and $\underline{k}$.

surfaces. The Poynting vectors $\underline{k}$ for rays of light travelling along and perpendicular to the optic axis are shown in Fig. 6.15 for a negative uniaxial crystal. The associated electric field oscillate in planes perpendicular to these vectors and are shown marked $E_{\parallel}$ and $E_{\perp}$. The "fast" direction is associated with the condition where the ray is travelling fastest (i.e. it is experiencing the smallest refractive index); but it refers to the direction of the associated electric field and not to the direction in which the ray is travelling. The "slow" direction is perpendicular to the "fast" direction.

Thus in Fig. 6.16, $\underline{k}_{\perp}$ is larger than $\underline{k}_{\parallel}$ so that the direction of its associated electric field $E_{\parallel}$ (viz. along the optic axis) is called the "fast" axis, and the refractive index in that direction, $n_{\parallel}$, is smaller than that for the perpendicular direction, $n_{\perp}$.

The retardation, Γ, of the two rays relative to each other is

$$\Gamma = (n_{\parallel} - n_{\perp})t \qquad (6.17)$$

where t is the thickness of the fibre. The difference, $n_{\parallel} - n_{\perp}$, is known as the birefringence, Δn, and so

$$\Gamma = \Delta n.t \qquad (6.18)$$

For a negative uniaxial crystal, such as calcite, the birefringence is less than zero; and for a positive uniaxial crystal, such as quartz, it is greater than zero.

6.4.1 The Physical Basis of Birefringence

During the passage of light through a medium, the oscillating electric field distorts the electron clouds within the constituent atoms or molecules. This distortion is known as polarisation. The (electron) polarisability relates the induced dipole moment, which is a measure of the charge separation, to the electric field causing it. At a given frequency

$$\underline{p} = \alpha \underline{E}_L \qquad (6.19)$$

where $\underline{p}$ is an induced dipole moment, α is the polarisability and $\underline{E}_L$ is the local electric field.

The continual reversal of the direction of polarisation in a medium through which light is passing results in the atoms themselves acting as radiators and emitting secondary waves. These waves are slightly retarded with respect to those of the incident light, and it is the interference between these two sets of waves that brings about the reduction in the velocity of light in the medium. The greater the polarisability, the greater is the amplitude of the secondary waves and the more the velocity is reduced (i.e. a larger refractive index).

Electronic polarisability and refractive index are related by means of the Lorentz-Lorentz equation*

$$\frac{n^2 - 1}{n^2 + 2} \cdot \frac{M}{\rho} = \frac{4\pi}{3} N_o \alpha \qquad (6.20)$$

where n is the refractive index, M is the molecular weight, ρ is the density, N_o is Avogadro's number and α is the electronic polarisability.

This equation can be applied to the component polarisabilities and refractive indices (Hartshorne and Stuart, 1970).

Thus

$$\left[\frac{n_{\parallel}^2 - 1}{n_{\parallel}^2 + 2} - \frac{n_{\perp}^2 - 1}{n_{\perp}^2 + 2} \right] \frac{M}{\rho} = \frac{4\pi}{3} N_o (\alpha_{\parallel} - \alpha_{\perp}) \qquad (6.21)$$

where the subscripts $\parallel$ and $\perp$ refer to the directions parallel and perpendicular to the optic axis (or fibre axis) respectively.

For the case of a polynucleotide, the molecular weight, M, and the polarisabilities, α, can be taken as being equal to those for the monomer unit. If the entire molecule were considered, both sides of equation (6.21) would simply be multiplied by N, the number of monomers in the molecule, as long as electronic interactions between the units were

---

* It should be noted, however, that this equation only takes into account the mutual induction effects of atoms linked by primary bonds, and ignores molecular interaction: it should therefore be applied cautiously with crystals of very low birefringence.

negligible.

In nucleic acids, it has been shown (Tsvetkov, 1963) that it is the bases which are anisotropic and result in the birefringence, the sugar-phosphate backbone being practically isotropic and contributing little to the birefringence. If electronic interactions between the bases were significant, then one side of Equation (6.21) would have to be multiplied by an interaction function, f(N). We will assume that these interactions are negligible (i.e. f(N) = 1), and that therefore the birefringence is independent of the number of nucleotides in a molecule.

Differentiating the Lorentz-Lorentz relationship gives

$$\frac{6n \cdot dn}{(n^2 + 2)^2} = K.d\alpha$$

where $K = \frac{4\pi}{3} \frac{N_o \rho}{M}$

If the birefringence is small ($\lesssim 0.3$, to maintain an accuracy of 0.1%), the differential equation may be applied to the finite differences -

$$\frac{6\bar{n}}{(\bar{n} + 2)^2} \cdot \Delta n = K.\Delta\alpha \qquad (6.22)$$

where

$$\bar{n} = \frac{n_{\parallel} + n_{\perp}}{2}$$

and $\Delta n = n_{\parallel} - n_{\perp}$.

Using values of $\Delta\alpha = -15\text{Å}^3$ (Frisman et al., 1962), M = 330, $\bar{n} = 1.6$ (Tsvetkov, 1963) and $\rho = 1.63\text{g cm}^{-3}$ (Seeds, 1951) results in a value for the birefringence of -0.4. This is at least four times larger than any experimental measurements on B-DNA (Porumb, 1976), though the disparity arises mainly through the value used for the density. A value of 1.63g cm^{-3} corresponds to the density of dry DNA, but in a fibre it will be considerably diluted by water and the dilution will result in smaller values for both the refractive indices and hence the birefringence. The actual water content will be a function of relative humidity, but the dilution factor would appear to be of the order of 4 - 6.

Transforming the Lorentz-Lorentz equation gives

$$n = \sqrt{\frac{3}{1 - K\alpha} - 2} \qquad (6.23)$$

where the constant K contains the density term as before. The form of this relationship is shown in Fig. 6.17 for different values of the density. If the density is less than or about 0.4g cm^{-3}, and $n_{\parallel}$ and $n_{\perp}$ are just below and just above 1.6 (their mean value), this would indicate that the polarisabilities $\alpha_{\parallel}$ and $\alpha_{\perp}$ are both greater than 100$\AA^3$, and are critically dependent on the density. This is in agreement with calculations for an adenine-uracil base-pair, using a simple Hückel scheme, which indicate that the π-electron polarisability in the plane of the base-pair (i.e. perpendicular to the helix axis) is around 175$\AA^3$ (Takashima, 1968).

6.4.2 Intrinsic and Form Birefringence

The birefringence of a fibre can be thought of as being composed of two parts: a term arising from the optical anistropy of the polynucleotide helices themselves (called the intrinsic birefringence), and a term resulting from a preferential orientation of the elongated helices (called the form birefringence). Even optically isotropic molecules embedded in an isotropic medium can possess a form birefringence which arises from the deformation of the electric field at anisotropically-shaped phase boundaries (Steiner and Beers, 1961).

By considering an arrangement of thin isotropic rods, of diameter smaller than the wavelength of light, orientated parallel to the fibre axis as a system of parallel capacitors it has been shown (Weiner, 1912) that

$$n_{\parallel}^2 - n_{\perp}^2 = \frac{\nu_o (n_o^2 - n^2)^2}{(\nu + 1) n_o^2 + \nu_o n^2} \qquad (6.24)$$

where ν, ν_o are the volume fractions of the rods and the material in which they are immersed: and n, n_o and the refractive indices of the rod and

Fig. 6.17 The Lorentz-Lorentz relationship between the refractive index, n, and the polarisability, α, for different densities, ρ.

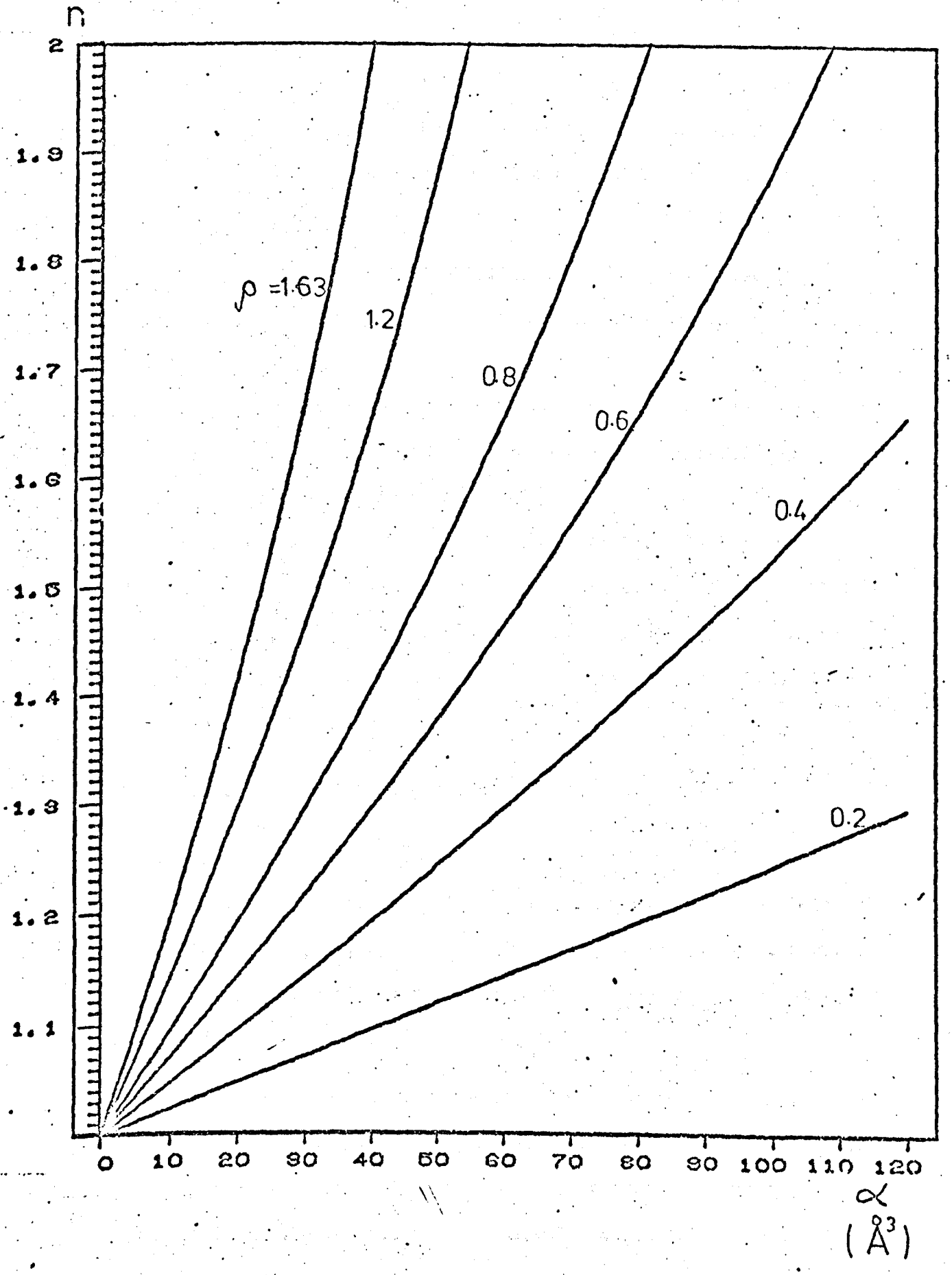

medium respectively. It can be seen that the form birefringence, Δn_f ($= n_{\parallel} - n_{\perp}$), is always positive in this case. Flow birefringence, light scattering and Kerr effect studies indicate that a rigid rod model can be invoked to explain the optical properties of DNA (Weill et al., 1963). Previous investigators (Hoshino et al., 1962, Tsvetkov, 1963; Porumb, 1976; Maeda, 1978) have treated the total birefringence of a fibre as being the sum of two terms - the intrinsic and the form birefringence,

$$\Delta n_{total} = \Delta n + \Delta n_f \qquad (6.25)$$

where Δn is related to bond polarisabilities, and Δn_f is related to Equation (6.24) in which the assumption had been made that the rods (viz. the DNA helices) were isotropic.

A more realistic approach would be to consider the rods as being anistropic from the beginning, and to compute the total birefringence when these rods are imbedded in an isotropic medium. In this treatment, the intrinsic and form effects would not be separable. It has been shown (Ninham and Sammut, 1976) for the case of infinitely long parallel cylinders of radius, a, and centre-to-centre spacing, α, immersed in an isotropic medium that the composite dielectric constants are given by

$$\varepsilon_c^{\parallel} = \varepsilon_m + f\,(\varepsilon_r^{\parallel} - \varepsilon_m) \qquad (6.26)$$

for the direction parallel to the cylinder axis, and

$$\varepsilon_c^{\perp} = \varepsilon_m\,(1 + 2f' \cdot \frac{\Delta rm}{1 - f\Delta rm}) \qquad (6.27)$$

for the perpendicular direction. In these equations, ε_m is the dielectric constant of the medium, $\varepsilon_r^{\parallel}$, $\varepsilon_r^{\perp}$ are the dielectric constants of the rods, f' is the volume fraction of the rods (and equals $\frac{2\pi a^2}{\sqrt{3}.\alpha^2}$ for hexagonal packing) and $\Delta rm = \frac{\varepsilon_r^{\perp} - \varepsilon_m}{\varepsilon_r^{\perp} + \varepsilon_m}$.

In using these expressions, the fibre is considered as being composed of DNA molecules, behaving like rigid rods, inbedded in a matrix of water molecules. This treatment does not take into account the symmetry connections between the individual DNA molecules (viz. the crystallinity

of A-DNA and semi-crystallinity of B-DNA), but since the polarisability of the base-pairs is almost isotropic in the plane of the bases (Takashima, 1968) these equations should apply to DNA systems.

The refractive indices of the composite fibre would be given by

$$n_c^{\perp} = n_m\left\{1 + \frac{f'\Delta_{rm}}{[\,1 - f'\Delta_{rm}\,]}\right\} \qquad (6.28)$$

and

$$n_c^{\parallel} \simeq n_m(1 + f'\delta) \qquad (6.29)$$

where $\delta = \dfrac{\epsilon_r^{\parallel} - \epsilon_m}{2\epsilon_m}$

The total birefringence is then

$$\Delta n_{total} = n_c^{\parallel} - n_c^{\perp}$$

$$\simeq n_m f'(A - f'B) \qquad (6.30)$$

where $A = \delta - \Delta_{rm}$ and $B = \Delta_{rm}^2$. The relationship between the total birefringence Δn_{total} and the volume fraction f' is parabolic, and is schematically displayed in Fig. 6.18. The parameters A and B are functions of ϵ_m, $\epsilon_r^{\parallel}$ and $\epsilon_r^{\perp}$. A value of $(1.33)^2$ can be taken for ϵ_m, but $\epsilon_r^{\parallel}$ and $\epsilon_r^{\perp}$ are unknown. The intrinsic birefringence of DNA, $n_r^{\parallel} - n_r^{\perp}$, is however considered to have a value of around -0.1 (Tsvetkov, 1963; Porumb, 1976) and values of the individual refractive indices have been assumed by various sources (Seeds, 1951; Tsvetkov, 1963) to lie in the approximate range 1.4 to 1.7. A plot of the birefringence, Δn_{total}, against the volume fraction, f', for various combinations of $n_{\parallel}$ and $n_{\perp}$ is shown in Fig. 6.19.

In a DNA fibre, as the relative humidity rises the fibre takes up water. This may result in a change in the diameter of the DNA helices, considered as rods, and/or in a change in the intermolecular separation. The values of both of these parameters can be measured from an X-ray diffraction photograph of the fibre at a particular humidity, and used to

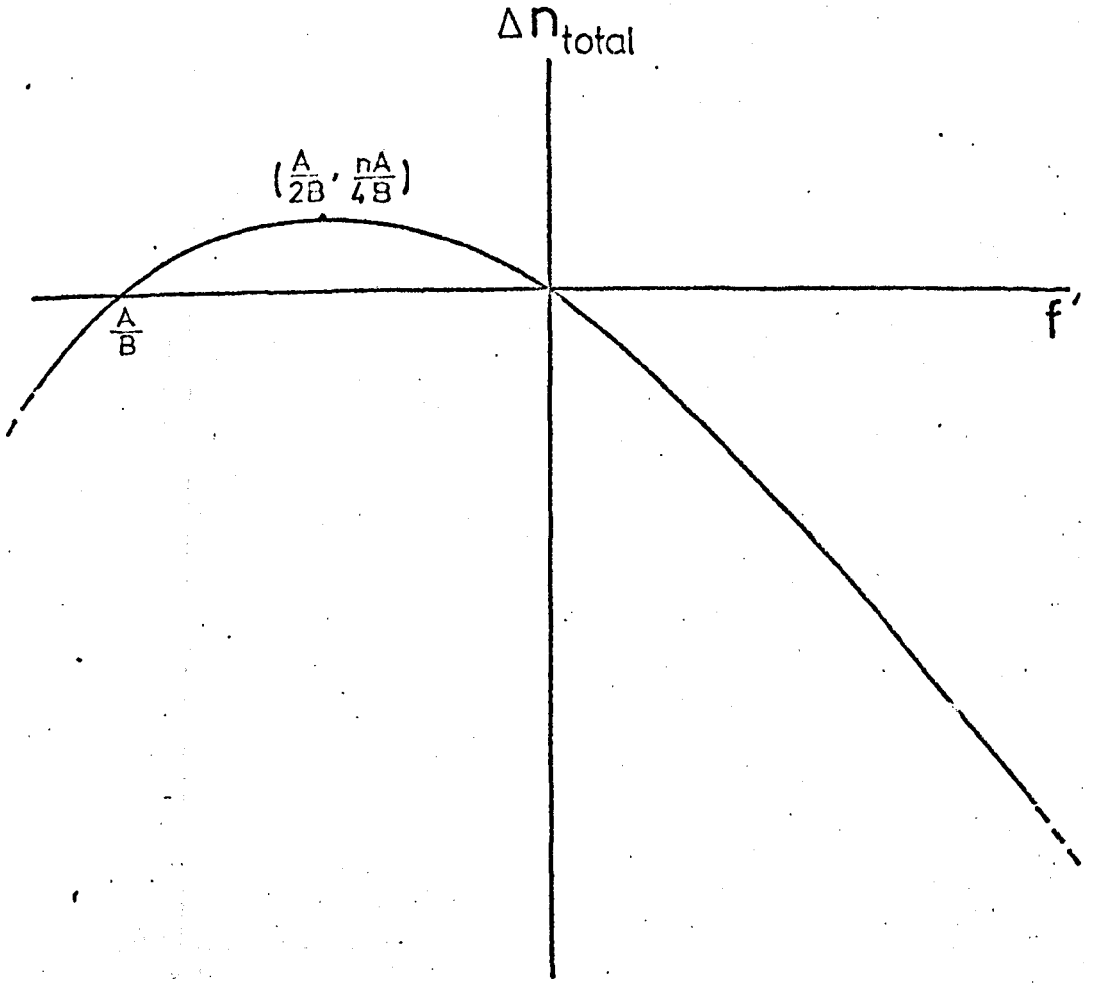

Figure 6.18. Schematic drawing of the relationship between the birefringence, Δn_{total}, and the volume fraction, f', for $n_{\parallel} < n_{\perp}$.

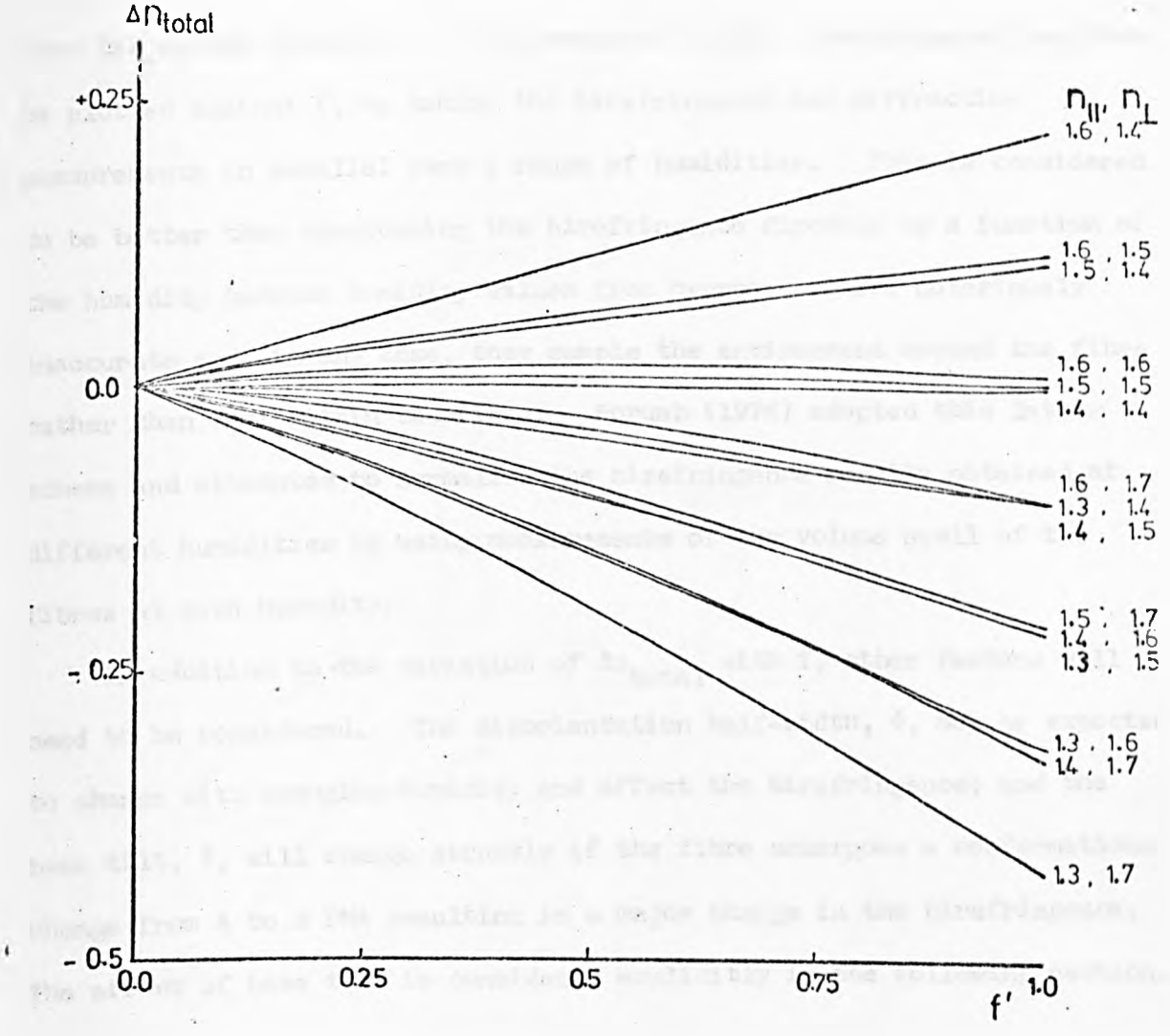

Figure 6.19 The total birefringence, Δn_{total}, as a function of the volume fraction, f', for various combinations of $n_{\parallel}$ and $n_{\perp}$.

give the volume fraction f'. The measured (total) birefringence can then be plotted against f', by taking the birefringence and diffraction measurements in parallel over a range of humidities. This is considered to be better than considering the birefringence directly as a function of the humidity because humidity values from hygrometers are notoriously inaccurate and, in any case, they sample the environment around the fibre rather than that within the fibre. Porumb (1976) adopted this latter scheme and attempted to normalise the birefringence results obtained at different humidities by using measurements of the volume swell of the fibres at each humidity.

In addition to the variation of Δn_{total} with f', other factors will need to be considered. The disorientation half-width, δ, may be expected to change with changing humidity and affect the birefringence; and the base tilt, θ, will change abruptly if the fibre undergoes a conformational change from A to B DNA resulting in a major change in the birefringence. The effect of base tilt is considered explicitly in the following section.

6.4.3 The Effect of Base Tilt (on the Intrinsic Birefringence)

Consider a fibre in which the bases are tilted by an angle θ to the plane perpendicular to the helix axis (Fig. 6.20). The polarisability perpendicular to the plane of the base-pair, α_L, is very small, and the polarisability in the plane of the base-pair, α_T, can be taken as isotropic (Takashima, 1968).

For a perfectly orientated fibre ($\beta = 0$), the normals ON to the plane of the base describe a cone of semi-angle θ about the fibre axis, OZ. The polarisabilities parallel and perpendicular to the fibre axis, $\alpha_\parallel$ and $\alpha_\perp$, are given by (Hartshorne and Stuart, 1970).

$$\alpha_\perp = \alpha_L \cos^2\Omega_\perp + \alpha_T \sin^2\Omega_\perp \qquad (6.31)$$

and

$$\alpha_\parallel = \alpha_L \cos^2\theta + \alpha_T \sin^2\theta \qquad (6.32)$$

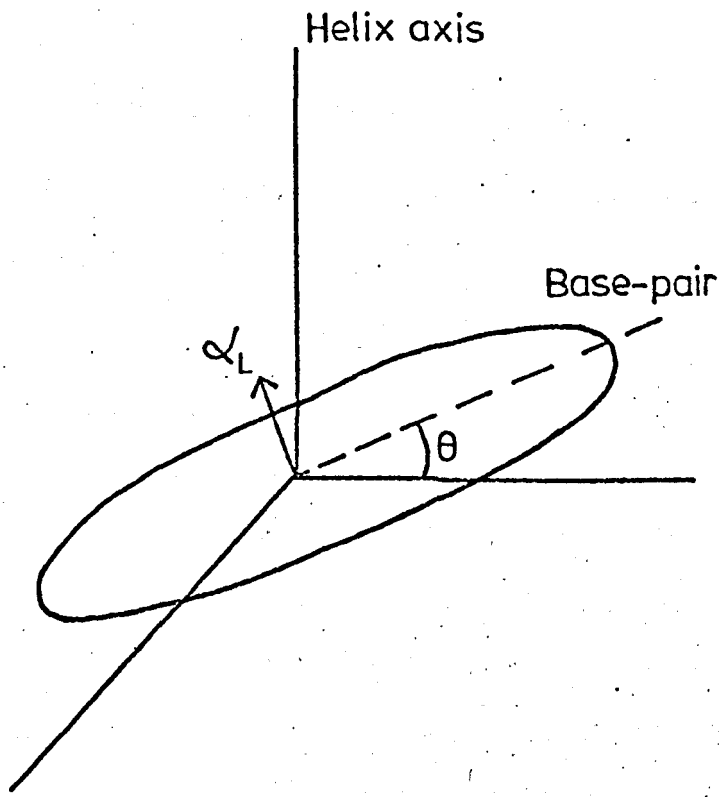

Figure 6.20. The system described in Section 6.4.3. α_L is small; α_T is isotropic in the plane of the base-pair.

since $\theta = \Omega_{\parallel}$, when $\beta = 0$. The angle $\Omega_{\perp}$ depends on the angular orientation, ϕ, of the base about the helix axis. Using vector geometry it can be shown that

$$\cos \Omega_{\perp} = \sin \theta \sin \phi$$

Substituting this into Equation (6.31) gives

$$\alpha_{\perp} = \alpha_L \sin^2\theta \sin^2\phi + \alpha_T (1 - \sin^2\theta \sin^2\phi) \qquad (6.33)$$

Subtracting Equation (6.33) from (6.32) and cylindrically averaging (i.e. integrating over ϕ) gives

$$\Delta\alpha = \alpha_{\parallel} - \alpha_{\perp} = (\alpha_L - \alpha_T)(1 - 1.5 \sin^2\theta) \qquad (6.34)$$

Using equation (6.22),

$$\Delta n = K (1 - 1.5 \sin^2\theta) \qquad (6.35)$$

where the constant K absorbs both the anisotropy in the polarisability and the concentration dependent terms. This relationship has been quoted by Porumb (1976) and is shown as the curve $\delta = 0^{\circ}$ in Fig. 6.21. When the tilt is zero the intrinsic component of the birefringence assumes its maximum negative value. It becomes zero for $\theta = 54^{\circ}44'$ (viz. $\sin^{-1}\sqrt{\frac{2}{3}}$), and for larger tilts it becomes positive. It is practically constant in the range $\theta = 0^{\circ} - 5^{\circ}$, and for a change of tilt from 0° to 20° (as encountered during the B to A transition in DNA) it drops in magnitude by 21%. Since the total birefringence includes a contribution from the form birefringence (which is always positive) the total birefringence would reduce to zero at an angle smaller than 54° 44'. Form birefringence and intrinsic birefringence are inter-linked, but Porumb (1976) has considered the case where the form term is arbitrarily given a value of 58% of the magnitude of the intrinsic term. For this case, the total birefringence would go to zero at $\theta = 32^{\circ}$, and its variation would be faster with θ than shown in Fig. 6.21 for the intrinsic component, but still slower than the variation in dichroic ratio with θ(Fig. 6.13).

Equation (6.35) holds for the case of a thin film as well. The dipole moments of the bases are not constrained to take up an orientation

Fig. 6.21 The intrinsic component of the birefringence of a fibre as a function of base tilt, θ, for various disorientation half-widths, δ.

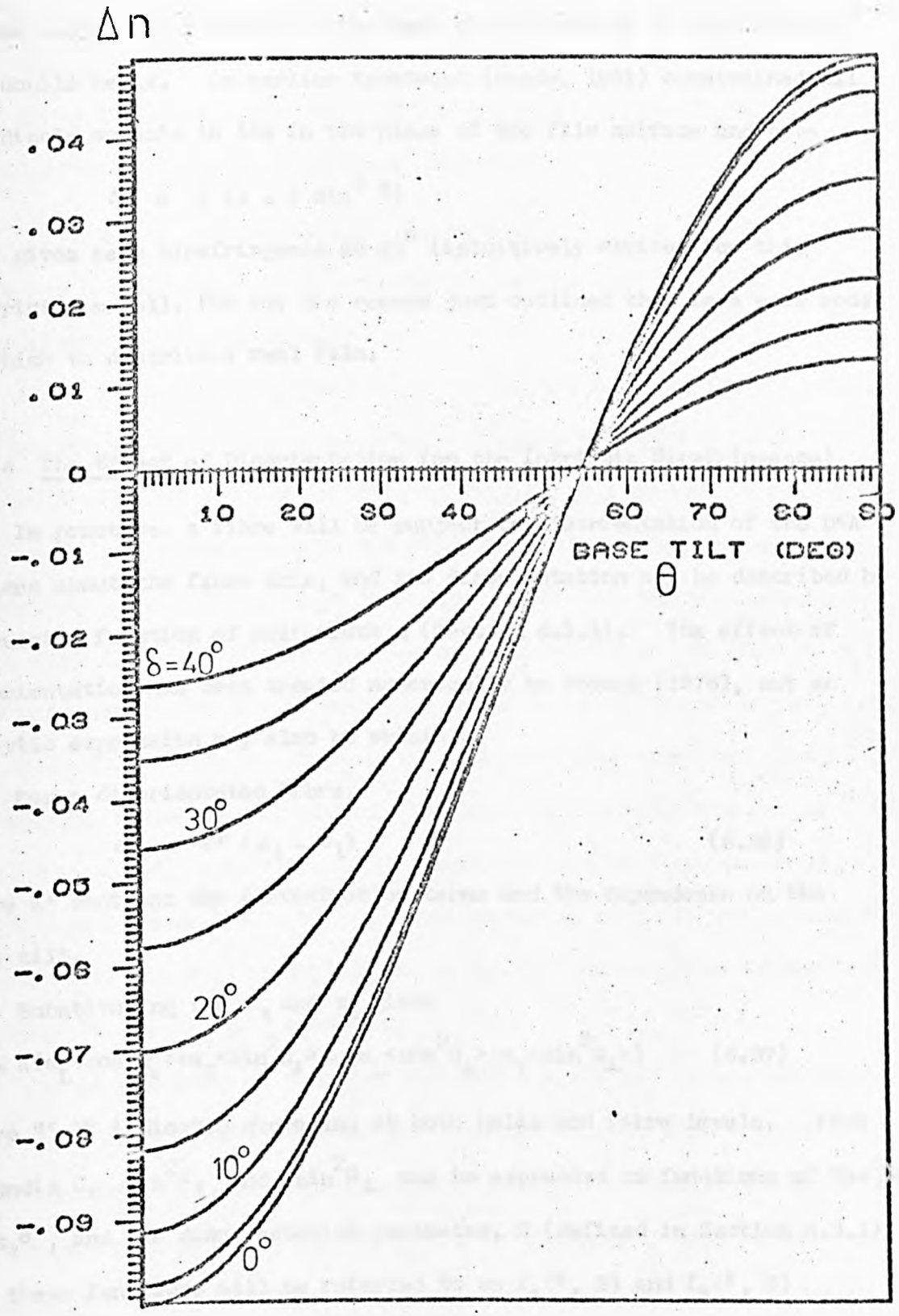

The vertical plotting is on a relative scale, since the constant K has been set to unity (Equation 6.39)

in the plane of the film surface. In fact, even if the dipole of one base were so positioned the dipole moment of the next one along the helix would have its polarisability at an angle to the surface of the film due to the continuous rotation of the base-pairs relative to each along a DNA double helix. An earlier treatment (Seeds, 1951) constrained all the dipole moments to lie in the plane of the film surface and gave

$$\Delta n = K (1 - 2 \sin^2 \theta)$$

This gives zero birefringence at 45° (intuitively obvious for this restricted model), but for the reason just outlined this is a poor model by which to describe a real film.

6.4.4 The Effect of Disorientation (on the Intrinsic Birefringence)

In practice, a fibre will be subject to disorientation of the DNA helices about the fibre axis, and the disorientation may be described by a gaussian function of half-width δ (Section 6.3.1). The effect of disorientation has been treated numerically by Porumb (1976), but an analytic expression may also be obtained.

For a disorientated fibre,

$$\Delta n = K' (\alpha_{\parallel} - \alpha_{\perp}) \qquad (6.36)$$

where K' contains the concentration terms and the dependence on the base tilt.

Substituting for $\alpha_{\parallel}$ and $\alpha_{\perp}$ gives

$$\Delta n = K\{\alpha_L \langle \cos^2 \Omega_{\parallel} \rangle + \alpha_T \langle \sin^2 \Omega_{\parallel} \rangle - (\alpha_L \langle \cos^2 \Omega_{\perp} \rangle + \alpha_T \langle \sin^2 \Omega_{\perp} \rangle) \qquad (6.37)$$

where "< >" indicates averaging at both helix and fibre levels. From Appendix C, $\sin^2 \Omega_{\parallel}$ and $\sin^2 \Omega_{\perp}$ can be expressed as functions of the base tilt, θ, and the disorientation parameter, S (defined in Section 6.3.1), and these functions will be referred to as $f_{\alpha}(\theta, S)$ and $f_{\beta}(\theta, S)$ respectively.

Since $\langle \cos^2 (\text{angle}) \rangle = 1 - \langle \sin^2 (\text{angle}) \rangle$, Equation (6.37) becomes

$$\Delta n = K' \{\alpha_L(1-f_\alpha(\theta,\phi)) + \alpha_T f_\alpha(\theta) - (\alpha_L(1-f_\beta(\theta,S)+\alpha_T f_\beta(\theta,S))\}$$

$$= K' (\alpha_L-\alpha_T)(f_\beta(\theta,S) - f_\alpha(\theta,S)) \qquad (6.38)$$

The relevant expressions for $f_\alpha(\theta,S)$ and $f_\beta(\theta,S)$ can then be substituted.

(i) The fibre case

Using the expressions for $f_\alpha(\theta,S)$ and $f_\beta(\theta,S)$, from Equations (C.3) and (C.4) respectively, in Equation (6.38) gives

$$\Delta n = K (1 - 1.5 \sin^2 \theta - 0.75SP) \qquad (6.39)$$

where $P = 3\cos^2\theta - 1$. This relationship is shown in Fig. 6.21 for various gaussian half-widths, δ.

For a perfectly orientated fibre S = 0, and Equation (6.39) reduces to Equation (6.35). For a completely disorientated fibre S = ⅔ (Appendix AIV) and the intrinsic birefringence goes to zero, as indeed it must. The expression predicts that there is a unique angle (viz. $54^\circ 44'$) at which the intrinsic component of the birefringence becomes zero, for all values of the disorientation parameter. The intrinsic birefringence of a fibre at zero tilt angle is proportional to (1 - 1.5S).

Fig. 6.21 should be compared with the computer simulated results of Porumb, reproduced in Fig. 6.22. The results are identical for $\delta=0^\circ$ (viz. a perfectly orientated fibre), and are very similar for small $\delta(\leq 10^\circ)$ and large $\delta(30^\circ - 40^\circ)$. They differ by up to 4% for intermediate values of δ, and this is thought to be due to the summation method used by Porumb to perform his averaging.

The contribution of the drug chromophores has not been considered explicitly in this treatment. The chromophores will have a large polarisability in their plane, probably larger than that of a base-pair. If they are orientated similarly to the base-pairs, as they would be if bound intercalatively, they will enhance the negative birefringence of the polynucleotide fibre.

Fig. 6.22 The computer-simulated results of Porumb (1976), showing the relative variation of Δn (in relative units) for a fibre with the base tilt, θ.

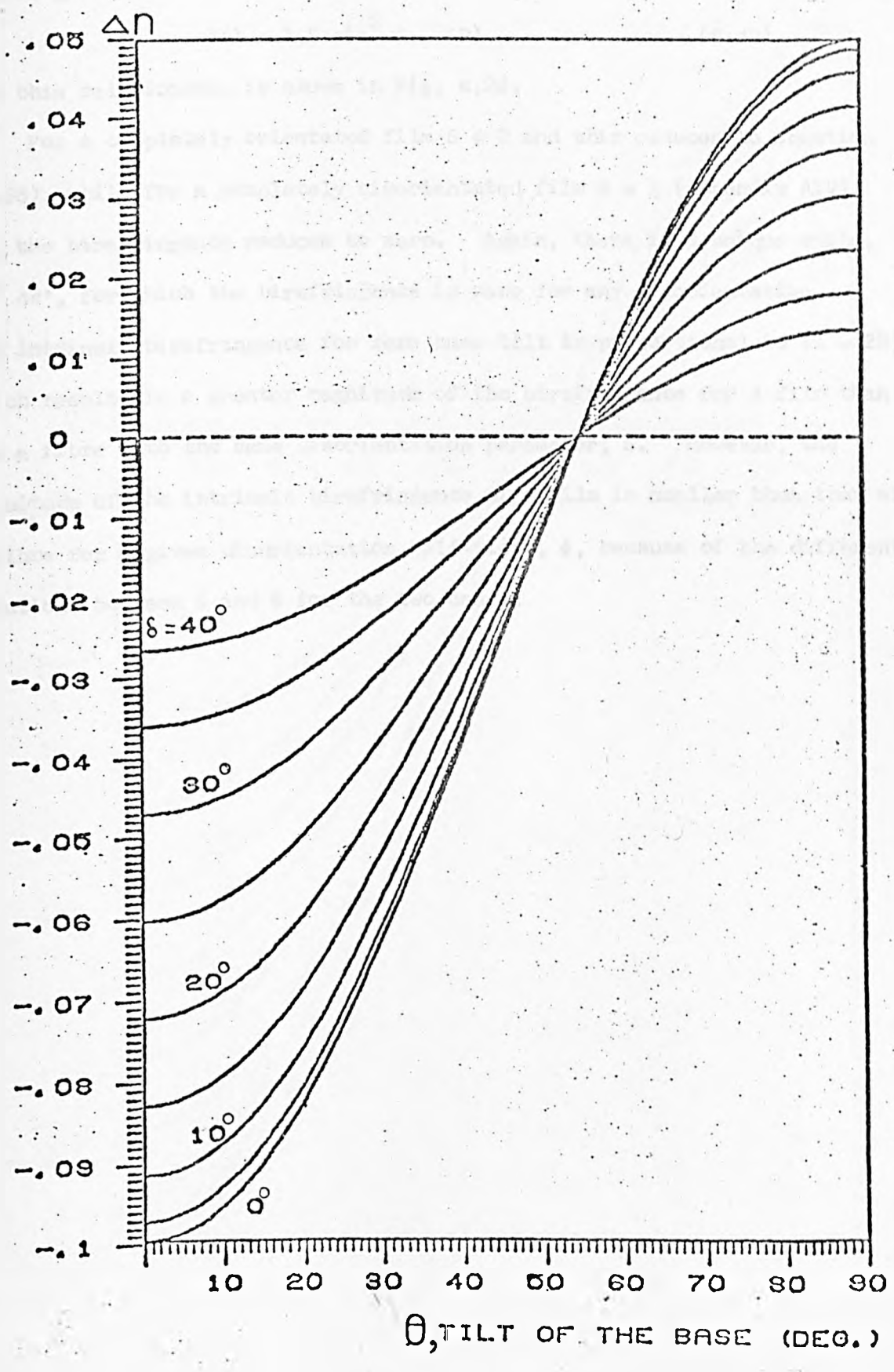

(ii) The film case

Substituting the expressions for $f_\alpha(\theta, S)$ and $f_\beta(\theta, S)$ relevant to the film from Equations (C.5) and (C.6) respectively, into Equation (6.38) gives

$$\Delta n = K(1 - 1.5 \sin^2 \theta - SP) \qquad (6.40)$$

and this relationship is shown in Fig. 6.23.

For a completely orientated film S = 0 and this reduces to Equation (6.35), while for a completely disorientated film S = ½ (Appendix AIV) and the birefringence reduces to zero. Again, there is a unique angle, 54° 44', for which the birefringence is zero for any disorientation. The intrinsic birefringence for zero base tilt is proportional to (1 - 2S), which results in a greater magnitude of the birefringence for a film than for a fibre with the same disorientation parameter, S. However, the magnitude of the intrinsic birefringence of a film is smaller than that of a fibre for a given disorientation half-width, δ, because of the different relations between S and δ for the two cases.

Fig. 6.23 The intrinsic component of the birefringence of a film as a function of base-tilt, θ, for various disorientation half-widths, δ.

K (Equation 6.40) has been set to unity.

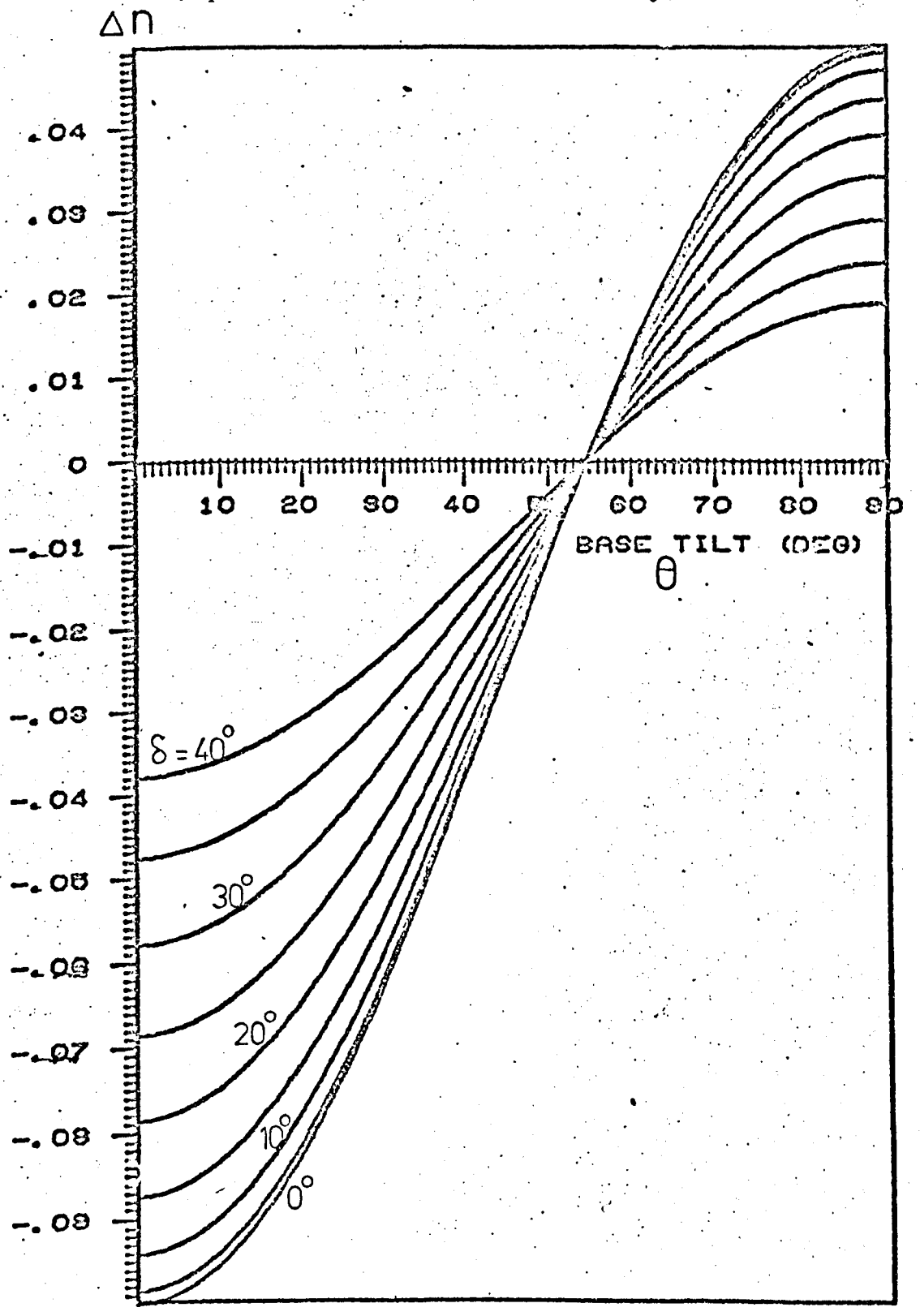

6.5 Summary

The more important equations that have been derived relating to the birefringence of a fibre are given in Table 6.1. In Chapter 7 the birefringence of DNA-drug fibres, of different DNA/drug contents, are measured at different humidities. Using the X-ray results of Chapter 5, in particular the relevant values of the intermolecular separation and the DNA helix diameter, the change in the birefringence with f (the volume fraction of the rods) may be followed to investigate the effect of water uptake on the fibres and to test the applicability of Equation (6.30).

TABLE 6.1

Summary of Some Birefringence Formulae

	$\Delta n_{total} = n_m f' (A - fB)$ where $A = \delta - \Delta_{rm}$ $B = \Delta_{rm}^2$	(6.30)
Completely orientated fibre	$\Delta n = K (1 - 1.5 \sin^2 \theta)$	(6.35)
Disorientated fibre	$\Delta n = K (1 - 1.5 \sin^2\theta - 0.75 SP)$	(6.39)

By comparing the values of the birefringence observed for DNA-drug fibres with those for DNA fibres, information on the orientation of the drug molecules and their anisotropy may be inferred (Equation (6.39)). The values for different drug contents at different humidities can be used to indicate the extent of binding at each humidity, and can be compared with the indications obtained from X-ray diffraction.

A summary of the expressions derived for the dichroic ratio of fibres is given in Table 6.2. The experimental results on DNA-drug fibres

presented in the next chapter will be analysed in terms of the relationship between the dichroic ratio, D, and the tilt of the drug (Equation (6.11)) since the direction of the transition dipole moment is not known for the three drugs used in this study. The values of dichroic ratio, obtained at different humidities can be used to indicate the orientation of one or more bound species using the predictions from the X-ray diffraction and birefringence results for the fractions bound at each humidity.

TABLE 6.2

Summary of Dichroic Ratio Formulae for Fibres

	D in terms of θ	D in terms of α
Disorientated Fibres	$\frac{1}{2} + \frac{2\cos^2\theta - SP}{2\sin^2\theta + SP}$ (Eqn. (6.11) & Fig. 6.13)	$\frac{\cos^2\alpha - \frac{SP'}{2}}{2\sin^2\alpha + SP'}$ (Eqn. (6.16) & Fig. 6.14)
Completely Orientated Fibres	$\frac{1}{2} + \cot^2\theta$ (Eqn. (6.3) & Fig. 6.5)	$\cot^2\alpha$ (Eqn. (6.2) & Fig. 6.3)

Where $P = 3\cos^2\theta - 1$

$P' = 3\cos^2\alpha - 2$

APPENDICES FOR CHAPTER 6

APPENDIX A

AI Expression for the Dichroic Ratio, D

From Section 6.3.1, a transition dipole moment T can be represented in the co-ordinate frame of the fibre as

$$T = \begin{pmatrix} x_1 \\ y_1 \\ z_1 \end{pmatrix} = L_1^{-1} L_2^{-1} \begin{pmatrix} 1 \\ 0 \\ 0 \end{pmatrix}$$

Using Equations (6.4) and (6.8), which refer to Figs. 6.9 and 6.10, this gives

$$T = \begin{pmatrix} x_1 \\ y_1 \\ z_1 \end{pmatrix} = \begin{pmatrix} \cos\phi_1 (\cos\psi_2 \cos\phi_2 - \cos\theta_2 \sin\phi_2 \sin\psi_2) \\ -\cos\theta_1 \sin\phi_1 (\cos\psi_2 \sin\phi_2 - \cos\theta_2 \cos\phi_2 \sin\psi_2) \\ +\sin\theta_1 \sin\phi_1 (\sin\theta_2 \sin\psi_2) \\ \\ \sin\phi_1 (\cos\psi_2 \cos\phi_2 - \cos\theta_2 \sin\phi_2 \sin\psi_2) \\ +\cos\theta_1 \cos\phi_1 (\cos\psi_2 \sin\phi_2 - \cos\theta_2 \cos\phi_2 \sin\psi_2) \\ -\sin\theta_1 \cos\phi_1 (\sin\theta_2 \sin\psi_2) \\ \\ 0 \\ \\ +\sin\theta_1 (\cos\psi_2 \sin\phi_2 - \cos\theta_2 \cos\phi_2 \sin\psi_2) \\ +\cos\theta_1 (\sin\theta_2 \sin\psi_2) \end{pmatrix} \qquad (A.1)$$

where ψ_1 has been set to zero as explained in the text (Section 6.3.1). The terms containing θ_2, the drug tilt, are of particular importance since they will remain in the final expression for the dichroic ratio when integration over the other angles has taken place.

$T.\hat{Y}_1$ and $T.\hat{Z}_1$, used to find D, are respectively the second and third terms in this column vector.

For the integrations, the following expressions are used

$$\int_0^{\pi \text{ or } 2\pi} \sin x \cos x \, dx = 0$$

$$\int_0^{\pi \text{ or } 2\pi} \sin^2 x \, dx = \frac{\pi}{2} \text{ or } \pi, \text{ respectively}$$

$$\int_0^{\pi \text{ or } 2\pi} \cos^2 x \, dx = \frac{\pi}{2} \text{ or } \pi, \text{ respectively}$$

(i) For a fibre

For a perfectly orientated fibre ($\theta_1 = 0$), averaging over ϕ_2 (from 0 to 2π), ψ_2 (from 0 to π), and ϕ_1 (from 0 to 2π) gives

$$D = \frac{\langle (T.\hat{Y}_1)^2 \rangle}{\langle (T.\hat{Z}_1)^2 \rangle} = \frac{\frac{1}{4}(1 + \cos^2\theta_2)}{\frac{1}{2}\sin^2\theta_2}$$

$$= \cot^2\theta_2 + \tfrac{1}{2}$$

which is the same as Equation (6.3), derived in Section 6.2 by a less general method.

For a disorientated fibre, $\theta_1 \neq 0$ (i.e. the helix axes are not aligned with the fibre axis) and the situation is more complicated.

$$\langle (T.\hat{Y}_1)^2 \rangle = \frac{1}{8}(1 + \cos^2\theta_2 + \langle \cos^2\theta_1 \rangle + \langle \cos^2\theta_1 \rangle \cos^2\theta_2 + 2\langle \sin^2\theta_1 \rangle \sin^2\theta_2)$$

Putting $S = \langle \sin^2\theta_1 \rangle$,

$$\langle (T.\hat{Y}_1)^2 \rangle = \frac{1}{8}(1 + \cos^2\theta_2 + (1-S) + \cos^2\theta_2 (1-S) + 2S \sin^2\theta_2)$$

$$= \frac{1}{8}(2(1 + \cos^2\theta_2) + S(1 - 3\cos^2\theta_2))$$

$$= \frac{1}{8}(2(1 + \cos^2\theta_2) - SP)$$

(A.2)

where $P = 3\cos^2\theta_2 - 1$

Similarly,

$$\langle (T.\hat{Z}_1)^2 \rangle = \langle \sin^2\theta_1 \rangle (\tfrac{1}{4} + \tfrac{1}{4}\cos^2\theta_2) + \tfrac{1}{2}\langle \cos^2\theta_1 \rangle \sin^2\theta_2$$

$$= \frac{S}{4}(1 + \cos^2\theta_2) + \tfrac{1}{2}(1 - S)\sin^2\theta_2$$

$$= \tfrac{1}{2}(\sin^2\theta_2 + \frac{SP}{2})$$

(A.3)

Thus, dropping the subscript on θ_2,

$$D = \frac{\frac{1}{8}\,(2\,(1 + \cos^2\theta_2) - SP)}{\tfrac{1}{2}\,(\sin^2\theta_2 + \frac{SP}{2})}$$

$$= \tfrac{1}{2}\left(\frac{2(\sin^2\theta + 2\cos^2\theta) - SP}{2\sin^2\theta + SP}\right)$$

$$= \tfrac{1}{2} + \frac{2\cos^2\theta - SP}{2\sin^2\theta + SP}$$

(A.4)

which is Equation (6.11) in the text.

(ii) For a film

In the case of a film, ϕ_1 is set to zero i.e. the film is considered so thin that there is no disorientation of the helices across any section perpendicular to the film surface. The density of states function, $N(\theta_1, \phi_1)$, and the probability function, $P(\theta_1)\,d\theta_1$, are defined for essentially a two-dimensional situation, as explained in detail in Fig. B.3. Integrating over ϕ_2 (from 0 to 2π) and ψ_2 (from 0 to 2π) gives

$$\langle(T.\hat{Y}_1)^2\rangle = \tfrac{1}{4}\{\langle\cos^2\theta_1\rangle + \langle\cos^2\theta_1\rangle\cos^2\theta_2 + 2\langle\sin^2\theta_1\rangle\sin^2\theta_2\}$$

$$= \tfrac{1}{4}\{(1-S)(1 + \cos^2\theta_2) + 2\,S\sin^2\theta_2\}$$

$$= \tfrac{1}{4}\{(1+\cos^2\theta_2) + S(2\sin^2\theta_2 - \cos^2\theta_2 - 1)\}$$

$$= \tfrac{1}{4}\{(1+\cos^2\theta_2) - SP\}$$

(A.5)

The denominator $\langle(T.\hat{Z}_1)^2\rangle$, is the same as for the fibre case. Thus

$$D = \frac{\tfrac{1}{4}\{(1 + \cos^2\theta) - SP\}}{\tfrac{1}{2}\{\sin^2\theta + \frac{SP}{2}\}}$$

$$= \tfrac{1}{2} + \frac{2\cos^2\theta - \frac{3}{2}SP}{2\sin^2\theta + SP}$$

(A.6)

which is Equation (B.2) in Appendix B.

AII The Disorientation Parameter, S

The disorientation, S, is defined as

$$S(\theta_1) = \langle \sin^2\theta_1 \rangle$$

$$= \frac{\int P(\theta_1) \sin^2\theta_1 \, d\theta_1}{\int P(\theta_1) \, d\theta_1}$$

where $P(\theta_1)$ is the probability function describing the distribution of DNA molecules about the fibre axis.

(i) For a fibre

As explained in the text

$$P(\theta_1) = \frac{1}{2\pi} \int_0^{2\pi} N(\theta_1, \phi_1) \sin\theta_1 \, d\phi_1$$

Assuming a gaussian distribution (viz. $N(\theta_1, \phi_1) \propto \exp\left(-\frac{\theta_1^2}{2\delta^2}\right)$) then

$$S = \frac{\int_0^{\frac{\pi}{2}} e^{-\frac{\theta^2}{2\delta^2}} \sin^3\theta_1 \, d\theta_1}{\int_0^{\frac{\pi}{2}} e^{-\frac{\theta_1^2}{2\delta^2}} \sin\theta_1 \, d\theta_1}$$

The upper integration limit for θ_1 may be increased to ∞; since they are both exponentially decaying odd functions this would result in the same scaling for both the numerator and the denominator. The denominator is similar to the standard integral (Abramowitz and Segun, 1968).

$$\int_0^{\infty} e^{-at^2} \sin(2xt) \, dt = \frac{1}{\sqrt{a}} e^{-\frac{x^2}{a}} \int_0^{\frac{x}{\sqrt{a}}} e^{t^2} \, dt$$

and the right-hand side of this can be expressed in terms of the Dawson integral

$$F(z) = e^{-z^2} \int_0^{z} e^{t^2} \, dt$$

Using these two equations, and setting $t = \theta_1$, $x = \frac{1}{2}$, $a = \frac{1}{2^2}$ and $z = \frac{x}{\sqrt{a}} = \frac{\delta}{\sqrt{2}}$ gives

$$\int_0^\infty e^{-\frac{\theta_1^2}{2\delta^2}} \sin\theta_1 \, d\theta_1 = \sqrt{2\delta^2}\left\{F(\frac{\delta}{\sqrt{2}})\right\}$$

and an extension of this, using $\sin^3\theta_1 = \frac{1}{4}(3\sin\theta_1 - \sin 3\theta_1)$ is

$$\int_0^\infty e^{-\frac{\theta_1^2}{2\delta^2}} \sin^3\theta_1 \, d\theta_1 = \sqrt{2\delta^2}\left\{3F(\frac{\delta}{\sqrt{2}}) - F(\frac{3\delta}{\sqrt{2}})\right\}$$

Using these standard integrations, the orientation parameters, S, is given by

$$S = \frac{1}{4}(3 - \frac{F(\frac{3\delta}{\sqrt{2}})}{F(\frac{\delta}{\sqrt{2}})})$$

which is Equation (6.14) in the text.

(ii) <u>For a Film</u>

For the film case

$$P(\theta_1) = N(\theta_1,\phi_1)\, d\theta_1$$

so that

$$S = \frac{\int_0^\pi e^{-\frac{\theta_1^2}{2\delta^2}} \sin^2\theta_1 \, d\theta_1}{\int_0^\pi e^{-\frac{\theta_1^2}{2\delta^2}} \, d\theta_1}$$

Both of these integrals are of a standard form (Abramowitz and Segun, 1968) and give

$$S = \frac{1}{2}(1 - e^{-2\delta^2})$$

quoted as Equation (B.3) in Appendix B.

AIII The Dawson Integral as a Series

$$F(z) = \frac{\sqrt{\pi}}{2i}\left(w(z) - e^{-z^2}\right)$$

where

$$w(z) = \sum_{n=0}^{\infty} \frac{(iz)^n}{\Gamma(\frac{n}{2}+1)}$$ (Abramowitz and Segun, 1968)

The even terms in the expansion of $w(z)$ are equal to the terms in the expansion of e^{-z^2} so these cancel (N.B. $\Gamma(1) = 1$ and $\Gamma(n+1) = n\Gamma(n)$).

The odd terms give

$$F(z) = \frac{\sqrt{\pi}}{2i}\left(\frac{iz}{\Gamma(\frac{3}{2})} + \frac{(iz)^3}{\Gamma(\frac{5}{2})} + \frac{(iz)^5}{\Gamma(\frac{7}{2})} + \ldots\ldots\right)$$

Now $\Gamma(\frac{1}{2}) = \sqrt{\pi}$ so that

$$F(z) = \frac{\sqrt{\pi}}{2} \sum_{r=1}^{\infty} \frac{(-1)^{r+1} z^{2r-1}}{\Gamma(r+\frac{1}{2})}$$

$$= \left(z - \frac{z^3}{\frac{3}{2}} + \frac{z^5}{\frac{5}{2}\cdot\frac{3}{2}} \ldots\ldots\right)$$

AIV Values of S for a Completely Disorientated Specimen

(i) For a Fibre

$$F(\delta) = \frac{\sqrt{\pi}}{2i}\left(w(\delta) - e^{-\delta^2}\right)$$

For large (i.e. large disorientation)

$$F(\delta) = \frac{\sqrt{\pi}}{2i}\, w(\delta)$$

$$= \frac{1}{2\delta} + O\left(\frac{1}{\delta^2}\right)$$

Therefore,

$$\frac{F\left(\frac{3\delta}{\sqrt{2}}\right)}{F\left(\frac{\delta}{\sqrt{2}}\right)} \sim \frac{1}{3}$$

Thus,

$$S = \langle \sin^2\theta \rangle = \tfrac{1}{4}\left(3 - \frac{F\left(\frac{3\delta}{\sqrt{2}}\right)}{F\left(\frac{\delta}{\sqrt{2}}\right)}\right) = \frac{2}{3}$$

(ii) For a Film

The expression $S = \tfrac{1}{2}\left(1 - e^{-2\delta^2}\right)$ takes the value 0.5 as δ goes to infinity (i.e. complete disorientation).

APPENDIX B

The Linear Dichroism of a DNA-Drug Film

Several experimental studies (Rupprecht et al., 1969; Kurucsev and Zdysiewicz, 1971; Kelly and Kurucsev, 1976) of linear dichroism have been carried out using DNA-drug films rather than fibres.

A previous analysis (Seeds, 1953) of a perfectly orientated film has considered the film to be so thin that the normal to the drug chromophore is constrained to be in the plane (YZ) of the film (Fig. B.1). With this assumption the angles previously referred to as θ and α are equivalent. Using Seed's notation,

$$D = \frac{E_{\perp} \cos^2 \alpha}{E_{\parallel} \sin^2 \alpha} = \cot^2 \alpha \qquad (B.1)$$

since $E_{\perp} = E_{\parallel}$ as before.

This relationship is shown in Fig. B.2. The dichroic ratio varies from zero to infinity, and takes the value of unity when $\alpha = 45^{\circ}$.

If disorientation within the film is considered, analytic expressions analogous to Equations (6.11) and (6.16) may be obtained. The transformation matrices given in Equations (6.6) and (6.8) still hold, but ϕ_1 can be considered equal to zero (i.e. the film is considered thin enough such that all the disorientation occurs in the plane of the film). The density of states function, $N(\theta_1, \phi_1)$ is defined somewhat differently (Fig. B.3) than in the case of a fibre and the gaussian probability function, $P(\theta_1)\, d\theta_1$, is shown graphically in Fig. B.4.

The dichroic ratio for a film can be shown to be given by

$$D = \tfrac{1}{2} + \frac{2 \cos^2 \theta - \frac{3}{2} SP}{2 \sin^2 \theta + SP} \qquad (B.2)$$

where P has its previous significance, and S is still $\langle \sin^2 \theta_1 \rangle$ but the

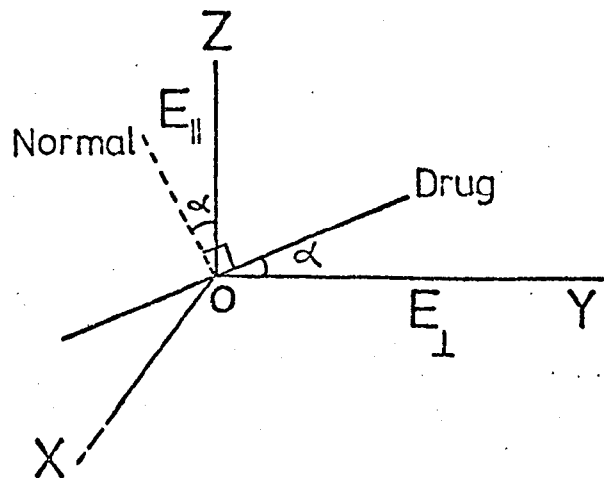

Figure B.1. The co-ordinate system for an infinitely thin, perfectly orientated film (after Seeds, 1963).

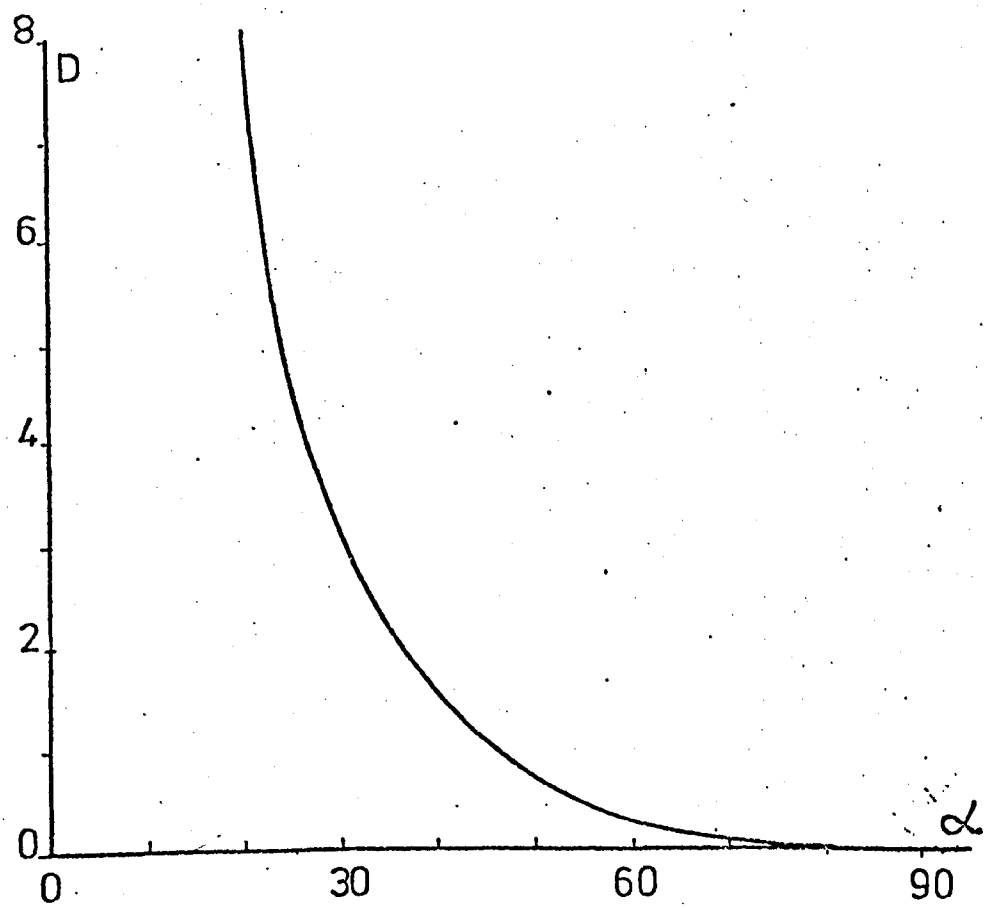

Figure B.2. A plot of the dichroic ratio, D, as a function of tilt angle, $\alpha(=\theta)$ (see Equation B.1).

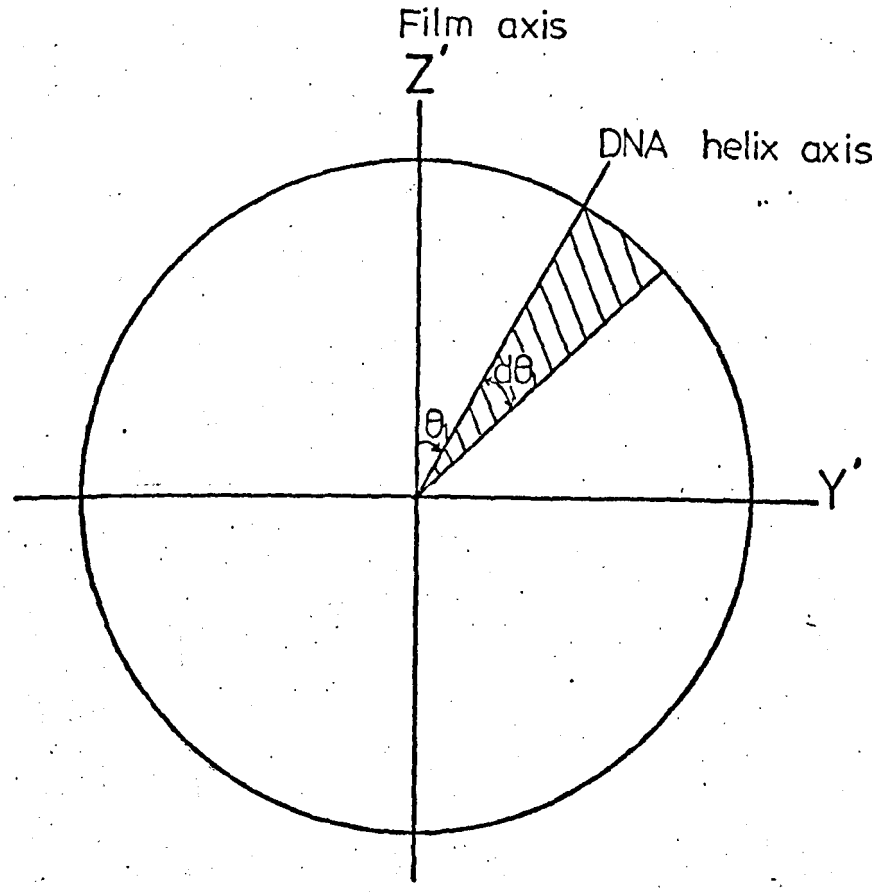

Figure B.3

The thin film is regarded essentially as a 2D case, there being no misalignment of the helices in the X' direction (viz. $\phi_1 = 0$).

$N(\theta_1, \phi_1)$ is the density of states function, again assumed gaussian in θ_1; it is proportional to the number of DNA helices pointing in a direction θ_1 from the film axis.

$P(\theta_1)d\theta_1$ is proportional to the probability of a DNA helix pointing within the limits θ_1 and $\theta_1 + d\theta_1$.

$$P(\theta_1)d\theta_1 = N(\theta_1, \phi_1)\, d\theta_1$$

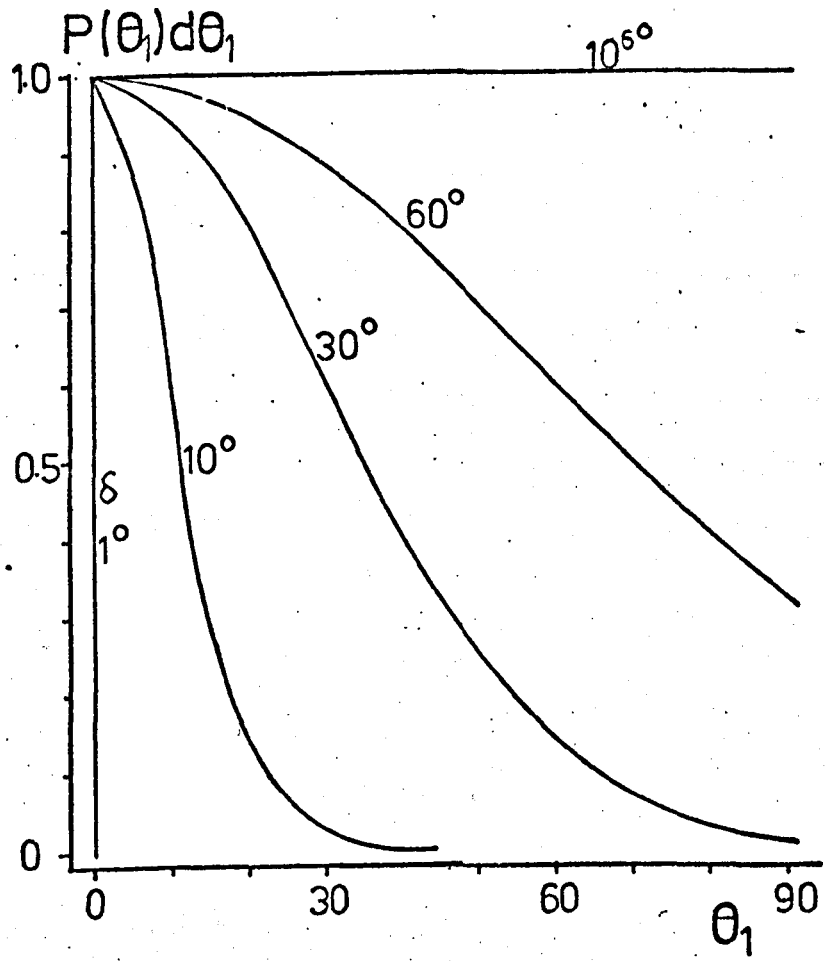

Figure B.4 The probability function $P(\theta_1)d\theta_1$ for a film. The probability function is a standard gaussian with half-width, δ. In the limit of complete disorientation ($\delta \to \infty$) it becomes a horizontal line, indicating that all values of θ_1 are equally probable.

integration is performed over θ_1 values from zero to π and no geometric $\sin\theta_1$ term appears in the expression i.e.

$$S = \frac{\int_0^{\pi} \sin^2\theta_1 \, P(\theta_1) \, d\theta_1}{\int_0^{\pi} P(\theta_1) \, d\theta_1}$$

$$= \tfrac{1}{2}\left(1 - e^{-2\delta^2}\right) \qquad \text{(B.3)}$$

The relationship given by Equation (B.2) is plotted in Fig. B.5; comparison should be made with Equation (6.6) and Fig. 6.13 pertaining to the fibre case. For the same value of S the dichroic ratio for a film is always smaller than that for a fibre, although for a given gaussian half-width, δ, the film values for D are larger than the fibre values. This results from the different relationship between S and δ in the two cases (compare Equations (6.14) and (B.3)).

Considering the special cases -

(i) For a perfectly orientated film S = 0 and Equation (B.2) reduces to Equation (6.3).

(ii) For a completely disorientated film

$$N(\theta_1, \phi_1) = 1$$

and the probability function can be represented by a straight horizontal line (Fig. B.4). S becomes equal to 0.5 (Appendix A Iv), and thus the dichroic ratio is equal to unity.

(iii) The dichroic ratio is always equal to unity when $\theta = 54^{\circ}44'$, irrespective of the value of the disorientation parameter, S.

(iv) For $\theta = 0$, the dichroic ratio is given by $D = \frac{1}{S} - 1$ which is the same as with a fibre.

Similarly, an expression for D in terms of α may be derived.

Figure B.5 The dichroic ratio, D, of a film as a function of θ, for various values of δ (Equation (B.2))

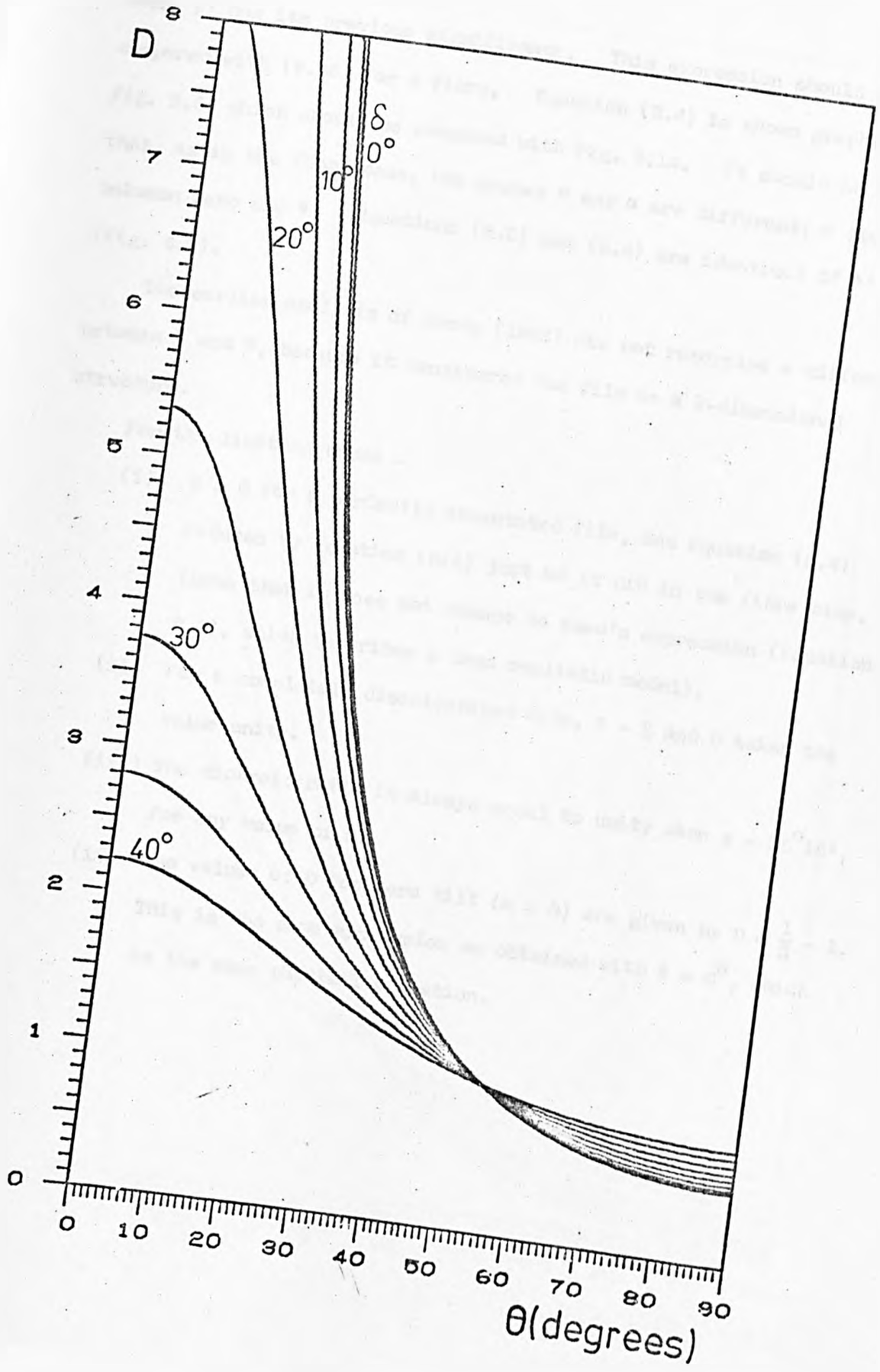

$$D = \frac{\cos^2 \alpha - SP'}{2 \sin^2 \alpha + SP'} \qquad (B.4)$$

where P' has its previous significance. This expression should be compared with (6.16) for a fibre. Equation (B.4) is shown graphically in Fig. B.6, which should be compared with Fig. 6.14. It should be noted that, as in the fibre case, the angles θ and α are different; α lies between zero and θ. Equations (B.2) and (B.4) are identical if $\phi' = 45^\circ$ (Fig. 6.2).

The earlier analysis of Seeds (1953) did not recognise a difference between θ and α, because it considered the film as a 2-dimensional structure.

For the limiting cases -

(i) S = 0 for a perfectly orientated film, and Equation (B.4) reduces to Equation (6.2) just as it did in the fibre case. (Note that it does not reduce to Seed's expression (Equation B.1), which describes a less realistic model).

(ii) For a completely disorientated film, S = ½ and D takes the value unity.

(iii) The dichroic ratio is always equal to unity when $\alpha = 35^\circ 16'$, for any value of S.

(iv) The values of D for zero tilt ($\alpha = 0$) are given by $D = \frac{1}{S} - 1$. This is the same expression as obtained with $\theta = 0^\circ$, which is the same physical situation.

Figure B.6 The dichroic ratio, D, of a film as a function of α, for various values of δ (Equation (B.4))

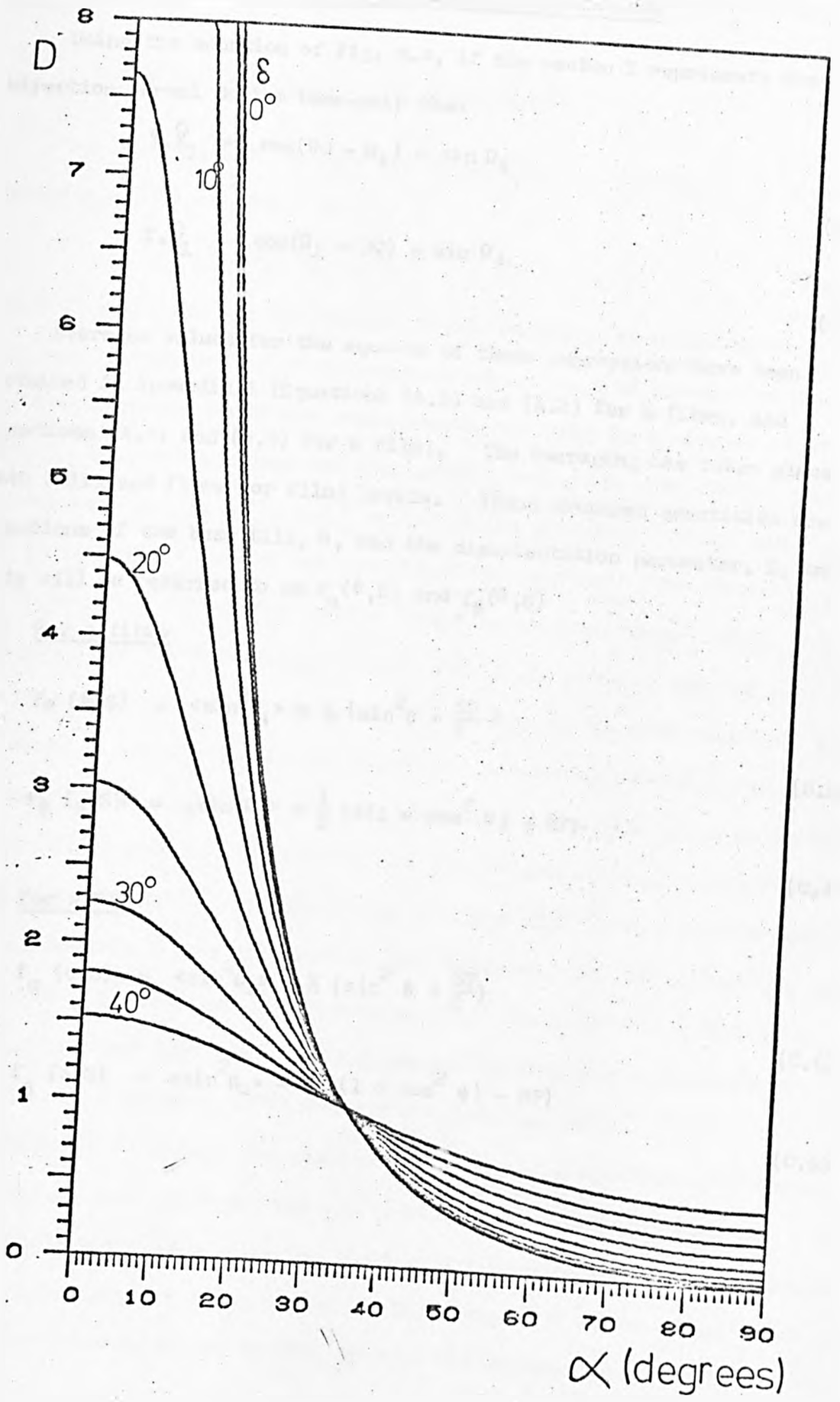

APPENDIX C

Expressions Relevant to the Birefringence Calculations

Using the notation of Fig. 6.4, if the vector T represents the direction normal to the base-pair then

$$T.\hat{Z}_1 = \cos(90 - \Omega_{\parallel}) = \sin \Omega_{\parallel} \qquad (C.1)$$

$$T.\hat{Y}_1 = \cos(\Omega_{\perp} - 90) = \sin \Omega_{\perp} \qquad (C.2)$$

Averaged values for the squares of these expressions have been obtained in Appendix A (Equations (A.3) and (A.2) for a fibre, and Equations (A.3) and (A.5) for a film). The averaging has taken place at both helix and fibre (or film) levels. These averaged quantities are functions of the base tilt, θ, and the disorientation parameter, S, and they will be referred to as $f_\alpha(\theta,S)$ and $f_\beta(\theta,S)$

(i) For a fibre

$$f_\alpha(\theta,S) = \langle \sin^2 \Omega_{\parallel} \rangle = \tfrac{1}{2} \{ \sin^2 \theta + \frac{SP}{2} \} \qquad (C.3)$$

$$f_\beta(\theta,S) = \langle \sin^2 \Omega_{\perp} \rangle = \frac{1}{8} \{ 2(1 + \cos^2 \theta) - SP \} \qquad (C.4)$$

(ii) For a Film

$$f_\alpha(\theta,S) = \langle \sin^2 \Omega_{\parallel} \rangle = \tfrac{1}{2} \{ \sin^2 \theta + \frac{SP}{2} \} \qquad (C.5)$$

$$f_\beta(\theta,S) = \langle \sin^2 \Omega_{\perp} \rangle = \tfrac{1}{4} \{ (1 + \cos^2 \theta) - SP \} \qquad (C.6)$$

CHAPTER 7

Linear Dichroism and Birefringence : Experimental Results

7.1 Technical Limitations on the Measurements

The absorbance of monochromatic radiation of wavelength, λ, by a specimen may be expressed as

$$A(\lambda) = \log I_o - \log I \qquad (7.1)$$

where I_o and I are the intensities of the radiation incident on the specimen and transmitted by it respectively. In a single-beam microspectrophotometer successive measurements are taken on a microscopic area with the specimen in place and then absent, using the same optical path. The measured values of I_o and I depend on the emissivity of the lamp (which is greater towards the red end of the spectrum), the spectral transmission of the optical system (which is greatest around 500nm, the wavelength at which the monochromator grating is blazed), and the frequency response of the photodetector (which is greater in the blue region of the spectrum). If the optical and electronic properties of the microspectrophotometer are unaltered during the time required to take these measurements, systematic errors will be reduced. A double-beam microspectrophotometer employs a beam-splitter to direct the incident light either alternatively or simulataneously to the specimen and the reference, but for microscopic use the attendant requirement for identical light paths is more difficult to satisfy than the time stability requirement in single-beam instruments (Clarke, 1972; Mielenz, 1972; Mielenz and Eckerle, 1972).

In order to measure the dichroic ratio, D, of a specimen in a single-beam system, four spectral runs are required (viz. the background and specimen-transmitted spectra for light polarised parallel and perpendicular to the optic axis of the specimen). This imposes a further restriction on the time stability of the system, because the optical and electronic

properties must remain constant over the increased length of time required to take these measurements. The birefringence of a specimen is measured in white light by rotating a compensator to find the dark compensation fringe (Section 7.3). There is no time stability restriction on this measurement since the effect of the different polarisations (giving rise to different refractive indices, $n_{\parallel}$ and $n_{\perp}$) is observed simultaneously and not sequentially.

7.1.1 An Alternative Technique for Measuring the Dichroic Ratio

The four log (transmission) curves can be collected in two spectral runs by using an adaptation of the method of Jaffe et al. (1967). A multiple waveplate of quartz, placed between the polariser and the specimen stage and oriented such that its optic axis is at 45° to the polarisation direction of the polariser, acts as a wavelength dependent polarisation modulator. The originally plane-polarised light will emerge from the waveplate elliptically polarised, due to the relative retardation, $\phi(\lambda)$, introduced.

$$\phi(\lambda) = \frac{2\pi}{\lambda} . \Delta n(\lambda) t \qquad (7.2)$$

where t is the waveplate thickness and $\Delta n(\lambda)$ is the birefringence of quartz at the wavelength λ. When $\phi(\lambda)$ equals an even multiple of π, the plane polarised light emerges with its polarisation unaltered; and when it equals an odd multiple of π, the light will emerge plane polarised in a direction at right angles to its polarisation direction on entry. The observed transmission will be that corresponding to the resultant polarisation. The frequency of these changes depends on the thickness of the waveplate.

With reference to Fig. 7.1,

$$\frac{\Delta n(\lambda_n)}{\lambda_n} - \frac{\Delta n(\lambda_{n+1})}{\lambda_{n+1}} = \frac{1}{t} \qquad (7.3)$$

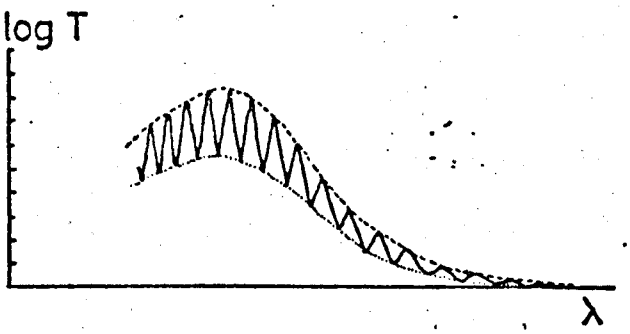

Figure 7.1 Schematic log(transmission) curves for a dichroic sample using a multiple waveplate of quartz

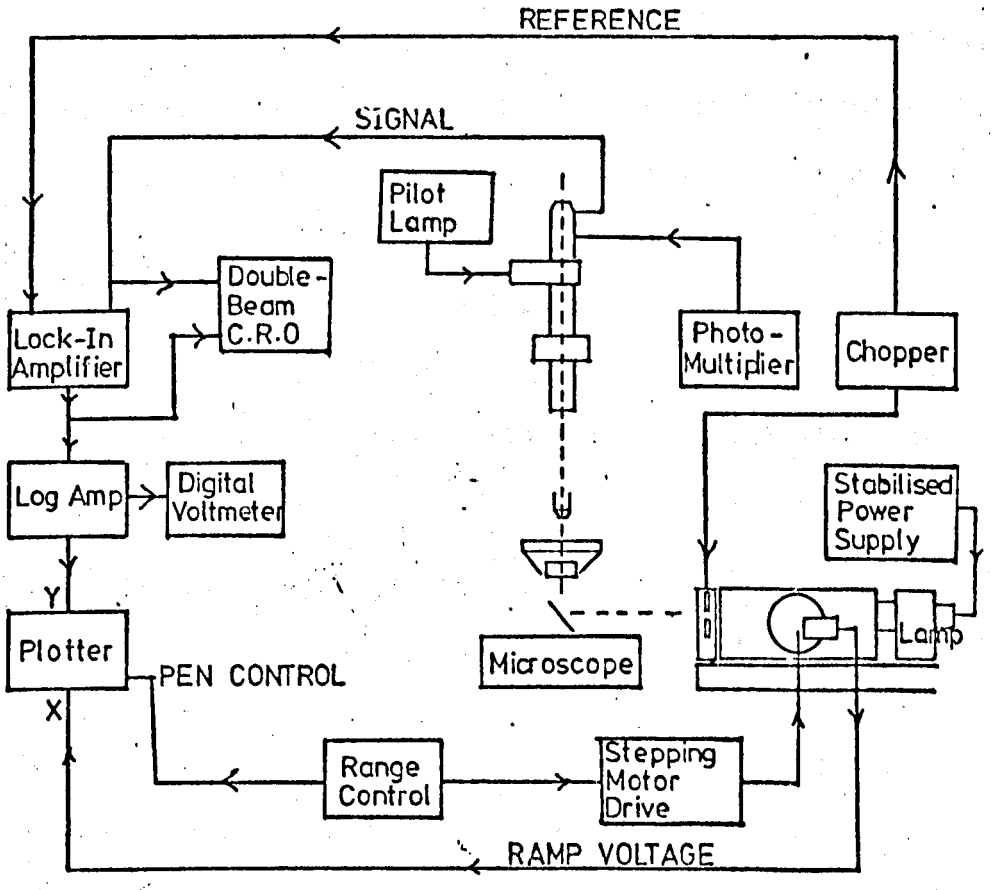

Figure 7.2 Schematic illustration of the full microspectrophotometer system.

The repeat, $\Delta\lambda(=\lambda_{n+1} - \lambda_n)$, should be chosen so that it is small enough to allow easy interpolation of the envelopes by eye, but large enough so that the spectral bandwidth passed by the monochromator does not diminish the magnitude of the oscillations because of averaging. For a repeat interval of around 5nm, $\Delta n(\lambda n)$ and $\Delta n(\lambda_{n+1})$ can be taken as equal for quartz. This is because the dispersion of the birefringence of quartz is small,

$$\frac{n(\lambda_F) - n(\lambda_C)}{\Delta n(\lambda_D)} = 3 \times 10^{-2}$$

where λ_F is 486.1nm, λ_C is 656.3nm and λ_D is 546.1nm. Thus

$$t = \frac{\lambda_{n+1} \cdot \lambda_n}{\Delta n(\lambda n) \cdot (\lambda_{n+1} - \lambda_n)} \qquad (7.4)$$

For example, with λ_n = 500nm and λ_{n+1} = 505nm, and Δn (500nm) = 0.00911 the required waveplate thickness is 5.5mm. A crystalline quartz optical flat, with its optic axis in the plane of the polished faces, 6mm. thick, flat to $\frac{\lambda}{2}$ and with faces parallel to 15 seconds of arc, was constructed to order by Gooch and Housego Ltd., Ilminster, Somerset. The expected repeat interval $\Delta\lambda$, according to Equation (7.4), is 4.6nm.

Spectra are taken with and without the specimen in position (viz. the 'specimen' and 'background' runs), the envelope of the oscillating traces providing the four data sets required. These are input via a D-Mac pencil follower to the program 'MICRO', which computes the dichroic ratio as a function of wavelength. This method is time-saving, and it reduces the time stability requirements of the system. Any difference in the envelopes for the 'background' case is due to non-uniformity of the polariser and/or variations in the polarisation sensitivity of the photomultiplier. In practice, these differences were so small that they were not resolved.

7.2 The Microspectrophotometer

A single-beam microspectrophotometer, with polarised light facilities, was used to investigate the birefringence of DNA and DNA-drug fibres and the linear dichroism of DNA-drug fibres. The system was described by Porumb (1976), and was operated over wavelengths from 400 to 650nm. The microspectrophotometer (Fig. 7.2) consists basically of two parts -

(i) The Optical System

The central part of this is a Zeiss polarising microscope. A fibre is placed in a humidity cell (Section 2.3) which is positioned on the rotating stage of the microscope. The specimen is illuminated by pulsed monochromatic light originating from a 12V, 100W quartz iodine lamp. The monochromator is of a symmetric Czerny-Turner design, equipped with a plane diffraction grating blazed at 500nm. The entrance slit determines the spectral bandwidth, and the exit slit determines the intensity of the light reaching the specimen. The settings normally used were 2nm for the bandpass and 0.5mm for the exit slit.

The emergent beam is periodically interrupted by a vibrating-vane chopper operating at 110Hz. The beam illuminates an adjustable field aperture, whose setting determines the area in the object plane to be illuminated. A 45° mirror joins up the optical axis of the monochromator section with the optical axis of the microscope. The optical bench supporting the lamp and monochromator were permanently decoupled from the support carrying the field aperture and 45° mirror, in order to facilitate alignment of the optical axes. The image of the condenser diaphragm and the field aperture were both in the centre of the field of view of the microscope when alignment

was completed. Before using the equipment each session the condenser lens was centred using the internal light source of the microscope, and minor adjustments were made, if necessary, to centre the field and measuring apertures accurately.

The light, having passed through the specimen, is detected and measured by an RCA 931 A photomultiplier tube operated at 1kV from its own stabilised power supply. A part of the beam is also directed to the inclined binocular head for viewing the fibre and the field aperture. The measuring aperture is located close to the photomultiplier window and can be viewed with the aid of a pilot lamp. It determines the fraction of the illuminated area that is sampled by the photomultiplier. The field aperture was set to illuminate a portion about ⅔rds of the width of a fibre to minimise the cylindrical lens effect of the fibre and yet allow sufficient light to pass through it (Porumb, 1976), and the measuring aperture was adjusted to give a slightly smaller area within the illuminated area. For the fibres used in this study the illuminated area is around 65μm x 100μm.

(ii) The Electronic System

This amplifies the output of the photomultiplier system, separating out the signal from the noise by phase sensitive detection i.e. it considers only that part of the photo-multiplier output that is in phase with a signal from the beam chopper (Abernethy, 1973). A d.c. signal proportional to the light intensity is directed to a log amplifier, which has been calibrated so as to deliver an increase in voltage output of 1V for every ten-fold increase in input. This output signal drives the Y deflection of a Bryans X-Y plotter. The Y deflection can be calibrated in absorbance units using voltages

measured on a digital voltmeter, since the deflection produced by a voltage of 1V is equivalent to 1 OD unit. The X deflection is linear with wavelength and is produced by a ramp voltage from a potentiometer which is turned by the monochromator shaft. A range control unit allows the spectra to be scanned between pre-selected wavelengths.

A DNA-drug fibre reduces the intensity of the transmitted light by such a large factor ($\sim 10^3 - 10^4$) that the logarithm of the photomultiplier output rather than the signal itself is recorded, in order to obtain the plots for the background and specimen over the full wavelength range on the scale of the plotter. There is an absolute limit to the absorbance which can be measured of about 3.8 OD units for a 2nm bandpass. This is due to stray light in the system. Stray light is defined as the radiation reaching the detector whose wavelengths are outside the region isolated by the monochromator (Slavin, 1963). It arises as scatter from the optics or from the walls in the monochromator, and from ambient light which has not passed through the chopper, reaching the detector. Electronic noise would start to be troublesome for optical densities greater than 4.0 (Porumb, 1976). Heterochromatic stray light may be reduced to some extent by reducing the exit slit to 1nm, but then the intensity of light transmitted through the fibre would be even lower. The optimum arrangement was when the background intensity was so high as to just avoid overloading the phase-sensitive detector (PSD) when it was set at its lowest sensitivity. With a fibre in position the PSD sensitivity could then be increased to record a measurable signal, which was still above the stray light level.

A spectrophotometer cannot measure absorbances higher than the stray light level, and even at levels below this limit the absorbance peaks will show some flattening (Technical Memo UV-71-2, Varian Instruments, 1971). The level at which this flattening becomes noticeable is around 3.5 OD units judged from the absorption spectra of fibres of differing M values. It was necessary to use thin fibres of fairly low drug/DNA ratios in order to minimise this effect. It was the intention of this thesis to make optical measurements on the same fibres as were used for the X-ray diffraction analysis. In order to obtain X-ray diffraction patterns within a reasonable exposure time, the fibres could be no thinner than about 80μm. The phenanthridines studied here have large absorptivities, and if the measured absorbance was to be less than about 3.5 OD units M could not be less than about 20 for fibres of this size.

The fluorescence emission spectrum of ethidium bromide has its maximum intensity at around 595nm and its fluorescence quantum efficiency is known to increase 21-fold on binding to double-stranded DNA (Le Pecq and Paoletti, 1967). Despite this, fluorescence will have no significant effect on the absorption spectrum, since it occurs in all directions and only a negligibly small proportion is collected at the very small solid angle sampled by the measuring aperture and photomultiplier.

It would be possible to automate the collection of the absorbance data by using a system such as that schematically illustrated in Fig. 7.3. The binary-coded decimal output of the auto-ranging digital voltmeter would be connected to a micro-computer, which would store the digital log intensity readings in memory. The micro-computer would also take the place of the range control unit in Fig. 7.2, and the user would input the

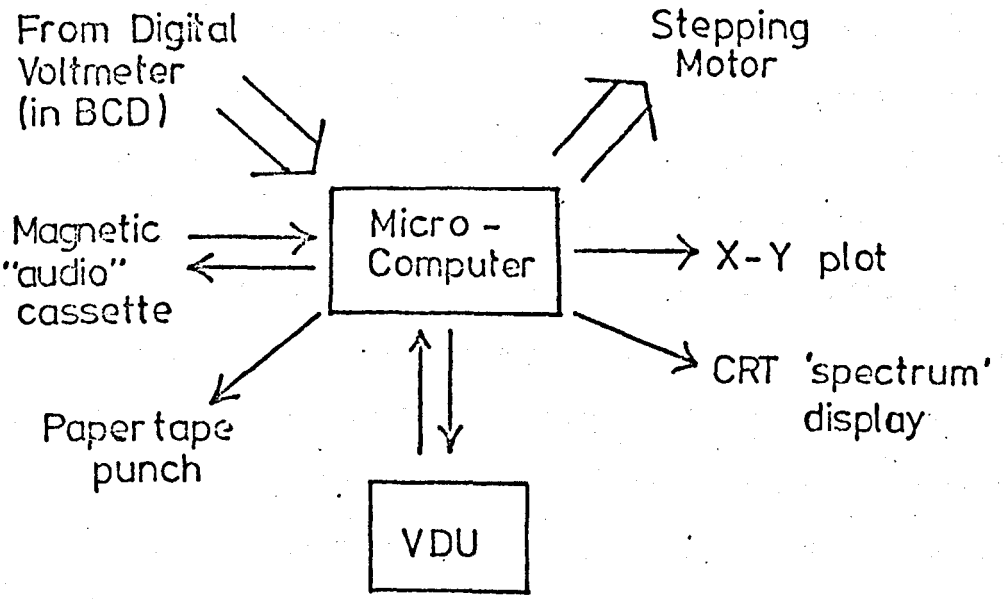

Figure 7.3 A schematic diagram to show the improvements suggested for the automation of data collection from the micro-spectrophotometer

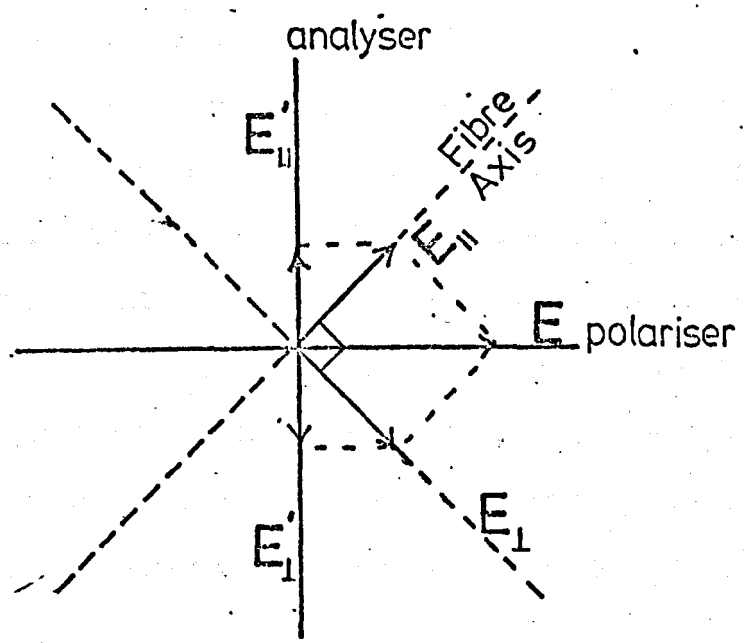

Figure 7.4 A birefringent fibre between crossed polariser and analyser

wavelength range over which each scan should be recorded, and the wavelength resolution required. Instead of using the ramp voltage from a potentiometer to calibrate the wavelength, the micro-computer would control the stepping motor directly by sending it appropriate current pulses. This would avoid the analogue-to-digital conversion that would be required if the ramp voltage scheme were retained. An initialising arrangement would need to be incorporated into the proposed scheme, for use at switch on, whereby a certain position of the monochromator drive shaft would be recognised by the stepping motor. Data could be routinely stored on a magnetic "audio" tape cassette, and nominated spectra could be translated on to paper tape for input to the program 'MICRO'. The user could communicate with the system via a video display unit, VDU, and the data could be displayed as it is being recorded on an XY plotter and/or on a cathode ray tube display.

The proposed scheme would eliminate the tedious and time-absorbing digitisation of the spectra by the D-Mac pencil follower which is currently employed. The user could communicate conveniently with the system and nominate the wavelength range and resolution through the VDU keyboard. He would obtain an instant graphical display of the data, and could choose either to abort the spectral run, change the resolution within it or accept the spectrum. Some minor adjustment of the optics is required before a series of spectral runs. A standard spectrum (of a filter, say) could be stored in the micro-computer and compared with a trial spectrum of the same filter at the beginning of a session. If they agree to within an acceptable tolerance the user would be instructed to proceed; if they did not, he would be requested to re-adjust the optical system.

7.3 Birefringence

In order to measure its birefringence, a fibre is placed in a humidity cell on the specimen stage of the polarising microscope such that the fibre axis is at 45° to the crossed polariser and analyser (Section 2.3.4.2). When reaching the fibre, the electric vector of the light is resolved into $E_{\parallel}$ and $E_{\perp}$ (Section 6.4). These two components travel through the fibre at different velocities, because of the different refractive indices $n_{\parallel}$ and $n_{\perp}$. They will travel different optical paths and will emerge generally out of phase. Along the axis of the analyser they will project as $E'_{\parallel}$ and $E'_{\perp}$ (Fig. 7.4). If their path difference is zero or an integral number of wavelengths, they will cancel and extinction will result. For white light all the wavelengths will cancel only for zero path difference, while for higher path differences only one wavelength at a time will be cancelled exactly. The others will be transmitted to varying extents to give what are known as Newton's colours. For large path differences the fringes overlap to such an extent that only white light is seen. In theory, if the central fringe can be identified uniquely then the white light fringes permit very accurate measurements to be made of optical path differences and hence birefringence.

The birefringence was measured using the internal white light source of the polarising microscope and an Ehringhaus rotary compensator. The fast direction of the compensator was superposed on the slow direction of the fibre. Rotation of the compensator changes its thickness in the light path and thus varies the retardation which it produces. The resultant path difference across the fibre plus compensator is reduced until the interference colours viewed in the microscope fall in Newton's scale. Continued rotation of the compensator produces a dark compensation band (the zeroth order band) in the middle of the fibre. The retardation produced by the calibrated compensator at this angle is equal and opposite

to that of the fibre. The birefringence Δn is calculated from

$$\Delta n = \frac{\text{path difference}}{\text{fibre thickness}} \qquad (7.5)$$

Exact compensation in white light can only be achieved if the relative dispersion of the birefringence of the compensator matches that of the fibre. Any marked difference between them will result in the compensation band being broadened and coloured, which leads to a phenomenon known as "fringe-jumping" i.e. the zeroth order band becomes coloured while an adjacent (formerly coloured band) appears black (Faust and Marrinan, 1955; Hartshorne and Stuart, 1970). This problem was encountered only for those fibres whose birefringence was so large that tilt angles of 20^{o} and above were required. For these fibres the problem was overcome as suggested by Hartshorne and Stuart (1970). The band that was dark at 95% R.H., when the birefringence was lowest, was assumed to be of genuine zeroth order. This band was followed as the specimen was dried down, as well as recording readings for the apparently dark band. At 55% R.H. the angles corresponding to the original band (now coloured) and the false dark band were determined. The readings at intermediate humidities were then corrected in proportion to this difference, and the corrected angles were converted into path differences by interpolation in the calibration table for the compensator.

7.3.1 Discussion of Results

The birefringence for a DNA fibre and for several DNA-phenanthridine fibres is shown as a function of relative humidity in Fig. 7.5. In each case the broken lines indicate the result of "normalising" the measured birefringence according to the method of Porumb (1976), to allow for the swelling of the fibres with increasing humidity. As the relative humidity of the fibres is increased, they swell and the substantial increase in volume (which can be of the order of 60-100% between 80% R.H. and 95% R.H.) causes a dilution in the polarisable material and a

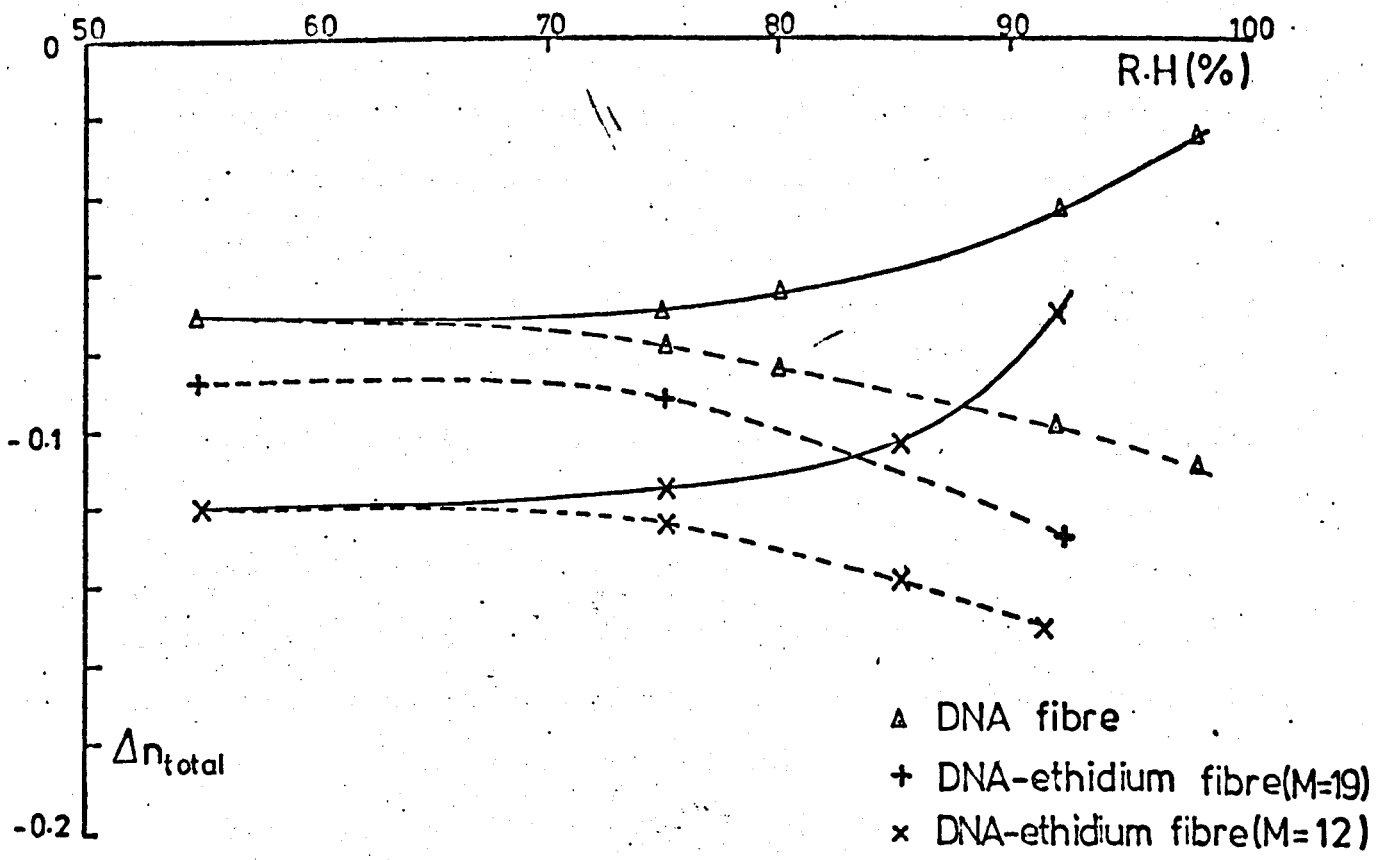

Figure 7.5 (i) The birefringence of a typical DNA fibre and typical DNA-ethidium fibres as a function of relative humidity. (The full lines indicate the measured birefringence, and the broken lines indicate the normalised birefringence.)

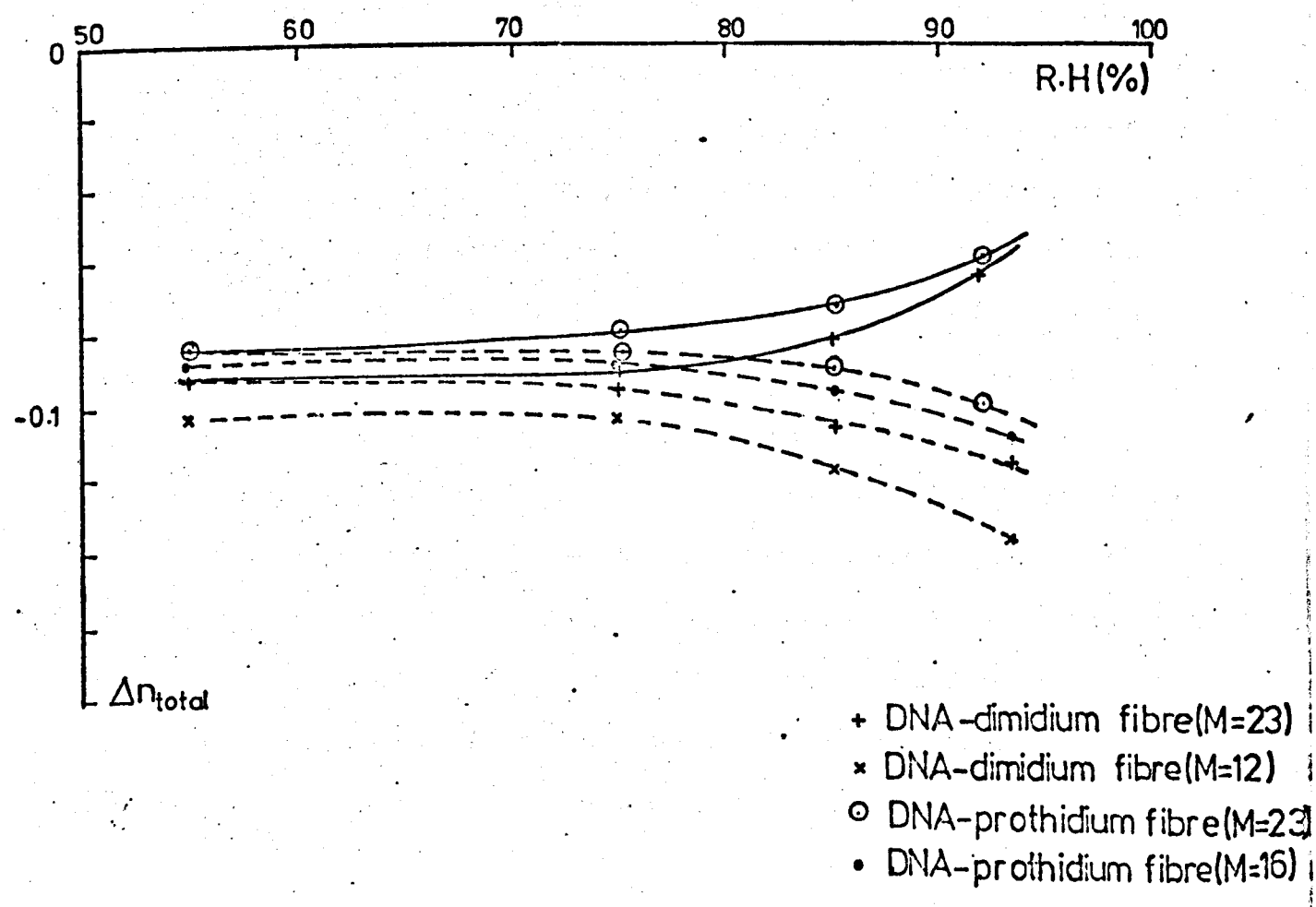

(ii) The birefringence of typical DNA-dimidium and DNA-prothidium fibres as a function of relative humidity

consequent reduction in the measured birefringence. Unless this effect is considered explicitly it will obscure all other trends. In any case, it makes the birefringence results rather difficult to interpret quantitatively.

In general, the swelling of a fibre is a macroscopic consequence of an increased separation of the oriented DNA helices and a swelling of the amorphous regions in the fibre due to uptake of water. Falk et al. (1963) have shown that water is adsorbed initially by the strongly hydrophilic PO_2 groups and then by the P-O-C and C-O-C oxygens as the humidity is increased to around 65% R.H. At this humidity, about six water molecules are adsorbed per nucleotide. The carbonyl groups and ring nitrogen atoms of the bases become hydrated above 65% R.H. At these humidities the helices are generally in the A-conformation. X-ray measurements show that the crystal packing parameters of the A-form do not change with relative humidity. The very small observed swelling of a fibre in this humidity range confirms this, and is probably a result of the expansion of the amorphous regions between the crystallites. At around 75%-80% R.H. the molecules hydrating the carbonyl groups and ring nitrogens fill the grooves of the DNA helix, which has by now completed the transition to the B-conformation. At about 80% R.H., all exposed hydration sites are probably filled and a further increase in the humidity causes the helices to move apart, resulting in the large observed increase in the dimensions of the fibre. X-ray diffraction measurements (Section 5.5.1) confirm the increase in intermolecular separation at these humidities.

In order to interpret the changes in the observed birefringence with humidity, due allowance would need to be made for these complicated changes. The birefringence itself depends in a complex manner on the amount of water in the system, even if changes in the DNA conformation and disorientation were not considered at this stage. Even in the simplified notion of the birefringence being the sum of two terms, the intrinsic and the form

birefringence, it should be noted that the form term does not vary linearly with the fraction of water in a fibre (Equation (6.24)), so that 'normalising' the observed birefringence according to the dimensions of the fibre at each humidity is inadequate. In the more realistic treatment (Section 6.4.2) in which the two terms are not separable, 'normalisation' is unnecessary. Nevertheless, the author has normalised his results in order to compare them with previous studies (e.g. Porumb, 1976).

The basic feature of the normalised birefringence is the increased magnitude with increasing humidity. Fig. 7.5 shows that all the fibres exhibit a normalised birefringence which is fairly constant at low humidities, and rises steeply at around 80% R.H. This is a similar trend to that observed with DNA-daunomycin and DNA-adriamycin fibres (Porumb, 1976). The size of the change is much too large to be explained in terms of a reduction in the disorientation of the DNA helices within the fibre. In any case, the results of Chapter 5 indicate a slight increase in disorientation as the humidity increases, which would cause a decrease in the magnitude of the birefringence and not the observed increase. With the proviso that the normalisation is reasonably adequate to describe the hydration effects, the observed (normalised) results are consistent with an A to B transition of the DNA conformation in the fibres at around 80% R.H.. The change in tilt angle from 20° to about 6° (Table 1.1) would result in a significant increase in the birefringence. Porumb (1976) has reported that if the form birefringence were taken as 58% of the intrinsic term, the total birefringence would increase by about 50% as the tilt angle changed from 6° to 20°.

The magnitude of the birefringence is larger for all the DNA-drug fibres than for the control DNA fibres, and it increases with increasing drug content within a fibre (Fig. 7.5). This indicates that a significant proportion of the total birefringence of the DNA-drug fibres is due to the anisotropy of the drugs, bound at a specific angle, adding to the anisotropy

of the base-pairs. If the drugs had been bound at a random orientation they would not contribute to the total birefringence. The birefringence values are lower for prothidium fibres than ethidium and dimidium fibres of the same M value, suggesting either that the prothidium chromophores are less anisotropic or that they bind at a larger angle to the plane perpendicular to the helix axis. Although prothidium contains an additional pyrimidyl moiety, this is unlikely to substantially affect the polarisibilities of the chromophore. Hence it is more likely that the lower observed values of birefringence with prothidium reflect binding at a larger tilt angle than is the case for ethidium and dimidium.

As the relative humidity is raised, the normalised birefringence of all the fibres increases. In the DNA control fibre, this is accounted for by the conformational change from A to B-DNA, which results in a reduction in the tilt of the base-pairs from 20° to 6°. For dimidium and ethidium fibres, the increase in the normalised birefringence over the same humidity range is at least as large as in the control DNA fibre. This suggests that as well as the base-pair tilt being reduced the tilt of the drugs also decreases at high humidity. It is consistent with a proportion of the drug leaving external binding sites and moving into intercalation sites as the humidity is increased. With the prothidium fibres the situation is more difficult to interpret. The bound drugs contribute less to the total birefringence, and the observed increase in birefringence at higher humidities may reflect the change in the tilt of the base-pairs with little, if any, rearrangement of the bound drug molecules.

The problem of normalisation is circumvented if the birefringence is considered as a function of f', the volume fraction defined in Section 6.4.2. Using this approach, the birefringence can be considered as a complete term, not as one comprising intrinsic and form components. In theory, the measured birefringence could be plotted against the volume

fraction and the trends interpreted directly. In practice, with DNA systems the situation is more complicated.

The parameter f' depends on the radius of the DNA helix, considered as a rod, and its intermolecular separation. The latter quantity is fairly readily deduced from X-ray diffraction patterns, but the radius of the helix is more difficult to measure especially from diffuse DNA-drug patterns. The radius of the helices does not change with humidity (although there may be a slight increase at humidities above about 85% R.H. if the hydration shell is included), and can probably be taken equal to the value for the control DNA at the same humidity for moderate drug loadings. The radius was taken as 9.96Å at low humidities ($\lesssim$ 80% R.H.) and 10.20Å at high humidities. These are the optimised distances of the O2 oxygen of the phosphate group from the helix axis in A-DNA and B-DNA respectively (Arnott and Hukins, 1972). The size of the crystal lattice of A-DNA does not vary with humidity, so that the intermolecular separation, α (and hence f'), will be constant over all the humidities over which the fibres are in a predominantly A-type configuration. In line with this, the measured values of the birefringence are essentially constant for all fibres which give A-type X-ray patterns. Consequently, all the birefringence measurements over a humidity range of 50% to 75% R.H. map on to a single value of f'. The parameter, α, was taken as 23.15Å for A-DNA (i.e. $\frac{1}{2}\sqrt{a^2 + b^2}$ where the lattice parameters are a = 22.24Å and b = 40.62Å (Fuller et al., 1965)). For B-like patterns, α is the intermolecular separation. For the control B-DNA, the values were 25.8Å and 26.4Å at 92% R.H. and 98% R.H. respectively, as measured in Section 5.5.1. For the DNA-drug fibres the intermolecular separation varied with the drug used and the M value of the fibre (Chapter 5). However, the variation was not great and all the DNA and DNA-drug birefringence measurements at high humidity map on to a small range of f' in the Δn_{total} vs. f' plot.

Fig. 7.6 shows the results of plotting the data for a control DNA fibre and a DNA-ethidium fibre (M = 12). The results appear to be consistent with the theoretical plots. The experimental data is confined to small regions in f'-space corresponding to the A and B conformations, and this makes interpretation of the results difficult. In particular, the expected discontinuity due to the A-B transition cannot be identified. It is possible to extend the range if a series of results were taken at 100% R.H., and the fibres were allowed to swell over a period of time. However, this would result in a loss of orientation within the fibre and it would be difficult to arrange for the X-ray diffraction patterns (from which α is measured) to be taken at exactly the same conditions of swelling as the birefringence measurements were taken. In any case, results at 100% R.H. will not help to characterise the discontinuity corresponding to the A-B transition.

The two schemes outlined are both rather unsatisfactory for the treatment of the birefringence data. In the first case, the theoretical simplifications and implicit assumptions are too far-reaching, and in the second case the experimental results are mapped on to two very small portions of the possible data area rendering the trends in the data virtually unrecognisable. However, it has been ascertained that the drugs bind to the DNA in a largely preferential orientation relative to the helix axis. With B-like patterns this orientation is probably close to perpendicular to the helix axis for ethidium and dimidium, because of the large increase in the observed birefringence of these fibres relative to the values for DNA fibres, and because the birefringence continues to increase with increased drug content. There are problems in separating out the relative contributions of the drugs and the base-pairs to the observed birefringence. Nevertheless, the smaller birefringence of the DNA-drug fibres at low humidity, compared with the values at high humidity, suggests that the chromophores are tilted at a considerable angle from the

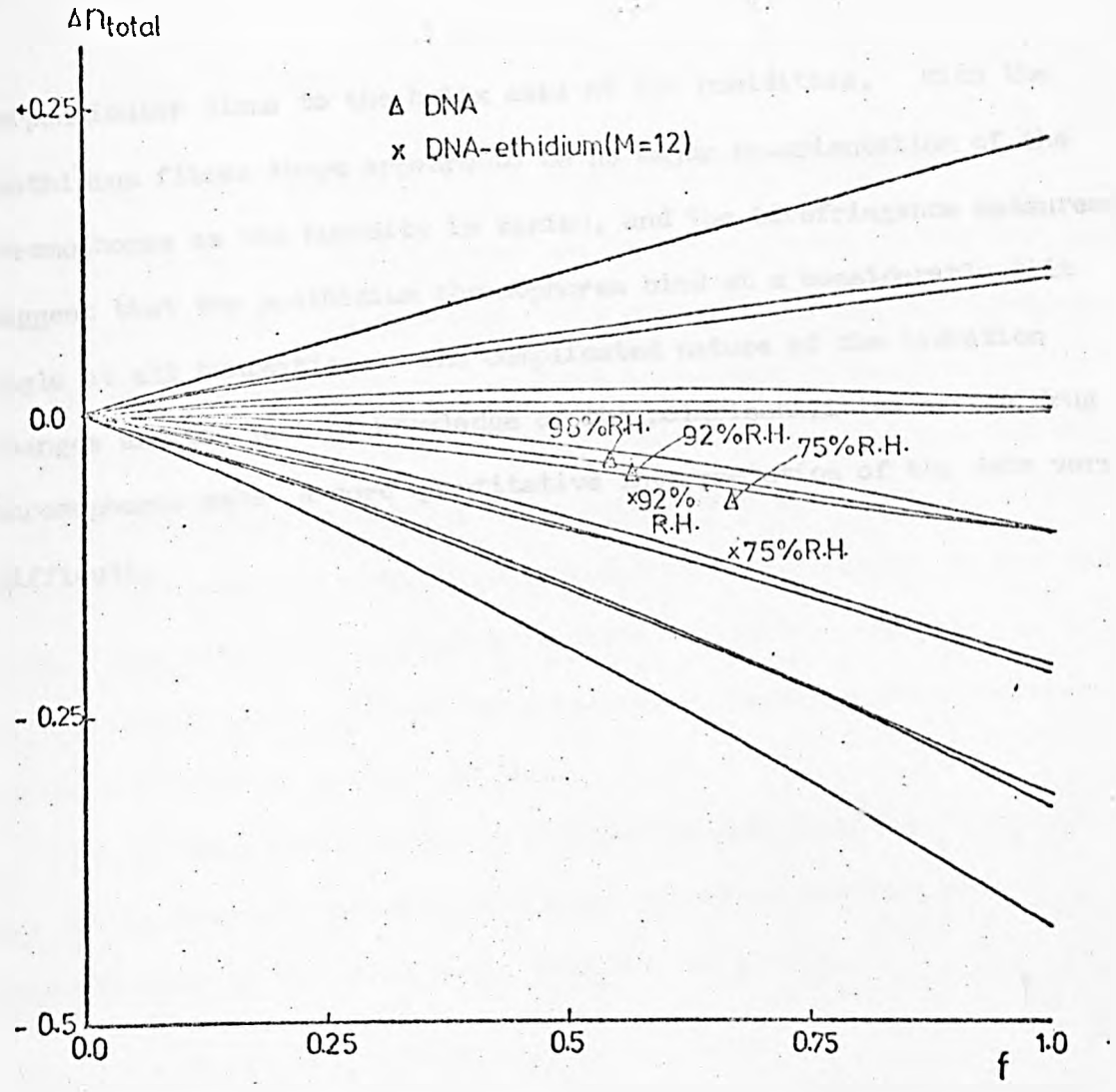

Figure 7.6 Observed birefringence as a function of the volume fraction f. (See Fig. 6.19 for an explanation of the full lines)

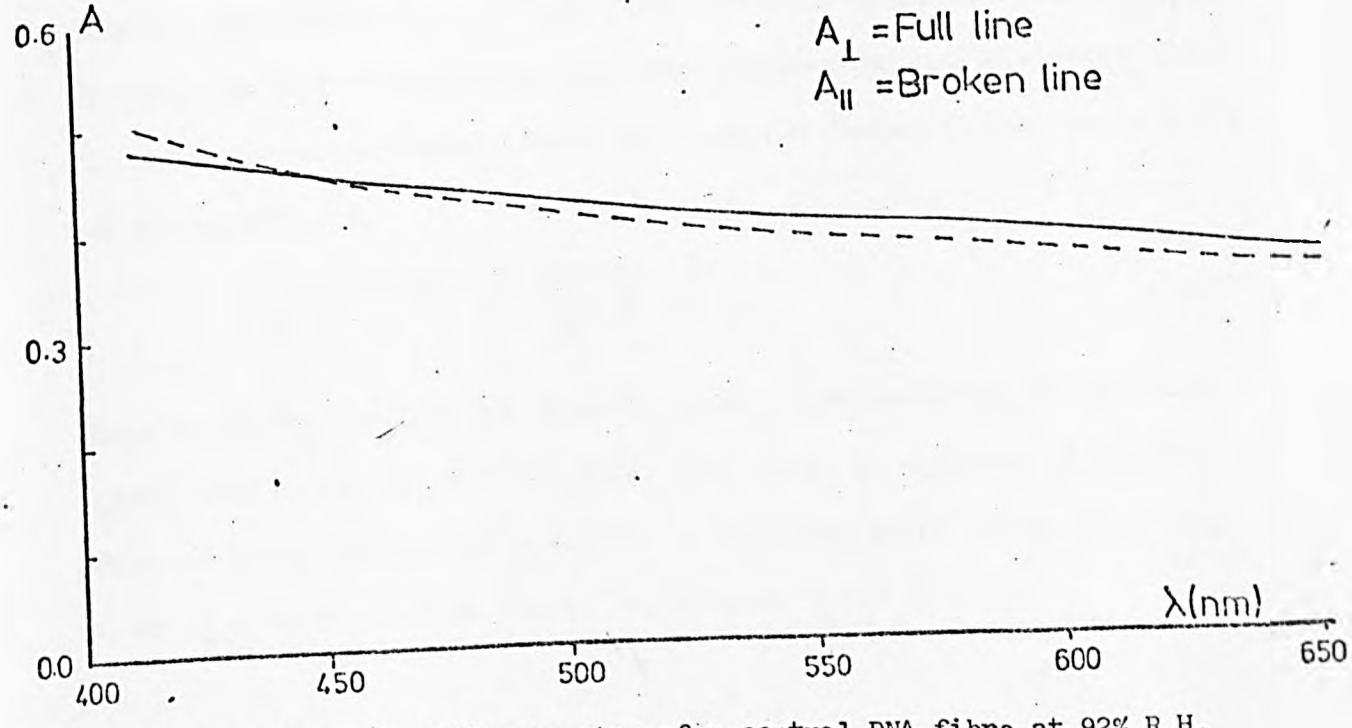

Figure 7.7 The absorption spectra of a control DNA fibre at 92% R.H.

perpendicular plane to the helix axis at low humidities. With the prothidium fibres there appears to be no major re-orientation of the chromophores as the humidity is varied, and the birefringence measurements suggest that the prothidium chromophores bind at a considerable tilt angle at all humidities. The complicated nature of the hydration changes and the lack of knowledge of the polarisabilities of the drug chromophores make a more quantitative interpretation of the data very difficult.

7.4 Linear Dichroism

7.4.1 Theory of Analysis in Terms of Two Bound Drug Species

The theoretical dependence of the linear dichroism on the tilt angle of the drug chromophores has been dealt with extensively in Chapter 6. For the visible absorption bands, light is assumed to be absorbed isotropically in the plane of the chromophore. Equation 6.11 and Fig. 6.13 represent this situation, for a single mode of binding in which the chromophores assume a preferential orientation with respect to the helix axis. The situation in which a fraction of the drug molecules is bound by a different mode, with either a different preferred orientation or a random orientation, is more difficult.

If the drug chromophores in a fibre are oriented, and if $A_{\parallel}$ and $A_{\perp}$ are the absorbances measured with light polarised parallel and perpendicular to the fibre axis, then the expression

$$A = \tfrac{1}{3}(A_{\parallel} + 2A_{\perp}) \qquad (7.6)$$

gives the isotropic value of the absorbance, which would be recorded using unpolarised light. This is also the value that would be recorded, for any direction of polarisation of the light, if the chromophores were randomly disorientated. If there are two bound species, one with the chromophores characterised by a distinct orientation and the other with the chromophores randomly disordered, then the measured dichroic ratio, D, can be expressed as

$$D = \frac{F'(D_A - 1) + (2D_A + 1)}{(2D_A + 1) - 2F'(D_A - 1)} \qquad (7.7)$$

where F' is the fraction of drug molecules bound according to the first scheme, and D_A is the dichroic ratio that would be measured if all the drug molecules bound by this method. This expression may be rearranged so as to give an equation for F' in terms of D and D_A

$$F = \frac{(2D_A + 1)(1 - D)}{(2D + 1)(1 - D_A)} \qquad (7.8)$$

If the chromophore orientation, θ, and the disorientation half-angle of the fibre, δ, are known then D_A can be found from Fig. 6.13. Measurement of the dichroic ratio, D, will then permit the solution of Equation (7.8) to find the fraction of drug bound with a specific orientation.

The situation may arise in which the drugs are distributed between two binding species, each of which is characterised by a distinct orientation to the helix axes. In this case the experimentally observed dichroic ratio, D, is given by

$$D = \frac{F(D_A - D_B) + D_B(2D_A + 1)}{(2D_A + 1) - 2F(D_A - D_B)} \qquad (7.9)$$

where F is the fraction bound in the first species, and D_A, D_B are the dichroic ratios if all the drug belonged to the first and second species respectively. This can be rearranged to give

$$F = \frac{(2D_A + 1)(D - D_B)}{(2D + 1)(D_A - D_B)} \qquad (7.10)$$

Equations (7.9) and (7.10) reduce to Equations (7.7) and (7.8) respectively, if the second species is randomly orientated, by setting $D_{ext} = 1$. In principle, one may write a relation of the type (7.10) for the fraction bound by scheme A at any relative humidity. In particular it can be applied at the lowest and highest relative humidities measured, viz. 55% and 92% respectively in this study. In general, there would be too many unknowns to solve for F' uniquely at both humidities. However, in a particular case, the results from using other techniques (such as X-ray diffraction) may provide sufficient data to solve the equations, especially if the data indicates simplifications that can be applied to the binding model.

7.4.2 Experimental Results

The spectra recorded from a control DNA fibre are shown in Fig. 7.7. DNA has no absorption band in this wavelength range and the recorded absorbance of about 0.4 OD units is the combined result of the cylindrical lens effect of the fibre (Section 7.2) and of light scattering by the specimen, particularly by salt crystallites and impurities present in the fibre. The measured absorbance depended on the thickness of the fibre but was always between 0.3 and 0.4 OD units at 650nm for the size of fibres normally used. These effects are also present presumably in the absorption spectra of the DNA-drug fibres, and allowance should be made for them in order to obtain absorbance values specific to the DNA-drug interaction. A correction for the vertical translation of the baseline was performed by subtracting the measured value of the absorbance at a wavelength where the drugs do not absorb (viz. 650nm) as suggested by Fraser (1953). The dichroic ratio should be constant over those wavelengths where absorbance arises from a single transition (Ding et al., 1972). The measured dichroic ratios were always constant to within ± 5% over the spectral range if a horizontal rather than an inclined baseline correction was used, so that the error introduced by using this method was not serious. In any case, a correction scheme which was a function of wavelength (to allow for differential scattering) could only be estimated and probably would be different for each fibre.

7.4.2.1. Ethidium and Dimidium

Typical absorbance spectra for a DNA-ethidium fibre at low and high humidities are shown in Fig. 7.8. In each case the spectra are similar to those obtained from the complex in solution (Chapter 4). From the positions and relative intensities of the peaks it can be deduced that most of the drug is bound to the DNA in the fibre.

Plots of the log of the intensity against wavelength using the multiwave quartz plate attachment were compared with the values obtained

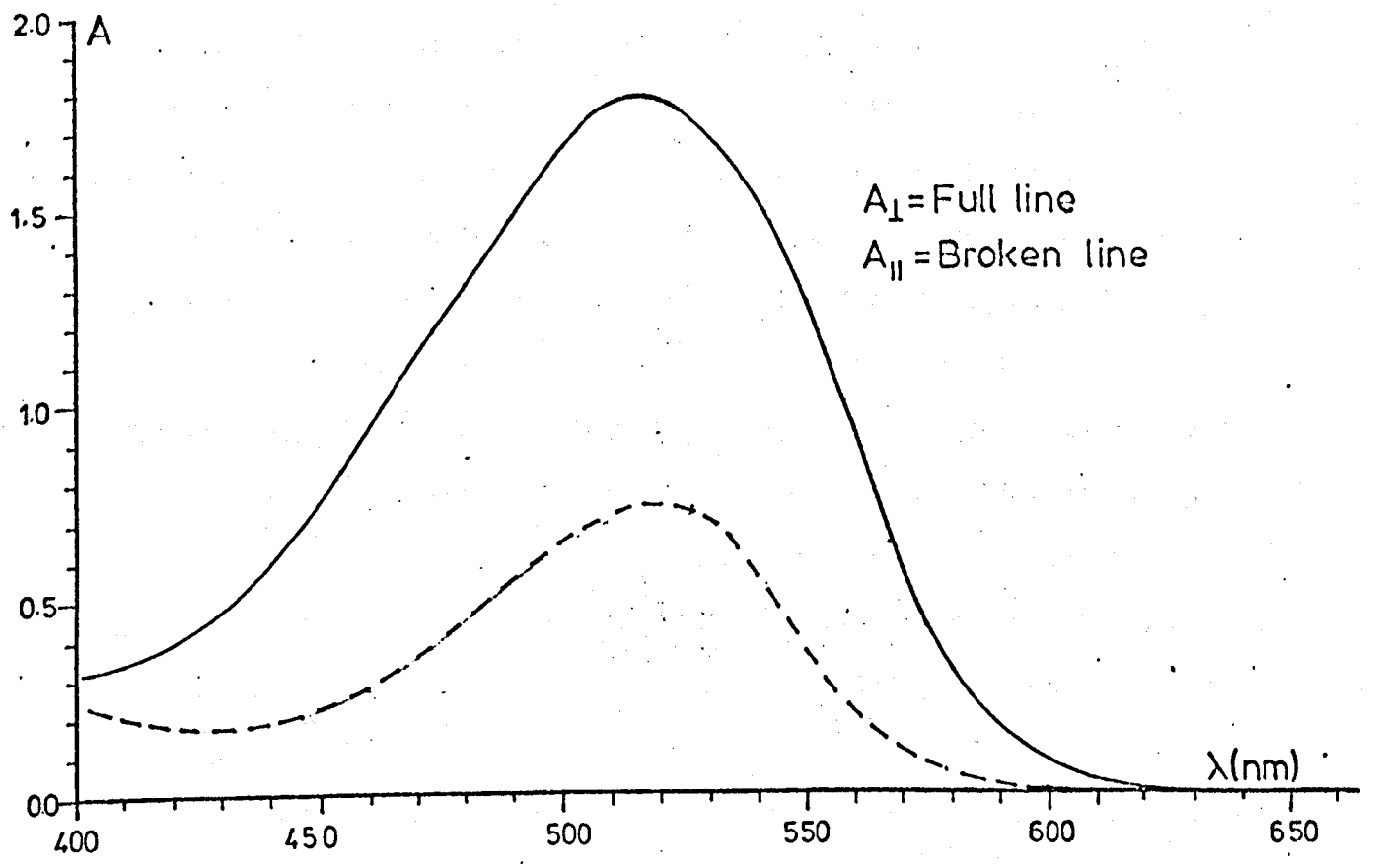

Figure 7.8 (i) The absorption spectra of a DNA-ethidium fibre (M=19) at 92% R.H.

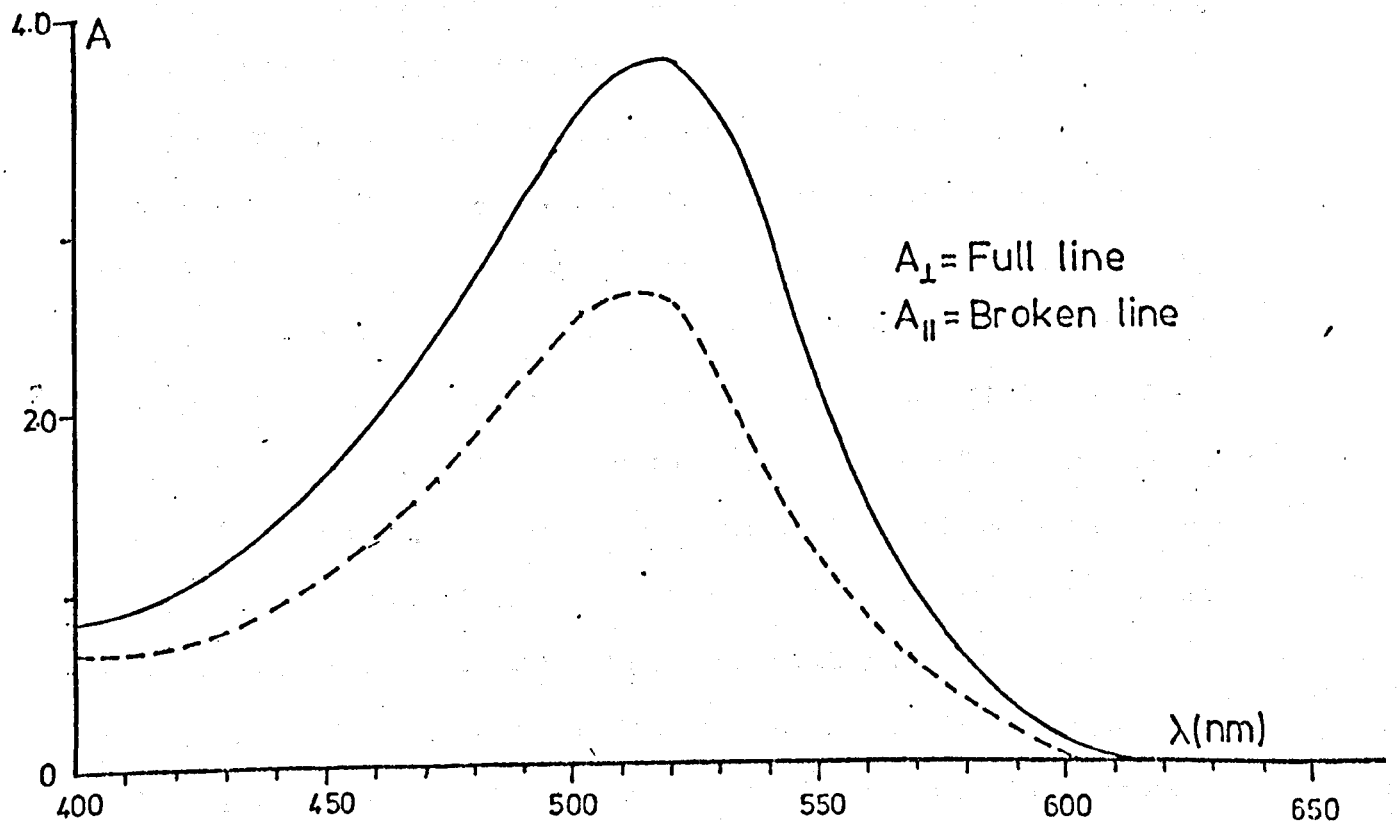

(ii) The absorption spectra of the same fibre at 55% R.H.

using separate spectral runs. The results taken with the quartz plate did not traverse the full intensity range between the separate traces. This may have been due to the time constant of the lock-in amplifier being set at too high a level. Reduction in the time constant results in additional noise being superimposed on the signal at these small signal strengths. Also the spectral band-pass of 2nm, required to obtain sufficient light through the DNA-drug fibres, is probably too large relative to the 5nm wavelength interval over which a complete oscillation occur. The method is likely to be more successful for thinner fibres, though these would not be amenable to X-ray study. For the present study, however, it was decided to take the spectral traces separately, without using the quartz plate.

As the relative humidity is increased the general tendency is that the absorbances decrease, due to the dilution effect caused by the swelling of the fibre. However, the absorbances, $A_{\parallel}$ and $A_{\perp}$, do not vary in the same proportion, presumably because simultaneous with the swelling there is a redistribution of the drug within the fibre. As a result of this, the dichroic ratio for ethidium and dimidium fibres changes with humidity as illustrated in Fig. 7.9 and Table 7.1.

In general, it is estimated that the dichroic ratios were obtained to an accuracy of around $\pm$ 8%. The variability of the results for a particular drug, at a given humidity and M value, can be accounted for by this uncertainty and by the differences in the disorientation half-angle, δ, amongst the fibres. Over the limited M value range that could be measured the dichroic ratio appears to be independent of the proportion of the drug in the fibre. There is no statistical significance to the small difference in the dichroic ratios of the two ethidium fibres (M = 19 and M = 24) presented in Fig. 7.9. An ethidium fibre with M = 24 was measured with a dichroic ratio as high as this M = 19 fibre (Table 7.1). Similarly, the dimidium fibres show no significant change in dichroic

TABLE 7.1

The Dichroic Ratios of some DNA-Drug Fibres as a Function of the Relative Humidity

Relative Humidity (%)	Ethidium				Dimidium			Prothidium		
	M=19		M=24		M=19	M=23		M=23		
55	1.55	1.40	1.30	1.50	1.40	1.40	1.35	1.10	1.00	1.04
65	1.55		1.50						1.02	
75	1.65			1.65	1.60	1.45	1.55	1.09		1.04
85		2.00				1.93				
92	3.08		2.80	3.10	3.00	2.65	2.95	1.00	1.00	1.02
95	3.10	2.90	2.70	3.05	3.05	2.60				

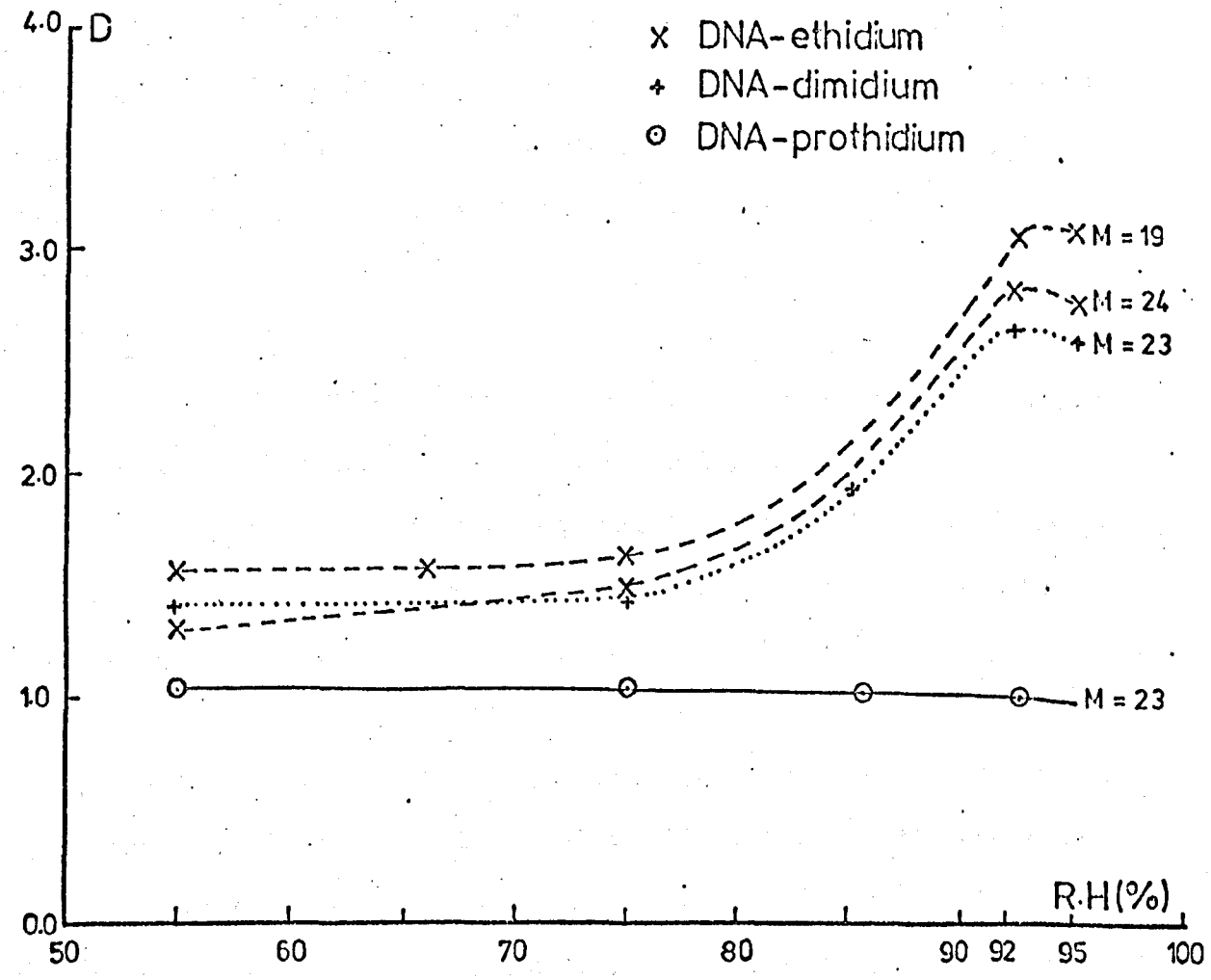

Figure 7.9 Representative traces of the dichroic ratios of DNA-phenanthridine fibres as a function of relative humidity

ratio with drug content. Indeed, the values for all the measured dimidium and ethidium fibres are the same for a particular humidity, within the estimated accuracy of the experimental method.

The problems of normalisation encountered with the birefringence measurements are avoided in this study, because the dichroic ratio, D, is a ratio rather than a difference of two quantities. Swelling corrections affect both the numerator and denominator equally, and therefore the ratio is independent of them. The consequent simplification in the analysis of the results is considerable, and the dichroic ratio measurements are much more amenable to quantitative interpretation than the birefringence measurements.

7.4.2.2 Prothidium

The results from DNA-prothidium fibres are very different (Fig. 7.9 and Table 7.1). The dichroic ratio of several fibres, at the minimum M value that could be measured (M = 23), were taken over the humidity range from 55% to 95% R.H. Fibres with M values less than 23 could not be measured successfully, because the high absorptivity of prothidium resulted in a flattening of the absorbance peaks at low humidities for fibres of 80-100μm in diameter. For all of the measured fibres the dichroic ratio stayed very close to unity, and maintained this value over the complete range. The absorbance spectra are similar to the solution spectra recorded at high M values (Section 4.4.3), suggesting that most of the drug in the fibre is located close to the DNA.

7.4.3 Discussion of the Results

7.4.3.1 Ethidium and Dimidium

The experimental values of the dichroic ratio for DNA-ethidium and DNA-dimidium fibres are greater than unity, indicating that the drug molecules have a preferential orientation in the fibre. In particular, they are consistent with the drug being orientated essentially perpendicular

to the fibre axis as would be the case for intercalation. The dichroic ratios reported here for these drugs are larger than those previously obtained using oriented DNA-acridine films (Neville and Davies, 1966; Kurucsev and Zdysiewicz, 1971), but are generally smaller than those obtained with DNA-anthracycline fibres (Porumb, 1976). Films are generally less well orientated than fibres, and the anthracyclines may bind preferentially perpendicular to the fibre axis at a higher binding fraction, F, than do the phenanthridines.

As previously mentioned, the measurements were limited to fibres with a low proportion of drug ($M \gtrsim 20$). The solution spectroscopy (Chapter 4) and X-ray diffraction results (Chapter 5) indicate that at these M values a high proportion of the bound ethidium or dimidium would be tightly bound to the DNA, and that at high humidities ($\gtrsim$ 80% R.H.) this is likely to be by intercalation. The intercalatively bound drug would assume an orientation similar to that of the base-pairs (viz. about 6^{o} from the plane perpendicular to the helix axis).

The observation that the dichroic ratio, at a particular relative humidity, does not vary with M for large M values suggests that, in these fibres, both ethidium and dimidium distribute themselves between the different binding modes in a constant proportion. The dichroic ratio does not reflect the absolute amount of drug in a fibre at a specific orientation, but rather the fraction of the bound drug assuming this particular orientation. At low M values the proportion of drug intercalated would drop, due to the excluded site effect, and more drug would be free or bound externally, so that the dichroic ratio would be expected to fall.

The fact that the dichroic ratio does not continue to rise at humidities greater than 92% R.H. confirms the conviction that no further intercalation takes place after 92% R.H. is reached. All of the drug cannot be intercalated at these humidities since the theory would predict

a dichroic ratio of about 11.6 in this case, for a drug tilt of 6° and a disorientation half-angle of about 7° to 9°. The small drop in the dichroic ratio above 92% R.H. recorded with some of the fibres correlates well with the increase in disorientation measured from the X-ray diffraction patterns at these high humidities. It is unlikely that the drop reflects any of the drug slipping out of the intercalation sites since the hydrophobic drive towards intercalation is expected to be even stronger at these high humidities.

The drop in the value of the dichroic ratio, for both ethidium and dimidium, as the relative humidity is reduced below 92% indicates a change in the distribution of the bound drug between the intercalated and externally-bound sites. The reduction implies that a proportion of the intercalated drug slips out of its site and becomes free or externally bound. The retention of the absorbance maximum at around 520nm indicates that all of the drug is maintained close to the DNA, and probably remains bound to it. Some care needs to be taken when comparing these spectra with the solution spectra of Chapter 4. In the latter case a maximum absorbance of 520nm was considered as proof that no free drug was present in a complex. In the case of a fibre it cannot be regarded as presumptive evidence since, in a fibre, all the drug molecules are likely to be constrained close to the DNA, and hence absorb at 520nm, whether they are bound to the DNA or not.

By the time 55% R.H. is reached all the DNA-drug fibres exhibit an A-type diffraction pattern and this would preclude any appreciable intercalation. The observation that the dichroic ratio remains greater than unity at this humidity indicates that all the externally bound molecules cannot be bound in a random orientation. If all the externally bound drug is considered to be bound according to a particular scheme, then the value of 1.4 ± 0.2 for the dichroic ratio at this humidity can be interpreted in a number of ways.

The molecules may be assumed to be loosely attached to the exterior of the DNA helices, with a mean orientation approximately perpendicular to the helix axes. The disorientation parameter corresponding to the measured dichroic ratio would then reflect both the disorientation of the helices in the fibre and the additional orientational freedom enjoyed by the externally bound drug. For this situation, Fig. 6.13 indicates a disorientation half-angle of around $45^{\circ} \pm 5^{\circ}$. This includes a value of about $5^{\circ} - 9^{\circ}$ for the disorientation of the helices, so that the drug molecules would be envisaged as "wobbling" over a half-angle of about $36^{\circ} - 40^{\circ}$. Although the external binding mode is largely ionic (Chapters 4 and 5), the charge on the dimidium and ethidium chromophores is delocalised. Therefore, binding is not directional and a "wobble" of this magnitude may be reasonable.

An alternative explanation of the measured values of the dichroic ratio is that the drugs are bound rigidly to the helix, such that their disorientation is the same as that of the helices, and their chromophores are oriented at a considerable angle to the plane perpendicular to the helix axes. Fig. 6.13 indicates that for a dichroic ratio of 1.4 ± 0.2 this angle would be $48^{\circ} \pm 3^{\circ}$ for an isotropic transition dipole moment. (Fig. 6.14 indicates that, for the case where the transition dipole moment direction is known, the dipole would be tilted at $31^{\circ} \pm 2^{\circ}$ from perpendicularity). This angle is somewhat larger than the angle of ascent of the DNA helices (approximately 27° for A-DNA, and 32° for B-DNA), but even if the externally bound dimidium and ethidium were envisaged as being attached to a sugar-phosphate chain, this does not preclude orientations of the chromophore larger than the angle of the chain. The experimental values could also be accounted for by an intermediate situation in which there is some "wobble" of the drug molecules, and they are bound at a tilt angle, θ, less than 48°.

As the humidity is increased to 92% R.H. the measured dichroic ratio rises to around 2.9 ± 0.25 indicating a substantial re-orientation of the

drug chromophores. A fraction, F, of the bound drugs can be considered as leaving the external binding site, and moving to an intercalation site. In this position the molecules are bound rigidly with a tilt, θ, of about 6° and a disorientation half-angle, δ, equal to that of the helices themselves, viz. $5^{\circ} - 9^{\circ}$. If all the drug was bound intercalatively the dichroic ratio would be 11.6 (from Fig. 6.13), and if it is all bound externally (as is proposed to be the situation at 55% R.H.) the dichroic ratio is 1.4 ± 0.2. Equation (7.10) may be applied to a DNA-ethidium fibre at 92% R.H. With the experimentally determined dichroic ratio, D, equal to 2.9 ± 0.25, and values of 11.6 and 1.4 ± 0.2 for D_A and D_B respectively, the expression predicts that the fraction of ethidium intercalated at this humidity is 0.52 ± 0.07. The value of F is fairly independent of the value of D_A, so long as it is large in comparison with D_B. It is almost proportional to the difference in the measured dichroic ratios at high (92% R.H.) and low (55% R.H.) humidities, $(D - D_B)$.

The values for DNA-dimidium fibres are very similar to those for DNA-ethidium, and considering the variability within fibres containing the same drug and the uncertainty in determining the dichroic ratios, the value of F, the proportion of dimidium drugs intercalated at 92% R.H., can be taken as being essentially the same as for ethidium i.e. 0.52 ± 0.07. As mentioned earlier this proportion appears to be independent of the drug content for large M values (M = 19-24).

This interpretation of the linear dichroism results can be compared with that for the X-ray diffraction results. Values for the fractions of ethidium and dimidium intercalated at 92% R.H. were calculated from the observed pitch values of the diffraction patterns in Sections 5.5 and 5.6, using Equation (5.9). The values for F depend on the unwinding angle assumed. The minimum unwinding angle consistent with intercalation is 12° (Pigram, 1968). If this figure is taken, a value for F of 0.90 is obtained for both ethidium and dimidium at moderate binding levels (i.e.

$M \simeq 5$). If a larger value for the unwinding is considered, then the value of F will be correspondingly lower. For instance, an unwinding of 26°, proposed in several publications (e.g. Wang, 1974; Pulleyblank and Morgan, 1975; Tsai et al., 1977), results in a value for F of 0.65 - 0.70.

The value of 0.52 ± 0.07 suggested by the linear dichroism studies is in fair agreement with the X-ray diffraction results that have assumed an unwinding of 26° at the intercalation site. This value of F can be used in conjunction with the X-ray results to suggest a value for the unwinding angle. However, the unwinding angle found in this way becomes very sensitive to the value of F, for F values considerably less than unity. For $F = 0.52 \pm 0.7$ the predicted unwinding angle, on the basis of the diffraction results, would be $34° \pm 8°$. This is similar to the revised estimate by Lerman (1964) of the unwinding angle, viz. 36°, though it is higher than the total unwinding of 29° (Tsai et al., 1975) and the unwinding at the intercalation site of 26° (e.g. Wang, 1974; Pulleyblank and Morgan, 1975; Tsai et al., 1977) proposed for ethidium bromide.

The value of F determined from the dichroism studies, and hence the predicted unwinding angle, depends on the accuracy of the dichroic ratio measurements and on the applicability of the theory used to analyse the results. The inaccuracy of the measurements is a consequence of the variability of the fibres, and the assumption of a horizontal base-line (Section 7.4.2), but both factors are considered to be included in the uncertainty estimates of D and D_B. The evaluation of F using the scheme adopted by the author does not depend on an interpretation of the binding at low humidities, although possible binding schemes have been proposed. The only assumption is that the drugs remain positioned in the same way at high humidities, except for a fraction F which slips into intercalation sites. If the drugs which are not intercalated at 92% R.H. substantially change their orientations then this would affect the analysis. In

particular, if these drugs change their positions such as to contribute a smaller amount to the total observed dichroic ratio, D, then the value of F obtained will be systematically lower than the actual fraction of intercalating drugs. If this were the case it would help to account for the difference in the value of F obtained in this chapter and that obtained in Chapter 5, assuming an unwinding angle of 26°.

7.4.3.2 Prothidium

The dichroic ratio of the DNA-prothidium fibres is close to unity over the complete range of relative humidities measured (Fig. 7.9). A value of unity can be interpreted in a number of ways. There could be complete disorder in the orientations of the molecules; or they could all be orientated at an angle of about 55° to the plane perpendicular to the helix axis (Fig. 6.13); or there could be a mixture of these two schemes. Since prothidium is doubly charged a substantial proportion of it is expected to bind strongly to two adjacent phosphate groups of the sugar-phosphate chain and these molecules would not be able to "wobble" appreciably (Chapter 8). An alternative method of binding would be between the two sugar-phosphate chains, but again this would appear to bind the drug rigidly (Chapter 8).

The observed dichroic ratio can best be explained in terms of some of the molecules being randomly oriented, and the remainder being tightly bound. These rigidly bound drugs may be distributed between a number of specific binding schemes, but the overall effect would be that they were equivalent to being all bound at $\theta = 55°$. Some of the drug could be bound along the sugar-phosphate chain, with a range of tilts probably around 40° (the angle of ascent of the helices), and some could be bound across two adjacent sugar phosphate chains, at a tilt angle close to 90°. The small observed values of the dichroic ratio exclude the possibility of any appreciable intercalative binding, in agreement with the X-ray diffraction results of Chapter 5.

There is no evidence of any significant re-orientation of the bound prothidium molecules as the humidity is changed. The dichroic ratio remains essentially constant. The association constant for prothidium binding to DNA is so large (Section 4.4.3) that, once bound, it is probably reluctant to leave its binding site. This can be interpreted in conjunction with the DNA-prothidium diffraction patterns, in which a significant proportion of A-type diffraction was observed for most fibres even at 92% R.H. This suggests that a considerable proportion of the drug may be bound across the two strands in DNA, and these may tend to resist the A to B conformational transition of the DNA as the humidity is increased.

7.5 Summary

The birefringence results are difficult to interpret uniquely. For ethidium and dimidium, they are consistent with a substantial proportion of the drug being bound perpendicular to the helix axis at 92% R.H., and most of it leaving this site to bind at larger tilt angles when the humidity is lowered to 55-75% R.H. For DNA-prothidium fibres of similar M values the birefringence is lower, and is only slightly higher than the DNA values, indicating that the prothidium molecules are oriented in such a way that they contribute little to the birefringence resulting from the anisotropy of the base-pairs. The prothidium molecules could be binding at sites with fairly large tilt angles.

The dichroic ratio measurements have been interpreted assuming that no intercalation is possible at low humidities. For all three drugs, the binding at low humidities is envisaged as being largely electrostatic in character. For ethidium and dimidium, the results can be interpreted as a mixture of fairly rigid binding to the sugar-phosphate backbones (with $\theta \approx 48^{\circ}$) and loose binding perpendicular to the helix axis, with the drug "wobbling" through a half angle of about 38°. The "wobble" would be less if chromophores were bound at an angle intermediate between 6° and 48°. For prothidium, the attachment to the DNA helices would be more rigid. A proportion of the drug may be bound along a sugar-phosphate chain, and some is probably bound between two adjacent chains. In addition, there are probably drugs bound in a random orientation.

As the humidity is raised to around 92% R.H., the dichroic ratio of the ethidium and dimidium fibres increases. The measured values indicate that about $52 \pm 7\%$ of the drug becomes intercalated at 92% RH. Together with the X-ray diffraction results, this suggests an unwinding angle of $34^{\circ} \pm 3^{\circ}$ at each intercalation site. This would be an overestimate of the unwinding if the externally bound drugs were to change their orientation as the

humidity was raised from 55% to 92% R.H., such as to contribute less to the dichroism at high humidity. The prothidium fibres maintain a low dichroic ratio as the humidity is raised to 92% R.H., implying no significant change in the orientation of the bound molecules.

The observation that the dichroic ratios of the DNA-ethidium and DNA-dimidium fibres at 92% R.H. is fairly independent of M, at the large M values used in this study, is an indication that kinking of the DNA is not an important feature of intercalation at these levels of binding. Bending or kinking of DNA alters the symmetry of the helix, thereby changing the spatial averaging of the transition dipole moments. Random distortions of the helix make DNA more isotropic, and would cause the value of the dichroic ratio to fall (Ding et al., 1972). If the dichroic ratios of fibres at a moderate drug loading ($M \sim 5$–15) were measured, the situation could be further resolved. If the drugs remained distributed between the binding schemes in the same proportions for this range of M values, a constant dichroic ratio would be evidence that the helix remains linear and is not kinked at an intercalation site.

Porumb (1976), in a preliminary study, has reported a value (viz. 3.2) for the dichroic ratio of a DNA-ethidium fibre at 92% R.H. similar to the values quoted here. However at low humidities he reported a much larger value (viz. 2.4) than those measured in this work. Since the measurements are taken at high humidities first, and then recorded as the humidity is lowered, it is possible that the fibre had not equilibrated properly to the low humidity conditions in his study. The ionic conditions and/or the degree of orientation in his fibre may have been somewhat different. The difference in the dichroic ratios at low and high humidities is critical in determining the fraction intercalated at high humidity. The much smaller difference suggested by Porumb (1976) results in a much smaller fraction of intercalative binding ($F \lesssim 0.20$) at 92% R.H., which would imply an unreasonably large value for the

unwinding angle.

Theoretically, it is possible to combine the linear dichroism and X-ray diffraction results to predict the unwinding caused by the intercalation of ethidium or dimidium, taking into account the disorientation within the fibres. In practice, however, the results are limited by the difficulty in comparing fibres of the same M value using the two techniques. The dichroic ratio could only be measured at M values greater than or about 20 for fibres that are sufficiently thick for X-ray diffraction, because of the large absorptivities of these drugs and the stray light limit of the microspectrophotometer. However, the pitch of these fibres is close to the pitch of the DNA control fibres, so that the ratio of the pitch of the drug fibres to that of the control cannot be estimated accurately. This would result in a very large uncertainty in the unwinding angle. Pitch values corresponding to M values of say, 5 to 15 can be distinguished much more readily from the pitch of the control DNA, but these fibres are different from those investigated by linear dichroism.

This work has considered the trend in the pitch values obtained by X-ray diffraction over a wide range of M. At low M ($M \lesssim 5$) the values of the pitch appear to saturate, probably due to excluded site effects. At high M($M \lesssim 20$) the values are difficult to distinguish from the control values, but the proportion of drug intercalated has been assumed to be similar to the proportion intercalated in fibres of moderate M value (M = 5–15). The F value from the dichroism measurements can then be used in parallel with fairly precise pitch measurements to obtain a reasonably precise estimate of the unwinding angle. The accuracy of this estimate depends on the validity of assuming that F is the same for a fibre at M = 20 as it is for a fibre of M = 5–15.

CHAPTER 8

CONCLUSIONS AND MODEL-BUILDING STUDIES

8.1 Conclusions from the Experimental Studies

The biological activity of a number of drugs, with a variety of anti-tumour, anti-leukaemia and antimicrobial action, has been shown to be due to their interaction with nucleic acids (e.g. Waring, 1964; Bolron et al., 1969). The main aim of this thesis was to characterise the interaction of three phenanthridine drugs with DNA, by combining information obtained from spectroscopy and equilibrium dialysis of the complexes in solution with results obtained from X-ray diffraction, birefringence and spectroscopic (including linear dichroism) studies of oriented fibre specimens of the same complexes. Some techniques such as visible spectroscopy are particularly convenient to apply to DNA-drug solutions, although this is hardly comparable with the physiological state; other valuable techniques such as high angle X-ray diffraction must be applied to semi-solid specimens such as fibres, in which the concentrations of DNA, ions and water are probably comparable to those in the chromosomal material of living cells. A major element of this study proved to be the development and/or detailed evaluation of a number of analytical techniques which can be applied to many DNA-ligand systems.

Ethidium bromide has been studied previously by a number of investigators (e.g. Waring, 1965; Le Pecq and Paoletti, 1967; Plumbridge and Brown, 1977), but this work has extended these studies in several areas. A detailed comparison of the binding to DNA of ethidium and the two related drugs, dimidium and prothidium, allows their properties to be related in some detail to the general features and specific differences in their structures. The results of this work have been related to detailed models of the binding of the individual drugs (Section 8.2.2), and it is hoped that this approach may contribute to the development of new, more specific chemotherapeutic

agents with reduced toxic side effects.

A detailed study of the binding parameters in solution was carried out for the three drugs, binding to various natural DNA samples of varying G-C content. The solution spectra of the complexes were taken for a large number of binding ratios using a novel mixing scheme developed by the author. The current work has obtained good isosbestism in the spectra of DNA-ethidium and DNA-dimidium complexes at low and high ionic concentrations, and fairly good isosbestism for DNA-prothidium complexes at high ionic concentrations. This indicates the existence of only one spectroscopically distinct binding mode in these instances. If more than one binding species exist, they must all involve binding close to the DNA base-pairs so that the effects on the drug spectra are similar.

The binding has been analysed according to the theory for the excluded-site model proposed by McGhee and Von Hippel (1974), using a computer program written by the author. In general, this theory provided a good fit to the experimental data, which lends credence to the applicability of this treatment. The data, presented in the form of Scatchard plots, is non-linear and cannot be treated realistically by the previously employed analysis (used by Waring (1965), Paoletti and Le Pecq (1967), and Plumbridge and Brown (1977)), which assumed no occlusion of neighbouring sites by a bound drug. Supplementary data from equilibrium dialysis measurements confirmed the results from the solution spectroscopy studies, although the dialysis data was not so precise and was not used in the curve-fitting program to find the binding parameters.

Values for the association constants and the binding site sizes have been obtained for each drug. For both ethidium and dimidium, the association constants are lower at high ionic concentration and the binding site size is increased at high ionic strength. This is accounted for by an ionic character to the binding. At higher ionic concentration the charged drug chromophores are in competition with a larger proportion of sodium cations, from the buffer, for attachment to the negatively charged

phosphate sites on the helix. The phosphate anions will be screened to a larger extent and this will inhibit drug binding. Fewer sites will be available for binding the drug, resulting in a large value for the apparent binding site size. Dimidium is bound less tightly than ethidium, and exhibits a slightly smaller binding site size. For prothidium, the association constant is much higher, rendering its determination more difficult. The value probably reflects the doubly-charged nature of the drug, and the multiplicity of possible binding sites (Section 2.2.3). Indeed, the binding curves suggest that at least two binding modes (with similar spectra but different binding parameters) are operating. These effects have contributed to an absence of isosbestism in the DNA-prothidium spectra at low ionic concentration, and these spectra were not analysed quantitatively. For clinical applications, drugs with very large affinities for DNA may prove to be very useful, provided that they also have some specificity. To this end, an ethidium bromide dimer has been synthesised and it exhibits a binding affinity for DNA about three orders of magnitude larger than that for the monomer (Gaugain et al., 1978).

Previous spectroscopic studies (Waring, 1965; Paoletti and Le Pecq, 1967) were unable to detect any specificity in the binding of ethidium bromide to natural DNA's, but more recent studies (Krugh et al., 1975; Krugh and Reinhardt, 1975; Patel and Canuel, 1976) using dinucleotide and tetranucleotide solutions have reported a binding preference for purine (5' - 3') pyrimidine sequences. The current work has been able to detect a strong G-C specificity in the binding of ethidium bromide to natural DNA polynucleotides. At low ionic concentration, the specificity is more marked and the drug prefers to bind to a sequence of two G-C pairs, although the precise nature of this sequence specificity (viz. whether GpC, CpG, GpG or CpC) could not be ascertained. Further studies of this type using synthetic polynucleotides may prove useful in clarifying the specificities operating, but difficulties are anticipated in differentiating between

consequences arising from the presence of different base-pairs and those arising from the conformational differences believed to occur with synthetic polynucleotides (Bram, 1972; Bram and Tougard, 1972; Bram, 1973). Nevertheless, detection of a specificity for ethidium binding to natural DNA's represents a significant advance on previous studies.

The binding of dimidium to DNA is less specific. At low ionic concentrations, it shows a preference for G-C pairs but at high concentration the specificity is only very slight. The specificity shown by both these drugs is not considered an absolute preference, but rather a relative preference, for G-C base-pairs. The level of binding at saturation is too high to be accounted for by binding to G-C base-pairs alone. It seems likely that dimidium binds more readily to A-T base-pairs than does ethidium, and this would explain the smaller binding site sizes obtained for dimidium. Its binding is able to continue to a higher level because it is not limited to such an extent by the absence of G-C pairs. For both drugs, the binding site size reflects a situation close to nearest-neighbour exclusion.

The results for prothidium binding to different DNA types are very different. Both the association constant and the binding site size are constant with varying G-C content, indicating that there is no specificity in the binding for a particular base-pair. The initial binding saturates at about $r = 0.5$ (viz. one bound drug for every two base-pairs) but then continues, presumably by a different mode, to larger levels. Since prothidium is a larger molecule than either ethidium or dimidium, this suggests that the binding modes operating with prothidium are different to the primary binding mode for ethidium and dimidium. In particular, if these latter two drugs are binding primarily by intercalation it suggests that prothidium may not bind intercalatively. In any case, the pyrimidyl moiety of prothidium would be expected to discourage the intercalation of prothidium because of possible steric hindrance (Section 8.2.2.3).

Previous X-ray investigations of the intercalation process (Neville

and Davies, 1966; Pigram, 1968; Porumb, 1976) have been extended or supplemented by considering the helix parameters of the complexes at a number of DNA/drug ratios and at different relative humidities. The DNA pitch rises markedly with increasing drug content to an asymptotic value of around 47Å for ethidium fibres, and 49Å for dimidium fibres. These asymptotes can be accounted for by a saturation of the binding due to neighbour exclusion effects, and the larger value for dimidium correlates well with the lower values for the binding site size of this drug obtained in the solution studies. The pitch increases can be more readily explained in terms of intercalative rather than external binding. At humidities less than about 80% R.H., the diffraction patterns revert to an A-type intensity distribution suggesting that all of the intercalated drug molecules have moved out of these binding sites, to become either free or externally bound. For prothidium, there is no measurable change in pitch relative to the control DNA fibres, at any humidity or drug concentration. This excludes intercalation as a major binding scheme, in agreement with the indications of the solution spectroscopy study.

It has been recognised (Neville and Davies, 1966; Pigram, 1968; Porumb, 1976) that the relative humidity of the fibre environment greatly affects the balance between intercalated and non-intercalated drug in the fibre. In particular, it has been suggested that at, say, 92% R.H. all the bound drug may not be intercalated. Due to a lack of knowledge of the fraction of drug intercalated, it is not possible to determine absolutely the unwinding angle of the DNA helix at the intercalation site by X-ray diffraction methods alone. However, if a value for the unwinding angle is assumed, the fraction of drug intercalated may be calculated. For an unwinding of 12° (Fuller and Waring, 1964), the pitch measurements obtained in this study at high humidity suggest that for ethidium 90% of the drug is intercalated at moderate binding levels ($M \approx 5$-15), and this proportion falls to about 67% when saturation is approached. For dimidium, with this

unwinding angle, the proportions are 90% and 76% respectively. If an unwinding angle of 26° is assumed (Wang, 1974; Pulleyblank and Morgan, 1975; Tsai et al., 1977), then about 68% of the ethidium would need to be intercalated at moderate binding levels, and 49% close to saturation. For dimidium the values would be 68% and 55% respectively.

The spectra of DNA-drug complexes can be recorded easily in solution to yield the fractions of free and bound drug, the very evidence which is required for the interpretation of the X-ray diffraction results on the fibre. Therefore, in parallel with the X-ray diffraction studies, the birefringence and linear dichroism of fibres were measured using a single-beam microspectrophotometer. Unfortunately, only the spectra and dichroic ratios of fibres of relatively low drug content ($M \gtrsim 20$) could be measured directly, for fibres of sufficient thickness ($\gtrsim 80\mu m$) to be suitable for X-ray diffraction. At smaller M values, the large absorptivities of the phenanthridines gave rise to absorbances greater than the stray light limit of the equipment. Scattering of light by the fibres resulted in a shifting of the baseline absorbance levels, but consistent results were obtained if corrections were applied by referring the baseline to a region where the drugs do not absorb viz. 650nm. The absorption spectra of the fibres were similar to the spectra of the corresponding DNA-drug complexes in solution where all the drug is bound. Thus, it appears that in the fibre state all of the drug is located close to DNA, and most of it is probably bound to DNA at all humidities between 55% and 95% R.H.

The theory of the birefringence and linear dichroism of fibres (such as those of DNA-drug complexes) has been developed in depth. The disorientation of the DNA helices has been considered explicitly in the analysis, by adopting a model in which the helices are considered to be oriented about the fibre axis according to a gaussian distribution function. Numerical solutions to the analyses have been presented.

There are difficulties in the interpretation of the birefringence

results because of a lack of knowledge on the polarisabilities of the drug chromophores, and because of the swelling of the fibres with increased hydration. Nevertheless, the results are consistent with a large proportion of the ethidium and dimidium chromophores being roughly perpendicular to the helix axis at high humidities, and this proportion being much less at low humidities. For prothidium, the chromophores would appear to be attached at a considerable angle to the plane perpendicular to the helix axis, and there is probably little reorganisation of the binding as the humidity is changed.

The dichroic ratio monitors the effect of all the drug molecules, whereas X-ray diffraction primarily reflects only the effect of specifically oriented molecules such as intercalated drugs. The linear dichroism results are easier to interpret than those for birefringence, since the DNA contributes no appreciable absorption to the fibre in the visible region of the spectrum. Values of the disorientation of the helices within a fibre are obtained from the arcing of the diffraction spots and are used in this analysis.

For ethidium and dimidium the dichroic ratio is low (1.4 ± 0.2) at low humidities (55 - 75% R.H.). The diffraction results have indicated no intercalation at these humidities, and the fibre absorption spectra indicate that probably all of the drug is bound. Some of the drug must be bound at specific orientations in order to give an observed dichroic ratio greater than unity, but the general ionic association of the drug to the DNA is unlikely to result in well-defined orientations. The binding is probably a combination of binding at random orientations with binding at preferred orientations. This latter group could include drug molecules almost perpendicular to the helix axis with a "wobble" of about 38° and molecules rigidly bound to the helix with a tilt angle of about 48°, but it is more likely to comprise molecules bound with parameters intermediate between these two extremes.

At 92% R.H. the dichroic ratio of the ethidium and dimidium fibres is larger (2.90 $\pm$ 0.25), and this can be identified with a substantial fraction of the drug becoming intercalated at this humidity with a tilt angle of about 6°. If it is assumed that the externally bound drugs retain the same distribution of orientations as they had at 55% R.H., then the results indicate that 52 $\pm$ 7% of the drugs are intercalated at 92% R.H.. The fraction intercalated appears to be constant with M, for large M values (M = 19-24) well away from nearest-neighbour exclusion effects. Ionic conditions within the fibre are expected to be an important factor in determining the balance between intercalated and externally bound drugs, since they will affect the association constants for the binding.

For prothidium fibres, the dichroic ratio is close to unity over the relative humidity range measured. This indicates that there is probably no substantial reorganisation of the bound drug molecules as the humidity is varied. A value close to unity suggests that a large proportion of the drug is probably bound with random orientations. Any molecules bound with a specific orientation must have an average tilt, θ, close to 55°, to maintain a dichroic ratio close to unity. This could result from some of these molecules being bound along a sugar-phosphate chain ($\theta \tilde{\sim} 40^{\circ}$) and some being bound between two adjacent chains ($\theta \tilde{\sim} 90^{\circ}$). In both instances the binding is likely to be fairly rigid, and no appreciable "wobble" is envisaged. The possible binding schemes consistent with the experimental results are discussed in detail in Section 8.2.2.

Unfortunately, the results from the linear dichroism and the X-ray diffraction studies cannot be strictly compared. The fibres used in the dichroism studies must have a small drug concentration, and the measured values of the pitch of these fibres are almost indistinguishable from the value for the control DNA fibres. This would be expected at these M levels, even for complete intercalation. However, if it is assumed that the same proportion of drugs is intercalated in fibres of moderate drug

content ($M \gtrsim 5$–15) as in those of low drug content ($M \gtrsim 20$), and that the externally bound drugs maintain a similar distribution of orientations at low and high humidities, then the results of the two studies may be combined to give some estimate of the unwinding angle. With these assumptions, the estimated unwinding at an intercalation site by either ethidium or dimidium is $34 \pm 8^{\circ}$. This cannot be regarded as an empirical determination of the unwinding angle, because of the simplifications assumed, but merely an estimate consistent with the results from both the X-ray and linear dichroism studies. The substantial uncertainty in this estimated value is mainly due to variability in the fibres leading to a range in the measured dichroic ratios. It is not accounted for by the different disorientations of the individual fibres. The estimated value is somewhat higher than the 26° unwinding proposed by Wang (1974) and others, but it is closer to this finding than to the earlier estimate of 12° suggested by Fuller and Waring (1964).

8.2 Model Building Studies

8.2.1 A Review of Previously Proposed Models

For a variety of drugs, their method of binding to DNA has long been envisaged as intercalation. Such an interaction was first proposed on the basis of X-ray diffraction, flow birefringence and low-angle X-ray scattering of DNA-proflavine complexes (Lerman, 1961). Lerman showed that the DNA would have to unwind at an intercalation site, and built a model with an unwinding of 45°. Later he revised this value to 36° (Lerman, 1964), but it should be emphasised that these were examples of possible models, not the best possible models resulting from extensive model-building studies. Since that time an accumulation of evidence, using many different physical techniques, has supported this binding scheme (see Section 1.2 for references), and intercalation is now accepted as the primary binding mode in the interaction with DNA of many drugs containing fused aromatic rings.

Fuller and Waring (1964) suggested that intercalated ethidium lies across and between successive base-pairs, with the phenyl and ethyl groups lying in the large groove of the DNA. Such a position allows the formation of hydrogen bonds between the 3- and 8-amino groups of the ethidium cation (Fig. 1.8) and phosphate groups on the two strands of DNA. The steric hindrance between the DNA and the phenyl and ethyl groups determines to a large extent the precise position of the intercalated chromophore. The complex is stabilised by the two hydrogen bonds, and by stacking interactions with the base-pairs with which there is good overlap. The aromatic triple ring is hydrophobic and the phenyl substituent is hydrophilic. The drug will be strongly driven towards intercalative binding on energetic grounds, because in this position the triple ring will be in a non-polar environment and the phenyl group will be projecting into an aqueous environment. The amino groups will also form favourable bonds.

On the basis of skeletal model building, Fuller and Waring (1964)

proposed that an unwinding angle of only 12° for each ethidium molecule was sufficient to allow intercalation, and that this small unwinding might be significant kinetically. From a detailed consideration of the DNA stereochemistry, Pigram (1968) concluded that 12° would be the minimum unwinding required for entry of any drug into an intercalation site and that models could be built for unwinding angles larger than this, up to at least 36° and possibly even 45°. More recently there have been a number of papers suggesting that the unwinding angle is significantly larger than this minimum value, and a value of 26° has been proposed for ethidium bromide (e.g. Wang, 1974).

Intercalation of ethidium bromide into the miniature double helix Gp iodoC has been observed at atomic resolution by X-ray crystallography (Jain et al., 1977) and a detailed molecular model has been proposed. These authors have postulated that drug intercalation gives rise to a helical screw axis dislocation in DNA, a variable whose magnitude determines the relative ring overlap between the intercalated drug chromophore and the adjacent base-pairs. For ethidium, the helical axes of B-DNA are estimated to be displaced by approximately 1Å (Sobell et al., 1977). Base-pairs on either side of the intercalation site are twisted by 10°, giving rise to an unwinding of 26° by the intercalated ethidium. The base-pairs are tilted relative to one another by about 8°, resulting in a "kink" at the intercalation site (Tsai et al., 1977; Jain et al., 1977). The large unwinding angle reflects the conformational changes in the sugar-phosphate chains accompanying intercalation. These primarily reflect the difference in sugar puckering about the intercalation site, C2' endo (5' - 3') C3' endo, rather than the C2' endo puckering assumed by Fuller and Waring (1964) for all the nucleotides, and alterations in the glycosidic torsional angles that describe the base-sugar conformation. Berman et al. (1978) have suggested that the unwinding angle can be directly related to the size of the intercalating drug, and they have reported that proflavine, which lacks the bulky ethyl and phenyl substituents, may intercalate into a dinucleoside

monophosphate with an unwinding angle as low as 3°.

Jain et al. (1977) report that the phenyl and ethyl groups of ethidium are found to lie in the narrow groove of the miniature double helix, exactly opposite to their orientation in the Fuller-Waring model. This difference could reflect the presence of the iodine atoms on the cytosine residues of the miniature double helix which, because of their bulk, may interfere with intercalation from the wide groove. The mixed sugar puckering necessarily predicts that intercalation be limited to every other base-pair at maximal binding ratios (i.e. a neighbour exclusion model), providing an attractive rationale for the observed limits to the binding in solution (Chapter 4) and the limits to the pitch increase in the fibre state (Chapter 5).

However, the details of drug binding to dinucleosides may not be a completely accurate model for drug-nucleic acid polymer associations, since the chemical structures and the environments are somewhat different in the two cases. For example, in the ethidium-dinucleoside complex there is only one phosphodiester link to each sugar, so there need be no consideration of the continuity of the sugar-phosphate chain. The structure of the 9-aminoacridine-dinucleoside complex (Seeman et al., 1975), showing successive bases parallel, but unstacked, and pointing away from each other and hydrogen bonded in a non-Watson-Crick fashion, clearly demonstrates that not every drug-dinucleoside structure may be appropriate for extrapolation to interactions involving polynucleotides. More detailed work on the linear dichroism of the DNA-drug fibres at a variety of M values may be able to indicate whether or not a kinking of the helix occurs at intercalation sites in the DNA polymer (Section 7.5).

Computerised model-building studies of drug-nucleic acid systems (Section 8.2.2) have been used to elucidate the details of the binding to a polynucleotide. These techniques allow best use to be made of the limited experimental data available by incorporating known stereochemical features of the structure into the analysis. Although they may produce

interesting and precise models, they are usually unable to consider all of the energetic aspects of the interactions satisfactorily.

8.2.1.1 The Kinetics of Intercalation

Kinetic studies of the mechanism of drug binding have proposed that intercalation occurs via a multi-step reaction (Li and Crothers, 1969; Sakoda et al., 1971; Schmechel and Crothers, 1971). The drug first attaches externally to the double helix in a fast-order process involving long range electrostatic forces, which is followed by the insertion of the drug between two adjacent base-pairs in a time roughly of the order of one millisecond. This phase will probably involve the effects of the drug perturbing the local dielectric and various more short range dipole interactions (which may account for a base-pair specificity).

The externally bound drug may partly overlap the base-pairs in some instances (Li and Crothers, 1969), which would explain why the two bound forms would have similar absorption spectra and be indistinguishable in equilibrium binding studies (Chapter 4). Even at low binding ratios, an appreciable amount of the drug may be externally bound in solution. Values range from 5% to 30% of the total drug bound for proflavine, and they are possibly even larger at very low salt concentrations not accessible in conventional temperature-jump experiments. Similar values have been suggested for ethidium (Bresloff, 1974). Larger amounts of externally bound drug are presumably present in the fibre state, due to the hydrophobic drive towards intercalation being smaller at lower humidities, and this is consistent with the values predicted in Chapters 5 and 7.

The conformational change in the DNA required if intercalation is to take place may be understood in terms of the natural flexibility of DNA along its helix axis. This allows an accordian-like longitudinal flexing of the DNA molecule. The resulting strain energy in the sugar-phosphate chains can be relieved by a simultaneous altering of the sugar pucker to the

mixed pattern across the dyad axis (Sobell et al., 1977). This results in a kinking of the helix with a consequent partial unstacking of the base-pairs. A conformational change such as this would require minimum stereochemical rearrangement and would also involve small energies. The change could result from normal modes in the DNA that are excited at thermal energies. Once formed, the kink could straighten and base-pairs separate to create the space for drug intercalation. The presence of externally bound drug molecules might further induce this change. The process would be continuous so that the DNA bases would soon overlap with the intercalated drug, and this would provide additional stacking interactions which would stabilise the interaction. The number of kinks present at any given time in a given region of DNA is likely to be a function of the base sequence (and to a lesser extent the base-pair composition), since the unstacking energy of the bases depends on the nature of the bases themselves. This dependence of the number of kinks on the base sequence could provide a rationale for the reported sequence specificity of ethidium (Krugh et al., 1975; Krugh and Reinhardt, 1975).

Kallenbach (1979) has examined the equilibrium and dynamics of transient base-pair breakage by following proton exchange rates using NMR techniques, and has concluded that there are transient open states analogous to Sobell's model of DNA 'breathing'. However, the basis for kinking, alternating sugar puckering about the intercalation site, has been challenged by the results of Berman et al. (1979), who find that for dinucleoside complexes the nature of the sugar pucker is unimportant. Rich (1979) has also examined the crystal structures of several of these model intercalation complexes, and concludes that the sugar puckering in them depends on whether or not the particular drug involved interacts with the phosphate group in the backbone.

8.2.2 Models for DNA-Phenanthridine Complexes

8.2.2.1 Ethidium Bromide

Alden and Arnott (1975) examined models for the intercalation of simple planar chromophores into DNA in search of a general intercalation mechanism compatible with an extended, but unstrained, DNA duplex in which base stacking is considered the principal binding force, and there are no drug-DNA interactions. They found that the most favourable conformation involved the changing of two torsion angles and a mixed sugar puckering (C3' exo (5' - 3') C3' endo) on either side of the intercalation site. The model had a rotation of 90° over three residues about the binding site, so that the total unwinding caused by intercalation was 18° - though this was not localised just to the two base-pairs adjacent to the intercalated drug.

Goodwin (1977) has extended these studies using a linked-atom model building computer program. Fig. 8.1 shows a computer drawn representation of the co-ordinates obtained by him for a general intercalation unit of four base-pairs (without an intercalated chromophore), in which all the sugar puckers are C2' endo and the untwist is 19°. The drawing was produced by a program 'DRAW' written by the author. It was displayed on an Imlac refresh tube, and photographed off the screen for inclusion in this thesis (Section 2.3.5). The hydrogen atoms have not been included in the drawing, although they were considered in the original model-building program. The drawing shows some unacceptably large geometric constraints. In particular, an oxygen atom of the lower phosphate group tends to interfere with the lower sugar ring giving rise to very short Van der Waal's contacts. Goodwin found that untwisting angles of 12° and 28° gave intercalation structures with the least Van der Waal's contact energy, and these were considered superior to structures with intermediate unwinding angles. If a mixed puckering scheme was adopted (either the C3' exo (5' - 3') C3' endo of Alden and Arnott (1975) or the similar C2' endo (5' - 3') C3' endo of

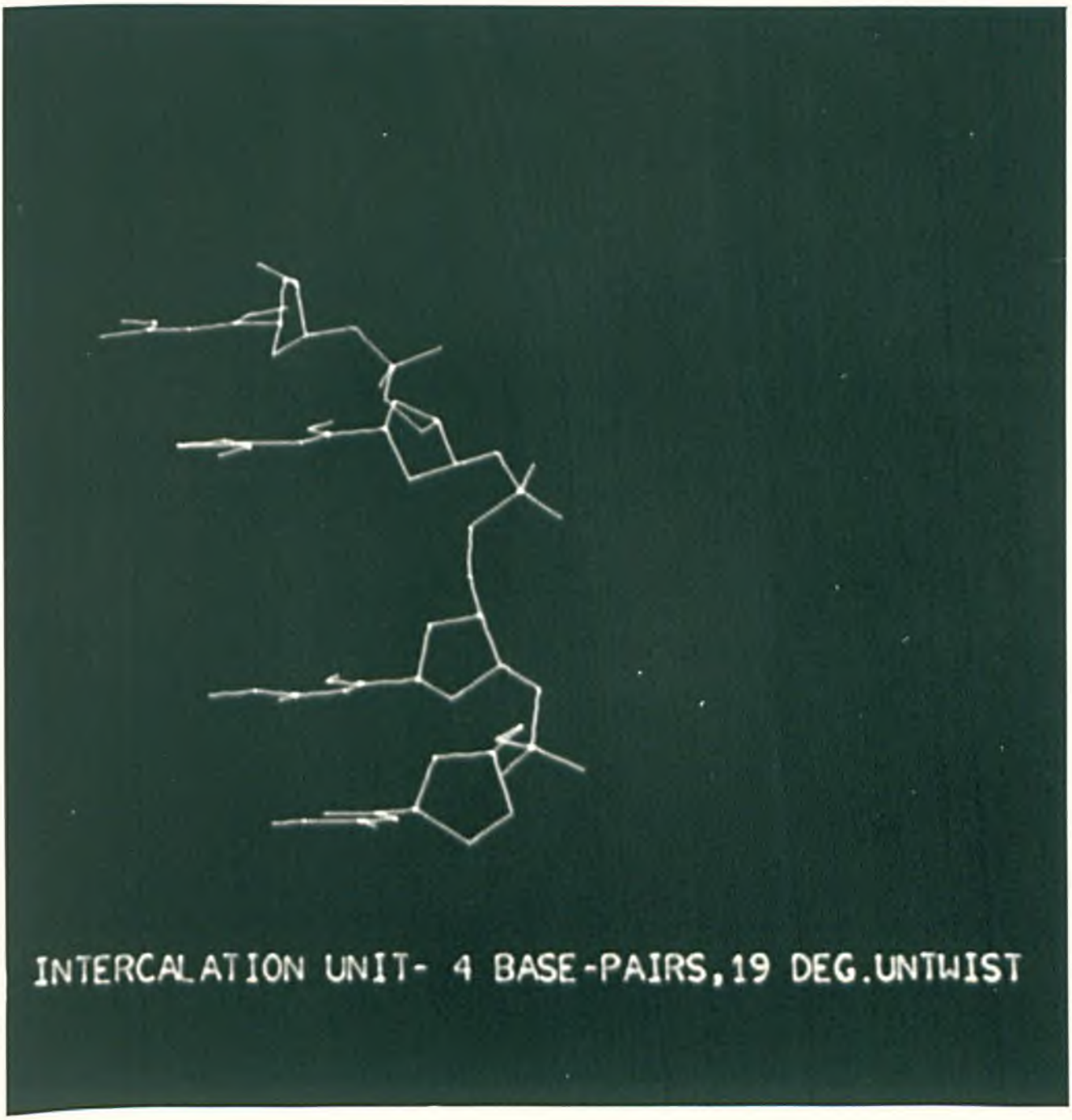

Figure 8.1 Computer-drawn general intercalation unit with an unwinding angle of 19^{o}. Only one sugar-phosphate chain is shown; the other is dyad related. The drug would be intercalated between base-pairs 2 and 3.

Sobell et al. (1975)) then the stereochemically most reasonable conformation was found to be one with an overall unwinding of 28°, incorporating a 26° unwinding at the intercalation site, and this was superior to the intercalation scheme where all the sugar puckers were C2' endo.

Goodwin (1977) also built a number of models incorporating an ethidium bromide molecule in the intercalation site. The previous general intercalation units were used as the starting points. The starting co-ordinates for the ethidium molecule were taken from Subramanian et al, (1971), and the DNA and ethidium conformations were co-refined. If the sugar puckers are all taken as C2' endo the best model energetically was found to be that in which the ethidium unwound the helix by 12°, and the ethyl and phenyl groups projected into the narrow groove of the DNA. However, the relatively close proximity of the two sugar-phosphate chains in this model seems likely to lead to short non-bonded atomic contacts. The difficulty in building a model in which these groups project into the large groove is due to the fact that the two outer rings of the ethidium chromophore approach too closely the atoms of the sugar-phosphate chain, when the ethidium molecule is in a position to achieve good overlap with the base-pairs. It is not possible on the basis of these studies alone to conclude which of these possibilities is the more likely to occur.

In models with all the sugars adopting a C2' endo pucker and with an untwist of 26° at the intercalation site, it is not possible to have hydrogen bonds between the amino groups of ethidium and the phosphate oxygens because these oxygens protrude out from the helix and not into the intercalation gap. A more superior model, stereochemically, can be built based on a mixed sugar pucker intercalation unit with an untwisting angle of 26°. The ethyl and phenyl groups project into the narrow groove of the DNA and the base overlap is good (Fig. 8.2). There are five rather poor non-bonded contacts with this model, but they all involve hydrogen atoms and hence are not apparent in the drawing. There is no kinking of

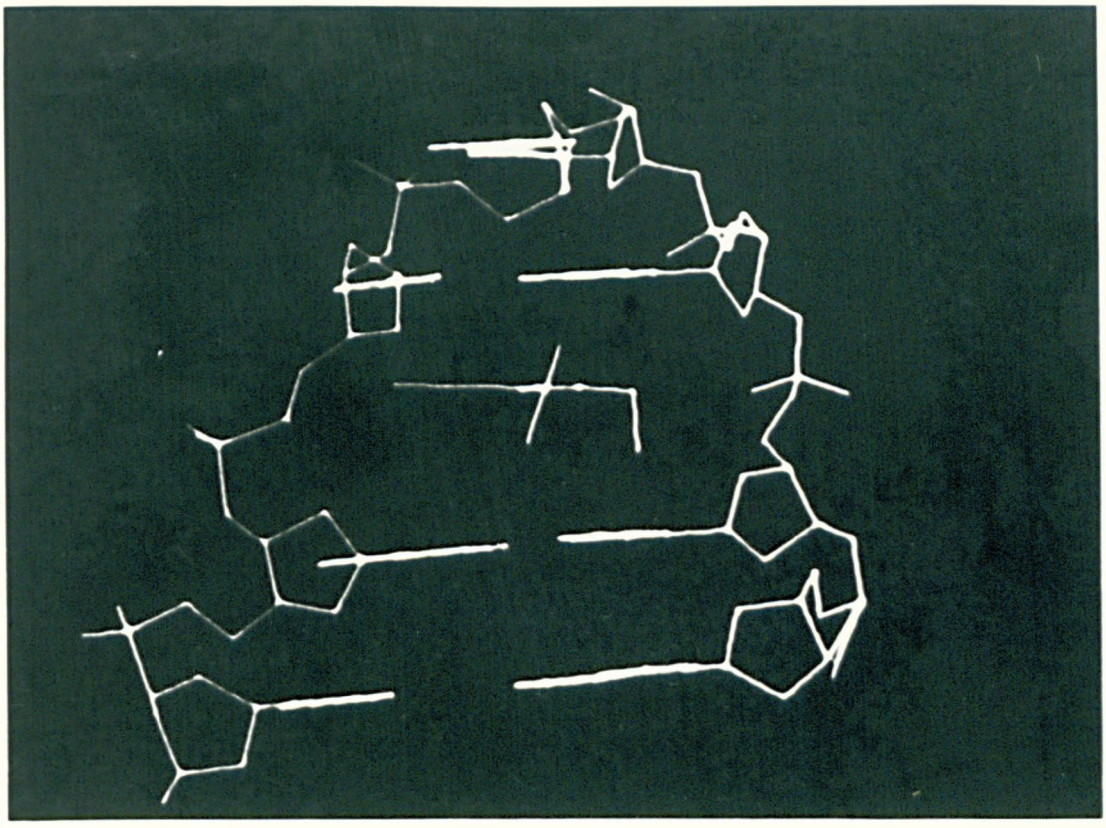

Figure 8.2 (i) Ethidium bromide built into a mixed pucker (C3 exo/C3 endo) intercalation unit, with an unwinding angle of 26°.

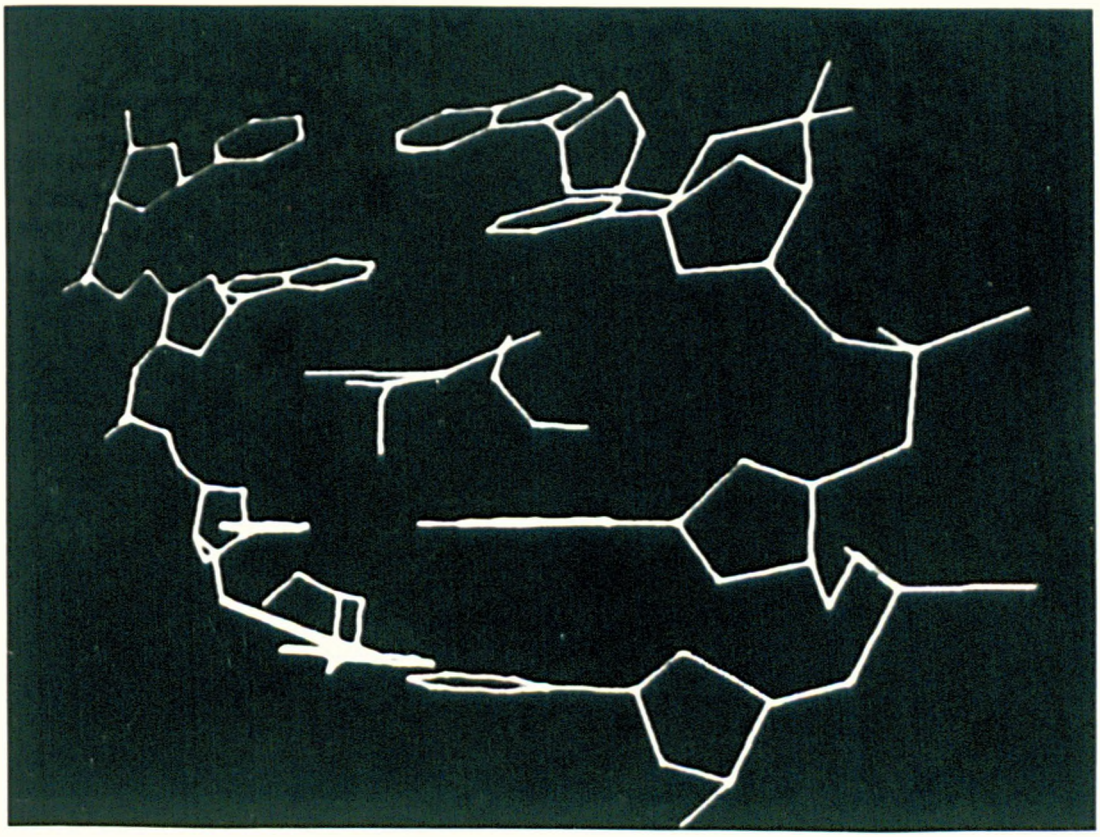

(ii) The view shown in (i), rotated anti-clockwise around the vertical axis by 75°.

the helix in this structure as proposed by Jain et al. (1977). Work is continuing within this research group to incorporate base-unstacking into the model-building program. The computer drawings produced using this model could then be compared with the computer sketches presented by Sobell et al. (1977) for ethidium-dinucleoside complexes.

Several ideas have been proposed by various authors (e.g. Krugh and Reinhardt, 1975; Kastrup et al., 1978) to explain the strong G-C specificity in the binding of ethidium to natural DNA's. Strong electrostatic binding to the exterior of the helix cannot be expected to exhibit any considerable specificity, since the drug interacts primarily with the phosphates which are uniformly placed along the sugar-phosphate chain irrespective of the base-pair composition. Any specificity is more likely to occur in the unwinding of the helix and unstacking of the base-pairs, and in the subsequent interactions between the intercalated drug chromophore and the base-pairs at the intercalation site. The energetics of both of these stages are likely to be sequence-dependent. The intercalation process involves a delicate interplay of hydrophobic, electrostatic, Van der Waals, hydrogen bonding and other forces, so that it will be some time before a unified theory is developed that adequately incorporates all of the effects operating.

A theoretical analysis (Pack and Loew, 1978) has shown that the stacking energies between the ethidium cation and the base-pairs are fairly constant for all combinations of bases at the intercalation site. In contrast, the energy involved in unwinding the double helix, to assume the geometry of the intercalation complex, shows substantial sequence differences. The results imply that there may be a large class of intercalating drugs which exhibit a purine (5' - 3') pyrimidine sequence specificity.

There may be other factors operating for a particular drug. In the minor groove of DNA, the hydrogen-bonding groups on both G-C and A-T base-pairs are identical, except for the 2-amino group of guanine. Binding to

G-C base-pairs would be preferred if the geometry of intercalation were such as to allow an additional stabilising hydrogen bound to be formed between the drug and this group on guanine. On the other hand, the amino group could interfere with intercalation of a drug if it were to provide steric hindrance. This latter possibility has been suggested to explain the A-T specificity of the intercalation of a chemically synthesised derivative of the quinoxaline antibiotic, triostin A (Lee and Waring, 1978).

Müller and Crothers (1975) have reported that, for a series of proflavine and acridine orange analogues, the G-C specificity of the binding increases as the visible absorption band of the free drug chromophore moves to longer wavelength. This implies a relationship between specificity and polarisability of the chromophore. The G-C basepair is more polar than A-T, and should therefore be able to interact more favourably with an easily polarised ring system, which is inferred from a long-wavelength absorbance spectrum. Since the dipole moment of a G-C pair is in a fixed direction, optimum specificity of binding should require that the local polarisation of the base-pair match the preferred polarisability axes of the chromophore. Steric effects can contribute to this specificity, since they will limit the possible binding geometries. A further possibility is that the base-pair sequence affects the formation of kinks in the DNA, which then become intercalation sites (Sobell et al., 1977).

If simple molecules such as ethidium can exhibit sequence preferences, then aromatic amino acids strategically located on enzymes may play an important role in the very selective recognition process involved in protein-nucleic acid interactions. Thus the "bookmark" hypothesis proposed by Brown (1970) is plausible, especially if the "bookmarks" (the aromatic residues of the protein) could also recognise the "pages of the book" (the intercalating sites).

8.2.2.2 Dimidium Bromide

The structure of dimidium is very similar to that of ethidium, the only

difference being the substitution of a methyl in place of the ethyl group on the quaternary ring nitrogen. Wakelin and Waring (1974) have found little difference between the two drugs in their unwinding of closed circular DNA. The equivalence binding ratio, at which closed and nicked circles cosediment, is centred around 0.050 for ethidium and 0.052 for dimidium. This current study has found small differences in the parameters of binding. However, at a molecular level, the binding would seem to be very similar to that of ethidium, so that the computer-refined models presented in Section 8.2.2.1 would hold just as well for dimidium. Sterically, there is little difference between the methyl group of dimidium and the ethyl group on ethidium.

It is interesting that Watkins (1952) reported that quaternisation of the ring nitrogen atom markedly increases its basicity, and causes significant changes in the curative powers of the drug. Ethidium was shown to be many times more active (and less toxic) than dimidium against Trypanosoma congolense in mice. Physical measurements on aqueous solutions of drugs at physiological pH's indicated that there were significant differences in the small concentration of drug present in the pseudo-base form, although these differences cannot be detected spectroscopically. The increased concentration of neutral component (either of the pseudo-base or ion-pair) was suggested as the explanation for the increased rate of diffusion of ethidium across the cell membrane and into the trypanosome cytoplasm. It is possible that this difference in the pseudo-base concentration may account for the observed differences in the binding parameters, and in particular the enhanced G-C specificity of ethidium.

It is unlikely that the small difference in the electron-withdrawing character of the ethyl and methyl groups could account for a change in the direction of the dipole moments in the chromophore, sufficiently large to explain the difference in the specificities on polarisability grounds. Since ethidium and dimidium were obtained from different sources (Section

2.1.2), it is possible that there was some difference in the purity of the samples. However, various previous studies have produced similar results for ethidium using samples from different suppliers, so that it is thought that this may not be a significant problem.

8.2.2.3 Prothidium

Prothidium binds very tightly to DNA, as evidenced by its large association constant. The attachment is considered to be strongly electrostatic, since the binding is strongly affected by the ionic concentration of the environment. Strong electrostatic binding would be expected to show no base-pair specificity, since the environment of all the DNA phosphates is similar. The results presented in Section 4.4.3 confirm this expected lack of specificity.

The birefringence and linear dichroism results suggest that the drug is bound at a considerable angle from perpendicular to the helix axis, and the X-ray diffraction patterns show that prothidium causes little if any change in the secondary structure of the DNA. Wakelin and Waring (1974) have reported that prothidium unwinds closed circular DNA, but they have not given any details. In any case, this is not evidence of intercalative binding. Steroidal diamines such as irehdiamine A and malouetine unwind the DNA helix (Waring, 1970; Waring and Chisholm, 1972), but irehdiamine A has a thickness of 5.9Å so that a conventional type of intercalation is not possible, and Gabbay and Glaser (1971) have suggested that the steroidal diamines bind in the minor groove of DNA.

In the prothidium molecule, both ring nitrogens are quaternised so that there is a strong charge localisation. The pyrimidyl moiety is fairly free to rotate about the amide bond to the phenanthridine triple ring. Nevertheless, the preferred conformation of the drug is likely to be when it is fully extended such that the pyrimidyl moiety makes an angle of about 120° with the triple aromatic ring, and lies on the same side of the triple ring as the main part of the aminated phenyl substituent. The separation

of the two positive charges is about 8Å (Cain et al., 1969), which corresponds to the distance between adjacent phosphate groups along a strand of the double helix. Electrostatic forces are much stronger than hydrogen bonds or hydrophobic effects, so that it is envisaged that electrostatic binding to neighbouring phosphates is the prime mode of attachment, certainly at low and moderate ionic concentrations. Fig. 8.3 shows a possible model for this situation, although the precise orientation of the drug is not known.

The prothidium molecule presents more groups for possible hydrogen bonding than does ethidium or dimidium. The amide group between the aromatic ring is likely to form only a weak hydrogen bond. On the pyrimidyl moiety, the lone pair is available for protonation and would normally participate in strong hydrogen bonds. However, the presence of the charged quaternary nitrogen is thought to shift this ability towards the attached amino group, which is then likely to become the stronger hydrogen bonding centre in this ring. The 3-amino group of the phenanthridine ring and the amino group in the 4-position of the phenyl ring are both likely to be even stronger hydrogen bonding centres. The inter-strand distance between phosphates across the minor groove in B-DNA is about 12.8Å, and across the major groove it is about 16.8Å. In A-DNA the interstrand separation of the phosphates is around 14.4 - 16.8Å. All of these distances are comparable with the separation of the various hydrogen bonding groups of prothidium. Thus, there is a multiplicity of possibilities for hydrogen bonding across the strands in DNA. A possible inter-strand binding scheme is shown in Fig. 8.4 for binding across the wide groove of B-DNA. It is possible that binding across the strands would resist the conformational change of DNA that occurs as the humidity is varied. This would account for the significant amount of A-type diffraction occurring at 92% R.H., and is consistent with the dichroism results. The models proposed are largely speculative and must remain so until more

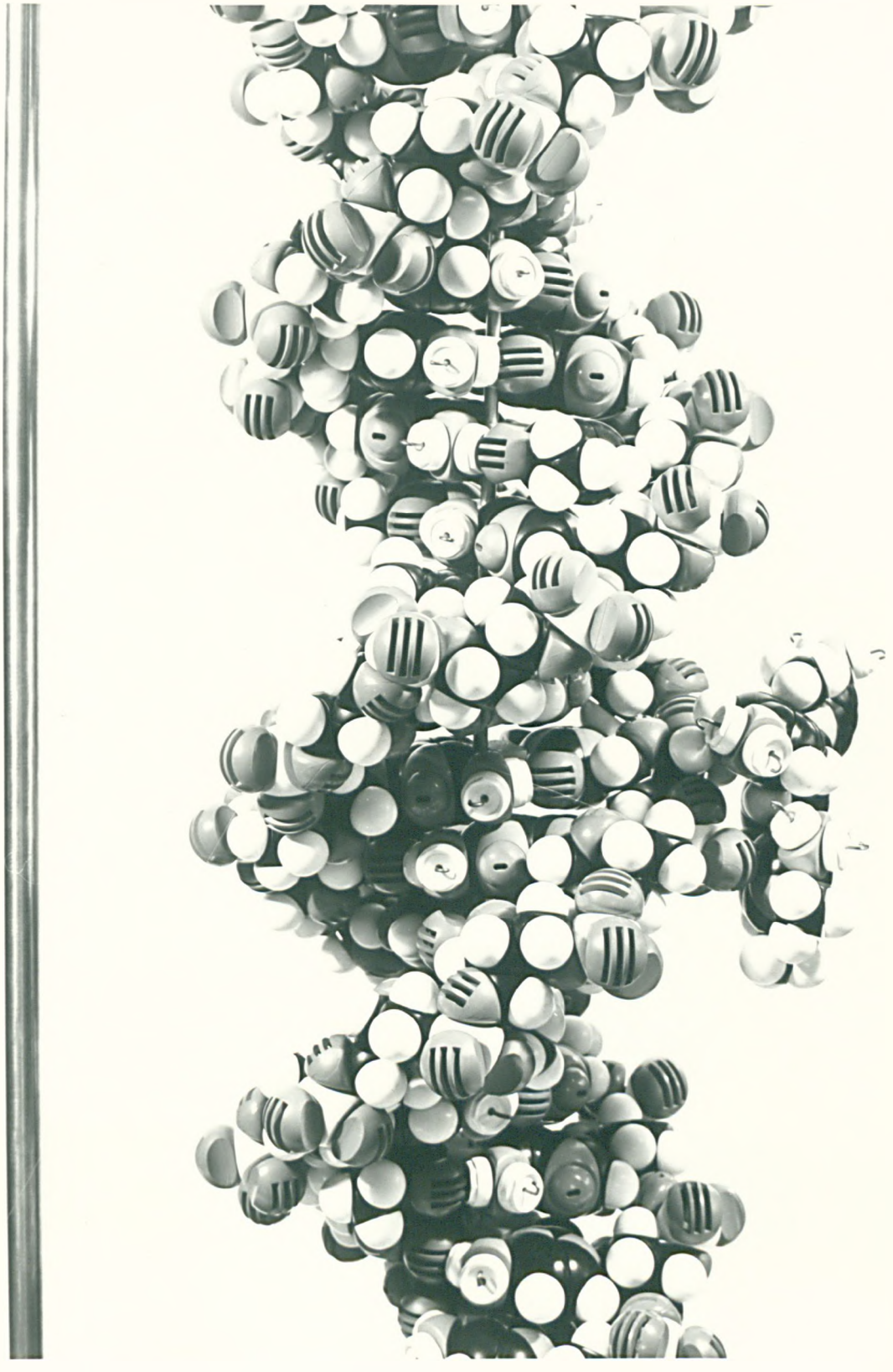

Figure 8.3. CPK model of B-DNA with a prothidium molecule externally bound by electrostatic attachment to two phosphate groups of the backbone.

Figure 8.4. CPK model of B-DNA with a prothidium molecule bound across the major groove.

definite data on the position and orientation of the bound drugs is obtained.

Intercalation could be considered as a possible mode of binding for prothidium, although it would be less favourable than with ethidium and dimidium. The bulky pyrimidyl group can provide steric hindrance to intercalation depending on its orientation, and it would control the depth of insertion of the chromophore if intercalation were to take place. Its orientation may also affect the direction of the dipole moment of the chromophore, which would change the strength of the drug/base-pair interaction.

It would be sterically possible for the prothidium to intercalate "sideways" by insertion of part of the triple ring between adjacent base-pairs approximately perpendicular to the helix axis. This is more likely to occur from the narrow groove of the DNA, since there is then the possibility of some additional stabilisation by the formation of a hydrogen bond to an amino group of a base-pair. This possibility is shown in Fig. 8.5. The poor overlap with the base-pairs makes it a less favourable position than the position adopted by ethidium and dimidium. The much lower unwinding angle which would result from this binding would lead to much smaller pitch increases in the DNA, and the fact that no increase in pitch was measured does not preclude a small fraction of the drug binding in this way. Indeed, "sideways" intercalation has been proposed for another bulky phenanthridine, RD 16101, to explain its binding parameters (Wakelin and Waring, 1974). Stereochemically it seems likely that this mode of binding could continue to fairly high binding levels, and it would not be so restricted by neighbour exclusion as the more established intercalation positions. Indeed, it may be that neighbour exclusion may be due, in part, to a thermodynamic limitation, which may be less restrictive for a drug of high DNA affinity.

It would be possible for prothidium to bind from the large groove into an intercalation position similar to that adopted by ethidium, but the

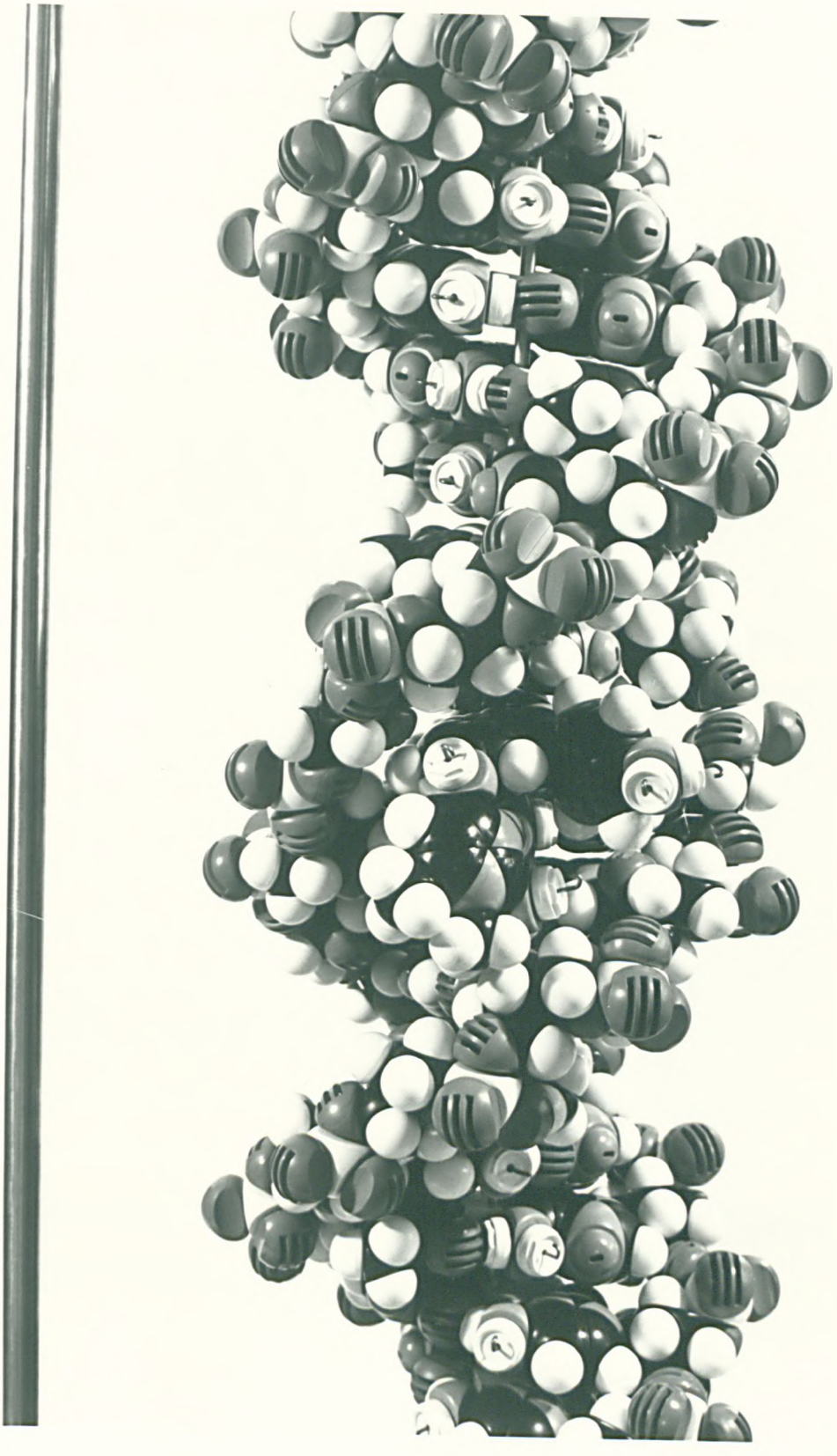

Figure 8.5. CPK model of B-DNA with a prothidium molecule intercalated sideways from the minor groove.

pyrimidyl moiety would need to be rotated close to the phenyl substituent (Fig. 8.6). This is not the preferred conformation of the prothidium molecule, but it could be constrained to adopt this conformation if the drive towards intercalation was large enough. A difficulty with this scheme is that it would probably result in the close approach of the amino-groups on the pyrimidyl and phenyl moieties.

In conclusion, intercalative binding seems to be less likely for prothidium. Strong electrostatic binding along a sugar-phosphate chain is proposed as the most likely binding scheme, and there may also be a considerable amount of binding across the grooves to an adjacent chain. These schemes involve such strong forces that it is unlikely that much of the drug would leave these sites and move into an intercalative position, although sterically intercalation cannot be excluded. The low solubility of prothidium suggests that the hydrophobic drive towards intercalation may not be large.

The large association constant for prothidium binding to DNA makes it an attractive chemotherapeutic agent. The fact that it does not intercalate to any great extent may not render it ineffectual provided that it could be given some specificity. The oligopeptide antibiotic netropsin is a non-intercalator, but it is thought to inhibit enzymes such as DNA polymerase by blocking access to the minor groove of DNA or by stabilising the double helix (Sutherland et al., 1978). Prothidium does have the disadvantage, however, of being doubly-ionised which would inhibit its passage through cellular membranes.

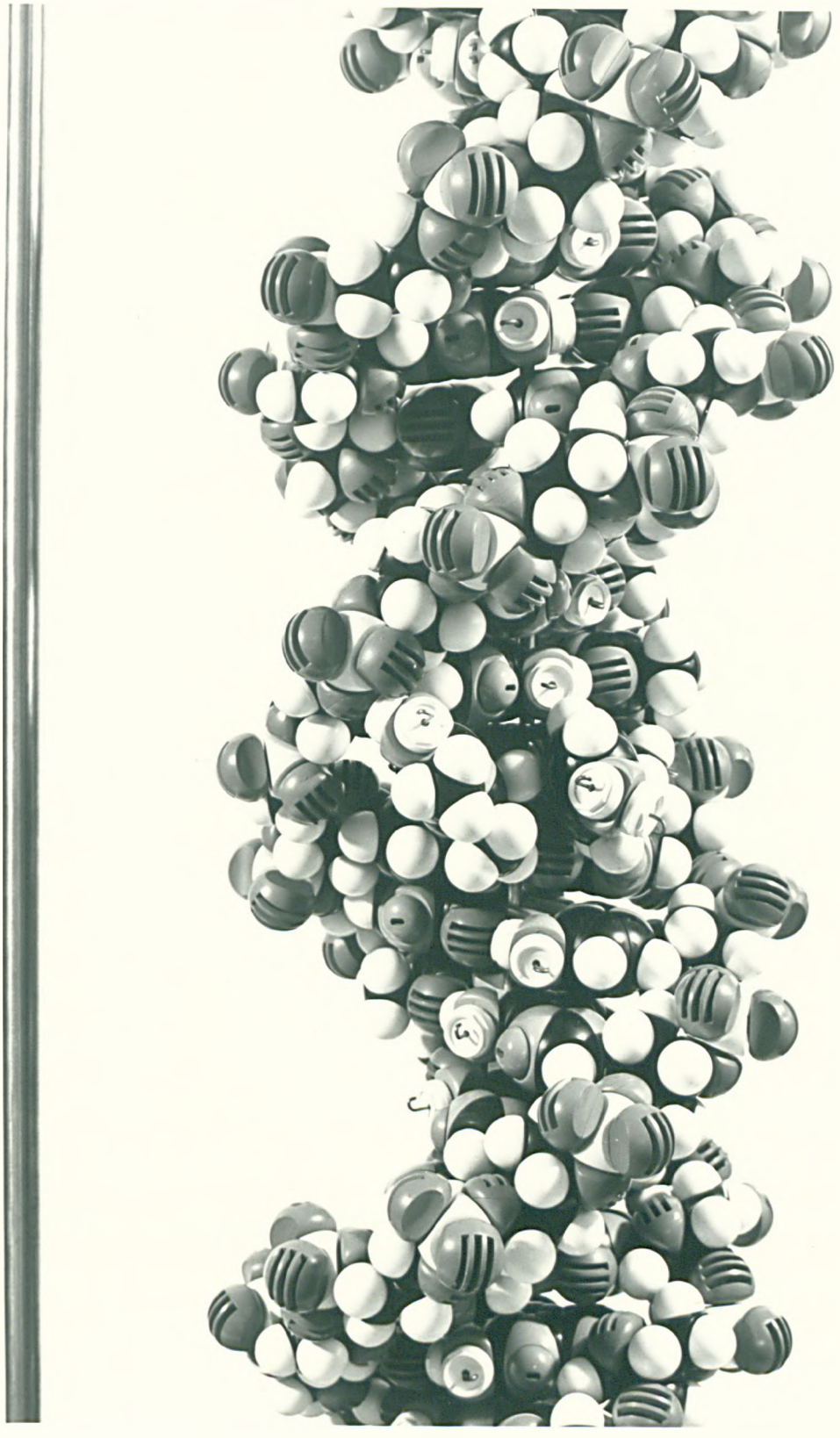

Figure 8.6. CPK model of B-DNA with a prothidium molecule intercalated from the major groove.

8.3 Summary and Proposals for Further Work

The theory of the analysis of solution spectra has been thoroughly appraised, and a program written to analyse the experimental data in terms of an excluded site model for the binding. The author has developed and tested a novel mixing scheme to facilitate the collection of accurate binding data, and this has been used to investigate the specificities of three phenanthridine drugs for particular base-pairs using three different natural DNA's.

The absorption spectra of DNA-drug fibres have been recorded on a microspectrophotometer, and the birefringence and linear dichroism of the fibres have been measured over a range of humidities. Unfortunately, these investigations have been limited to fibres of low drug content ($M \gtrsim 20$) because of the stray light limit of the microspectrophotometer. The fibres have been somewhat variable in quality, but it has been the experience of this research group that ionic considerations, and the viscosity of the gel from which the fibre had been pulled, are important factors in determining the quality of a fibre. Other drugs may result in better fibres than those obtained with the phenanthridines.

The X-ray diffraction studies have been somewhat supplementary to the spectral investigations, although they have confirmed earlier results on DNA-ethidium systems and shown that the binding of dimidium causes a similar unwinding of the DNA-helix. In contrast, the binding of prothidium does not increase the pitch of DNA. The methods described could be applied to an extensive X-ray diffraction investigation of new drugs. Some model-building studies have been undertaken, especially for the binding of prothidium (di)bromide. The results for prothidium must remain rather speculative until more precise data on the orientation of the drug is obtained from other techniques.

The solution spectra of DNA-prothidium complexes were particularly difficult to analyse. It may prove useful if spectra were obtained at

intermediate salt concentrations, and the results extrapolated to low salt concentration using the scheme of Record et al. (1976). The investigation of the binding could be supplemented by an extended equilibrium dialysis study. It would be particularly interesting to investigate the binding of the dimethylated form of prothidium, although difficulty in dissolving it in aqueous solution is envisaged. Removal of the positive charges should result in a compound which would find intercalation a more attractive proposition.

The approach developed in this thesis could be extended to the investigation of other drugs interacting with nucleic acids. It should be possible to find the fraction of these drugs intercalated at particular relative humidities, and obtain an estimate of their unwinding angles. The estimates would be more certain if the variability in the quality of fibres could be reduced, and if the dichroic ratio could be measured for moderate M values ($M \tilde{>} 5$–15). This may be possible using films or fibre sections, if sufficiently good orientation can be achieved. The theory of the birefringence and dichroism of films has been presented in this thesis along with that for fibres. It would seem that a polymer such as cis-polybutadiene would be a very suitable substrate for making films, since it will stretch but will not allow the drug to penetrate it. A solution of a DNA-drug complex could be gently poured on to the substrate, as it floated on a mercury bath to maintain a horizontal disposition. When the complex had dried, it could be orientated by stretching the polymer substrate and its optical properties measured. If a DNA-drug film of about 5 - 10μm were prepared, then films with small M values ($M \sim 2$) could be measured. These films could then be folded to produce a thickness suitable for X-ray diffraction. In this way specimens over a range of M values could be compared directly by the two techniques, and a better estimate of the unwinding angle of an intercalating drug could be obtained.

It would be interesting to extend these studies to the cytotoxic antibiotic nogalamycin. This drug has two bulky sugar residues, yet it

still appears to intercalate (Al-Jubory, 1978). The antibacterial agents, steffimycin and steffimycin B, have been shown to intercalate and micro-crystals of the DNA-steffimycin complex appear to crystallise out at low humidity. It would be useful to apply the dichroism techniques to fibres containing these drugs, in order to characterise the orientation of the drugs. The formation of drug micro-crystals is of special interest in relation to cancer therapy, where the drug crystals could be implanted near to a tumour. This could provide a steady, prolonged release of the drug to a localised region. A further area for fruitful study would be the drugs such as echinomycin, which are believed to be bisintercalators (Wakelin and Waring, 1976). Investigations by the methods proposed in this thesis would shed light on the conformation adopted by these drugs on binding and the extent to which they intercalate.

REFERENCES

ABERNETHY, J.D.W. (1973). Phys. Bull., 24, 591.

ABRAMOWITZ, M. and SEGUN, I.A. (1968). Handbook of Mathematical Functions, Dover Pub., New York.

ALBERT, A., ARMAREGO, W.L.F. and SPINNER, E. (1961). J. Chem. Soc., 2689.

ALDEN, C.J. and ARNOTT, S. (1975). Nuc. Acids. Res., 2, 1701.

AL-JUBORY, T.T. (1978). Ph. D. Thesis, University of Keele.

ANGERER, L.M. and MOUDRIANAKIS, E.N. (1972). J. Mol. Biol., 63, 505.

ARMSTRONG, R.W., KURUCSEV, T. and STRAUSS, U.P. (1970). J. Amer. Chem. Soc., 92, 3174.

ARNOTT, S. and HUKINS, D.W.L. (1972). Biochem. Biophys. Res. Commun., 47, 1504.

BAUER, W. and VINOGRAD, J. (1970). J. Mol. Biol., 47, 419.

BERMAN, H.M., NEIDLE, S. and STODOLA, R.K. (1978). Proc. Natl. Acad. Sci. USA, 75, 828.

BIDET, R., CHAMBRON, J. and WEILL, G. (1971). Biopolymers, 10, 225.

BLAKE, A. and PEACOCKE, A.R. (1968). Biopolymers, 6, 1225.

BLAKE, A. and LEFOLEY, S.G. (1978). Biochim. Biophys. Acta, 518, 233.

BLAKELEY, P.J. (1976). Ph.D. Thesis, University of Keele.

BLOOMFIELD, V.A., CROTHERS, D.M. and TINOCO, Jr., I. (1974). Physical Chemistry of Nucleic Acids, Harper and Row.

BOLRON, M., JAQUILLAR, C., WEIL, M., TANZER, J., LEVY, D., SULTAN, C. and BERNARD, J. (1969). Lancet, 1, 330.

BOND, P.J., LANGRIDGE, R., JENNETTE, K.W. and LIPPARD, S.J. (1975). Proc. Natl. Acad. Sci. USA, 72, 4825.

BRADLEY, D.F. and FELSENFELD, G. (1959). Nature, 184, 1920.

BRAM, S. (1972). Biochem. Biophys. Res. Commun., 48, 1088.

BRAM, S. (1973). Proc. Natl. Acad. Sci. USA, 70, 2167.

BRAM, S. and TOUGARD, P. (1972). Nature New Biol., 239, 128.

BRENNER, S., BARNETT, L., CRICK, F.H.C. and ORGEL, A. (1961). J. Mol. Biol., 3, 121.

BRESLOFF, J.L. (1974). Ph.D. Thesis, Yale University.

BRESLOFF, J.L. and CROTHERS, D.M. (1975). J. Mol. Biol. 95, 103.

BROWN, P.E. (1970). Biochim. Biophys. Acta, 213, 282.

BURDIN, M.L. and PLOWRIGHT, W. (1952). Nature, 169, 666.

BUTOUR, J.L., DELAIN, E., COULAUD, D., LE PECQ, J.B., BARBET, J. and ROQUES, B.P. (1978). Biopolymers, 17, 873.

CAIN, B.F., ATWELL, G.J. and SEELYE, R.N. (1969). J. Med. Sci., 12, 199.

CAIRNS, J. (1962). Cold Spring Harbor Symp., 27, 311.

CALENDI, E., DI MARCO, A., REGGIANI, A., SCARPINATO, B. and VALENTINI, L. (1965). Biochim. Biophys. Acta, 103, 25.

CARCHMAN, R.A., HIRSCHBERG, E. and WEINSTEIN, I.B. (1969). Biochim. Biophys. Acta, 179, 158.

CELLA, R.J., BYUNGKOOK, L. and HUGHES, R.E. (1970). Acta Cryst. A26, 118.

CHAN, L.M. and VAN WINKLE, Q. (1969). J. Mol. Biol., 40, 491.

CLARKE, F.J.J. (1972). J. Res. natn. Bur. Stand., 76A, 375.

COCHRAN, W., CRICK, F.H.C. and VAND, V. (1952). Acta Cryst., 5, 581.

COOPER, P.J. and HAMILTON, L.D. (1966). J. Mol. Biol., 16, 562.

CRAIG, M. and ISENBERG, I. (1970). Biopolymers, 9, 689.

CRICK, F.H.C., WANG, J.C. and BAUER, W.R. (1979). J. Mol. Biol., 129, 449.

CROTHERS, D.M. (1968). Biopolymers, 6, 575.

CYRIAX, B. and GÄTH, R. (1978). Naturwissenschaften, 65, 106.

DALGLEISH, D.G., PEACOCKE, A.R., FEY, G. and HARVEY, C. (1971). Biopolymers, 10, 1853.

DALGLEISH, D.G., DINGSØYR, E. and PEACOCKE, A.R. (1973). Biopolymers, 12, 445.

DING, D., RILL, R. and VAN HOLDE, K.E. (1972). Biopolymers, 11, 2109.

DUANE, M. (1972). Eur. J. Biochem., 26, 207.

ELLIS, K.J. and DUGGLEBY, R.G. (1978). Biochem. J., 171, 513.

FALK, M., HARTMAN, Jr., K.A. and LORD, R.C. (1963). J. Am. Chem. Soc., 85, 387.

FAUST, R.C. and MARRINAN, H.J. (1955). Brit. J. Appl. Phys., 6, 351.

FELSENFELD, G. and HIRSCHMAN, S.Z. (1965). J. Mol. Biol., 13, 407.

FOWLER, R. and GUGGENHEIM, E. (1952). Statistical Thermodynamics, Cambridge.

FRANKLIN, R.E. and GOSLING, R.G. (1953). Acta Cryst., 6, 678.

FRANKLIN, R.E. and KLUG, A. (1955). Acta Cryst., 8, 777.

FRASER, R.D.B. (1953). J. Phys. Chem., 21, 1511.

FRASER, R.D.B. (1955). Nature, 176, 358.

FRASER, R.D.B., MACRAE, T.P., MILLER, A. and ROWLANDS, R.J. (1976). J. Appl. Cryst., 9, 81.

FRISMAN, E.V., VOROBYEV, V.I., SHCHAGINA, L.V. and YANOVSKA, L.V. (1962). Vysokomol. Soedin., 4, 762.

FULLER, W. (1961). Ph.D. Thesis, University of London.

FULLER, W. (1966). Genetic Elements, Properties and Function, 17-39, Academic Press.

FULLER, W. and WARING, M.J. (1964). Ber Bunsenges. Phys. Chem., 68, 805.

FULLER, W., WILKINS, M.H.F., WILSON, H.R. and HAMILTON, L.D. (1965). J. Mol. Biol., 12, 60.

GABBAY, E.J. and GLASER, R. (1971). Biochemistry, 10, 1665.

GALE, E.F., CUNDLIFFE, E., REYNOLDS, P.E., RICHMOND, M.H. and WARING, M.J. (1972). The Molecular Basis of Antibiotic Action, John Wiley.

GAUGAIN, B. (1978). Biochemistry, 17, 5078.

GENEST, D. and WAHL, P. (1972). Biochim. Biophys. Acta, 259, 175.

GERSCH, N.F. and JORDAN, D.O. (1965). J. Mol. Biol., 13, 138.

GIACOMONI, P.U. and LE BRET, M. (1973). FEBS Letters, 29, 227.

GOLDSTEIN, H. (1964). Classical Mechanics, Addison-Wesley.

GOODWIN, D.C. (1977). Ph.D. Thesis, University of Keele.

GRADSHTEYN, I.S. and RYZHIK, I.M. (1965). Table of Integrals, Series and Products, 4th Edition, Academic Press.

GRAY, D.M., HAMILTON, F.D. and VAUGHAN, M.R. (1978). Biopolymers, 17, 85.

GROVES, W.E., DAVIES, Jr., F.C. and SELLS, B.H. (1968). Analytical Biochemistry, 22, 195.

GURSKII, G.V., ZASEDATELEV, A.S. and VOL'KENSHTEIN, M.V. (1972). Molecular Biology, 6, 385.

HAMILTON, L.D., BARCLAY, D.M.R.K., WILKINS, M.H.F., BROWN, G.L., WILSON, H.R., MARVIN, D.A., EPHRUSSI-TAYLOR, H. and SIMMONS, N.S. (1959). J. Biophys. Biochem. Cytol., 5, 397.

HARTSHORNE, N.H. and STUART, A. (1970). Crystals and the Polarising Microscope, 4th Edition, Edward Arnold.

HILL, T.L. (1957). J. Polymer Sci., 23, 549.

HOGAN, M., DATTAGUPTA, N. and CROTHERS, D.M. (1979). Biochemistry, 18, 280.

HOLMES, K.C. and BARRINGTON LEIGH, L. (1974). Acta Cryst., A30, 635.

HONG, S.J. and PIETTE, L.H. (1976). Cancer Research, 36, 1159.

HOSHINO, S., POWERS, J., LEGRAND, D.G., KAWAI, H. and STEIN, R.S. (1962). J. Polym. Sci., 58, 185.

HOUSSIER, C., HARDY, B. and FREDERICQ, E. (1974). Biopolymers, 13, 1141.

HUDSON, B., UPHOLT, W.B., DEVINNY, J. and VINOGRAD, J. (1969). Proc. Natl. Acad. Sci. USA, 62, 813.

INGRAHAM, L.L. and JOHANSEN, H. (1969). Archives of Biochemistry and Biophysics, 132, 205.

JAFFE, J.H., JAFFE, H. and ROSENHECK, K. (1967). Rev. Sci. Inst., 38, 935.

JAIN, S.C., TSAI, C.-C. and SOBELL, H.M. (1977). J. Mol. Biol., 114, 317.

JONES, R.N. (1945). J. Am. Chem. Soc., 67, 2127.

JOSSE, J., KAISER, A.D. and KORNBERG, A. (1961). J. Biol. Chem., 236, 864.

KALLENBACH, N.R. (1979). Nature, 279, 475.

KANDASWAMY, T.S. and HENDERSON, J.F. (1962). Biochim. Biophys. Acta, 61, 86.

KASTRUP, R.V., YOUNG, M.A. and KRUGH, T.R. (1978). Biochemistry, 17, 4855.

KELLER, W. (1975). Proc. Natl. Acad. Sci. USA, 72, 4876.

KELLER, W. and WENDEL, I. (1974). Cold Spring Harbor Symp. Quant. Biol., 39, 199.

KELLY, G.R. and KURUCSEV, T. (1976). Biopolymers, 15, 1481.

KERRIDGE, D. (1958). J. Gen. Microbiol., 19, 497.

KERSTEN, W., KERSTEN, H. and SZYBALSKI, W. (1966). Biochemistry, 5, 236.

KLEINWÄCHTER, V., BALCAROVA, Z. and BOHAČEK, J. (1969). Biochim. Biophys., Acta, 174, 188.

KLOTZ, I.M. and HUNSTON, D.L. (1971). Biochemistry, 10, 3065.

KOLTUN, W.L. (1965). Biopolymers, 3, 665.

KRUGH, T.R. and REINHARDT, C.G. (1975). J. Mol. Biol., 97, 133.

KRUGH, T.R., WITTLIN, F.N. and CRAMER, S.P. (1975). Biopolymers, 14, 197.

KURUCSEV, T. and ZDYSIEWICZ, J.R. (1971). Biopolymers, 10, 593.

LANGRIDGE, R., MARVIN, D.A., SEEDS, W.E. and WILSON, H.R. (1960). J. Mol. Biol., 2, 19.

LEE, J.S. and WARING, M.J. (1978). Biochem. J., 173, 115.

LENG, M., RAMSTEIN, J., DEUBEL, V. and DROCOURT, J.L. (1973). Stud. Biophys., 40, 83.

LE PECQ, J.B. and PAOLETTI, C. (1967). J. Mol. Biol., 27, 87.

LERMAN, L.S. (1961). J. Mol. Biol., 3, 18.

LERMAN, L.S. (1963). Proc. Natl. Acad. Sci. USA, 49, 94.

LERMAN, L.S. (1964). J. Cell. Comp. Physiol., 64, Suppl., 1, 1.

LESKO, Jr., S.A., HOFFMANN, H.D., TS'O, P.O.P. and MAHER, V.M. (1971). Prog. Mol. Subcell. Biol., 2, 347.

LEVITT, M. (1978). Proc. Natl. Acad. Sci. USA, 75, 640.

LIBERTINI, L.J., BURKE, C.A., JOST, P.C. and GRIFFITH, O.H. (1974). J. Mag. Res., 15, 460.

LIU, L.F. and WANG, J.C. (1975). Biochim. Biophys. Acta, 395, 405.

LI, H.J. and CROTHERS, D.M. (1969). J. Mol. Biol., 39, 461.

LUZZATI, V., MASSON, F. and LERMAN, L.S. (1961). J. Mol. Biol., 3, 634.

McGHEE, J.D. and VON HIPPEL, P.H. (1974). J. Mol. Biol., 86, 469.

MAEDA, Y. (1978). Eur. J. Biochem., 90, 113.

MARMUR, J. (1961). J. Mol. Biol., 3, 208.

MARVIN, D.A., SPENCER, M., WILKINS, M.H.F. and HAMILTON, L.D. (1958) Nature, 182, 387.

MARVIN, D.A., SPENCER, M., WILKINS, M.H.F. and HAMILTON, L.D. (1961). J. Mol. Biol., 3, 547.

MASSIE, H.R. and ZIMM, B.H. (1965). Biochemistry, 54, 1636.

MAUSS, Y., CHAMBRON, J., DAUNE, M. and BENOIT, H. (1967). J. Mol. Biol., 27, 579.

MIELENZ, K.D. (1972). J. Res. natn. Bur. Stand., 76A, 455.

MIELENZ, K.D. and ECKERLE, K.L. (1972). Tech. Not. natn. Bur. Stand., 729.

MÜLLER, W. and CROTHERS, D.M. (1968). J. Mol. Biol., 35, 251.

MÜLLER, W. and CROTHERS, D.M. (1975). Eur. J. Biochem., 54, 267.

MULLER, W., CROTHERS, D.M. and WARING, M.J. (1973). Eur. J. Biochem., 39, 223.

NEVILLE, D.M. and DAVIES, D.R. (1966). J. Mol. Biol., 17, 57.

NINHAM, B.W. and SAMMUT, R.A. (1976). J. Theor. Biol., 56, 125.

O'BRIEN, F.E.M. (1948). J. Scient. Instrum., 25, 73.

O'BRIEN, R.L., ALLISON, J. and HAHN, F.E. (1969). Biochim. Biophys. Acta, 129, 622.

PACK, G.R. and LOEW, G. (1978). Biochim. Biophys. Acta, 519, 163.

PAGE, E.S. (1959). J. Roy. Stat. Soc. (Ser. B), 21, 364.

PAOLETTI, J. and LE PECQ, J.B. (1971). J. Mol. Biol., 59, 43.

PATEL, D.J. and CANUEL, L.L. (1976). Proc. Natl. Acad. Sci. USA, 73, 3343.

PATEL, D.J. and CANUEL, L.L. (1977). Biopolymers, 16, 857.

PATEL, D.J. and SHEN, C. (1978). Proc. Natl. Acad. Sci. USA, 75, 2553.

PEACOCKE, A.R. and SKERRETT, J.N.H. (1956). Trans. Far. Soc., 52, 261.

PHILPOTT, M.R. (1970). J. Chem. Phys., 53, 968.

PIGRAM, W.J. (1968). Ph.D. Thesis, University of London.

PIGRAM, W.J., FULLER, W. and HAMILTON, L.D. (1972). Nature New Biol., 235, 17.

PILET, J. and BRAHMS, J. (1972). Nature New Biol., 236, 99.

PILET, J. and BRAHMS, J. (1973). Biopolymers, 12, 387.

PLUMBRIDGE, T.W. and BROWN, J.R. (1977). Biochim. Biophys. Acta, 479, 441.

PLUMBRIDGE, T.W. and BROWN, J.R. (1979). Biochim. Biophys. Acta, 563, 181.

PLUMBRIDGE, T.W., AARONS, L.J. and BROWN, J.R. (1978). J. Pharm. Pharmac., 30, 69.

POHL, W.F. and ROBERTS, G.W. (1978). J. Math. Biol., 6, 383.

PORUMB, H. (1976). Ph.D. Thesis, University of Keele.

PORUMB, T. and SLADE, E.F. (1976). Eur. J. Biochem., 65, 21.

PORUMB, T. and SLADE, E.F. (1976). Quantum Chemistry Exchange Programs, QCEP 295, University of Indiana.

PORUMB, T. and SLADE, E.F. (1976). J. Mag. Res., 22, 219.

PREMILAT, S. and ALBISER, G. (1975). J. Mol. Biol., 99, 27.

PULLEYBLANK, D.E. and MORGAN, A.R. (1975). J. Mol. Biol., 91, 1.

RAMSTEIN, J. and LENG, M. (1975). Biophys. Chem., 3, 234.

RAMSTEIN, J., DOURLENT, M. and LENG, M. (1972). Biochem. Biophys. Res. Comm., 47, 874.

RECORD, Jr., M.T., LOCHMAN, T.M. and DE HASSETH, P. (1976). J. Mol. Biol., 107, 145.

RICH, A. (1979). Nature, 279, 475.

ROBSON, J. (1961). Vet. Record, 73, 641.

RODLEY, G.A., SCOBIE, R.S., BATES, R.H.T. and LEWITT, R.M. (1976). Proc. Natl. Acad. Sci. USA, 73, 2959.

RUPPRECHT, A., RIGLER, R., FORSLIND, B. and SWANBECK, G. (1969). Eur. J. Biochem., 10, 291.

SAKODA, M., HIROMI, K. and AKASAKA, K. (1971). Biopolymers, 10, 1003.

SASISEKHARAN, V. and PATTABIRAMAN, N. (1976). Curr. Sci., 45, 779.

SASISEKHARAN, V., PATTABIRAMAN, N. and GUPTA, G. (1977). Curr. Sci., 46, 763.

SASISEKHARAN, V., PATTABIRAMAN, N. and GUPTA, G. (1978). Proc. Natl. Acad. Sci. USA, 75, 4092.

SCATCHARD, G. (1949). Ann. N.Y. Acad. Sci., 51, 660.

SCHELLMAN, J.A. (1974). Isr. J. Chem., 12, 219.

SCHILDKRAUT, C.L., MARMUR, J. and DOTY, P. (1962). J. Mol. Biol., 4, 430.

SCHMECHEL, D.E.V. and CROTHERS, D.M. (1971). Biopolymers, 10, 465.

SCHWARZ, G. (1970). Eur. J. Biochem., 12, 442.

SEEDS, W.E. (1951). Ph. D. Thesis, University of London.

SEEDS, W.E. (1953). Progr. Biophys. and Biophysic. Chem., 3, 27.

SEEMAN, N.C., DAY, R.O. and RICH, A. (1975). Nature, 253, 324.

SHUGALIN, A.V., FRANK-KAMENETSKII, M.D. and LAZURKIN, YU. S. (1971). Molecular Biology, 5, 613.

SHURE, M. and VINOGRAD, J. (1976). Cell, 8, 215.

SLAVIN, W. (1963). Anal. Chem., 35, 561.

SOBELL, H.M. (1973). Progress in Nucleic Acid Research and Molecular Biology (COHN, W.E. and DAVIDSON, J.N., Eds.), 13, 153-190, Academic Press, New York.

SOBELL, H.M. and JAIN, S.C. (1972). J. Mol. Biol., 68, 21.

SOBELL, H.M., JAIN, S.C. and SAKORE, T.D. (1971). Nature New Biol., 231, 200.

SOBELL, H.M., TSAI, C-C., JAIN, S.C. and GILBERT, S.G. (1977). J. Mol. Biol., 114, 333.

STANDKE, K-H.C. (1975). Nucl. Acids Res., 2, 1839.

STEINER, R.F. and BEERS, R.F. (1961). Polynucleotides, 290-311, Elsevier.

STREISINGER, G., OKADA, Y., EMRICH, J., NEWTON, J., TSUGITA, A., TERZAGHI, E. and INOUYE, M. (1966). Cold Spring Harbor Symp. Quant. Biol., 31, 77.

STUBBS, G.J. (1974). Acta Cryst., A30, 639.

SUBRAMANIAN, E., TROTTER, J. and BUGG, C.E. (1971). J. Cryst. Mol. Struct., 1, 3.

SUTHERLANDS, J.C., DUVAL, J.F. and GRIFFIN, K.P. (1978). Biochemistry, 17, 5088.

TAN, C., TASAKA, H., YU, K., MURPHY, M.L. and KARNOESKY, D.A. (1967). Cancer, 20, 333.

TAKASHIMA, S. (1968). Biopolymers, 6, 1437.

THOMAS, G. and ROQUES, B. (1972). FEBS Letters, 26, 169.

TOMCHIK, R. and MANDEL, H.G. (1964). J. Gen. Microbiol., 36, 225.

TSAI, C-C., JAIN, S.C. and SOBELL, H.M. (1975). Proc. Natl. Acad. Sci. USA, 72, 628.

TSAI, C-C., JAIN, S.C. and SOBELL, H.M. (1977). J. Mol. Biol., 114, 301.

TSVETKOV, V.N. (1963). Polym. Sci., 4, 1448.

VAN, S.P., BIRRELL, G.B. and GRIFFITH, O.H. (1974). J. Mag. Res. 15, 30.

WAKELIN, L.P.G. and WARING, M.J. (1974). Molec. Pharmac., 10, 544.

WAKELIN, L.P.G. and WARING, M.J. (1976). Biochem. J., 157, 721.

WANG, J.C. (1974). J. Mol. Biol., 89, 783.

WANG, J.C. (1978). Cold Spring Harbor Symp. Quant. Biol., 43.

WANG, J.C. (1979). Proc. Natl. Acad. Sci. USA, 76, 200.

WARD, D.C., REICH, E. and GOLDBERG, I.H. (1965). Science, 149, 1259.

WARING, M.J. (1965). J. Mol. Biol., 13, 269.

WARING, M.J. (1970). J. Mol. Biol., 54, 247.

WARING, M.J. and CHISHOLM, J.W. (1972). Biochim. Biophys. Acta, 262, 18.

WARTELL, R.M., LARSON, J.E. and WELLS, R.D. (1974). J. Biol. Chem., 249, 6717.

WATKINS, T.I. (1952). J. Chem. Soc., 3059.

WATSON, J.D. and CRICK, F.H.C. (1953). Nature, 171, 737.

WEILL, G., HORNICK, C. and STOYLOV, S. (1968). Journal de Chimie Physique, 64, 182.

WEINER, V.O. (1912). Abh. Sachs. Ges. (Akad.) Wiss., 32, 507.

WILKINS, M.H.F., STOKES, A.R. and WILSON, H.R. (1953). Nature, 171, 738.

ZANKER, V., HELD, M. and RAMMENSEE, H. (1959). Z. Naturforsch, 146, 789.

ZASEDATELEV, A.S., GURSKII, G.V. and VOL'KENSHTEIN, M.V. (1971). Molecular Biology, 5, 194.

ZBINDEN, R. (1964). Infra-red Spectroscopy of High Polymers, Academic Press, New York.

ZUNINO, F., GAMBETTA, R., MARCO, A. and ZACCARA, A. (1972). Biochim. et Biophys. Acta, 277, 489.